

**The Structure and Life-Cycle of Midlatitude Mesoscale
Convective Complex**

by
Robert A. Maddox

Department of Atmospheric Science
Colorado State University
Fort Collins, Colorado



**Department of
Atmospheric Science**

Paper No. 336

THE STRUCTURE AND LIFE-CYCLE OF
MIDLATITUDE MESOSCALE CONVECTIVE COMPLEXES

by

Robert A. Maddox

Department of Atmospheric Science

Colorado State University

Fort Collins, Colorado

June, 1981

Atmospheric Science Paper No. 336

"The aims of scientific thought are to see the general in the particular and the eternal in the transitory."

-Alfred North Whitehead-

"...nature shows us only surfaces, but she is a million fathoms deep."

-Ralph Waldo Emerson-

ABSTRACT

Enhanced infrared satellite imagery has been used to document the existence and frequent occurrence, over middle latitudes of the United States, of large, convectively driven weather systems. These systems, names Mesoscale Convective Complexes (MCCs), have not been heretofore recognized or documented in the scientific literature. It is shown that these systems frequently produce a variety of severe convective weather phenomena (such as tornadoes, hailstorms and flash floods) that significantly impact human activities. A preliminary climatology of MCCs, based on satellite data from two warm seasons, indicates that these systems frequently affect United States agricultural regions and it is hypothesized that MCCs produce a highly significant portion of the growing season precipitation over these areas.

Objective analyses of composited meteorological conditions attending ten MCC weather systems have revealed a number of distinctive characteristics and interactions with their larger scale environment. These analyses are used to develop a physically realistic model of the life-cycle of the typical midlatitude Mesoscale Convective Complex. The systems develop within a relatively weak and stagnant large-scale setting and are usually closely linked to the eastward progression of a weak middle tropospheric short-wave trough. Initial thunderstorms develop within a region of mesoscale convergence and lifting that is primarily forced by low-level warm advection. The MCC system rapidly grows and takes on a mesoscale organization while it moves slowly eastward ahead of the short-wave trough. Diabatic heating eventually

produces a system that is warm core in the middle troposphere and cold core in lower and upper levels. The mature MCC, although it occurs within a considerably different large-scale setting, exhibits many similarities to tropical convective systems. Strong inflow within the lower half of the troposphere forces an intense mesoscale updraft that maintains a region of moist ascent and widespread precipitation. Thickness increases within this meso-updraft produce anomalously high heights in the upper-troposphere above the MCC and an intense outflow jetstreak develops along the northern periphery of the system in the region where the height gradient has increased. As the system decays atmospheric response to residual temperature perturbations results in intensification of the pre-existent short-wave trough within the upper half of the troposphere. Decay occurs when the system moves east of the conditionally unstable airmass and region of warm advection over the Plains. Although the demise of the intense, highly organized convective system is abrupt, residual cloudiness and light shower activity may persist for many hours and affect large regions of the eastern United States. It is found that synoptic data (i.e., data taken at 12 h intervals) are not sufficient to quantitatively describe the energetics or the small-to-medium scale processes and interactions attending these systems.

ACKNOWLEDGMENTS

The research effort that resulted in this dissertation was accomplished while the author was affiliated with both Colorado State University and the Office of Weather Research and Modification, NOAA, Environmental Research Laboratories. Portions of this work completed at Colorado State University have been supported by the National Science Foundation under Grant ATM-7918513. The Office of Weather Research and Modification has partially supported this effort by allowing the author to complete portions of the research as an integral part of his work.

The author acknowledges and thanks his graduate committee, Professors T. H. Vonder Haar, W. R. Cotton, T. B. McKee, and P. W. Mielke for their continued support, guidance and encouragement. In addition to his committee, the author thanks a number of his colleagues and associates for their comments, suggestions and stimulating discussions during the course of this work; in particular thanks are due: Dr. C. A. Doswell III, National Severe Storms Forecast Center; Drs. J. M. Fritsch, J. M. Brown, S. L. Barnes, C. F. Chappell, and L. R. Hoxit, NOAA-ERL; Professors L. F. Bosart, State University of New York; W. M. Gray, Colorado State University; F. Sanders, Massachusetts Institute of Technology; and Dr. E. J. Zipser, NCAR.

Dr. R. Scofield, NOAA-NESS, kindly provided several figures that were used in Section II and Dr. A. H. Thompson, Texas A&M University, loaned the author numerous satellite images that were utilized during the course of the work. W. Dietrich and K. Crysler, NOAA-ERL, and G. Walters, NCAR, provided invaluable assistance in data reduction and processing. M. Howes and J. Sorbie drafted many of the complex figures and A. Adams skillfully prepared the final typescript. Most

importantly, the author's wife, Becky, and sons, Tim and Jason, not only tolerated innumerable long work days and working weekends during the past five years, but also provided continued support and sincere encouragement without which this dissertation could not have been completed.

TABLE OF CONTENTS

| <u>Section</u> | <u>Page</u> |
|---|-------------|
| I. INTRODUCTION..... | 1 |
| II. MESOSCALE CONVECTIVE COMPLEXES..... | 13 |
| II.1 Definition..... | 16 |
| II.2 Contrast Between MCCs and A Severe Squall Line..... | 18 |
| II.3 Climatology of Central U.S. MCCs..... | 39 |
| III. ANALYSIS OF METEOROLOGICAL CONDITIONS ASSOCIATED WITH MCCs.. | 53 |
| III.1 Conditions Over the Genesis Region (GR)..... | 54 |
| III.2 Conditions Over the MCC Region (MR)..... | 65 |
| III.3 Conditions Over the Decay Region (DR)..... | 75 |
| III.4 Relative Flow Fields..... | 85 |
| III.5 Vertical Profiles..... | 98 |
| III.6 Cross-Section Analyses..... | 109 |
| IV. THE MCC LIFE-CYCLE: A MODEL..... | 124 |
| IV.1 Genesis..... | 124 |
| IV.2 Organization..... | 126 |
| IV.3 Mature..... | 127 |
| IV.4 Dissipation..... | 128 |
| IV.5 Structure of the Mature System..... | 128 |
| V. MODEL VALIDATION..... | 132 |
| V.1 Macroscale Setting..... | 132 |
| V.2 Mesoscale Analyses..... | 135 |
| V.3 The MCC Moisture Budget..... | 167 |
| V.4 Kinetic Energy Budgets in the MCC Region..... | 174 |
| VI. SUMMARY AND CONCLUSIONS..... | 193 |

TABLE OF CONTENTS (Continued)

| <u>Section</u> | <u>Page</u> |
|---|-------------|
| VII. REFERENCES..... | 202 |
| APPENDIX A. A SCALE SEPARATION TECHNIQUE BASED ON NUMERICAL FILTERING..... | 214 |
| 1. Lowpass Objective Analysis..... | 214 |
| 2. Bandpass Objective Analysis..... | 216 |
| 3. Scale Separation..... | 217 |
| 4. Determination of λ_{\max} | 220 |
| 5. Analysis Example..... | 223 |
| APPENDIX B. OBJECTIVE ANALYSIS OF THE COMPOSITE DATA SETS..... | 227 |
| APPENDIX C. OVERVIEW OF THE CASES COMPOSITED..... | 235 |
| 1. MCC of 23/24 April 1975..... | 236 |
| 2. MCC of 6/7 May 1978..... | 243 |
| 3. MCC of 18 May 1978..... | 261 |
| 4. MCC of 30/31 May 1978..... | 267 |
| 5. MCC of 3/4 June 1978..... | 272 |
| 6. MCC of 19/20 June 1978..... | 279 |
| 7. MCC of 19/20 July 1978..... | 285 |
| 8. MCC of 20/21 July 1978..... | 291 |
| 9. MCC of 3/4 August 1977..... | 296 |
| 10. MCC of 4/5 August 1977..... | 303 |

LIST OF TABLES

| <u>Table</u> | <u>Page</u> |
|--|-------------|
| 1. Mesoscale Convective Weather Systems..... | 4 |
| 2. Mesoscale Convective Complex (MCC) -- Definition..... | 17 |
| 3. 1978 and 1979 Mesoscale Convective Complexes..... | 40 |
| 4. Characteristics of Orogenic and Plains MCCs..... | 48 |
| 5. Characteristics of Orogenic and Plains MCCs During July and August..... | 48 |
| 6. Mean Relative Humidities and Precipitable Water Surface to 300 mb..... | 106 |
| 7. Composite MCC Rainfall..... | 168 |
| 8. Kinetic Energy Budget SW Corner..... | 186 |
| 9. Kinetic Energy Budget Center Grid Point..... | 187 |
| 10. Kinetic Energy Budget NE Corner..... | 188 |
| C1. The Composite MCC Systems..... | 235 |

LIST OF FIGURES

| <u>Figure</u> | <u>Page</u> |
|--|-------------|
| 1. Enhanced infrared (IR) satellite image for 0630 GMT 20 May 1979..... | 3 |
| 2a. Enhanced IR satellite image for 1200 GMT 7 May 1978..... | 8 |
| 2b. Enhanced IR satellite image for 0900 GMT 12 July 1979..... | 8 |
| 2c. Enhanced IR satellite image for 0300 GMT 11 May 1979..... | 10 |
| 2d. Enhanced IR satellite image for 0930 GMT 15 October 1979..... | 10 |
| 2e. Enhanced IR satellite image for 0232 GMT 13 September 1979... | 11 |
| 2f. Enhanced IR satellite image for 1102 GMT 3 May 1980..... | 11 |
| 3. MB digital enhancement curve..... | 13 |
| 4a. Enhanced IR image for 0100 GMT 14 June 1976 with the temperature ranges from Fig. 3 shown..... | 14 |
| 4b. Regular IR image for 0100 GMT 14 June 1976..... | 14 |
| 5a. Enhanced IR (analog enhancement used in 1975) image for 0300 GMT 26 August 1975..... | 15 |
| 5b. Radar (10 cm) PPI display from St. Louis, Missouri, for 0300 GMT 26 August 1975..... | 16 |
| 6a. Enhanced IR image for 1130 GMT 20 May 1979..... | 18 |
| 6b. Radar summary chart for 1135 GMT 20 May 1979..... | 20 |
| 6c. Surface analysis for 1200 GMT 20 May 1979..... | 20 |
| 6d. 850 mb analysis for 0000 GMT 20 May 1979..... | 22 |
| 6e. 500 mb analysis for 0000 GMT 20 May 1979..... | 22 |
| 7a. Enhanced IR image for 0900 GMT 12 July 1979..... | 23 |
| 7b. Radar summary chart for 0835 GMT 12 July 1979..... | 25 |
| 7c. Surface analysis for 0900 GMT 12 July 1979..... | 25 |
| 7d. 850 mb analysis for 0000 GMT 12 July 1979..... | 28 |
| 7e. 500 mb analysis for 0000 GMT 12 July 1979..... | 28 |
| 7f. Time series of surface weather for Huron, South Dakota, on 11 and 12 July 1979..... | 29 |

LIST OF FIGURES (Continued)

| <u>Figure</u> | <u>Page</u> |
|---|-------------|
| 8a. Enhanced IR image for 0600 GMT 20 June 1979..... | 31 |
| 8b. Radar summary chart for 0535 GMT 20 June 1979..... | 31 |
| 8c. Surface analysis for 0600 GMT 20 June 1979..... | 32 |
| 8d. 850 mb analysis for 0000 GMT 20 June 1979..... | 34 |
| 8e. 500 mb analysis for 0000 GMT 20 June 1979..... | 34 |
| 8f. Time sequence of surface weather for Minneapolis, Minnesota, on 19 and 20 June 1979..... | 36 |
| 9a. Enhanced IR image for 0730 GMT 12 April 1980..... | 38 |
| 9b. Radar summary chart for 0735 GMT 12 April 1980..... | 38 |
| 10. MCC cloud top area with $T_{BB} \leq -32^{\circ}\text{C}$ at the time of maximum extent..... | 44 |
| 11a. Tracks of 1978 and 1979 Mesoscale Convective Complexes during March-May..... | 44 |
| 11b. Tracks of 1978 and 1979 Mesoscale Convective Complexes during June..... | 45 |
| 11c. Tracks of 1978 and 1979 Mesoscale Convective Complexes during July-August..... | 46 |
| 12. Enhanced IR images documenting the life-cycle of an MCC weather system during a 16 h period on 12 July 1979..... | 49 |
| 13a. Enhanced IR image for 0030 GMT 29 June 1979..... | 51 |
| 13b. Enhanced IR image for 0600 GMT 29 June 1979..... | 51 |
| 14. Analysis grids used in objective analyses..... | 53 |
| 15a. Analysis of surface features 12 h before the MCC..... | 55 |
| 15b. Analysis of surface features 12 h before the MCC..... | 56 |
| 16. Analysis of 850 mb level 12 h before the MCC..... | 57 |
| 17. Analysis of 700 mb level 12 h before the MCC..... | 60 |
| 18. Analysis of 500 mb level 12 h before the MCC..... | 60 |
| 19. Analysis of 300 mb level 12 h before the MCC..... | 61 |

LIST OF FIGURES (Continued)

| <u>Figure</u> | <u>Page</u> |
|---|-------------|
| 20. Analysis of 200 mb level 12 h before the MCC..... | 64 |
| 21. Analysis of the Totals stability index 12 h before the MCC... | 64 |
| 22a. Analysis of surface features at the time of the MCC..... | 66 |
| 22b. Analysis of surface features at the time of the MCC..... | 67 |
| 23. Analysis of 850 mb level at the time of the MCC..... | 68 |
| 24. Analysis of 700 mb level at the time of the MCC..... | 69 |
| 25. Analysis of 500 mb level at the time of the MCC..... | 71 |
| 26. Analysis of 300 mb level at the time of the MCC..... | 72 |
| 27. Analysis of 200 mb level at the time of the MCC..... | 74 |
| 28. Analysis of the Totals stability index at the time of the MCC | 74 |
| 29a. Analysis of surface features 12 h after the MCC..... | 77 |
| 29b. Analysis of surface features 12 h after the MCC..... | 77 |
| 30. Analysis of 850 mb level 12 h after the MCC..... | 80 |
| 31. Analysis of 700 mb level 12 h after the MCC..... | 80 |
| 32. Analysis of 500 mb level 12 h after the MCC..... | 81 |
| 33. Analysis of 300 mb level 12 h after the MCC..... | 82 |
| 34. Analysis of 200 mb level 12 h after the MCC..... | 84 |
| 35. Analysis of the Totals stability index 12 h after the MCC.... | 84 |
| 36a. 850 mb relative flow 12 h before the MCC..... | 85 |
| 36b. 850 mb relative flow at the time of the MCC..... | 86 |
| 36c. 850 mb relative flow 12 h after the MCC..... | 88 |
| 37a. 700 mb relative flow 12 h before the MCC..... | 90 |
| 37b. 700 mb relative flow at the time of the MCC..... | 90 |
| 37c. 700 mb relative flow 12 h after the MCC..... | 91 |
| 38a. 500 mb relative flow 12 h before the MCC..... | 92 |

LIST OF FIGURES (Continued)

| <u>Figures</u> | <u>Page</u> |
|---|-------------|
| 38b. 500 mb relative flow at the time of the MCC..... | 93 |
| 38c. 500 mb relative flow 12 h after the MCC..... | 94 |
| 39a. 200 mb relative flow 12 h before the MCC..... | 95 |
| 39b. 200 mb relative flow at the time of the MCC..... | 96 |
| 39c. 200 mb relative flow 12 h after the MCC..... | 97 |
| 40. Hodographs of precursor relative wind fields..... | 97 |
| 41. Mean divergence over 12 grid points within the MCC region.... | 98 |
| 42. Mean omega over 12 grid points within the MCC region..... | 100 |
| 43. Vertical profiles of winds aloft and θ_e before, during and after the MCC..... | 102 |
| 44. Pressure surface heights along cross-section at 40°N..... | 110 |
| 45. Layer thicknesses along cross-section at 40°N..... | 112 |
| 46a. Omega along cross-section at 40°N 12 h before the MCC..... | 115 |
| 46b. Temperature advection by the total wind along cross-section at 40°N 12 h before the MCC..... | 115 |
| 46c. Relative vorticity of the total wind and the u-component of the wind along cross-section at 40°N 12 h before the MCC..... | 116 |
| 47a. Omega along cross-section at 40°N at the time of the MCC..... | 117 |
| 47b. Temperature advection by the total wind along cross-section at 40°N at the time of the MCC..... | 118 |
| 47c. Relative vorticity of the total wind and the u-component of the wind along cross-section at 40°N at the time of the MCC.. | 119 |
| 48a. Omega along cross-section at 40°N 12 h after the MCC..... | 120 |
| 48b. Temperature advection by the total wind along cross-section at 40°N 12 h after the MCC..... | 121 |
| 48c. Relative vorticity of the total wind and the u-component of the wind along cross-section at 40°N 12 h after the MCC..... | 122 |
| 49. Enhanced infrared satellite photographs documenting the life-cycle of an MCC..... | 125 |

LIST OF FIGURES (Continued)

| <u>Figures</u> | <u>Page</u> |
|---|-------------|
| 50. Schematic drawing of the mature MCC and its near environment | 129 |
| 51. South to north cross-section through a mature MCC and its near environment..... | 130 |
| 52a. Macroscale analysis of the 500 mb level 12 h prior to the MCC..... | 134 |
| 52b. Macroscale analysis of the 500 mb level at the time of the MCC..... | 134 |
| 52c. Macroscale analysis of the 500 mb level 12 h after the MCC.. | 135 |
| 53a. Mesoscale analysis of the 850 mb level 12 h prior to the MCC | 137 |
| 53b. Mesoscale analysis of the 850 mb level 12 h prior to the MCC | 137 |
| 53c. Mesoscale analysis of the 850 mb level at the time of the MCC..... | 140 |
| 53d. Mesoscale analysis of the 850 mb level at the time of the MCC..... | 140 |
| 53e. Mesoscale analysis of the 850 mb level 12 h after the MCC... | 142 |
| 53f. Mesoscale analysis of the 850 mb level 12 h after the MCC... | 142 |
| 54a. Mesoscale analysis of the 500 mb level 12 h prior to the MCC | 143 |
| 54b. Mesoscale analysis of the 500 mb level 12 h prior to the MCC | 145 |
| 54c. Mesoscale analysis of the 500 mb level at the time of the MCC..... | 145 |
| 54d. Mesoscale analysis of the 500 mb level at the time of the MCC..... | 147 |
| 54e. Mesoscale analysis of the 500 mb level 12 h after the MCC... | 147 |
| 54f. Mesoscale analysis of the 500 mb level 12 h after the MCC... | 148 |
| 55a. Mesoscale analysis of the 200 mb level 12 h prior to the MCC | 150 |
| 55b. Mesoscale analysis of the 200 mb level 12 h prior to the MCC | 150 |
| 55c. Mesoscale analysis of the 200 mb level at the time of the MCC..... | 152 |
| 55d. Mesoscale analysis of the 200 mb level at the time of the MCC..... | 152 |

LIST OF FIGURES (Continued)

| <u>Figure</u> | <u>Page</u> |
|--|-------------|
| 55e. Mesoscale analysis of the 200 mb level 12 h after the MCC.... | 155 |
| 55f. Mesoscale analysis of the 200 mb level 12 h after the MCC.... | 155 |
| 56. Average mesoscale temperature perturbations for the 12 interior grid points following the MCC..... | 156 |
| 57a. West to east cross-section of mesoscale perturbations 12 h prior to the MCC..... | 157 |
| 57b. West to east cross-section of mesoscale perturbations 12 h prior to the MCC..... | 158 |
| 58a. West to east cross-section of mesoscale perturbations at the time of the MCC..... | 159 |
| 58b. West to east cross-section of mesoscale perturbations at the time of the MCC..... | 160 |
| 59a. South to north cross-section of the mesoscale perturbations at the time of the MCC..... | 162 |
| 59b. South to north cross-section of the mesoscale perturbations at the time of the MCC..... | 163 |
| 60a. West to east cross-section of mesoscale perturbations 12 h after the MCC..... | 164 |
| 60b. West to east cross-section of mesoscale perturbations 12 h after the MCC..... | 165 |
| 61. Vertical profiles of mean mixing ratio following the MCC..... | 169 |
| 62a. Total horizontal flux divergence of water vapor into the Genesis Region..... | 171 |
| 62b. Total horizontal flux divergence of water vapor into the MCC Region..... | 171 |
| 62c. Total horizontal flux divergence of water vapor into the Decay Region..... | 172 |
| 63a. Vertical profiles of kinetic energy of the SW grid point..... | 177 |
| 63b. Vertical profiles of kinetic energy of the center grid point. | 177 |
| 63c. Vertical profiles of kinetic energy of the NE grid point..... | 178 |
| 64a. Change in k before-during the MCC within the 850-700 mb layer following the system..... | 180 |

LIST OF FIGURES (Continued)

| <u>Figure</u> | <u>Page</u> |
|---|-------------|
| 64b. Change in k during-after the MCC within the 850-700 mb layer following the system..... | 180 |
| 65a. Change in k before-during the MCC at 500 mb following the system..... | 183 |
| 65b. Change in k during-after the MCC at 500 mb following the system..... | 183 |
| 66a. Change in k before-during the MCC at 200 mb following the system..... | 185 |
| 66b. Change in k during-after the MCC at 200 mb following the system..... | 185 |
| 67a. Generation of k at 850 mb at the time of the MCC..... | 189 |
| 67b. Generation of k at 500 mb at the time of the MCC..... | 191 |
| 67c. Generation of k at 200 mb at the time of the MCC..... | 191 |
| A1. Response curves for the filters used for objective scale separation..... | 219 |
| A2. Observation weight curves..... | 220 |
| A3. Surface analysis for 2100 GMT 24 April 1975..... | 221 |
| A4. Structure function for the observed temperature field at 2100 GMT 24 April 1975..... | 223 |
| A5. Mesoscale temperature perturbations for 2100 GMT 24 April 1975..... | 224 |
| A6. Macroscale temperature analysis for 2100 GMT 24 April 1975... | 225 |
| A7. Total temperature analysis for 2100 GMT 24 April 1975..... | 226 |
| B1. Composite analysis grids..... | 228 |
| B2. Structure function for composite 500 mb winds..... | 230 |
| B3. Response curves utilized in the objective analyses of the composite data fields..... | 232 |
| B4. Locations of the soundings used in the composite analyses.... | 232 |
| C1. Enhanced IR image for 0900 GMT 24 April 1975..... | 238 |
| C2. Maximum observed winds aloft for 0000 GMT 24 April 1975..... | 238 |

LIST OF FIGURES (Continued)

| <u>Figure</u> | <u>Page</u> |
|--|-------------|
| C3. Maximum observed winds aloft for 1200 GMT 24 April 1975..... | 240 |
| C4. Stability chart for 0000 GMT 24 April 1975..... | 240 |
| C5. Accumulated precipitation from 0000 to 1200 GMT..... | 242 |
| C6. Twelve hour LFM forecast..... | 242 |
| C7. Enhanced IR image for 1200 GMT 7 May 1978..... | 245 |
| C8. Maximum observed winds aloft for 0000 GMT 7 May 1978..... | 245 |
| C9. Maximum observed winds aloft for 1200 GMT 7 May 1978..... | 247 |
| C10. Stability chart for 0000 GMT 7 May 1978..... | 247 |
| C11. Accumulated precipitation from 0000 to 1200 GMT..... | 248 |
| C12. Twelve hour LFM forecast..... | 249 |
| C13. Surface observation time-series..... | 250 |
| C14. Surface weather reports for 1100 GMT 7 May 1978..... | 251 |
| C15. Vertical profiles for Longview, Texas..... | 254 |
| C16. Vertical profiles for Lake Charles, Louisiana..... | 254 |
| C17. Vertical profiles for Centerville, Alabama..... | 256 |
| C18. Vertical profiles for Jackson, Mississippi..... | 256 |
| C19. Vertical profiles for Little Rock, Arkansas..... | 258 |
| C20. Vertical profiles for Nashville, Tennessee..... | 258 |
| C21. Vertical profiles for Monett, Missouri..... | 260 |
| C22. Vertical profiles for Salem, Illinois..... | 260 |
| C23. Enhanced IR image for 1330 GMT 18 May 1978..... | 261 |
| C24. Maximum observed winds aloft for 0000 GMT 18 May 1978..... | 263 |
| C25. Maximum observed winds aloft for 1200 GMT 18 May 1978..... | 263 |
| C26. Stability chart for 0000 GMT 18 May 1978..... | 264 |
| C27. Accumulated precipitation from 0000 GMT 1200 GMT..... | 266 |

LIST OF FIGURES (Continued)

| <u>Figure</u> | | <u>Page</u> |
|---------------|---|-------------|
| C28. | Twelve hour LFM forecast..... | 266 |
| C29. | Enhanced IR image for 0900 GMT 31 May 1978..... | 267 |
| C30. | Maximum observed winds aloft for 0000 GMT 31 May 1978..... | 269 |
| C31. | Maximum observed winds aloft for 1200 GMT 31 May 1978..... | 269 |
| C32. | Stability chart for 0000 GMT 31 May 1978..... | 270 |
| C33. | Accumulated precipitation from 0000 to 1200 GMT..... | 271 |
| C34. | Twelve hour LFM forecast..... | 272 |
| C35. | Enhanced IR image for 1200 GMT 4 June 1978..... | 273 |
| C36. | Maximum observed winds aloft for 0000 GMT 4 June 1978..... | 274 |
| C37. | Maximum observed winds aloft for 1200 GMT 4 June 1978..... | 276 |
| C38. | Stability chart for 0000 GMT 4 June 1978..... | 276 |
| C39. | Accumulated precipitation from 0000 to 1200 GMT..... | 278 |
| C40. | Twelve hour LFM forecast..... | 278 |
| C41. | Enhanced IR image for 0630 GMT 20 June 1978..... | 281 |
| C42. | Maximum observed winds aloft for 0000 GMT 20 June 1978..... | 281 |
| C43. | Maximum observed winds aloft for 1200 GMT 20 June 1978..... | 283 |
| C44. | Stability chart for 0000 GMT 20 June 1978..... | 283 |
| C45. | Accumulated precipitation from 0000 to 1200 GMT..... | 284 |
| C46. | Twelve hour LFM forecast..... | 285 |
| C47. | Enhanced IR image for 0800 GMT 20 July 1978..... | 287 |
| C48. | Maximum observed winds aloft for 0000 GMT 20 July 1978..... | 287 |
| C49. | Maximum observed winds aloft for 1200 GMT 20 July 1978..... | 288 |
| C50. | Stability chart for 0000 GMT 20 July 1978..... | 290 |
| C51. | Accumulated precipitation from 0000 to 1200 GMT..... | 290 |
| C52. | Twelve hour LFM forecast..... | 291 |

LIST OF FIGURES (Continued)

| <u>Figure</u> | <u>Page</u> |
|---|-------------|
| C53. Enhanced IR image for 0930 GMT 21 July 1978..... | 292 |
| C54. Maximum observed winds aloft for 0000 GMT 21 July 1978..... | 292 |
| C55. Maximum observed winds aloft for 1200 GMT 21 July 1978..... | 293 |
| C56. Stability chart for 0000 GMT 21 July 1978..... | 295 |
| C57. Accumulated precipitation from 0000 to 1200 GMT..... | 295 |
| C58. Twelve hour LFM forecast..... | 296 |
| C59. Enhanced IR image for 1000 GMT 4 August 1977..... | 297 |
| C60. Maximum observed winds aloft for 0000 GMT 4 August 1977..... | 297 |
| C61. Maximum observed winds aloft for 1200 GMT 4 August 1977..... | 299 |
| C62. Stability chart for 0000 GMT 4 August 1977..... | 299 |
| C63. Accumulated precipitation from 0000 to 1200 GMT..... | 300 |
| C64. Twelve hour LFM numerical forecast..... | 302 |
| C65. Surface observation time-series..... | 302 |
| C66. Enhanced IR image for 0900 GMT 5 August 1977..... | 305 |
| C67. Maximum observed winds aloft for 0000 GMT 5 August 1977..... | 305 |
| C68. Maximum observed winds aloft for 1200 GMT 5 August 1977..... | 306 |
| C69. Stability chart for 0000 GMT 5 August 1977..... | 308 |
| C70. Accumulated precipitation from 0000 to 1200 GMT..... | 308 |
| C71. Twelve hour LFM forecast..... | 309 |
| C72. Enhanced IR image for 0030 GMT 4 August 1977..... | 310 |
| C73. Enhanced IR image for 0014 GMT 5 August 1977..... | 311 |

I. INTRODUCTION

Each year during spring the primary weather forecast problem for much of the continental United States gradually shifts from prediction of traveling cyclones with their broad shields of stratiform cloud and stable precipitation, to prediction of smaller scale weather systems characterized by deep convective clouds. Prediction of convective weather phenomena is extremely complex and the forecaster must deal with thunderstorm systems that vary from the classic pre-frontal squall line with attendant tornadoes, wind and hail, to nocturnal storms with locally heavy rainfalls, to isolated afternoon air mass storms. The scales associated with midlatitude convective systems are usually defined to be on the order of 1 to 10 km for an individual thunderstorm and 10 to 100 km for a squall line (Holton, 1972; and La Seur, 1974). Since the average spacing of upper-air observations over the United States is ~ 350 -400 km, the operational prediction of convective systems and their precipitation has traditionally been perceived as a subgrid scale problem. Various approaches have been used to attack this challenge. Forecasters at the National Severe Storms Forecast Center anticipate the development of severe thunderstorms and tornadoes utilizing large-scale observations and numerical and statistical forecasts in conjunction with complex, synoptic pattern recognition procedures (see Magor, 1959; Miller, 1967; Charba, 1979; and Reap and Foster, 1979). On the other hand, the National Meteorological Center has attempted to cope with convective precipitation utilizing statistical techniques in combination with numerical model output (refer to Glahn and Lowry, 1972; Klein and Glahn, 1974; and Bermowitz and Zurndorfer, 1979).

The problem of forecasting (and also of understanding) the development, movement and eventual demise of intense convective weather systems has been considerably complicated by the fact that the spacing of conventional observations (upper-air soundings, surface observations and even the synoptic radar network) has been far too coarse to observe the life-cycle of such systems adequately. However, the advent of the geostationary meteorological satellite during the early 1970's added an important new dimension (continuous observations ranging in scale from synoptic cloud patterns down to individual cumulus clouds) to the observation system that could be brought to bear on convective problems (see Vonder Haar, 1969; Sikdar et al., 1970; Ludwig, 1974; and Purdom, 1976 and 1979). Indeed, a survey of Geostationary Operational Environmental Satellite (GOES) imagery for the warm seasons (March through September) of 1978 and 1979 has revealed that large (diameters 500 - 1000 km), persistent, and highly organized convective storm complexes frequently occur over the central and eastern United States. Two such systems are captured in the satellite photograph shown in Fig. 1. These systems, which have been named Mesoscale Convective Complexes (MCCs), exhibit dynamic and thermodynamic structure characteristically different from the more classic midlatitude thunderstorm systems documented in the literature.

Other types of medium scale, convectively driven, weather systems have been extensively studied because of the significant and often extreme meteorological events they produce and also because of their potentially important role in the general circulation that results from interactions with both smaller and larger scale atmospheric features. The MCC weather systems considered here are ones that grow to truly

Fig. 1. Enhanced infrared (IR) satellite image for 0630 GMT 20 May 1979. Black, gray and white contours indicate increasingly cold infrared black body temperatures.

significant horizontal extent. In order to define and discuss these systems more clearly, scale terminology proposed by Orlanski (1975) is used (with slight modification) throughout the remainder of this paper as a logical way to subdivide a wide range of medium scale meteorological phenomena, as follows:

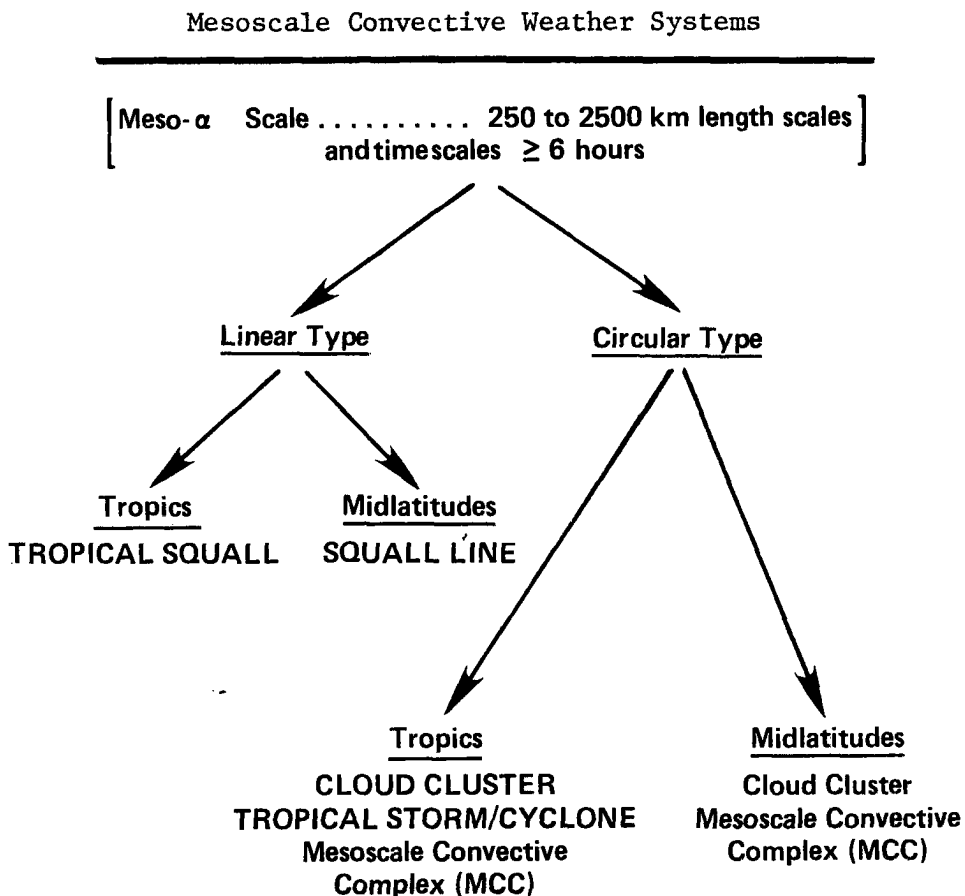
meso- α ...length scales of 250 to 2500 km with duration ≥ 6 hours,
meso- β ...length scales of 25 to 250 km with duration < 6 hours.

These categorizations are by no means comprehensive (e.g., systems with meso- β length scales may on occasion persist more than 6 hours, etc.). Convective weather systems also occur on a broad, nearly continuous spectrum of length and time scales; however, these particular definitions are employed because the mesoscale convective weather systems studied occurred primarily over the central U.S. where the separation between upper-air sounding sites ranges from about 225 to

450 km. Thus, atmospheric circulation and features associated with meso- α scale convective weather systems are usually detected, but not always clearly defined, by the U.S. synoptic data set.

Meso- α scale, convectively driven weather systems can be further classified according to their physical characteristics, organization, and their location of occurrence. Such a classification scheme is presented in Table 1 (note that meso- β scale systems could be similarly classified). Upper case letters indicate system types that have previously been extensively studied while lower case letters indicate types of systems that have been considered infrequently, if at all. Note that nearly circular, large convective weather systems (MCCs) have

Table 1



not been previously identified or studied in the midlatitudes. Satellite imagery indicates that similar systems may also occur over the tropics.

Tropical convective systems have been widely examined since they are the predominant weather systems of low latitudes. The structure and evolution of the tropical storm have been documented in detail by numerous researchers and physical and numerical models have been developed (e.g., Palmén, 1948; Palmén and Riehl, 1957; Malkus and Riehl, 1960; Riehl and Malkus, 1961; Kasahara, 1961; Yanai, 1961; Charney and Eliassen, 1964; Ogura, 1964; Ooyama, 1964; Gray, 1968; Rosenthal, 1970; Frank, 1977). Although the tropical cloud cluster has been more elusive (e.g., Simpson et al., 1967; Reed and Recker, 1971; Williams and Gray, 1973; and Ruprecht and Gray, 1976), a number of tropical experiments (VIMHEX, BOMEX, and GATE for example) have gathered data on the meso-scale, within and near tropical weather systems. An understanding of the organization and structure of tropical mesosystems is evolving as researchers study these special data sets (e.g., Zipser, 1969; Martin and Sikdar, 1975; Riehl, 1978; Frank, 1978; Zipser and Gautier, 1978; Ogura et al., 1979; and Leary and Houze, 1979). These data sets have also been useful in studying the tropical squall line (as identified by Hamilton and Archbold, 1945). While numerous physical and numerical models of the linearly organized, tropical squall have been developed (e.g., Riehl et al., 1974; Grover, 1974; Betts et al., 1976; Moncrieff and Miller, 1976; Houze, 1977; Mansfield, 1977; Zipser, 1977; and Brown, 1979), most of the models have considered meso- β scale systems that may, or may not, have been embedded within larger scale weather systems.

Midlatitude convective systems have not been studied as intensively as those of the tropics. This is probably because these convective features are often embedded within macroscale baroclinic weather systems whose circulations are considered dominant. Much of the study, to date, has been motivated by the need to warn the public of the severe weather phenomena (i.e., tornadoes, hail and damaging winds) that often attend midlatitude thunderstorm systems. Therefore, efforts have focused on the individual severe thunderstorm (super-cell or multi-cell) or the intense (frontal or pre-frontal) squall line. The linearly organized, midlatitude squall line (see Table 1) has been extensively studied, resulting in physical and numerical models of these important systems (e.g., Williams, 1948; Newton, 1950; Brunk, 1953; Fujita, 1955; Newton and Newton, 1959; Bates, 1961; Miller, 1967; Hane, 1973; and Ogura and Liou, 1980). [Note that Lilly (1979) has reviewed numerical models of both tropical and midlatitude thunderstorms and squall lines.] Studies of other midlatitude mesoscale systems have not been as numerous and have tended to be of meso- β scale, linearly organized systems (e.g., Fujita, 1959a; Pedgley, 1962; Dirks, 1969; Sanders and Paine, 1975; Sanders and Emanuel, 1977; Ogura and Chen, 1977; Philipp, 1979; and Fritsch and Chappell, 1980).

Newton and Katz (1958), Fujita and Brown (1958), Newton and Newton (1959) and Fujita (1959b) studied large, long-lived convective mesosystems that had some characteristics similar to those of the MCCs considered here. Indeed, careful review of the squall line studies of Brunk (1953) and Porter et al. (1955) indicates that some of their cases may have been MCC systems. Satellite imagery provides the all encompassing perspective required to identify the high degree of

organization, large size and extended life time of MCC weather systems. Lacking this, past investigators were not able to differentiate these systems (MCCs) from squall lines - nor at times even from large scale weather systems - or to document their true extent and systematic life-cycle and movement. For example, MCCs appear to be, in large part, responsible for the nocturnal maximum of precipitation and thunderstorms over the central Plains. However, many investigators have studied these climatological features assuming that certain physical mechanisms must act to trigger storms in situ over the central Plains (e.g., Means, 1944; Newmann, 1950; Bleeker and Andre, 1951; Pitchford and London, 1962; and Wallace, 1975); whereas, satellite imagery clearly illustrates the frequent movement of MCC weather systems across this region during the nighttime. More recently, George (1979), Clark et al. (1980), Bosart and Sanders (1981), Cotton et al. (1981) and Wetzal et al. (1981) have examined the life-cycles and precipitation characteristics of several MCC type convective systems.

Figure 2 presents satellite images that depict several types of meso- α scale convective weather systems. Large MCC systems over the north central and southern U.S. are shown in Figs. 2a and b - note the nearly circular, continuous cold cloud shield that characterizes the MCCs. A midlatitude squall line is depicted in Fig. 2c. Regions of colder cloud top and intense convection are embedded within the line which stretches from the Great Lakes to Texas. An example of a tropical cloud cluster is presented in Fig. 2d (this particular cluster had developed into a tropical depression). The cluster, located over the Caribbean Sea south of Cuba, presents (in the enhanced IR imagery) a chaotic cloud shield with a number of meso- β scale convective components

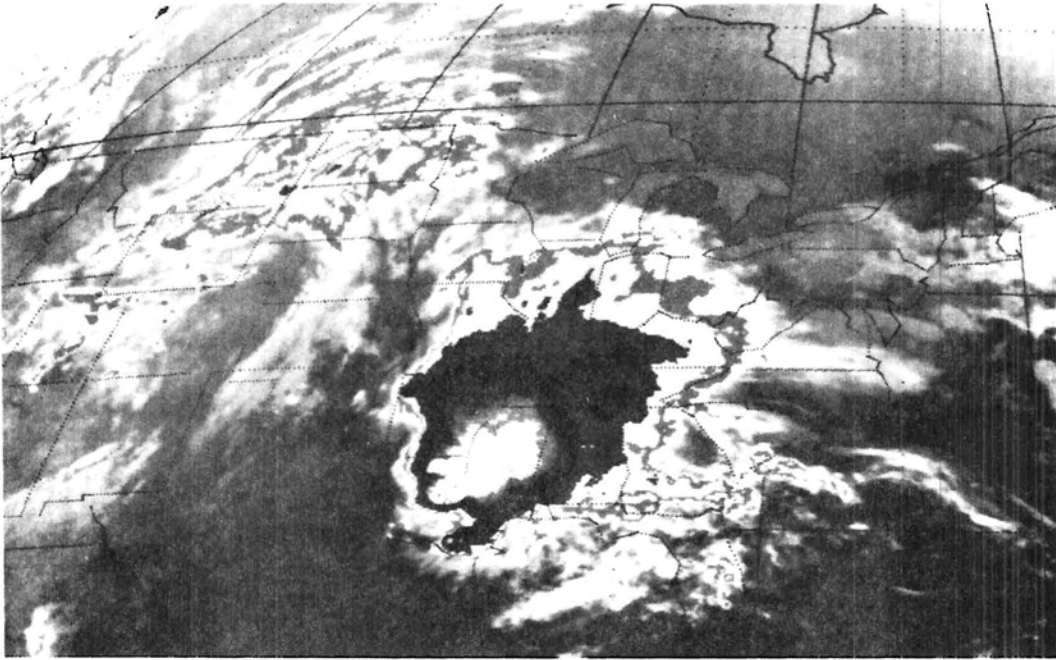


Fig. 2a. Enhanced IR satellite image for 1200 GMT 7 May 1978.

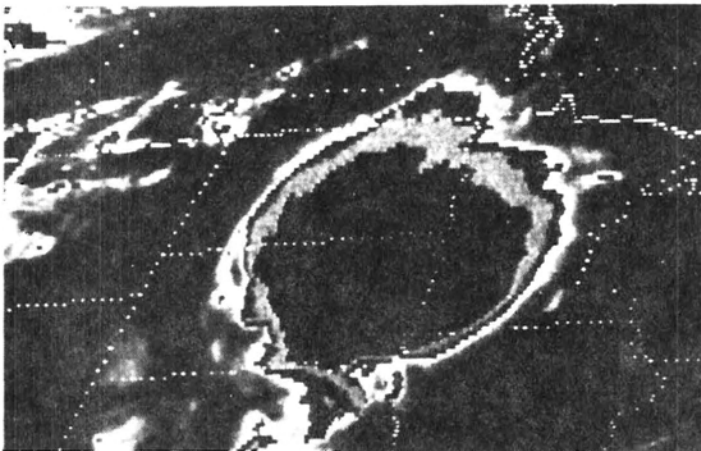
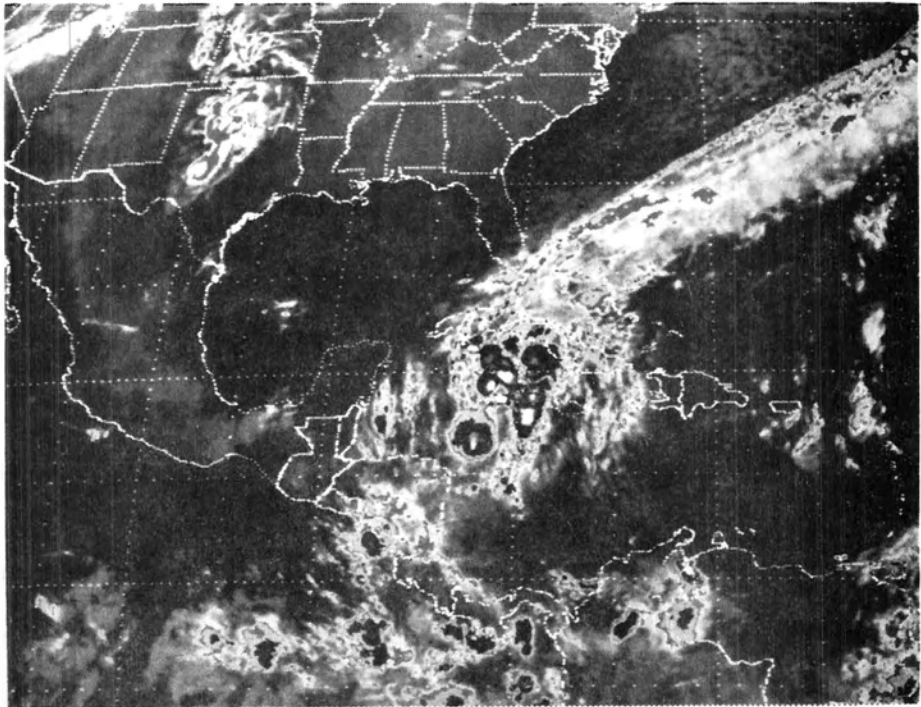
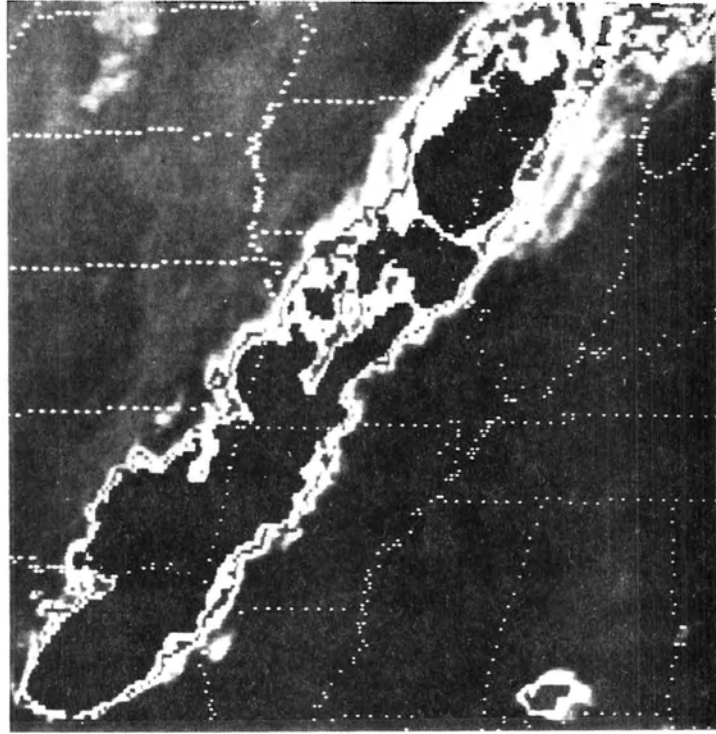


Fig. 2b. Enhanced IR satellite image for 0900 GMT 12 July 1979.

Fig. 2c. Enhanced IR satellite image for 0300 GMT 11 May 1979.

Fig. 2d. Enhanced IR satellite image for 0930 GMT 15 October 1979.



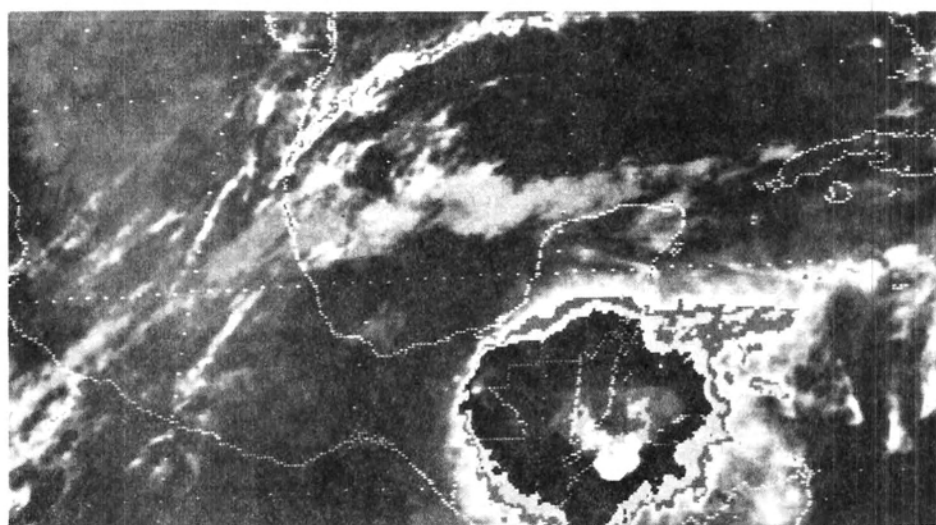
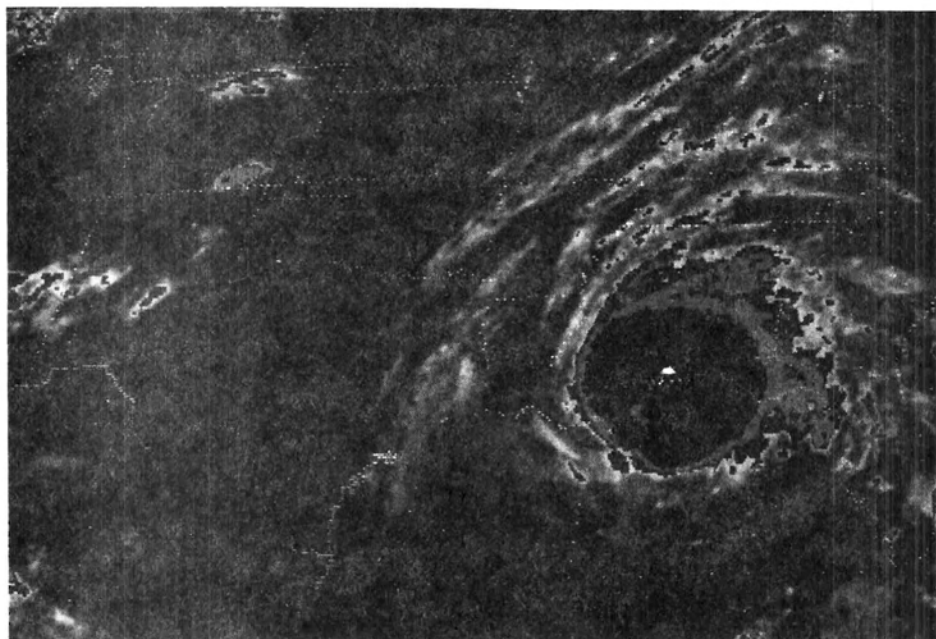


Fig. 2f. Enhanced IR satellite image for 1102 GMT 3 May 1980.

The survey of 1978 and 1979 satellite imagery indicated that their physical characteristics (size, lifetime, etc.) render MCCs amenable to study with conventional, routinely available surface and upper-air observations. Selected data sets have been used to study the medium

and large scale aspects and interactions of MCC weather systems over the midlatitude of the U.S. Detailed composite and case study analyses of MCCs have been completed.

A quantitative MCC definition (based upon satellite-observable characteristics), a comparison of the physical characteristics of MCCs with those of squall lines, and a brief climatology of central and eastern United States MCCs are all presented in Section II. Results of detailed objective analyses of meteorological conditions spanning the life-cycle of a composite, or "typical", MCC are presented in Section III. These findings were used to develop the physical model of the MCC and its life-cycle that is discussed in Section IV. A consideration of both the macroscale and mesoscale features of meteorological fields associated with the composite MCC is presented in Section V to substantiate various aspects of the MCC physical model. A brief overview of the moisture and kinetic energy budgets during the life-cycle of the "typical" MCC is also available in Section V.

II. MESOSCALE CONVECTIVE COMPLEXES

It was found that sequences of enhanced IR satellite images from the Geostationary Operational Satellite (GOES) were particularly useful for studying the development and evolution of convective weather systems. This type image provides contrasting shades of black, gray and white to indicate specific ranges of IR black body temperature (T_{BB}). The enhancement curve (MB curve) used is shown in Fig. 3. An example, with the T_{BB} ranges indicated is shown in Fig. 4a with the corresponding raw IR image presented in Fig. 4b. The enhanced product is clearly more suited for monitoring areas of cold cloud top.

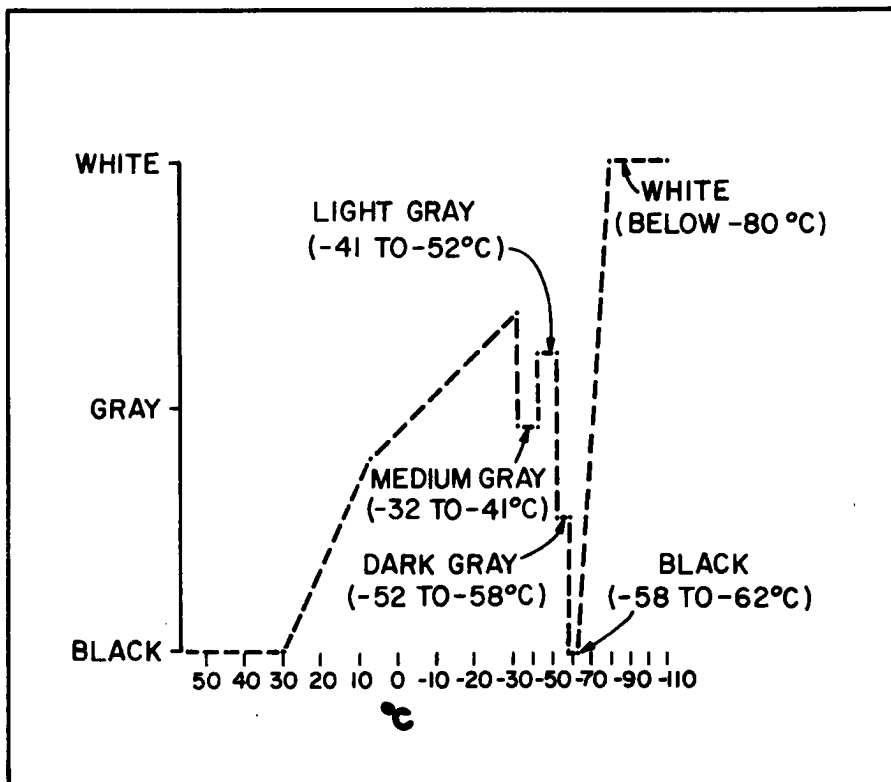


Fig. 3. MB digital enhancement curve. T_{BB} ranges and corresponding shading are indicated.

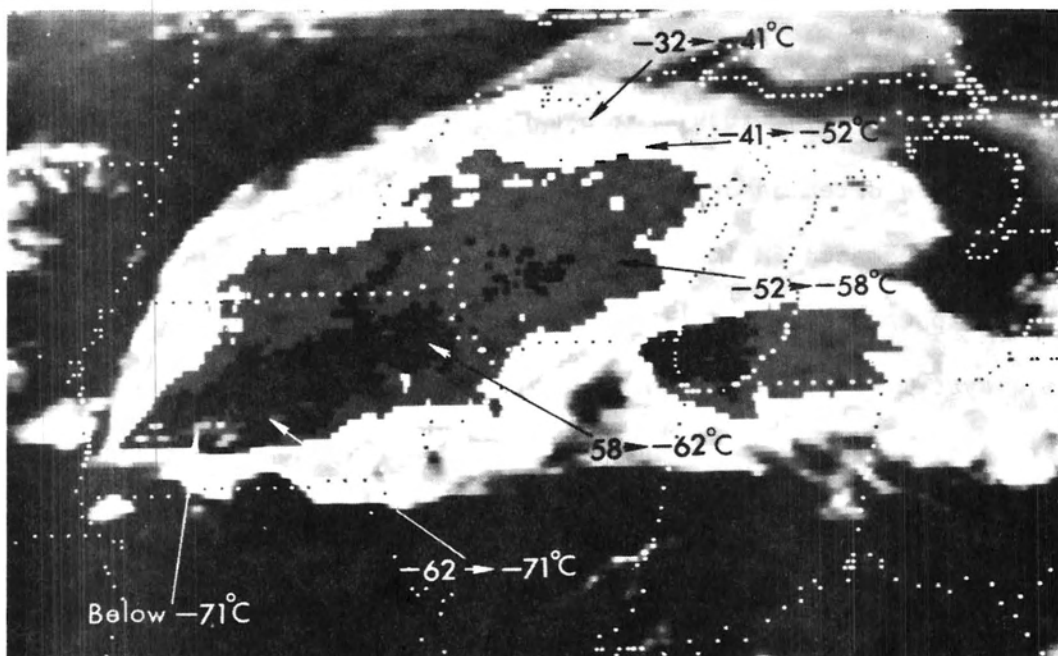


Fig. 4a. Enhanced IR image for 0100 GMT 14 June 1976 with the temperature ranges from Fig. 3 shown.

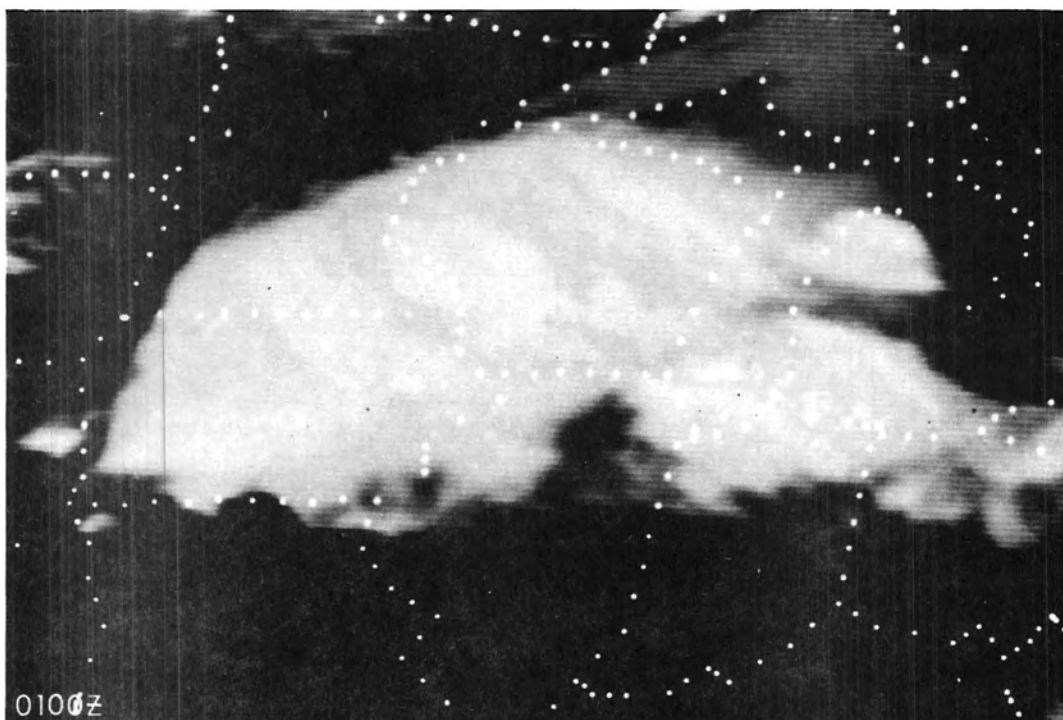


Fig. 4b. Regular IR image for 0100 GMT 14 June 1976.

It has been shown (Woodley et al., 1972; Follansbee and Oliver, 1975; Griffith et al., 1978; and Reynolds and Smith, 1979) that cold IR cloud tops are often associated with deep precipitating convective clouds. An enhanced IR image (Fig. 5a) qualitatively illustrates this relationship when compared to the concurrent radar depiction of a convective system (Fig. 5b). [Note that intense convective elements are occurring along the eastern and southern edges of the system and that a widespread region of light precipitation is indicated to the north and west.] It is important to note that enhanced GOES IR imagery provides the basis for the Scofield and Oliver (1977) operational technique for estimating convective rainfall from satellite data.

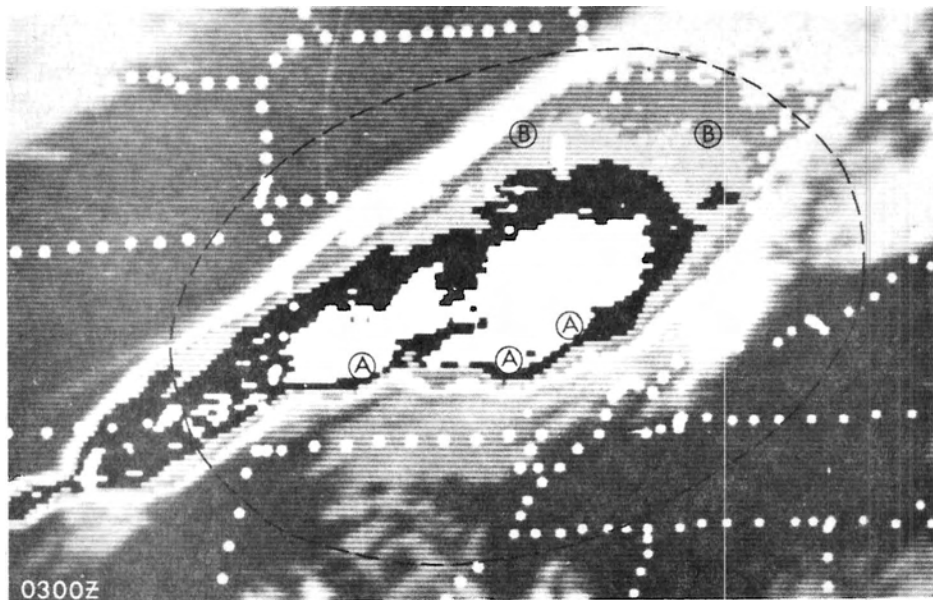


Fig. 5a. Enhanced IR (analog enhancement used in 1975) image for 0300 GMT 26 August 1975.

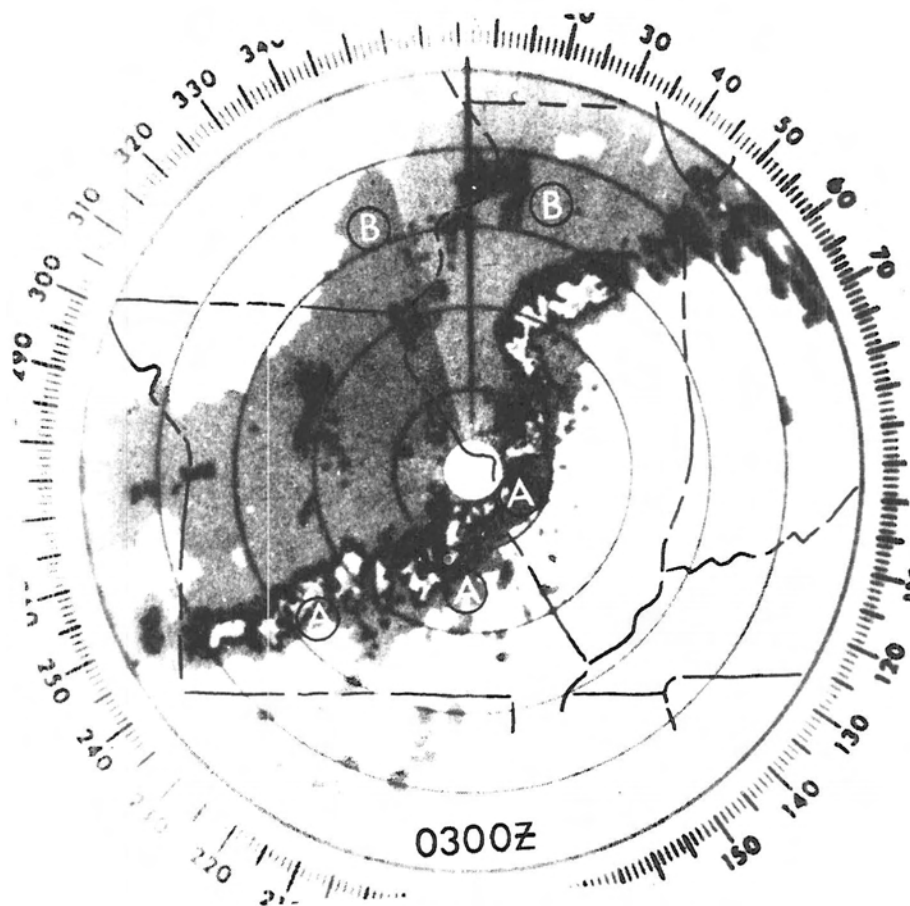


Fig. 5b. Radar (10 cm) PPI display from St. Louis, Missouri, for 0300 GMT 26 August 1975.

II.1 Definition

The working definition developed for midlatitude MCCs is presented in Table 2. It is based solely upon physical characteristics observable in enhanced IR satellite imagery. Size and duration criteria were set large and long enough so that, at least over the central U.S., the system's meso- α scale features were likely to be sampled, at some point in its life-cycle, by several synoptic upper-air soundings. The requirement that a large portion of the MCC cloud shield have an IR $T_{BB} < -52^{\circ}\text{C}$ ensures that the system is active and that precipitation is falling over a significant area. [Note that Scofield and Oliver's (1977) satellite rainfall estimation scheme begins accumulating precipitation after T_{BB}

Table 2

Mesoscale Convective Complex (MCC) - Definition

[Based Upon Analyses of Enhanced IR Satellite Imagery]

Physical Characteristics

| | |
|------------------------|---|
| <u>Size:</u> | A - Continuous cold cloud shield with IR temperature $\leq -32^{\circ}\text{C}$ must have an area $\geq 100,000 \text{ km}^2$ |
| | B - Interior cold cloud region with temperature $\leq -52^{\circ}\text{C}$ must have an area $\geq 50,000 \text{ km}^2$ |
| <u>Initiate:</u> | Size definitions A and B are first satisfied |
| <u>Duration:</u> | Size definitions A and B must be met for a period ≥ 6 hours |
| <u>Maximum Extent:</u> | Continuous cold cloud shield (IR temp. $\leq -32^{\circ}\text{C}$) reaches maximum size |
| <u>Shape:</u> | Minor axis/Major axis ≥ 0.7 at time of maximum extent |
| <u>Terminate:</u> | Size definitions A and B no longer satisfied |

reaches -32°C .] The shape criterion in Table 2 was arbitrarily specified in an attempt to discriminate line-type convective systems from MCCs.

The size of an MCC system, as defined in Table 2, is huge in comparison to individual thunderstorms. For example, IR depictions of mature, air mass thunderstorms indicate an average cold cloud shield area $< -32^{\circ}\text{C}$ of approximately 700 km^2 ; whereas, Reynolds and Vonder Haar (1979) documented 38 multi-cell thunderstorms over eastern Montana and found that the average total cloud top area was about 1400 km^2 . The cold cloud top area of an MCC is required to be at least $100,000 \text{ km}^2$ and its size may thus exceed that of an individual ordinary thunderstorm by more than two orders of magnitude!

II.2 Contrast Between MCCs and A Severe Squall Line

The satellite image of Fig. 6a captures an MCC weather system over the central U.S. at 1130 GMT on 20 May 1979. A nearly concurrent (1135 GMT) radar summary chart (Fig. 6b) shows that the highest echo tops were coincident with the region of coldest cloud top indicated in Fig. 6a. A large region of weaker echo attended the system and the shape of the echo area was similar to that of the cold cloud shield depicted in the satellite image. The thick, cold cirrus shield extended north and east of the echo area indicating that the IR $T_{BB} < -32^{\circ}\text{C}$ region did not exactly correspond with active precipitation areas. However, during this study it was noted that surface stations located beneath cloud regions with $T_{BB} < -52^{\circ}\text{C}$ almost always were reporting precipitation. A 1200 GMT surface analysis (Fig. 6c) shows that the MCC was occurring with a large scale environment characterized by weak pressure gradients and light

Fig. 6a. Enhanced IR image for 1130 GMT 20 May 1979.

Fig. 6b. Radar summary chart for 1135 GMT 20 May 1979. Interior hatched and shaded areas indicate regions of stronger echo. Echo tops are shown in hundreds of feet above sea level.

Fig. 6c. Surface analysis for 1200 GMT 20 May 1979. Surface features are indicated, along with 2 mb isobars. Winds are in kt (full barb = 10 kt or $\sim 5 \text{ m s}^{-1}$) and squall symbols with frontal barbs indicate positions and movements of cold air outflow boundaries. Six hour precipitation amounts, in inches, are also shown.

Fig. 6d. 850 mb analysis for 0000 GMT 20 May 1979. Height contours are solid lines, isotherms ($^{\circ}\text{C}$) dashed and region where dewpoint exceeds 14°C is shaded. Winds are in kt with full barb 10 kt ($\sim 5 \text{ m s}^{-1}$).

Fig. 6e. 500 mb analysis for 0000 GMT 20 May 1979. Height contours are solid lines, isotherms ($^{\circ}\text{C}$) dashed and 12 h height changes (dam) are plotted. Winds are in kt with full barb 10 kt ($\sim 5 \text{ m s}^{-1}$) and flag 50 kt ($\sim 25 \text{ m s}^{-1}$).

winds and that it was producing a significant area of general precipitation (note the reports of steady light rain).

Analyses of the 850 and 500 mb levels at 0000 GMT on the 20th emphasize the benign character of the meteorological setting in which this MCC developed. At 850 mb (Fig. 6d) southerly flow was evident in the moist air over the southern Plains with a pool of very high dewpoints located over the central Plains. Winds at 500 mb (Fig. 6e) were not particularly strong and the shear within the lower half of the troposphere was obviously quite weak. Temperature gradients were not pronounced and the lack of large height changes indicates that the large scale pattern was stagnant.

The enhanced IR image in Fig. 7a shows a large MCC, that produced widespread rains of up to an inch or more, over the northern Plains at 0900 GMT 12 July 1979. The radar summary chart for GMT (Fig. 7b) indicated that this system's echo configuration was also quite similar

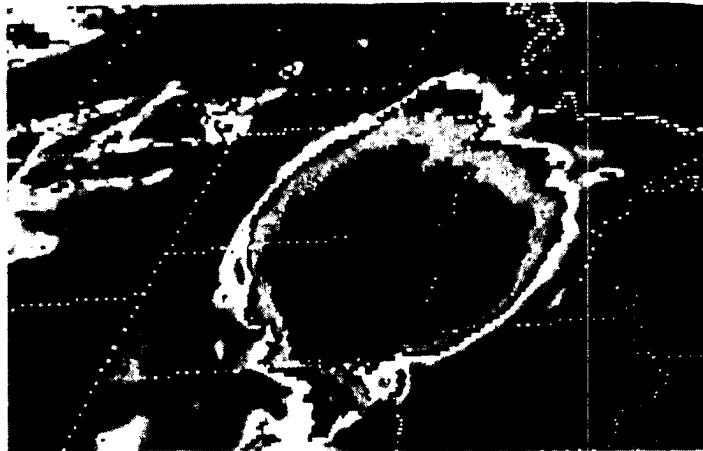


Fig. 7a. Enhanced IR image for 0900 GMT 12 July 1979.

Fig. 7b. Radar summary chart for 0835 GMT 12 July 1979. Interior regions indicate stronger echoes. Echo tops are shown in hundreds of feet above sea level. Arrows with barbs indicate movement of echo areas and arrows with numbers indicate cell movement (both in kt).

Fig. 7c. Surface analysis for 0900 GMT 12 July 1979. Details are similar to Fig. 6c.

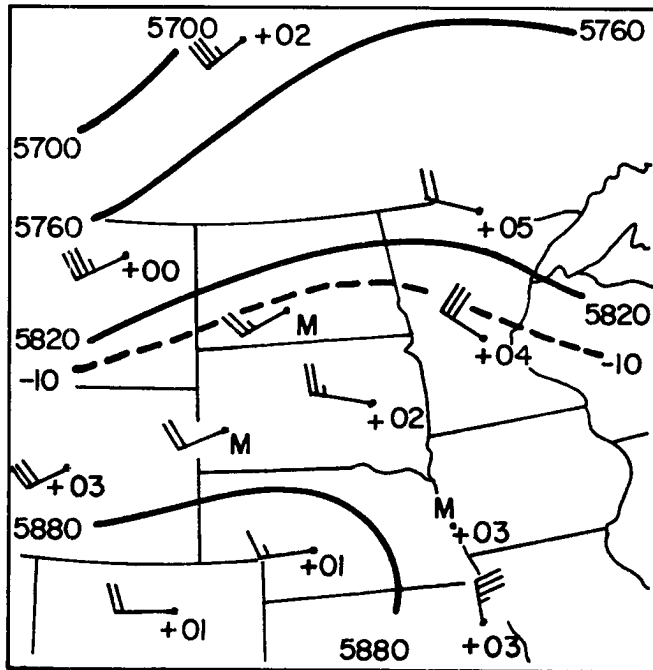
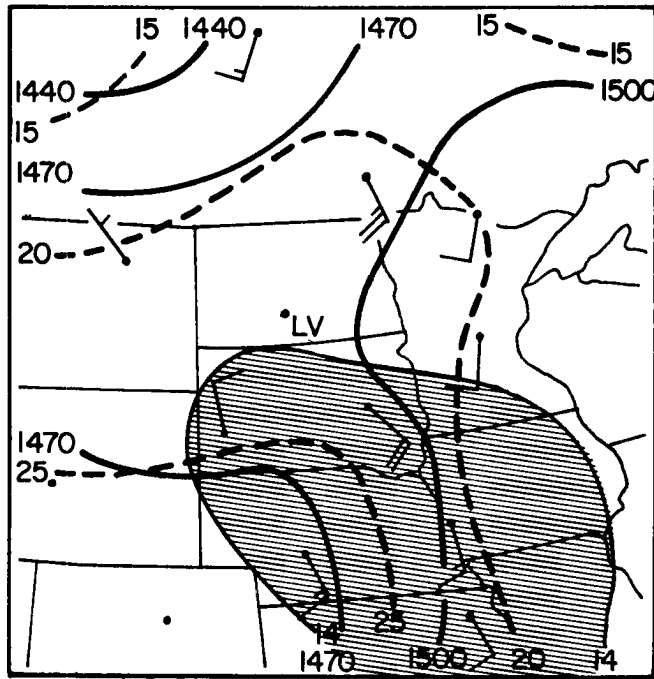
to that of its cold cloud shield. An analysis of surface conditions at 0900 GMT (Fig. 7c) shows that this MCC was occurring within a large scale environment characterized by weak pressure gradients and light winds and that the important surface features were the outflow boundary, pressure trough and mesohighs directly associated with the convective system.

Analyses of the 850 and 500 mb levels 9 h earlier at 0000 GMT again emphasize the absence of significant synoptic weather systems. The most significant features at 850 mb (Fig. 7d) were the south-southeasterly winds of 15 to 20 kt (~ 7 to 10 m s^{-1}) and the large pool of very high dewpoint air over the Plains (also note the extremely weak height gradients). At 500 mb (Fig. 7e) winds were very light indicating that the large scale environment was characterized by weak vertical shear and slowly changing patterns (note the 12 h height changes).

A time-series of surface observations from Huron, South Dakota, is shown in Fig. 7f. It shows that the temperature and dewpoint temperature dropped rapidly when the leading edge of the system moved across the station. The wind shifted briefly to the southwest and gusted to 32 kt ($\sim 15 \text{ m s}^{-1}$) before becoming light and variable for the duration of the event. The pressure rapidly rose and then fell about 2 mb, after which it remained almost steady. An initial burst of heavy rain was followed by more than 4.5 h of continuous light rain showers and thunder. This sequence of MCC weather events and especially the long period of light rainfall is similar to the characteristics exhibited by tropical convective systems studied by Betts et al. (1976), Houze (1977) and Zipser (1977 and 1979).

Fig. 7d. 850 mb analysis for 0000 GMT 12 July 1979. Details as in Fig. 6d.

Fig. 7e. 500 mb analysis for 0000 GMT 12 July 1979. Details as in Fig. 6e.



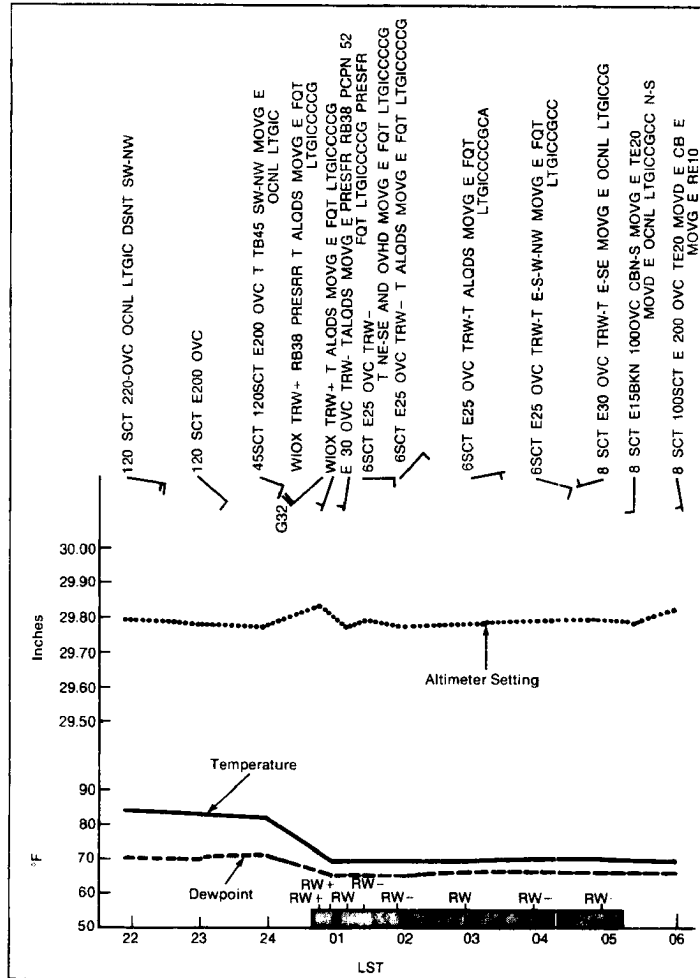
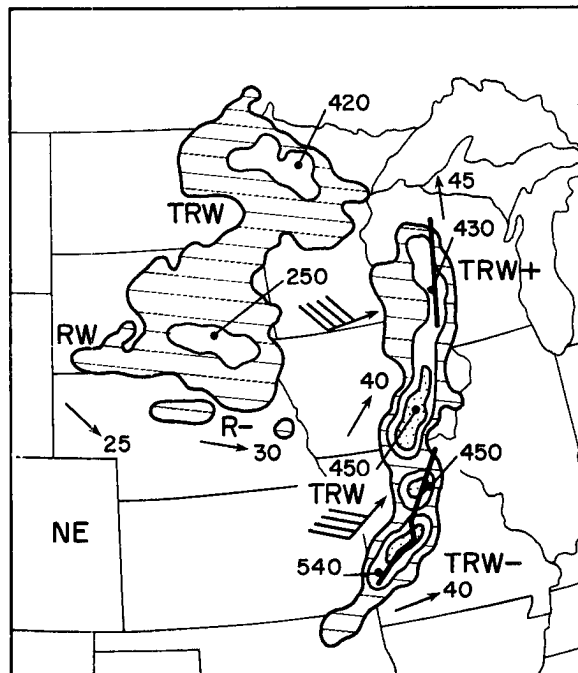
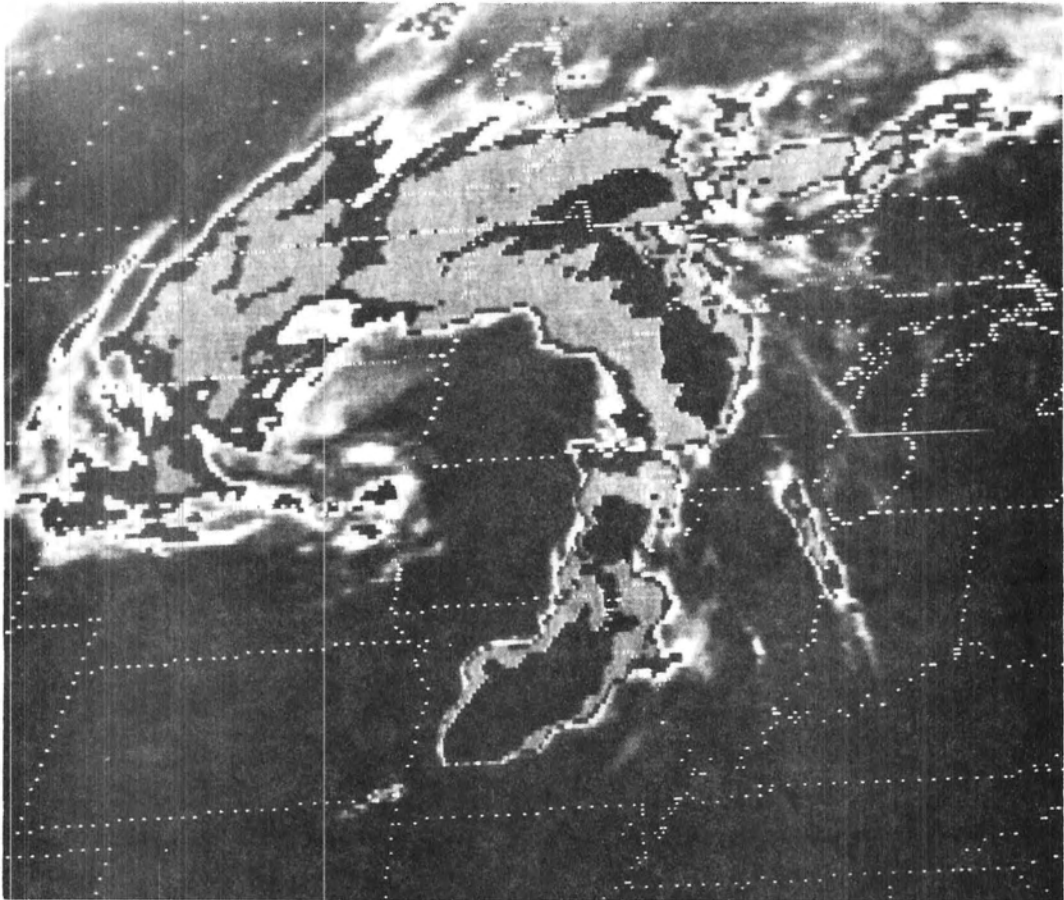


Fig. 7f. Time series of surface weather (from the WBAN-10 form) for Huron, South Dakota (station HON on Fig. 7c) on 11 and 12 July 1979. Surface winds are plotted in kt with north at top of page. Note that GMT = LST + 6 hours.

In contrast, the enhanced IR image in Fig. 8a (0600 GMT on 20 June 1979) shows a severe squall line (note that the length of the $\leq -52^{\circ}\text{C}$ region that arcs from northern Minnesota to Missouri is much greater than its width) over the north-central U.S. This squall produced tornadoes, large hail and straight-line winds exceeding 75 kt. A radar summary chart for 0535 GMT (Fig. 8b) illustrates the "line type" characteristics of the system (compare with Figs. 6b and 7b). The 0600 GMT surface analysis of Fig. 8c (compare with Figs. 6c and 7c) shows that

Fig. 8a. Enhanced IR image for 0600 GMT 20 June 1979.

Fig. 8b. Radar summary chart for 0535 GMT 20 June 1979. Details are similar to Fig. 7b.



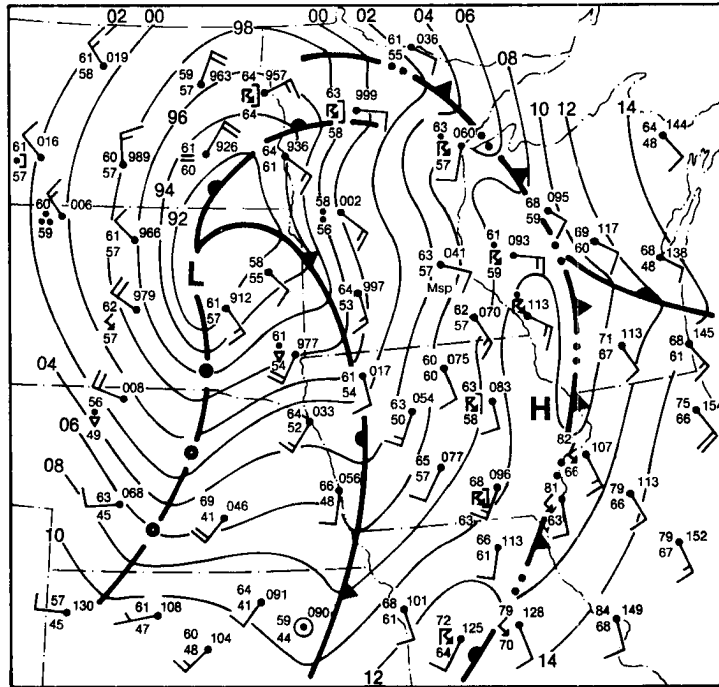


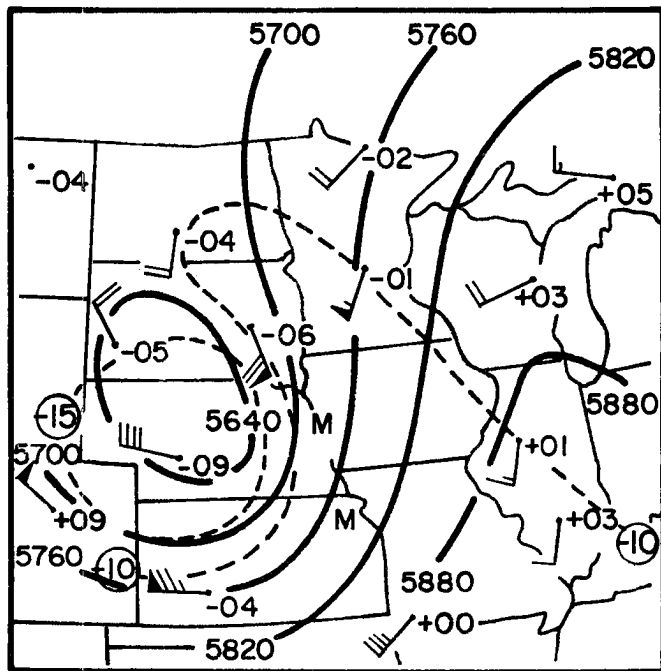
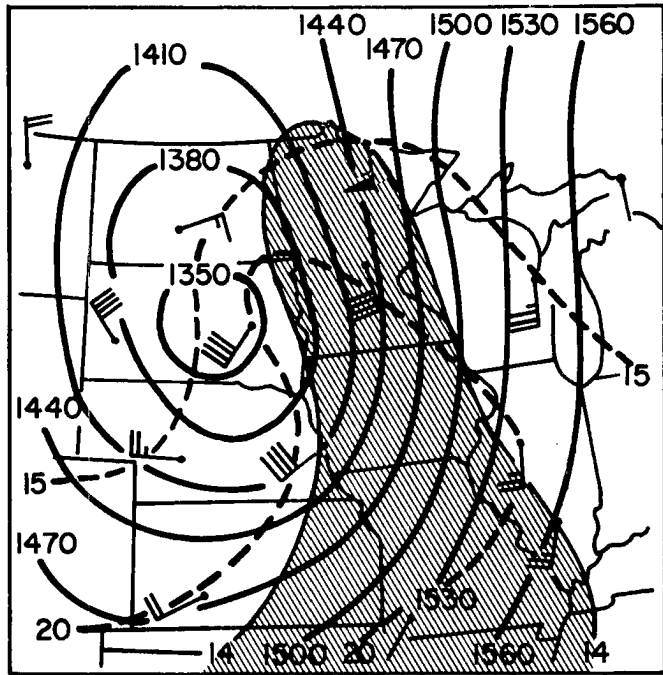
Fig. 8c. Surface analysis for 0600 GMT 20 June 1979. Details are similar to Fig. 6c.

the squall line was occurring within the warm sector of an intense, large scale cyclone that was centered over the Dakotas.

Analyses of 850 and 500 mb levels 6 h earlier more dramatically illustrate the intensity of the synoptic environment that generated this particular severe squall line. The 850 mb (Fig. 8d) height gradient was very strong, especially to the east and southeast of the deep cyclone over the Dakotas. The resultant strong southerly jet had pulled a tongue of warm and very moist air northward in the warm sector of the cyclone. The 500 mb (Fig. 8e) setting was likewise intense with very strong winds indicated around the periphery of a significant, rapidly moving short-wave trough (note the strong rise/fall height change couplet). The vertical wind shear was obviously quite strong in the squall environment. Indeed, the large scale setting of the 20 June severe squall line was quite similar to that generalized by Newton

Fig. 8d. 850 mb analysis for 0000 GMT 20 June 1979. Details are in Fig. 6d.

Fig. 8e. 500 mb analysis for 0000 GMT 20 June 1979. Details as in Fig. 6e.



(1962), who listed the following conditions as being favorable for severe convective storms:

- a) Conditional instability
- b) Availability of abundant moisture in lower levels
- c) Bands of strong winds in lower and upper levels, usually veering with height
- d) Some dynamical mechanism which can cause the release of instability (i.e., the approach of a strong baroclinic wave).

A time-series of surface observations for Minneapolis, Minnesota (Fig. 8f), depicts the sequence of weather events as the severe squall line moved across the station. As the squall hit, the temperature and dewpoint dropped rapidly while the pressure rose rapidly (~ 6 mb). The wind shifted to the west-southwest and gusted to 49 kt (~ 25 m s⁻¹). A thunderstorm-associated mesohigh, followed by a wake depression, passed the station as precipitation persisted for about 2.5 h and the wind gradually backed to the east-southeast. Although this sequence of events is much different than that produced by the MCC (see Fig. 7d), it is typical of severe squall lines (see Williams, 1948; Newton, 1950; Brunk, 1953; and Fujita, 1955).

These analyses demonstrate that, in these particular cases, the MCC and squall line weather systems manifested themselves, both in satellite and radar data and in the surface weather they produced, as distinctly different types of convective systems. The 850 and 500 mb analyses illustrated that the MCCs occurred within large scale environments characterized by light winds and vertical shear and by weak height and temperature gradients; whereas, the severe squall line occurred in conjunction

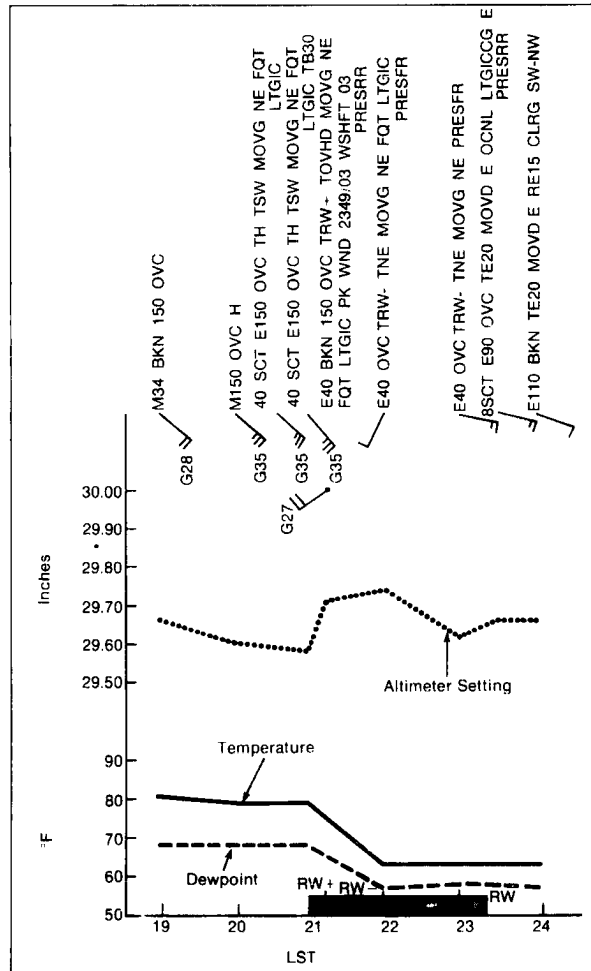


Fig. 8f. Time sequence of surface weather (from the WBAN-10 form) for Minneapolis, Minnesota (station Msp on Fig. 8c) on 19 and 20 June 1979. Details are similar to Fig. 7f.

with an intense cyclone within an environment characterized by strong winds and shear. The severe squall's large scale setting was changing rapidly while the MCC's environments appeared quite stagnant.

It is hypothesized that the persistent, nearly circular, continuous cold cloud shield of MCCs is a direct reflection of these differing large scale environments and that it indicates that convectively-driven, mesoscale circulations can dominate those of the large scale. This is in contrast to severe prefrontal squall lines, as typified by the 20 June case, whose "line" nature is imposed and modulated by larger

scale features and dynamics [e.g., boundary layer convergence ahead of a surface front, a narrow tongue of moist, unstable air in the warm sector, a strong mid-level short-wave trough, meso- α scale flow instabilities (Emanuel, 1979), etc.]. An analogy can be drawn with the air mass thunderstorm, as described by Byers et al. (1949), even though it is much smaller in scale. Such storms typically occur within a weakly sheared environment and anvil-level outflow tends to be nearly uniform in all directions as opposed to the highly elliptical anvils of severe storms in strong shear (also contrast anvil configurations of modeled storms under shear vs. no shear, e.g., Hane, 1972). The net result is that air mass storms appear nearly circular when viewed in satellite imagery much like MCCs do on a larger scale.

It is interesting to note that intense convective cells within the mature MCC sometimes exhibit a line-type internal substructure. However, when this occurs the line usually is oriented parallel to mid-level steering winds instead of nearly orthogonal as in the severe squall situation. The line also tends to occur on the right side of the convective system (nearest the unstable fuel supply) instead of along the leading edge. Limited areas can thus be subjected to repeated passage of intense storm cells and very heavy rains. Such a situation is illustrated by the satellite image in Fig. 9a and the corresponding radar summary chart in Fig. 9b. Note that the line of intense echoes in the southwestern portion of the MCC is oriented parallel to both the system's movement and to internal cell movement. The differences between the severe prefrontal squall line and internal MCC line structure can also be seen in the contrast between Figs. 8b and 9b.

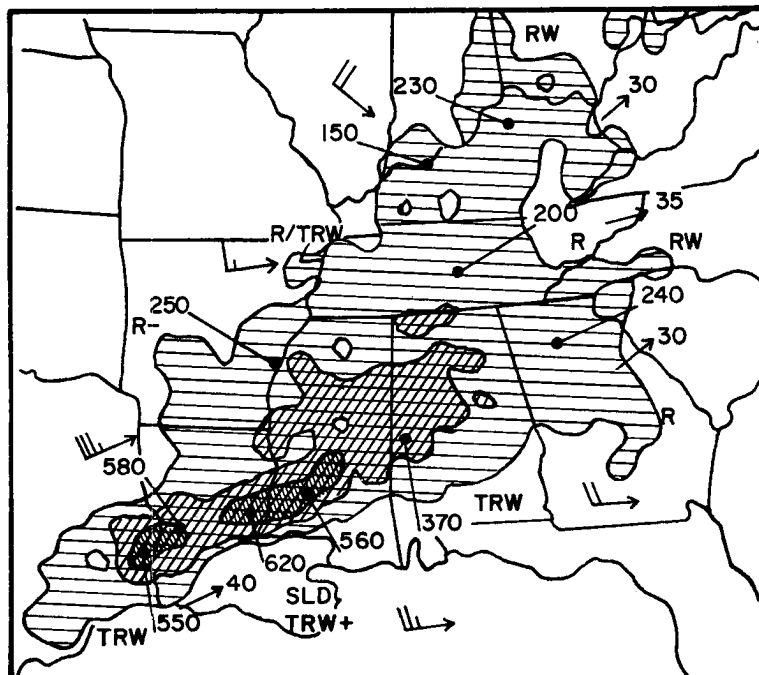
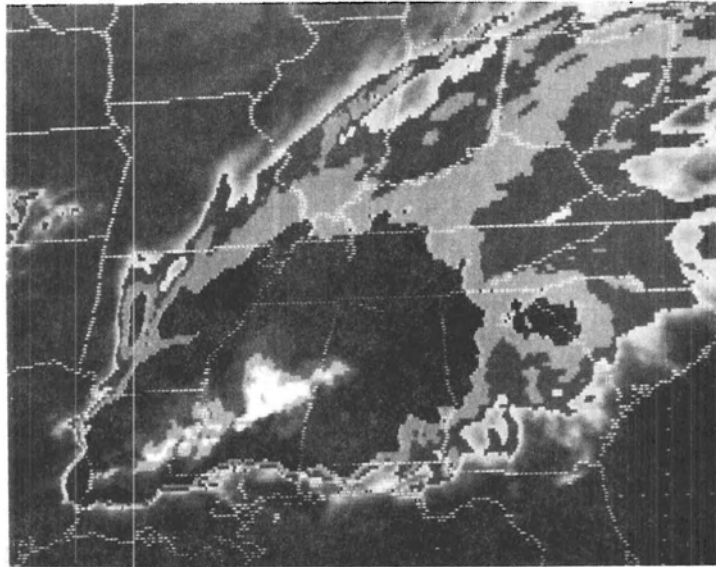


Fig. 9b. Radar summary chart for 0735 GMT 12 April 1980. Arrows with barbs indicate movement of echo areas and arrows with numbers indicate cell movement (both in kt).

II.3 Climatology of Central U.S. MCCs

Enhanced IR satellite images (operational data routinely available from the Kansas City Satellite Field Service Station at intervals of approximately 30 minutes) for the period March through September of 1978 and 1979 were examined to develop an MCC climatology. Although the image set was far from complete (machine trouble, power outages, wrong sectors available, etc.) the life-cycles of 71 MCCs were documented. Specific information for these systems is presented in Table 3 (refer to Table 2 for the terminology definitions). Areas were computed by outlining the boundaries encompassing $T_{BB} \leq -32^\circ$ and $\leq -52^\circ$ onto maps and then fitting a number of rectangles to each region. Significant weather (from the NOAA, EDIS publication Storm Data) that each system produced during the period between initiation and termination is also listed in Table 3. Severe thunderstorm phenomena (tornadoes, wind and hail), as well as torrential rains and flash floods; were often associated with the systems and almost one of every four produced injuries or deaths. Therefore, the MCCs studied were truly significant convective weather systems that spawned a variety of severe convective weather.

Although the first thunderstorms typically developed during the afternoon, the transition to large, highly organized mesosystems usually did not occur until early evening. An average of $16\frac{1}{2}$ hours elapsed between first thunderstorm development and the time that the MCC began to decay (terminate). Most systems grew to maximum size (as indicated by the satellite imagery) after midnight and persisted until after sunrise. The size of the systems was indeed huge with an average cold cloud shield ($T_{BB} \leq -32^\circ\text{C}$) of more than $300 \times 10^3 \text{ km}^2$ at the time of maximum extent.

Table 3

1978 and 1979 Mesoscale Convective Complexes

| No. | Date | First Storms | Time (GMT) | | | Cloud Top Area at Max. Extent x 10 ³ km ² ≤ -32°C | Significant Weather |
|-----|-----------------|--------------|------------|----------------|------------|---|---------------------|
| | | | Initiate | Maximum Extent | Terminate | | |
| 1 | 22/23 Mar 78 | 2200 | 0200 | 0600 | 1430 | 281 | None Reported |
| 2 | 11/12 Apr 79 | 1330 | 2000 | 0130 | 0630 | 789 | T,W,H,R,F,D,I |
| 3 | 11/12 Apr 79 | 2100 | 0600 | 1100 | 1300 | 393 | W,R,F |
| 4 | 12/13 Apr 79 | 1230 | 1600 | 0200 | 0400 | 246 | T,W,R,F,D,I |
| 5 | 22/23 Apr 78 | 1700 | 2100 | 1500 | 2200 | 568 | T,W,H |
| 6 | 2/3/4 May 78 | 1600 | 2200(3rd) | 1230(3rd) | UNKN | 612 | T,W,H,R,F,D,I |
| 7 | 2/3 May 79 | 2130 | 0030 | 1100 | 1600 | 322 | T,W,H,R,I |
| 8 | 3/4 May 79 | 1230 | 1530 | 0500 | 0930 | 927 | T,W,H,R,F,D,I |
| 9 | 6/7 May 78 | 2230 | 0200 | 1200 | 2230 | 924 | T,W,H,R,F,D,I |
| 10 | 9/10 May 79 | 2100 | 0000 | 0630 | 1000 | 271 | T,H,R,F |
| 11 | 11/12 May 78 | 1800 | 2200 | 0300 | 0800 | 574 | T,W,H,I |
| 12 | 17/18 May 78 | 1500 | 1800 | 2330 | 0400 | 218 | T,W,H,R,F |
| 13 | 18 May 78 | 0300 | 0730 | 1330 | 1600 | 224 | None Reported |
| 14 | 18/19 May 78 | 2200 | 0130 | 0600 | 1000 | 212 | T,H |
| 15 | 19 May 78 | 0230 | 0730 | 1130 | 1530 | 188 | None Reported |
| 16 | 19/20 May 79 | 2230 | 0230 | 0630 | 0830 | 221 | W,R |
| 17 | 19/20 May 79 | 1930 | 0600 | 1000 | 1400 | 252 | W,R,F,I |
| 18 | 26/27 May 78 | 1800 | 2200 | 0600 | 1000 | 198 | T,W,H,R,F,D,I |
| 19 | 26/27 May 78 | 2100 | 0300 | 0600 | 1000 | 166 | T,W |
| 20 | 30/31 May 78 | 2030 | 2330 | 0900 | 1500 | 405 | T,W,H |
| 21 | 2/3 Jun 78 | 2200 | 0000 | 0600 | 1500 | 391 | W,R |
| 22 | 3/4 Jun 78 | 2200 | 0600 | 1230 | 1430 | 174 | T,H |
| 23 | 5/6 Jun 78 | 2100 | 0200 | 0615 | 1330 | 230 | W,H |
| 24 | 13/14 Jun 78 | 1930 | 0500 | 1100 | 1400 | 235 | H |
| 25 | 15/16 Jun 79 | 2000 | 0100 | 0600 | 0830 | 165 | T,W,H |
| 26 | 15/16/17 Jun 79 | 2000 | 0600(16th) | 1130(16th) | 0400(17th) | 242 | T,W,H,R,F |
| 27 | 19 Jun 79 | 0030 | 0900 | 1430 | 1930 | 257 | None Reported |

Table 3 (Continued)

| No. | Date | First Storms | Time (GMT) | | | Terminate | Cloud Top Area at Max. Extent x 10 ³ km ² ≤ -32°C | Significant Weather |
|-----|-----------------|--------------|------------|----------------|------|-----------|---|---------------------|
| | | | Initiate | Maximum Extent | | | | |
| 28 | 19/20 Jun 78 | 1930 | 0030 | 0630 | 1430 | 546 | T,W,H,R | |
| 29 | 21/22 Jun 78 | 1200 | 1500 | 2100 | 0000 | 185 | T,W,H | |
| 30 | 21/22 Jun 79 | 1930 | 0000 | 0500 | 1100 | 349 | W,H,R,F,D,I | |
| 31 | 22/23 Jun 79 | 1930 | 2300 | 0400 | 0630 | 150 | T,W,H | |
| 32 | 22/23 Jun 79 | 2200 | 0000 | 0400 | 1030 | 167 | W,H,R,F | |
| 33 | 23 Jun 78 | 0600 | 1200 | 1700 | 2000 | 164 | W,R | |
| 34 | 23/24 Jun 78 | 1800 | 2230 | 0500 | 1800 | 300 | W,H | |
| 35 | 24/25 Jun 78 | 2000 | 0030 | 0500 | 0830 | 250 | T,H,R | |
| 36 | 24/25 Jun 78 | 2100 | 0130 | 0400 | 0730 | 167 | T,H | |
| 37 | 24/25 Jun 78 | 2030 | 0430 | 1000 | 1915 | 446 | W,H,R,F,D,I | |
| 38 | 26/27 Jun 79 | 2330 | 0230 | 0700 | 0930 | 233 | T,W | |
| 39 | 26/27 Jun 79 | 1700 | 1400 | 1030 | 1300 | 198 | None Reported | |
| 40 | 27/28 Jun 78 | 1800 | 2200 | 0430 | 0900 | 382 | H | |
| 41 | 27/28 Jun 79 | 1530 | 0730 | 1030 | 1430 | 235 | W | |
| 42 | 29/30 Jun 78 | 2200 | 0330 | 0630 | 1030 | 125 | R | |
| 43 | 29/30 Jun 78 | 1800 | 0000 | 0630 | 1100 | 322 | None Reported | |
| 44 | 30 Jun/1 Jul 78 | 2000 | 0030 | 0500 | 1000 | 262 | R,F,D | |
| 45 | 30 Jun/1 Jul 79 | 2130 | 0500 | 0900 | 1300 | 144 | None Reported | |
| 46 | 1/2 Jul 78 | 1900 | 0030 | 0800 | 1030 | 271 | W,R,F,D | |
| 47 | 3/4 Jul 78 | 2000 | 0030 | 0500 | 1000 | 262 | T | |
| 48 | 4/5 Jul 79 | 2000 | 2330 | 0630 | 1000 | 378 | T,W | |
| 49 | 5/6 Jul 78 | 1830 | 2300 | 0430 | 0800 | 454 | T,W,H,R,F,D | |
| 50 | 6 Jul 78 | 0100 | 0700 | 1100 | 1330 | 233 | W,H | |
| 51 | 8/9 Jul 78 | 2000 | 0330 | 0630 | 1200 | 190 | W,R | |
| 52 | 8/9 Jul 79 | 2130 | 0600 | 0900 | 1400 | 180 | W | |
| 53 | 11/12 Jul 79 | 2100 | 0330 | 0900 | 1500 | 245 | T,W | |
| 54 | 12/13 Jul 79 | 2200 | 0330 | 0630 | 1000 | 161 | T,R,F | |
| 55 | 13 Jul 78 | 0130 | 0700 | 1100 | 1600 | 186 | None Reported | |

Table 3 (Continued)

| No. | Date | First Storms | Time (GMT) | | | Cloud Top Area at Max. Extent x 10 ³ km ² ≤ -32°C | Significant Weather |
|----------------|--------------|--------------|------------|-------------------|-----------|---|------------------------|
| | | | Initiate | Maximum Extent | Terminate | | |
| 56 | 13/14 Jul 79 | 1900 | 0300 | 0830 | 1130 | 238 | T,W,H,R |
| 57 | 14/15 Jul 78 | 1700 | 0000 | 0500 | 0830 | 326 | W,H,R,F |
| 58 | 19/20 Jul 78 | 1900 | 0300 | 0800 | 1430 | 238 | None Reported |
| 59 | 20/21 Jul 78 | 1830 | 0200 | 0930 | 1300 | 243 | T |
| 60 | 21/22 Jul 78 | 1930 | 0000 | 0630 | 1100 | 429 | W,I |
| 61 | 22/23 Jul 79 | 1830 | 0230 | 0630 | 1000 | 189 | None Reported |
| 62 | 29/30 Jul 79 | 2130 | 0500 | 0930 | 1300 | 414 | T,W,H,R,F,I |
| 63 | 7/8 Aug 79 | 2030 | 0145 | 0615 | 1145 | 192 | T,H |
| 64 | 17 Aug 78 | 0100 | 0730 | 1100 | 1800 | 216 | None Reported |
| 65 | 17/18 Aug 78 | 1700 | 0130 | 0430 | 0830 | 382 | None Reported |
| 66 | 22/23 Aug 78 | 1800 | 2130 | 0500 | 0800 | 338 | R |
| 67 | 22/23 Aug 78 | 1930 | 0100 | 0730 | 1700 | 375 | R |
| 68 | 23/24 Aug 78 | 1730 | 0230 | 0730 | 0900 | 150 | W,H,R,F |
| 69 | 25/26 Aug 78 | 1200 | 2130 | 0130 | 0930 | 239 | W |
| 70 | 28/29 Aug 79 | 2200 | 0100 | 0845 | 1400 | 340 | T,W,H,D,I |
| 71 | 30/31 Aug 79 | 0300 | 0600 | 1100 | 1830 | 230 | None Reported |
| AVERAGE VALUES | | 2000 | 0145 | 0730 | 1230 | 301 | |

T = Tornadoes
W = Wind
F = Flooding
D = Deaths
H = Hail
R = Heavy Rain
I = Injuries

Figure 10 shows a plot of the number of MCCs whose area at maximum extent fell into specific intervals. The great majority of MCC weather systems had maximum areas in the range 150 to 300,000 km². While larger systems occur less frequently (note that the lower end of the distribution may partially reflect the artificiality of the MCC definition requiring $\geq 100,000$ km² area for at least 6 h), Table 3 indicates that these "super" MCCs were usually very severe.

The paths that these MCCs followed are shown in Figs. 11a through c (tracks are for the centroid of the $\leq -32^{\circ}\text{C}$ cloud shield). The solid lines indicate the tracks of the systems from the time that they initiated until they terminated and the circles denote the MCC position at the time of maximum extent. The circled numbers correspond with the systems documented in Table 3. Dashed lines indicate the region in which the first thunderstorms developed and their movements prior to MCC initiation. Once the systems developed their movement tended to be with the mean flow in the 700-500 mb layer. The tracks seem to indicate that many of the systems moved eastward of a large scale ridge position before they began to decay. This anticyclonic turning of the systems as they weakened is emphasized by a tendency for dissipation to begin preferentially within the northern portions of the MCCs.

The system tracks and the data shown in Table 3 indicate that MCCs are likely responsible, in large part, for the well known nocturnal maxima in thunderstorm and precipitation frequencies over the central U.S. (Kincer, 1916; and Wallace, 1975). The nocturnal maximum of thunderstorm incidence reported by Wallace extends from Oklahoma northward to Minnesota, Wisconsin and northern Michigan and is strongly peaked at about 0100 local time (about 0700 GMT), the time that MCC systems

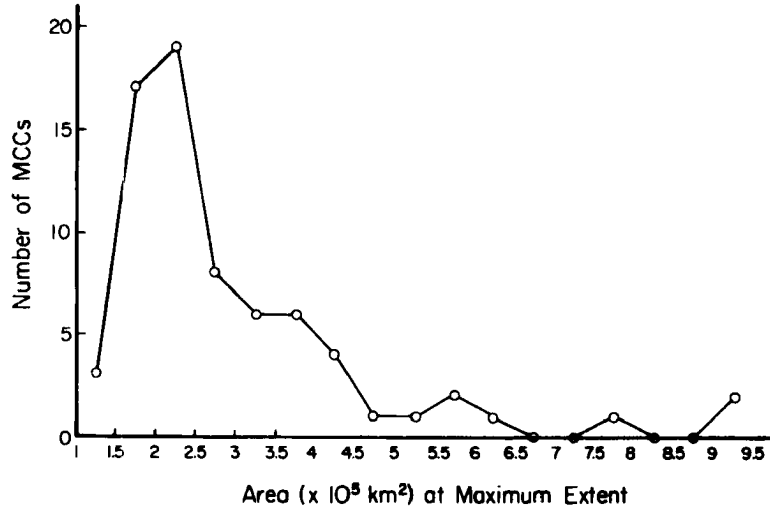


Fig. 10. MCC cloud top area with $T_{BB} \leq -32^\circ\text{C}$ at the time of maximum extent. Data were summed over intervals of $.5 \times 10^5 \text{ km}^2$.

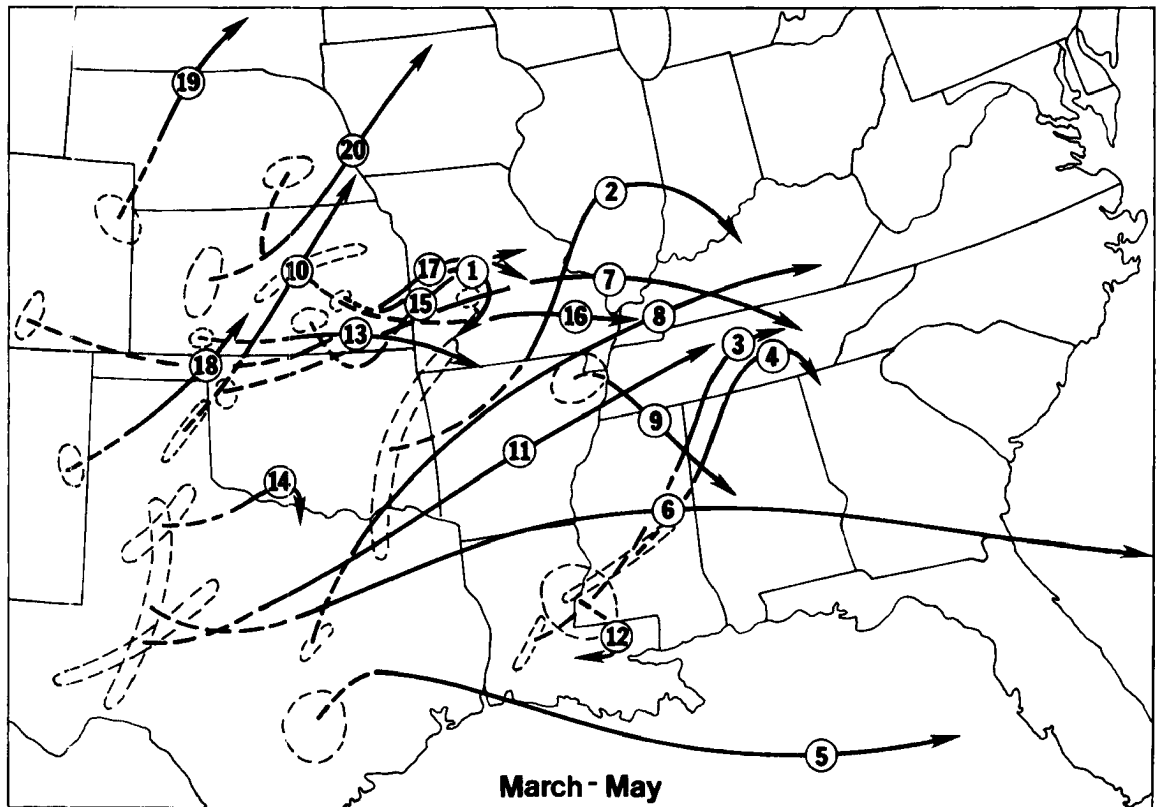


Fig. 11a. Tracks of 1978 and 1979 Mesoscale Convective Complexes during March-May. Dashed lines indicate regions and movements of the first thunderstorm developments. Heavy arrows show movement of systems from initiation to termination. Circles indicate system position at maximum extent.

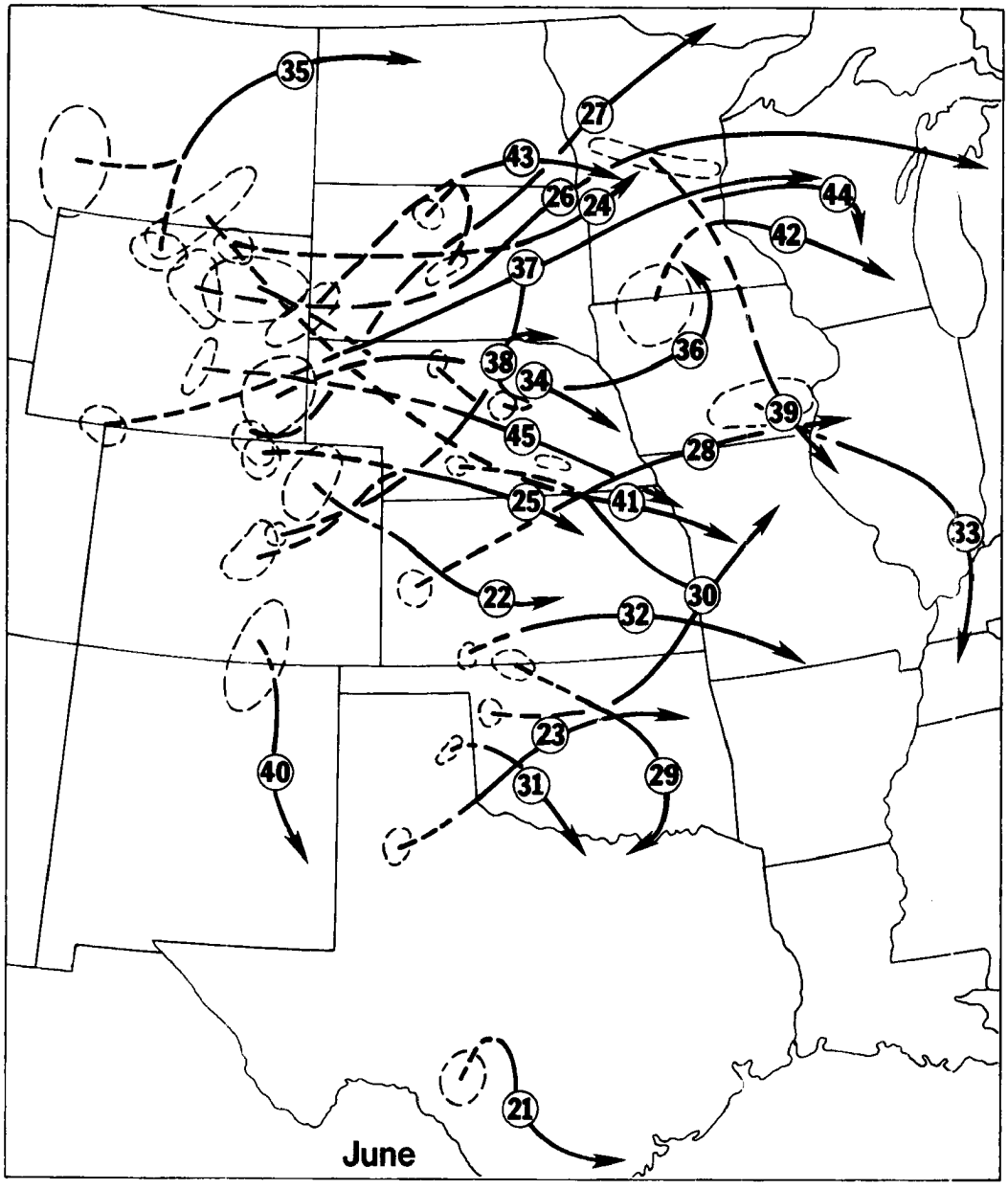


Fig. 11b. Tracks of 1978 and 1979 Mesoscale Convective Complexes during June.

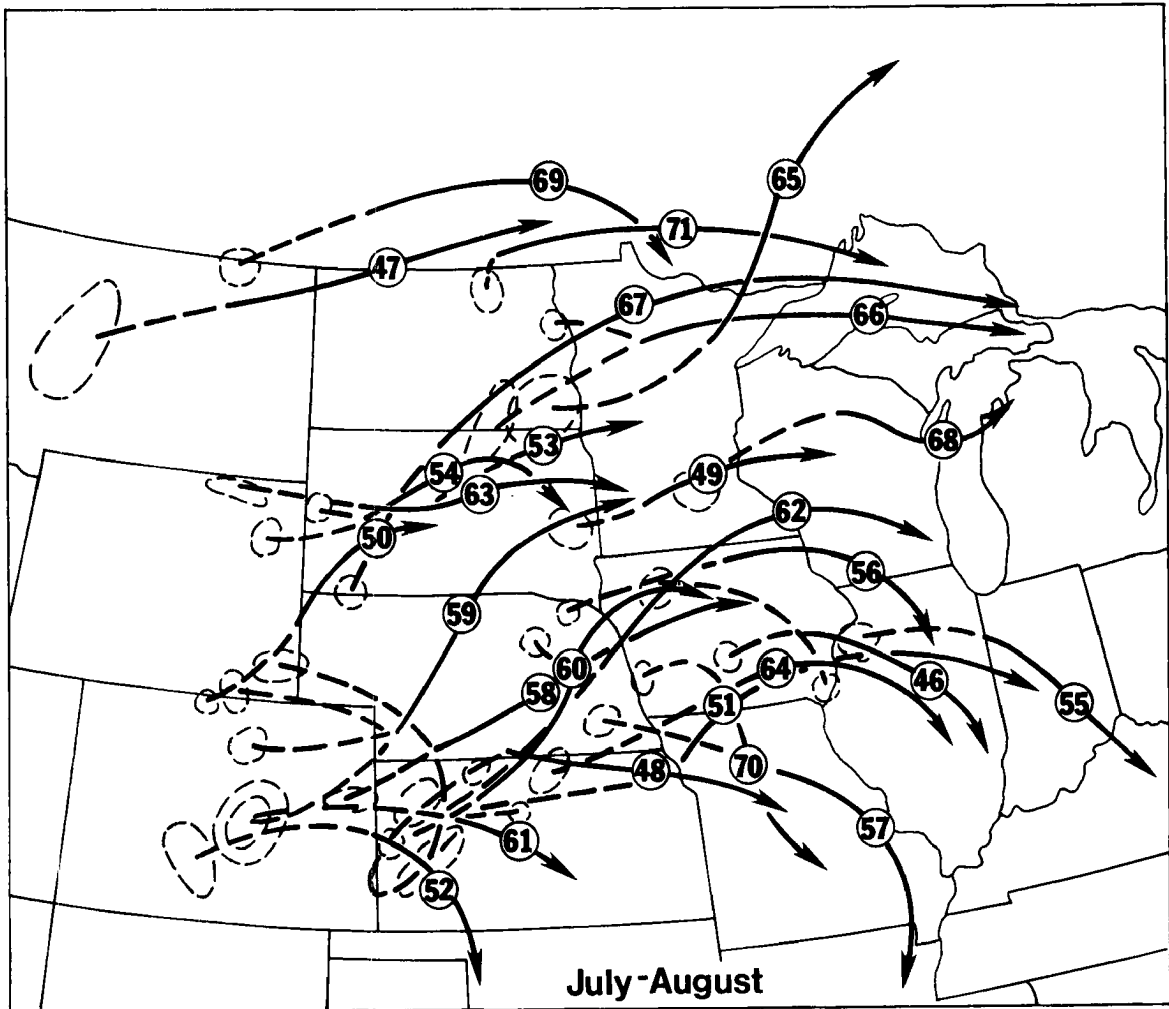


Fig. 11c. Tracks of 1978 and 1979 Mesoscale Convective Complexes during July-August.

typically reach their greatest extent. It is important to note (see Fig. 11) that even though many of the MCCs studied moved into or across the nocturnal precipitation region these systems had their roots in thunderstorm activity that developed far to the west. Maddox et al. (1979) found that significant flash floods in the eastern 2/3rds of the U.S. often occurred during nighttime hours and it is felt that MCCs are largely responsible for this nocturnal flash flood characteristic (Table 3 indicates that at least 32 of the 71 systems produced heavy rains). A recent climatology of heavy precipitation events by Crysler et al.

(1981) also supports this idea. They show that heavy precipitation events [> 4.0 in. (101.6 mm) in < 8 h] in Missouri and Illinois have a maximum frequency near local midnight -- just the time of day that these regions are often affected by large, mature MCCs.

The 1978 and 1979 satellite imagery served to illustrate a number of interesting aspects of MCCs (see again Fig. 11). Many systems resulted from mergers and interactions between groups of storms that developed in different locations. Some of the systems were initially squall line developments that acquired MCC characteristics as they persisted and grew in size. As the warm season progressed the favored region of MCC occurrence shifted slowly northward so that by July and August the systems primarily affected the north-central states.

Dirks (1969), Philipp (1979) and George (1979) have studied the eastward propagation of convective systems from the mountains onto the plains of Colorado. George has also noted that many systems that develop over the mountains (he termed these "orogenic" systems) eventually grow into large nocturnal precipitation systems over the Plains. He suggested that the eastward movement of these systems into the central Plains is related to the nocturnal precipitation maximum and the data of Table 3 and Fig. 11 certainly support this idea. About a third of the systems documented (Fig. 11) had their origins in activity that was first detected (via satellite images) over the Rocky Mountains or the eastern slopes (i.e., within the states of Montana, Wyoming, Colorado or New Mexico). Physical characteristics were averaged for the orogenic MCCs and the Plains systems and the results are shown in Table 4. Orographic systems were characterized by a slightly earlier time of initial storm development; however, the Plains systems grew to reach MCC size criteria

Table 4

Mean Characteristics of Orogenic and Plains MCCs

| | <u>First Storms</u> | <u>Time (GMT)</u> <u>Initiate</u> | <u>Time (GMT)</u> <u>Max. Extent</u> | <u>Terminate</u> | <u>Cloud Top Area at</u> <u>Max. Extent x 10³ km²</u> <u>≤ -32°C</u> |
|------------------------|---------------------|--------------------------------------|---|------------------|--|
| Orogenic (23 cases) | 1930 | 0300 | 0745 | 1300 | 238 |
| Plains (48 cases) | 2015 | 0030 | 0715 | 1215 | 332 |

much more quickly. It is important to note that both Orogenic and Plains systems reached maximum extent about the same time and that both types of systems persisted until near sunrise. Plains systems were also considerably larger than systems coming off the mountains.

These statistics are somewhat biased by the very large and impressive late spring MCCs that primarily affect the south Plains and Gulf Coast (see Table 3 and refer back to Figs. 2a and 9a). Thus the statistics were re-computed for only the July and August MCCs and the tabulations are shown in Table 5. The main change is that the average time of initiation was considerably later for the summertime Plains systems (0200 instead of 0030 GMT). The ratio was still approximately two Plains systems for each

Table 5

Mean Characteristics of Orogenic and Plains MCCs During July and August

| | <u>First Storms</u> | <u>Time (GMT)</u> <u>Initiate</u> | <u>Time (GMT)</u> <u>Max. Extent</u> | <u>Terminate</u> | <u>Cloud Top Area at</u> <u>Max. Extent x 10³ km²</u> <u>≤ -32°C</u> |
|------------------------|---------------------|--------------------------------------|---|------------------|--|
| Orogenic (10 cases) | 1945 | 0300 | 0715 | 1200 | 208 |
| Plains (18 cases) | 2030 | 0200 | 0730 | 1215 | 301 |

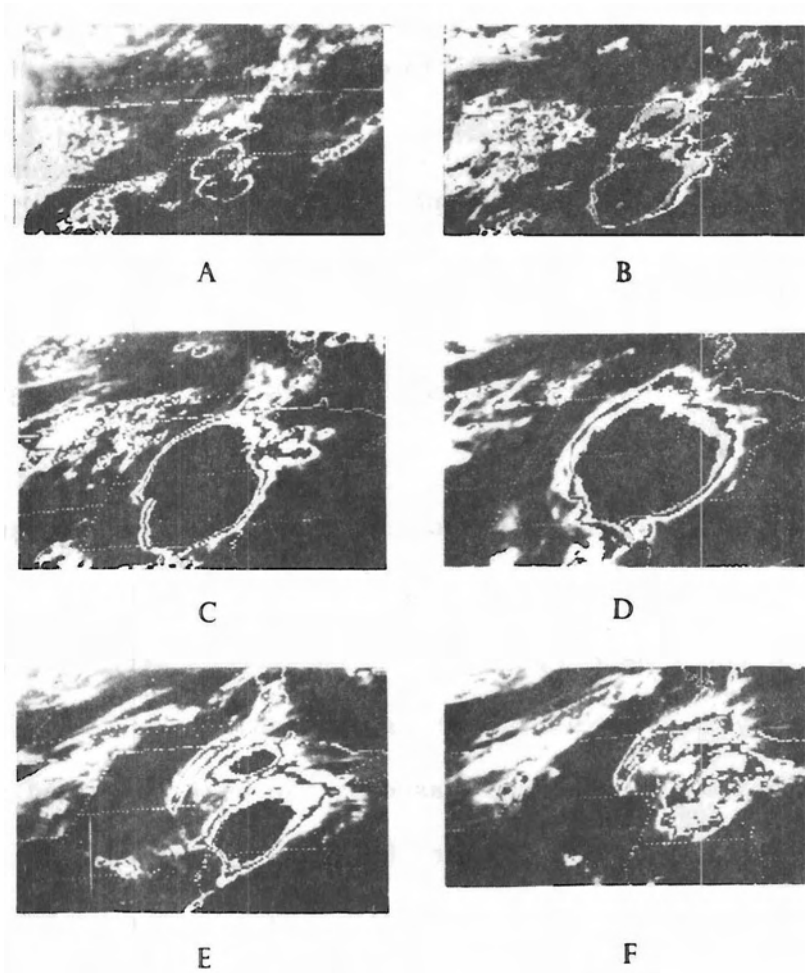


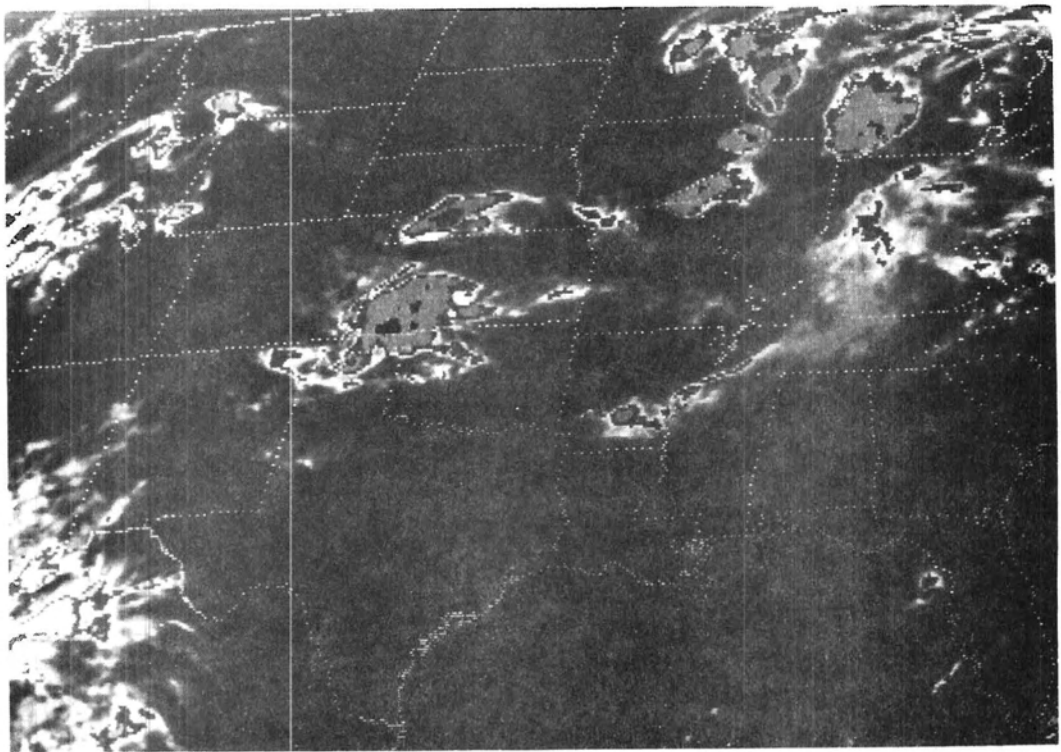
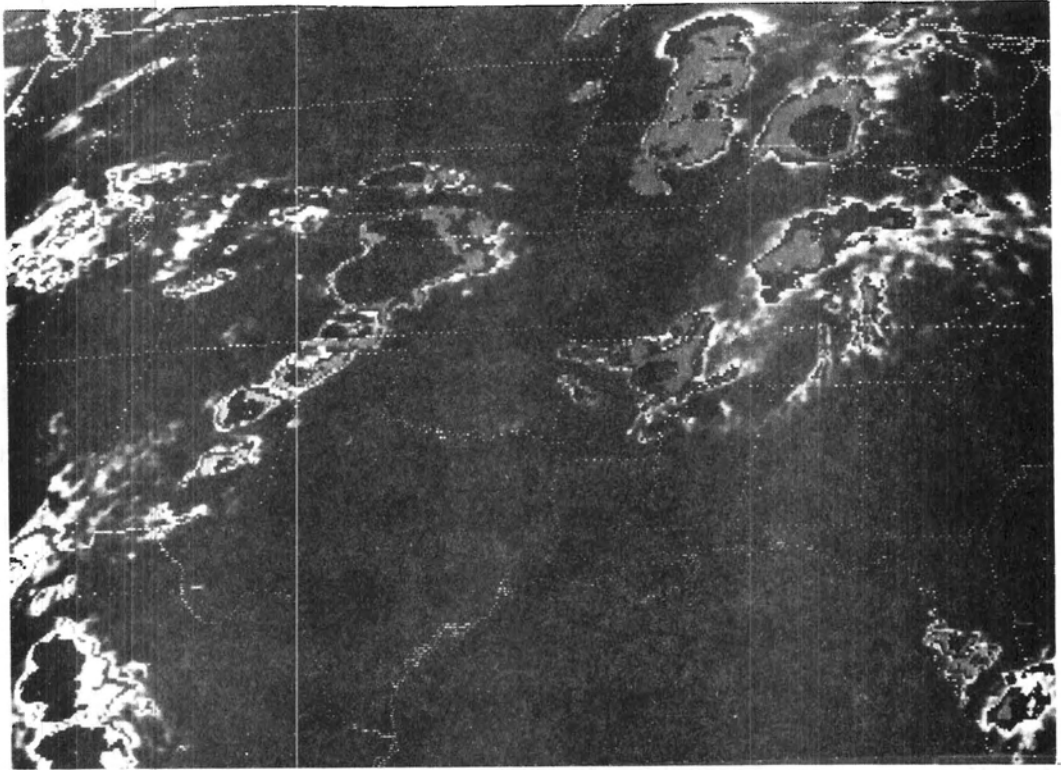
Fig. 12. Enhanced IR images documenting the life-cycle of an MCC weather system during a 16 h period on 12 July 1979. The image times are: A) 0030 GMT, B) 0300 GMT, C) 0600 GMT, D) 0900 GMT, E) 1430 GMT and F) 1630 GMT.

orogenic system and Plains systems remained considerably larger than orogenic systems (probably because they existed in a more moist and unstable air mass for a longer period than did the orogenic systems).

Regardless of where the systems originate MCCs have their roots in thunderstorm activity that first developed during the late afternoon. This is in distinct contradiction with Bleeker and Andre (1951),

Fig. 13a. Enhanced IR image for 0030 GMT 29 June 1979.

Fig. 13b. Enhanced IR image for 0600 GMT 29 June 1979.



Pitchford and London (1962), and Wallace (1975) who presupposed that the nocturnal precipitation maximum was attributed to thunderstorms that developed in situ over the central and northern Plains. The typical life-cycle sequence of events is illustrated in the satellite images shown in Figs. 12a-f which span a 16 h period. It is important to realize that many convective systems develop and begin to organize similarly, but do not persist and blossom into MCCs. Figures 13a and b illustrate this more common situation. At 0030 GMT large convective systems (quite characteristic of the developments that grow into MCCs) were over western Kansas and Wisconsin. By 0600 GMT these systems still retained their identity but had weakened dramatically as they moved eastward.

Under favorable meteorological conditions, MCCs persist and reach maximum size shortly after midnight -- about the time that the nocturnal low-level jetstream both reaches maximum strength and is located nearest the surface (Hoxit, 1975; and Thompson et al., 1976). Thus, the nocturnal jet seems to act primarily in a large scale sense, providing the MCC its maximum influx of moist static energy. This idea is consistent with the findings of Bonner (1966), Hoxit (1975) and Paegle (1978). However, the early stages of MCC development do not appear closely linked to the diurnal wind oscillations (see again Fig. 11). The entire MCC life-cycle appears to reflect a favorable interaction between large, medium and convective scale features that occurs most frequently over the central and north central U.S.

III. ANALYSIS OF METEOROLOGICAL CONDITIONS ASSOCIATED WITH MCCs

Upper-air sounding data have been composited upon a common analysis grid relative to 10 different MCCs positioned at the center of the domain. The grid, which is moved with the convective system during a 24 h period, is shown in Fig. 14. [Crosses indicate 12 grid points within the composite system over which a number of meteorological parameters were averaged; circles denote 5 grid points for which vertical soundings were extracted from analyzed significant level data.] An objective analysis procedure has been used to grid the large number of individual soundings involved upon a 2 degree latitude/longitude analysis mesh. Small scale noise was filtered from the analyses and a scale separation technique applied so that gridded fields representing the total,

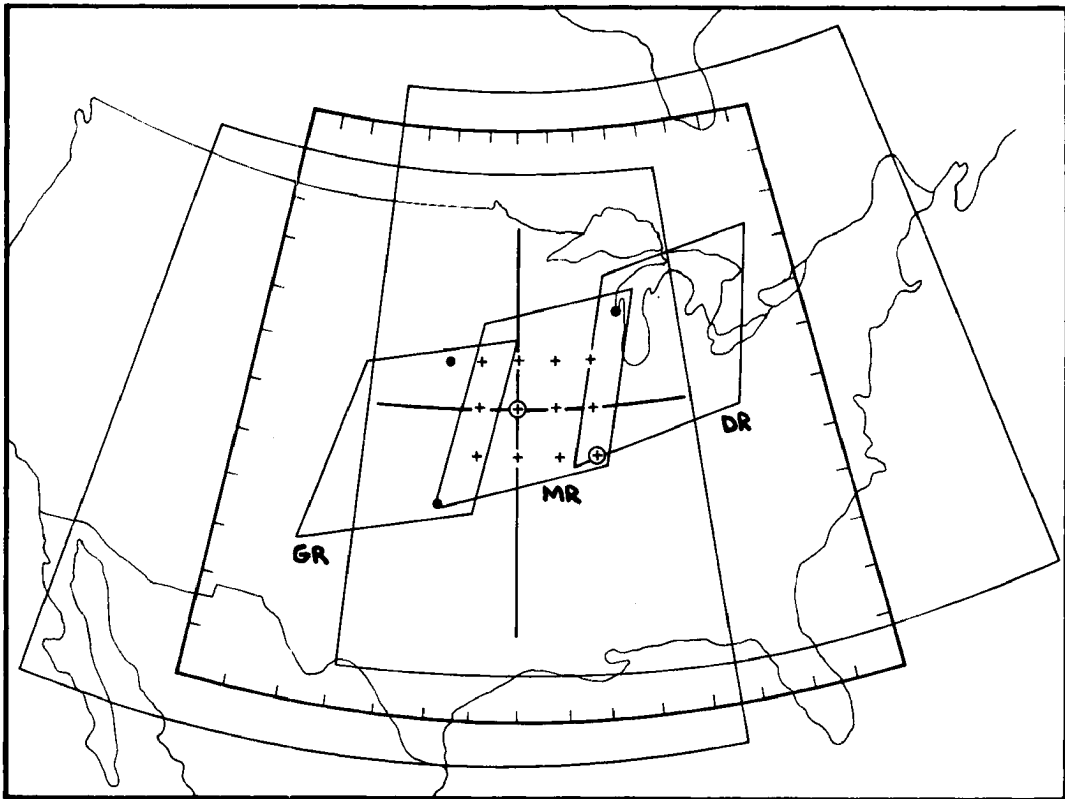


Fig. 14. Analysis grids used in objective analyses, see text for details.

macroscale and mesoscale meteorological environments were obtained. The objective analysis techniques are described in detail in Appendix A while the data compositing procedures are explained in Appendix B.

The analysis procedures suppress variability between differing meteorological situations as well as small scale details. This allows detection and evaluation of important repetitive meteorological features that attend MCCs. This filtering process also damps the magnitude of some features present in individual situations so that characteristics of the final composite system are not as intense, or occasionally spectacular, as in individual cases. Descriptions and specific analyses of the ten cases composited are presented in Appendix C. Objective analyses of the composite, total meteorological fields attending MCC weather systems are considered first.

III.1 Conditions Over the Genesis Region (GR)

Composite analyses for 0000 GMT, 12 h prior to the time of the MCC, were centered about the region where initial storm developments presumably occurred. This determination was based upon MCC movement during its mature phase. An analysis of surface features, pressure (reduced to sea level) and divergence ($\times 10^{-5} \text{ s}^{-1}$) is presented in Fig. 15a. Surface winds are plotted at every other analysis grid point and the quadrilateral (solid dark line) in the center of the domain indicates the approximate Genesis Region (GR) of the thunderstorms that develop into the MCC. The dashed quadrilateral to the east indicates the MCC Region (MR) where the convective system will be located 12 h later (see Appendix B). Surface observations indicate that a weak large scale frontal boundary stretches from the western portion of the analysis domain east-northeastward across the northern portion of the GR. A surface trough

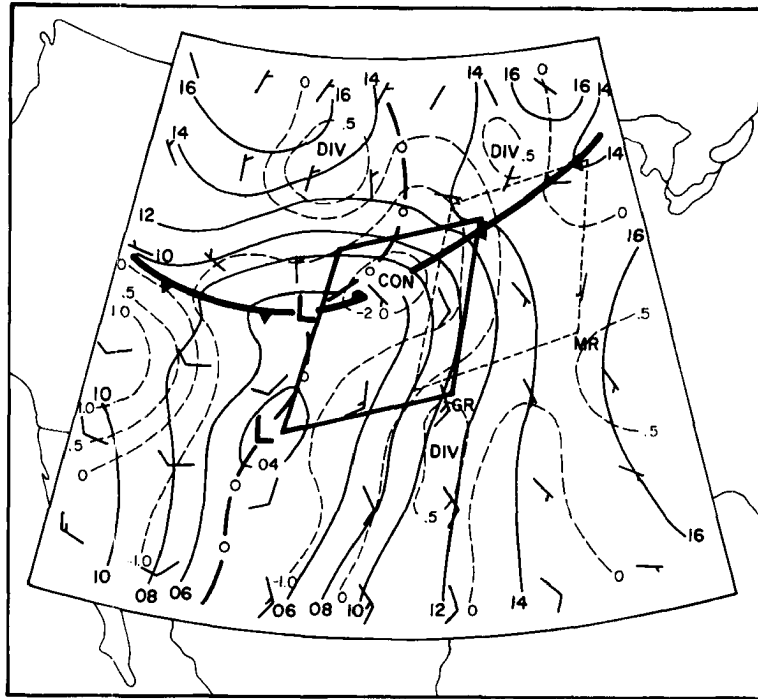


Fig. 15a. Analysis of surface features 12 h before the MCC. Surface winds are plotted at every other grid point and are plotted in kt (note that a full barb = 10 kt or $\sim 5 \text{ m s}^{-1}$). Isobars of surface pressure reduced to sea level are shown as solid lines with surface divergence ($\times 10^{-5} \text{ s}^{-1}$) shown as dashed lines.

over the Plains east of the mountains (see details concerning the analysis domain in Appendix B) stretches from south to north across the western portion of the GR. Surface winds are south to southwesterly within the GR and are strongest over the southeastern 1/3 of the GR. To the east winds are light over the MR where the MCC will be in 12 h.

The divergence pattern is generally characterized by divergence over lower elevations with convergence over the elevated terrain (see Appendix B). This pattern is consistent with that to be expected over the sloping terrain of the Plains during late afternoon (see Bleeker and Andre, 1951; Paegle and McLawhorn, 1973; and Paegle, 1978a). The major exception to this is the strong surface convergence that extends eastward into the Plains along the frontal zone. Maximum convergence ($< -2 \times 10^{-5} \text{ s}^{-1}$)

occurs over the northern GR with the entire GR covered by convergence. Further east the flow over the MR is predominantly divergent at the surface.

Figure 15b presents analyses of the surface temperature and mixing ratio. Temperatures are highest and mixing ratios lowest to the south and southwest of the GR. Very cool temperatures are present northwest of the GR. A tongue of high moisture values (12 to 16 g/kg) curves north-westward from the Gulf of Mexico into the eastern portion of the GR and southern portion of the MR. Many MCCs are heavily precipitating systems (see Appendix C) and their low-level moisture source is clearly the Gulf of Mexico. Comparison with Fig. 15a indicates increasing low-level moisture in the GR due to both convergence and advection. The entire GR is also a region of apparent warm advection. Early studies on thunderstorm forecasting in the central U.S. (Means, 1944, 1952 and 1954;

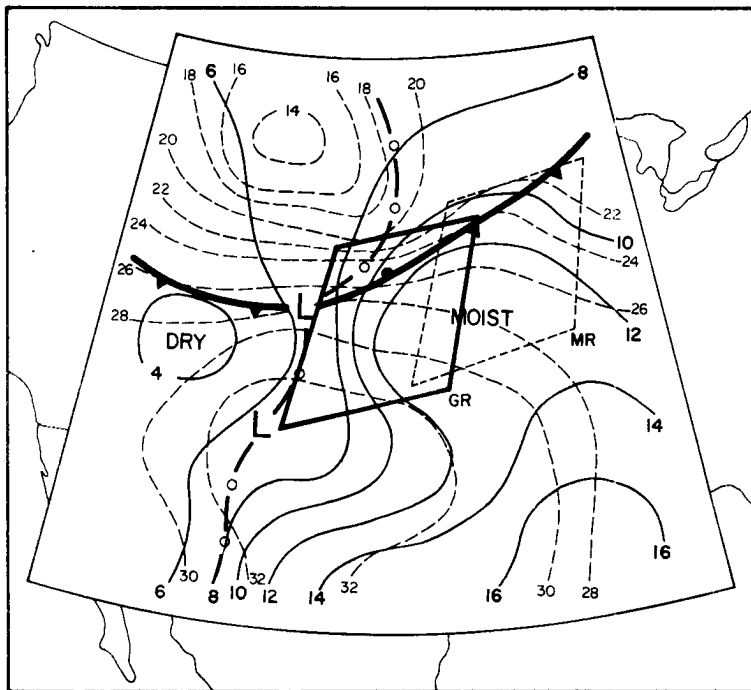


Fig. 15b. Analysis of surface features 12 h before the MCC. Isopleths of mixing ratio (g/kg) are solid lines and dashed lines are isotherms ($^{\circ}\text{C}$).

Whiting, 1957; Whiting and Bailey, 1957; Darkow et al., 1958) noted the frequent occurrence of a pronounced warm advection pattern (the dynamic importance of this pattern will be discussed later). There are significant east-west moisture gradients and very strong north-south temperature gradients present within the GR. The wind and divergence fields also exhibit considerable horizontal variations in both the x and y directions.

A detailed analysis of the 850 mb level (note that the smoothed surface elevation extends above the 850 mb level within the hatched region) is shown in Fig. 16. The height field is generally characterized by a broad trough over the western (higher elevation) portion of the analysis domain with a high over the southeast, while a very weak high is

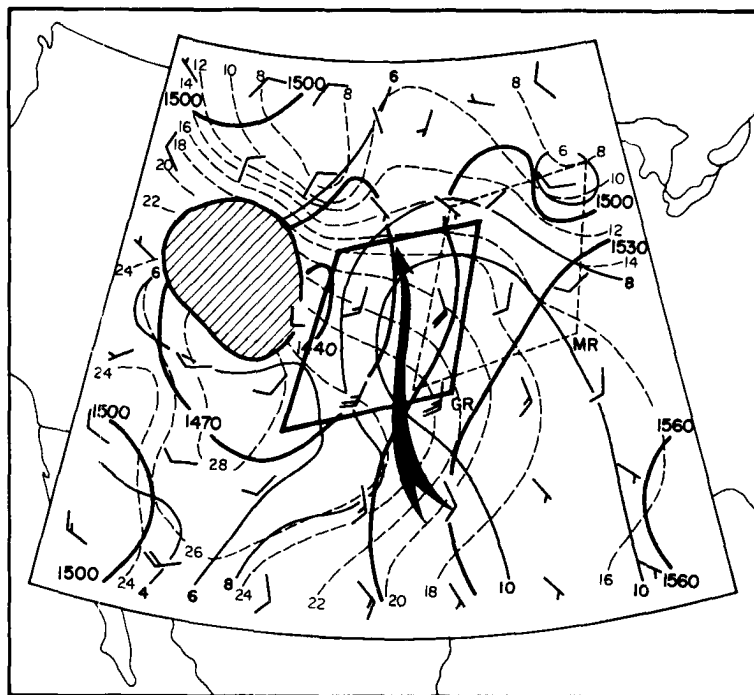


Fig. 16. Analysis of 850 mb level 12 h before the MCC. Heights (m) are shown as heavy solid contours with isotherms ($^{\circ}\text{C}$) dashed and mixing ratio (g/kg) light solid contours. Winds (full barb = 10 kt or $\sim 5 \text{ m s}^{-1}$) are plotted at every other grid point and the shaded arrow shows the axis of maximum wind speeds. The cross-hatched region indicates terrain elevations above the 850 mb level.

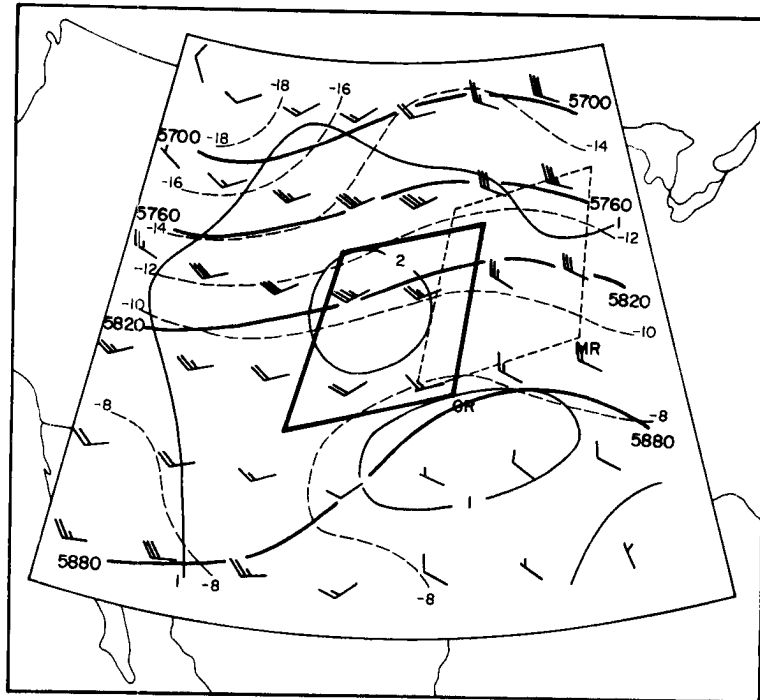
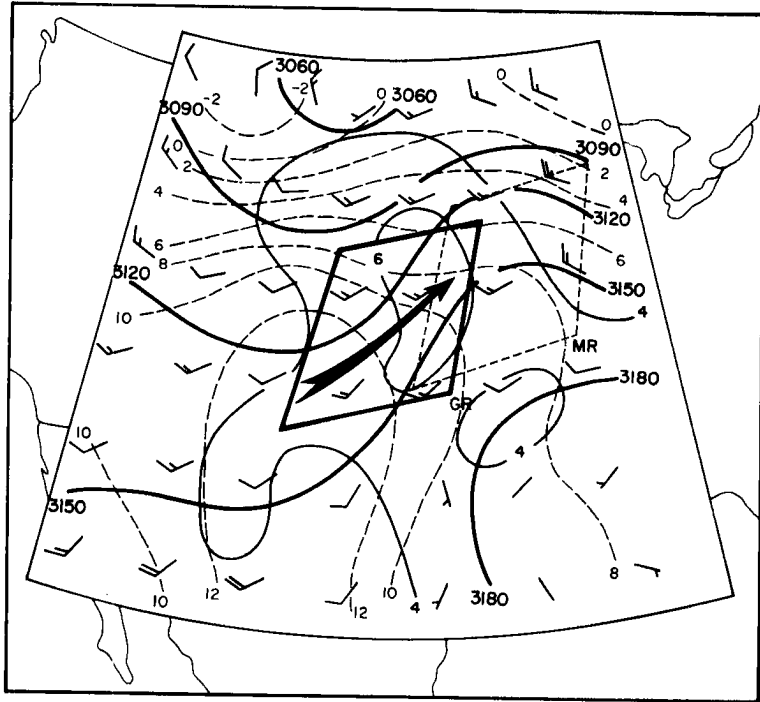
indicated to the northeast of the GR. Warm and dry conditions are present west and southwest of the GR. Moisture contents are distinctly high (> 10 g/kg) within an arc from the Gulf of Mexico into the eastern portion of the GR and southwestern portion of the MR. A strong south to north temperature gradient is present over the western portion of the domain while a moderate west to east gradient is present over the southeastern portion of the analysis region. The most pronounced feature of the wind field is the presence of a relatively strong 850 mb jet [speeds > 20 kt (~ 10 m s $^{-1}$)] over the Plains that extends into the eastern and central GR. Thus, a low-level jetstream is a recurrent feature of the MCCs' precursor environment. The flow at 850 mb is diffluent and weak over the MR. Pronounced warm advection is indicated over most of the GR. Conditions at 850 mb are quite asymmetric with west to east height and moisture gradients, south and north temperature gradients and a wind field characterized by a strong southerly jet bisecting the GR.

Conditions at 700 mb are portrayed in Fig. 17. Winds over the GR have veered and weakened (relative to the 850 mb level) considerably. The wind and height fields suggest that a very weak short-wave trough is moving across the northern portion of the domain. Temperatures generally decrease from south to north with the warmest region being southwest of the GR. Warm advection is again indicated over the GR and much of the MR. At 700 mb the atmosphere is distinctly moist (mixing ratios > 6 g/kg) over the eastern portion of the GR.

At 500 mb (see Fig. 18) winds have veered and become west to west-southwesterly over the GR (note that at 500 mb winds are west-northwesterly over the MR and that a ridge-line is present between the GR and MR).

Fig. 17. Analysis of 700 mb level 12 h before the MCC. Details are similar to Fig. 16.

Fig. 18. Analysis of 500 mb level 12 h before the MCC. Details are similar to Fig. 16.



There is now considerable horizontal speed shear across the GR with speeds increasing from about 15 kt ($\sim 7 \text{ m s}^{-1}$) to $> 35 \text{ kt}$ ($\sim 18 \text{ m s}^{-1}$) from south to north. There is an accompanying south to north temperature gradient although thermal advection appears nearly neutral over both the GR and MR. The mixing ratio analysis indicates moist conditions over all of the Plains with a pocket of high moisture present over the northern portion of the GR. This region of high moisture content may be partly a result of vertical transport by mountain and east slope afternoon thunderstorms. Conditions are considerably drier to the south of the GR and MR area. The wind, height and moisture fields again suggest that a weak short-wave trough is approaching the GR (the Limited Fine Mesh numerical forecasts shown in Appendix C for each individual case support this conclusion).

Figure 19 shows analyses of the 300 mb level. Again, as at 500 mb, there is little apparent thermal advection over the domain. Moisture

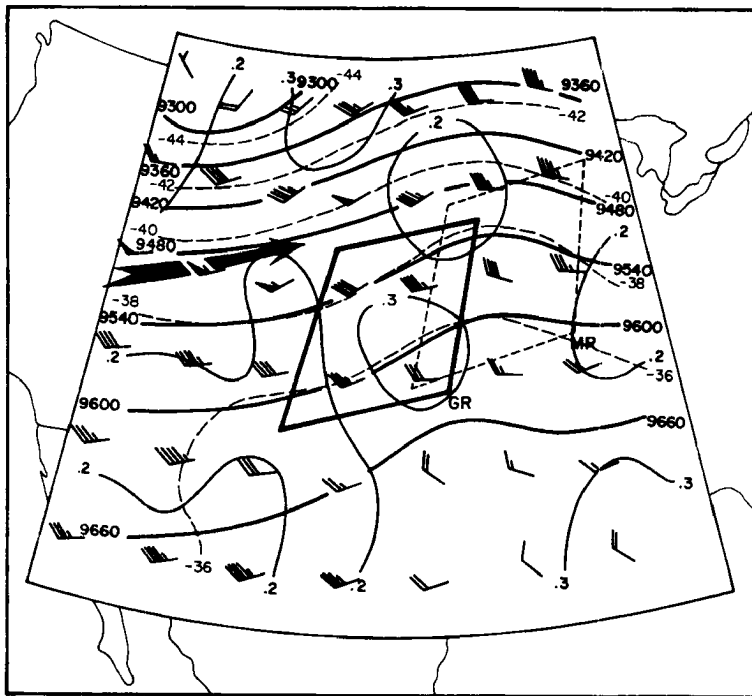


Fig. 19. Analysis of 300 mb level 12 h before the MCC. Details are similar to Fig. 16.

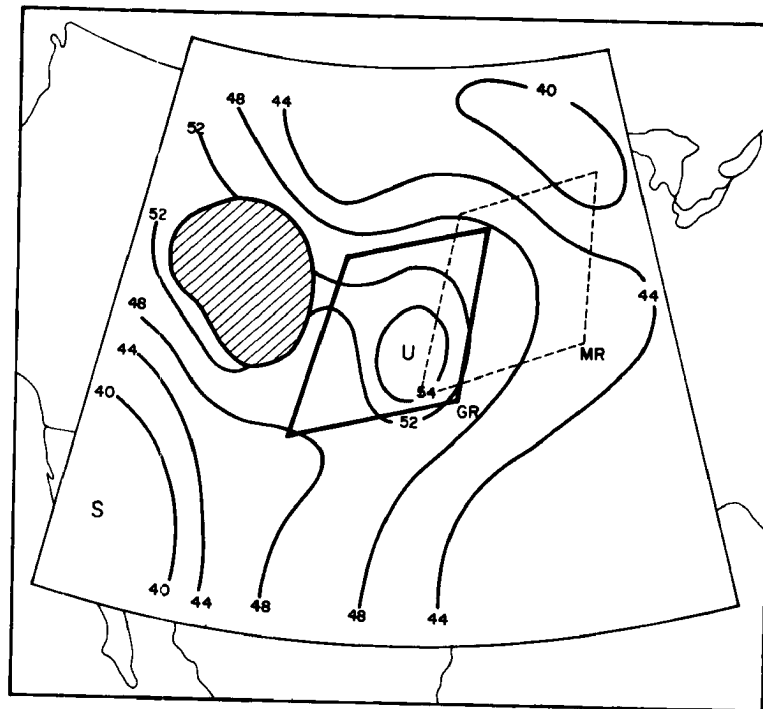
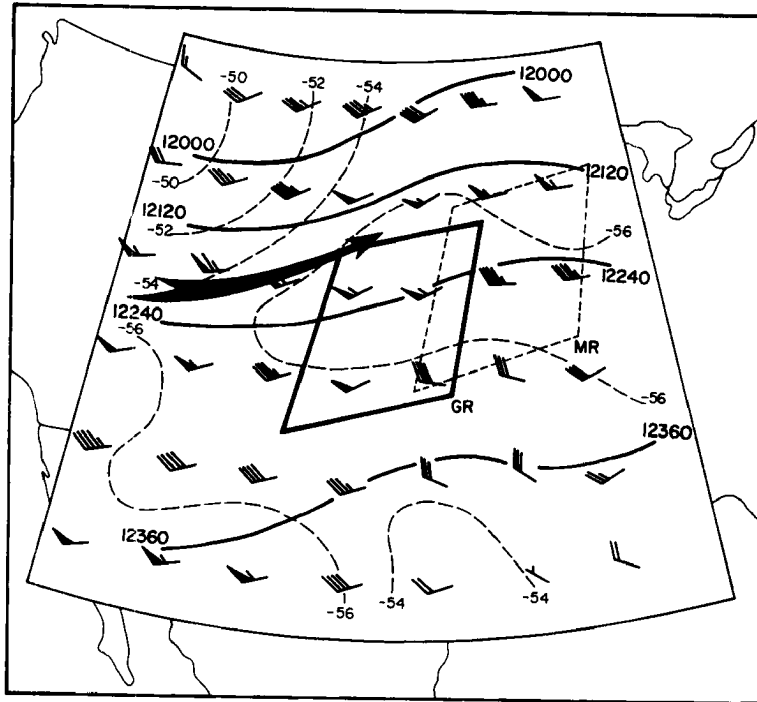
contents are high suggesting that middle and upper tropospheric moisture may be related to the Southwest monsoon flow in many MCC cases (see Cotton *et al.*, 1981). Moisture contents are maximized, however, over the GR. Note that a weak jet streak [speeds ~ 60 kt (~ 30 m s $^{-1}$)] is located just northwest of the GR. This indicates that initial storm development and MCC genesis are occurring within the right exit zone of the jet -- a region usually considered unfavorable for intense storm development (see Riehl *et al.*, 1952; Beebe and Bates, 1955; McNulty, 1978; and Uccellini and Johnson, 1979). Convective instability and lower tropospheric forcing must dominate vertical circulations associated with this jet in the MCC cases. Analyses for the 200 mb level are presented in Fig. 20. The jet streak is present at this level also with speeds of ~ 65 kt (~ 32 m s $^{-1}$). The flow appears weakly diffluent over the GR and coldest temperatures ($\leq -56^{\circ}\text{C}$) are located within the ridge to the right of the jet.

An analysis of a stability index (the Totals Index, computed with composite data from the 850 to 500 mb levels; see Miller, 1967) is shown in Fig. 21. [Values of the Totals greater than 44 indicate increasingly favorable conditions for deep convection; values greater than 54 indicate a potential for intense convection -- a lifted index of -6 is somewhat analogous to a Total of 54.] Notice that values of the Totals increase to the west as the 850 mb level nears the surface (i.e., very warm temperatures); however, a distinct pocket of very unstable air is present over the Plains within the south and east portion of the GR. This is the air mass which feeds the developing MCC.

The stability analysis and the other fields discussed above illustrate that the MCC develops within a large scale environment that is

Fig. 20. Analysis of 200 mb level 12 h before the MCC. Details are similar to Fig. 16.

Fig. 21. Analysis of the Totals stability index 12 h before the MCC. Cross-hatched region is area where terrain elevation is above the 850 mb level.



strongly three-dimensional (i.e., significant temperature, moisture and stability gradients along with considerable horizontal variations in both horizontal and vertical wind shear). This environment appears different from the somewhat homogeneous environment within which many tropical convective systems develop (e.g., Riehl, 1954; Williams and Gray, 1973; Riehl, 1978). The analysis series indicates that the MCC develops on the anticyclonic side of a broad, and relatively weak, westerly jet. Further, the system initiates in the vicinity of a large scale frontal zone that is generally oriented west to east. Meridional temperature gradients are pronounced whereas zonal gradients are relatively weak. A weak short-wave trough apparently moves eastward within the zonal current and enhances the favorability for convective developments. The most pronounced features within the genesis environment are the pre-existence of a moist and conditionally unstable environment in the GR and MR. Within the lower troposphere there is a substantial southerly wind maximum present along with significant warm advection [indicating, if differential vorticity advection is weak, low-level forcing of upward motion by quasi-geostrophic processes (e.g., Holton, 1972; Sanders, 1976)] over the Plains. Thus the MCC precursor environment is significantly different from that classically associated with severe squall lines wherein large scale features are characterized by intense zonal gradients, strong fronts and an intense polar jetstream (e.g., Newton, 1950; Fujita, 1955; Ludlum, 1966; and Miller, 1967).

III.2 Conditions Over the MCC Region (MR)

It is emphasized in Appendix C that the 1200 GMT composite data does not, in the mean, capture the convective system at the time of maximum extent or intensity but rather represents a period in the MCC life-cycle

after maximum intensity but prior to its rapid decay. An analysis of surface features, pressure and divergence is shown in Fig. 22a at the time of the MCC. The large scale front has slowly subsided southward across the entire domain. However, its southward displacement was least over the MR. Pressures have risen over the entire analysis region during the night. These rises were generally less than 2 mb. To the west of the MCC however they exceeded 4 mb. The pressure increases were a result of both diurnal cooling and the southward push of the front. The MCC has left behind the region of surface convergence and the MR is characterized by weak divergence. The divergence pattern suggests the presence of a very weak mesohigh and outflow boundary (this is verified by mesoscale perturbation analyses). One surface low remains but it is now considerably to the west of the MCC. Note that surface winds

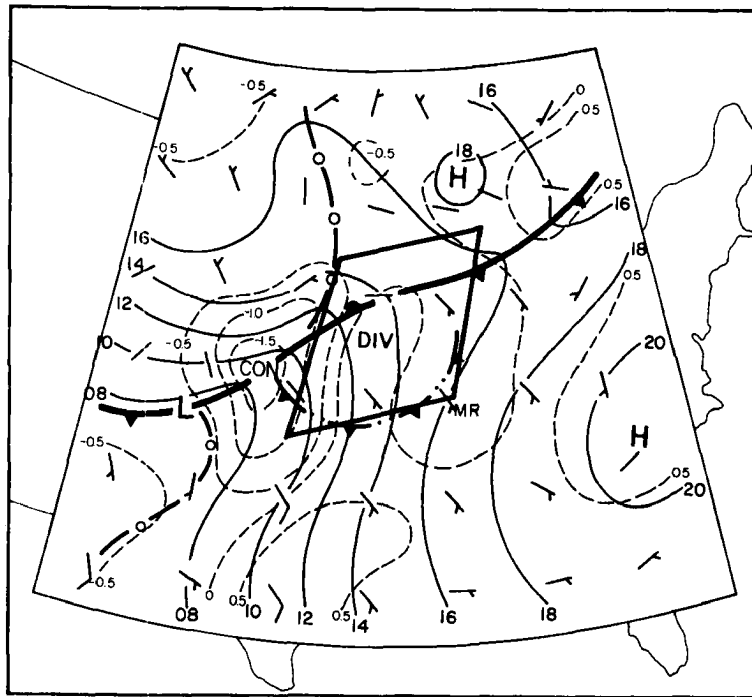


Fig. 22a. Analysis of surface features at the time of the MCC. Details are similar to Fig. 15a.

are very light at this observation time. Corresponding surface analyses of temperature and mixing ratio are shown in Fig. 22b. The thermal ridge is now much more pronounced within the MR. This explains the subtle nature of the mesohigh observed at 1200 GMT. Presumably, the thermal ridge is due to the persistent cloud cover, rain and moistening that has occurred during the night in the MR. By 1200 GMT the surrounding large scale environment has cooled more rapidly (clear skies) than has the region beneath the MCC cloud shield. [Note that earlier in the MCC life-cycle surface temperature drops can be dramatic, as can the pressure fluctuations (refer to the surface observation time-series shown in Section II and Appendix C).] Absolute moisture contents have increased significantly within the MR (mixing ratios now exceed 15 g/kg). This is

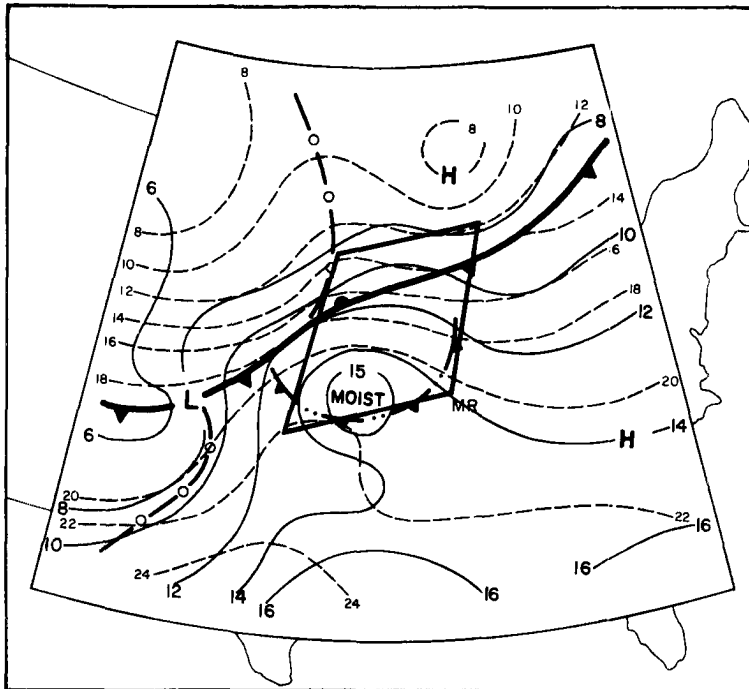


Fig. 22b. Analysis of surface features at the time of the MCC. Details are similar to Fig. 15b.

undoubtedly due to rainfall evaporation since relative humidities are near 100% across the entire MR!

An analysis of the 850 mb level is shown in Fig. 23. During the 12 h period separating analyses the MCC has developed and moved east-northeastward through the region of high moisture contents. A pocket of high mixing ratios (≥ 10 g/kg) is located in the southwestern portion of the MR. Temperatures have cooled markedly over the western third of the analysis area but have changed little over the MR. Temperature gradients remain strong and are primarily meridional. The most significant change at 850 mb has been the slight increase in wind speed and the substantial veering that has occurred as the diurnal cooling cycle has helped amplify the low-level jet (e.g., Pitchford and London, 1962; Bonner, 1966 and 1968; and Thompson et al., 1976). The veering of the low-level wind

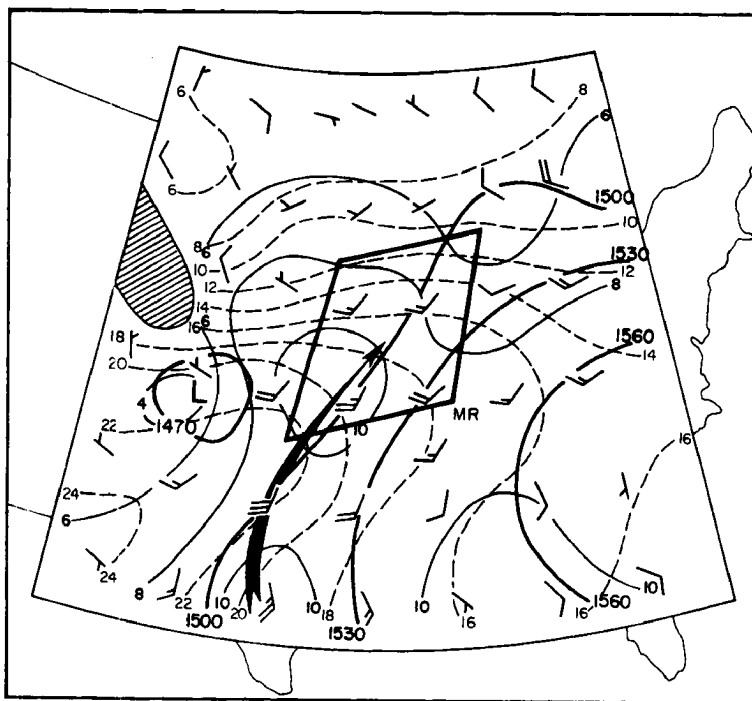


Fig. 23. Analysis of 350 mb level at the time of the MCC. Details are similar to Fig. 16.

presumably reflects both the advance of the aforementioned short-wave trough and inertial oscillations caused by the rapid change in eddy viscosity that takes place around sunset (i.e., the decoupling of the lower several kms from the surface friction layer, see Hoxit, 1975). A strong [> 30 kt (~ 15 m s $^{-1}$)] southwesterly low-level jet now enters the southwestern portion of the MR. Note that this low-level jet has not developed in response to strong cyclogenesis over the Plains (see Uccellini, 1980). Also observe that the MR is still located within a region of strong warm advection.

The 700 mb analysis (Fig. 24) at the time of the MCC indicates significant changes. Flow over the MR is now west-southwesterly (as it was 12 h earlier over the GR) and has increased dramatically in speed [> 10 kt (~ 5 m s $^{-1}$)] so that a distinct jet is present over the MR

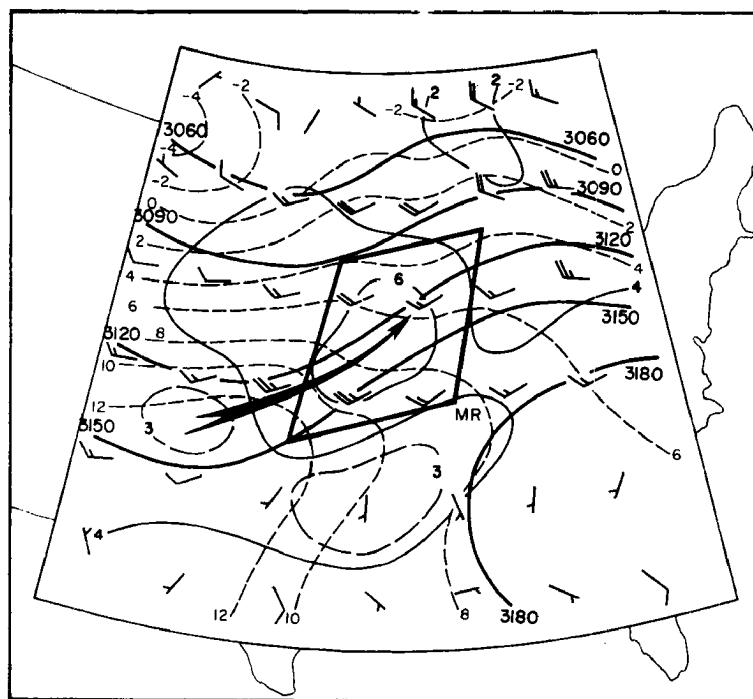


Fig. 24. Analysis of 700 mb level at the time of the MCC. Details are similar to Fig. 16.

(note that speeds are about the same as at 850 mb). The short-wave trough/ridge pattern has clearly moved eastward at about the speed of the system. A strong south to north temperature gradient is still present. It is important to notice that 700 mb temperatures in the MR region have changed very little in the face of almost 12 continuous hours of apparent strong warm advection. Bosart and Sanders (1981) noted similar characteristics with the long-lived convective system that they studied. At 1200 GMT the region of significant cross isotherm flow almost perfectly delineates the MCC region. It is likely that the small actual temperature changes are explained by persistent ascent based somewhere below 700 mb. Moisture contents are now very high over the MR (maximum relative humidities are $\sim 80\%$) with pronounced drying apparent to the south of the MCC's track.

At 500 mb (Fig. 25) a number of important changes are evident. The MR is characterized by high moisture contents and central relative humidities exceeding 85%. Mixing ratios now exceed 3 g/kg which is considerably larger than any values present over the entire domain 12 h earlier. This increase is due to vertical advection from lower layers. The short-wave trough/ridge pattern has moved eastward with heights rising to the northeast of the MR and falling to the northwest. Height and wind contours appear to reflect both the short wave and a local perturbation within the MR so that precise location of the short wave is difficult. The isotherm pattern indicates a distinct warm ridge over the MR with cold advection to the east and northeast. Winds at 500 mb have veered and increased slightly to the rear of the MCC with maximum speeds now exceeding 40 kt ($\sim 20 \text{ m s}^{-1}$).

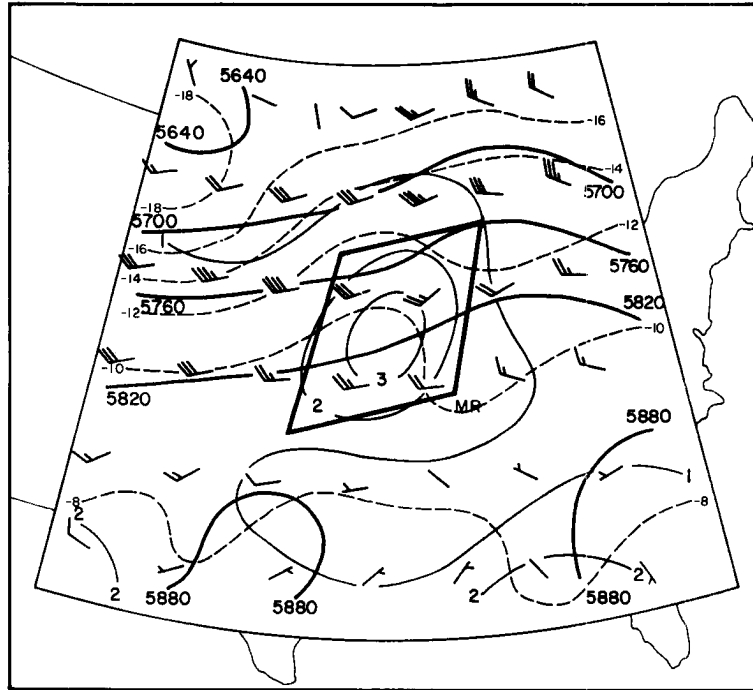


Fig. 25. Analysis of 500 mb level at the time of the MCC. Details are similar to Fig. 16.

At 300 mb (Fig. 26) effects of the MCC are even more apparent. A large "bullseye" of high moisture contents is centered over the MR, apparently reflecting a large region of ascent and/or moistening by mixing from convective towers. The MCC exhibits a very distinct warm core at 300 mb with cold advection occurring on the west side of the MR and warm advection on the east side. The development of this distinct warm core may be partly due to differential radiation effects (strongest nocturnal cooling occurring in the clear regions surrounding the MCC). McBride and Gray (1980a and b) have shown that radiational forcing may play an important role in the maintenance of tropical cloud clusters and this could also be true for MCCs. Winds have changed dramatically, veering and decreasing southwest of the MR while backing and increasing over the western portion of the MR. A strong jetstreak has developed

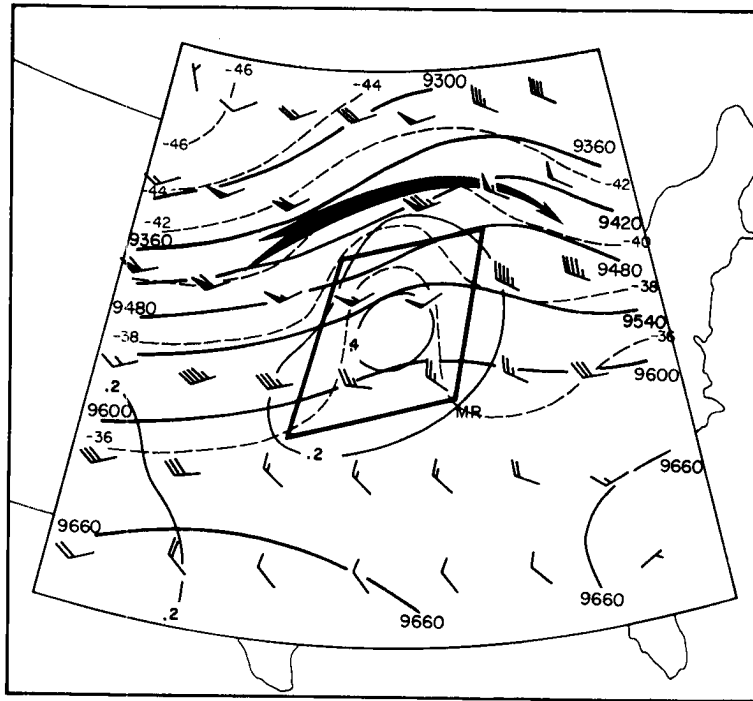


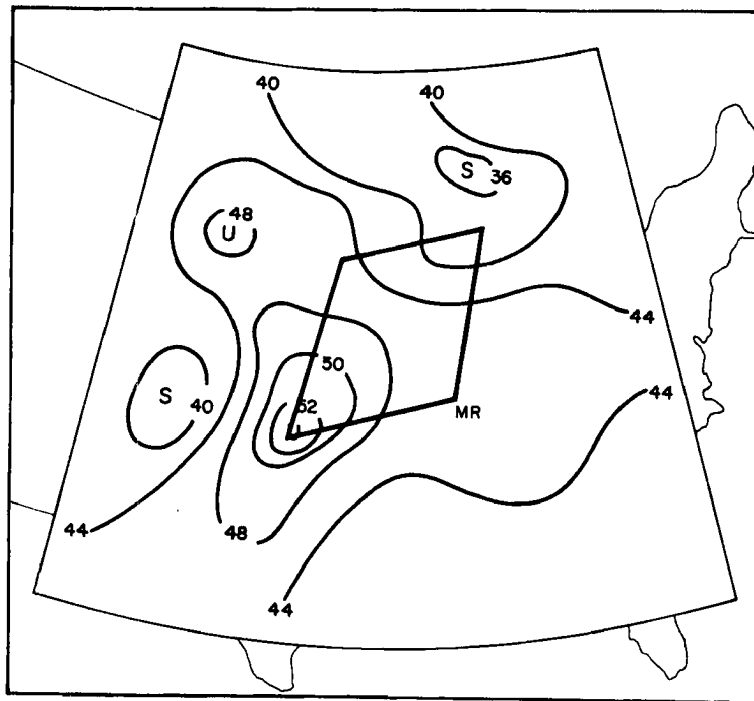
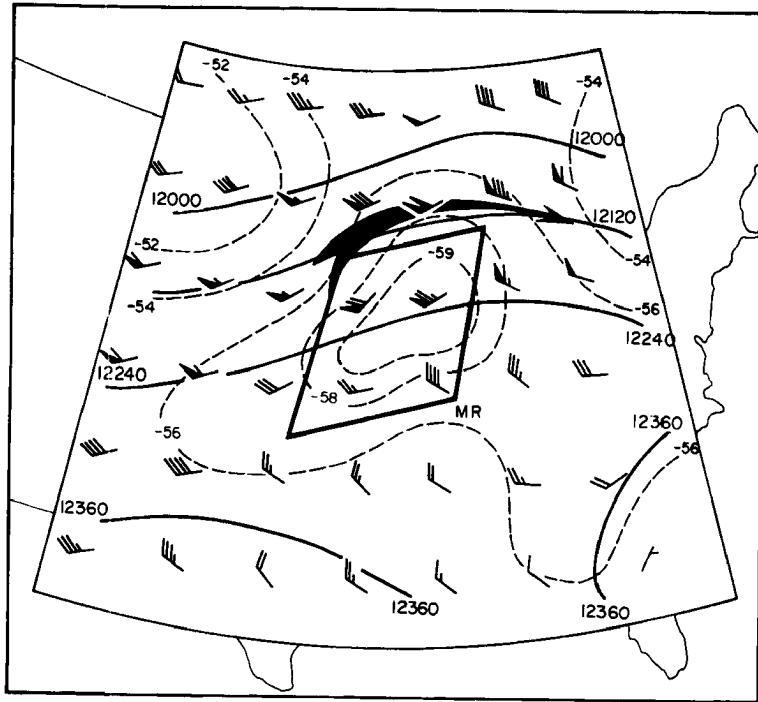
Fig. 26. Analysis of 300 mb level at the time of the MCC. Details are similar to Fig. 16.

just to the north of the MCC (speeds to the north of the MR far exceed any speeds analyzed 12 h earlier) and the flow is much more diffluent over the MR region.

Features at 200 mb, shown in Fig. 27, exhibit similar significant changes. Winds have increased dramatically north of the MR while substantially decreasing to its southwest. An anticyclonically curved jet-streak [speeds, now ~ 100 kt (~ 50 m s $^{-1}$), exceed any 200 mb speeds analyzed 12 h earlier by > 30 kt (~ 15 m s $^{-1}$)] has developed along the northern and northeastern periphery of the MCC. Strong diffluence is now evident (contrast Fig. 27 with Fig. 20). Similar increases in upper-level diffluence over smaller convective storm systems has been found by Shmeter (1969), Fankhauser (1969 and 1974) and Ninomiya (1971a and b). Temperatures are much cooler ($> 3^{\circ}\text{C}$) over the system indicating a distinct cold core at this level. This cooling is probably a reflection of

Fig. 27. Analysis of 200 mb level at the time of the MCC. Details are similar to Fig. 16.

Fig. 28. Analysis of the Totals stability index at the time of the MCC.



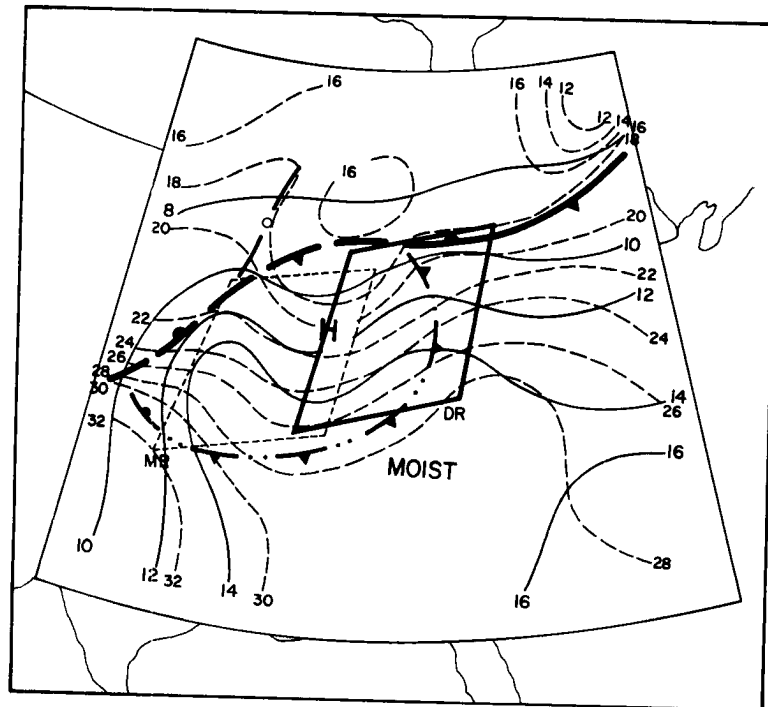
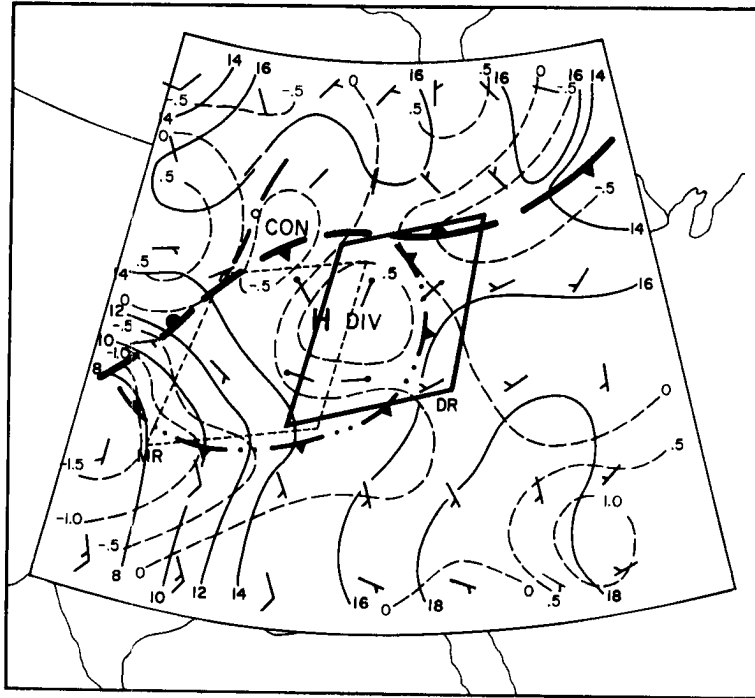
radiation effects (see Griffith et al., 1980) and persistent meso- α scale lifting at 200 mb. The stability analysis for the time of the system (Fig. 28) shows a continuing pocket of very unstable air present over the southwest corner of the MR. However, it appears that the MCC is moving east-northeastward into a region characterized by a much more stable air mass.

III.3 Conditions Over the Decay Region (DR)

An analysis of surface features, sea level pressure and divergence for 12 h after the MCC (Fig. 29a) shows that features have generally become very diffuse and difficult to locate. An anticyclonic circulation and attendant divergence mark the region of the decayed MCC. The MCC mesohigh is apparently still (12 h later) attended by a weak outflow boundary. Convergence along this feature may on occasion play an important role in triggering convection on the afternoon following the MCC (see Miller, 1967; Purdom, 1979; Bosart and Sanders, 1981; and Wetzel et al., 1981). The region of lower surface pressures and strong convergence has been left behind over the Plains. The large scale frontal zone appears to have weakened over the Plains. Surface temperature and mixing ratio fields (shown in Fig. 29b) indicate that the DR is within and just ahead of a pronounced cool thermal trough (note that 12 h earlier the MR was characterized by a warm thermal ridge -- Fig. 22b). This change in thermal characteristics most likely results from decreased insolation in the DR due to cloud cover and to evaporational cooling associated with the weakening region of shower activity. Meridional temperature gradients remain strong while longitudinal gradients remain weak. Mixing ratios are higher over the DR and comparison with Fig. 22b shows that a moist axis is associated with the decaying MCC.

Fig. 29a. Analysis of surface features 12 h after the MCC. Details are similar to Fig. 15a.

Fig. 29b. Analysis of surface features 12 h after the MCC. Details are similar to Fig. 15b.



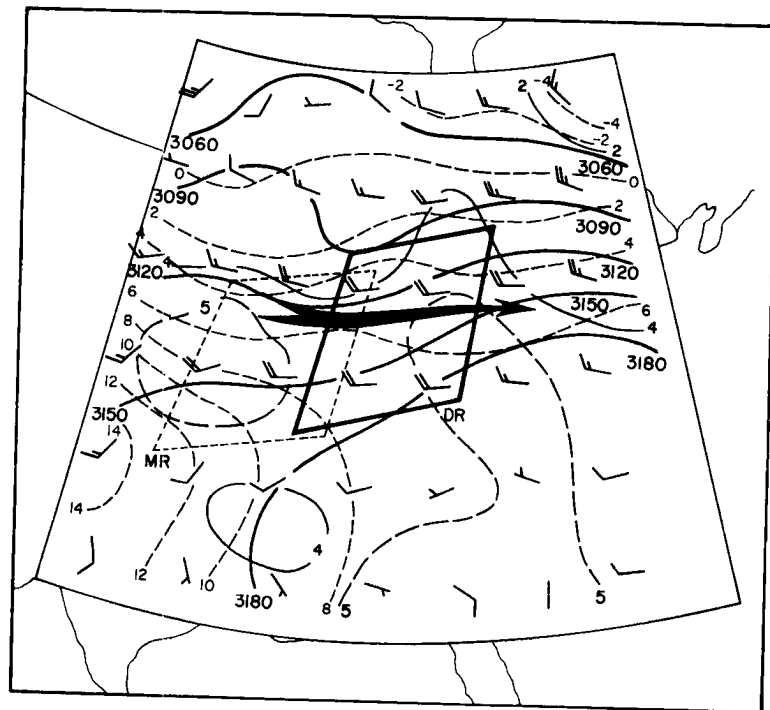
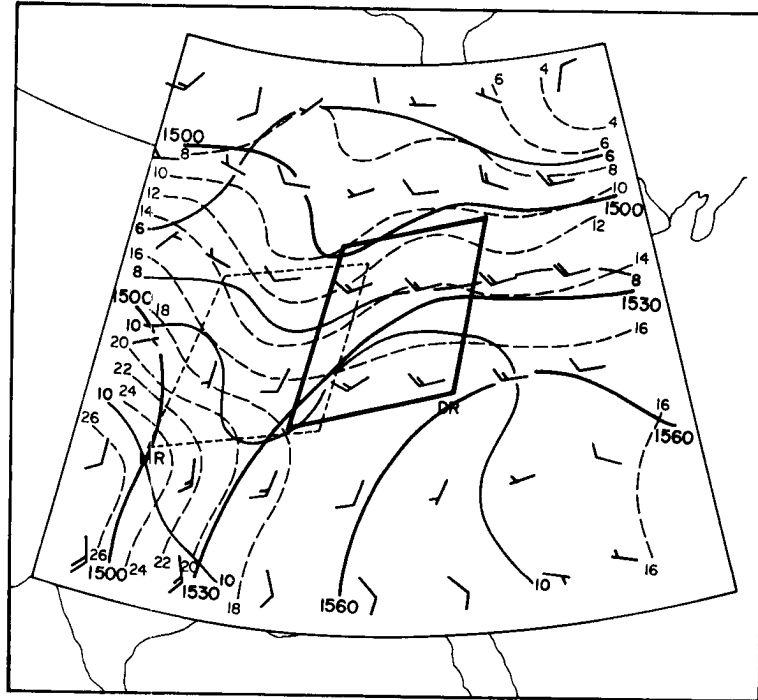
The 850 mb analysis shown in Fig. 30 indicates that significant changes have occurred during the 12 h that elapsed since Fig. 23. Although the strongest temperature gradients remain meridional, a cold trough is evident at the western edge of the DR. Most striking is the change in temperature advection patterns. The DR now contains a region of cool advection, whereas 12 h earlier the entire MR had been characterized by strong warm advection. A pronounced low-level jet is no longer present anywhere over the analysis domain and winds over the DR parallel the MCC's direction of movement. Drying has occurred over the MR, with slight moistening over the DR (maximum relative humidity over the MR is $\sim 75\%$). Over the MR region winds have backed and weakened over the south 2/3rds and veered over the northern 1/3 as the weak short-wave trough moved northeastward.

At 700 mb (Fig. 31) a ridge of higher moisture contents (a reflection of the weakening precipitation system and its attendant cloud debris) is moving east-northeastward with the MCC. The flow is now characterized by a broad band of westerlies with speeds near 20 kt ($\sim 10 \text{ m s}^{-1}$). The change in character of the thermal advection patterns is again remarkable. The DR is dominated by neutral or cool advection. The short-wave trough is now more pronounced in the height and temperature fields but the wind and height fields indicate geostrophic imbalance.

At 500 mb (Fig. 32) the short-wave trough is very pronounced in the height and temperature fields. However, the wind fields are again not well balanced with the height field. There is now pronounced cold advection into the ridge east of the DR and slight warm advection into the trough to the west of the DR. A pocket of relatively high mixing ratios has continued eastward with the system (also note that significant drying

Fig. 30. Analysis of 850 mb level 12 h after the MCC. Details are similar to Fig. 16.

Fig. 31. Analysis of 700 mb level 12 h after the MCC. Details are similar to Fig. 16.



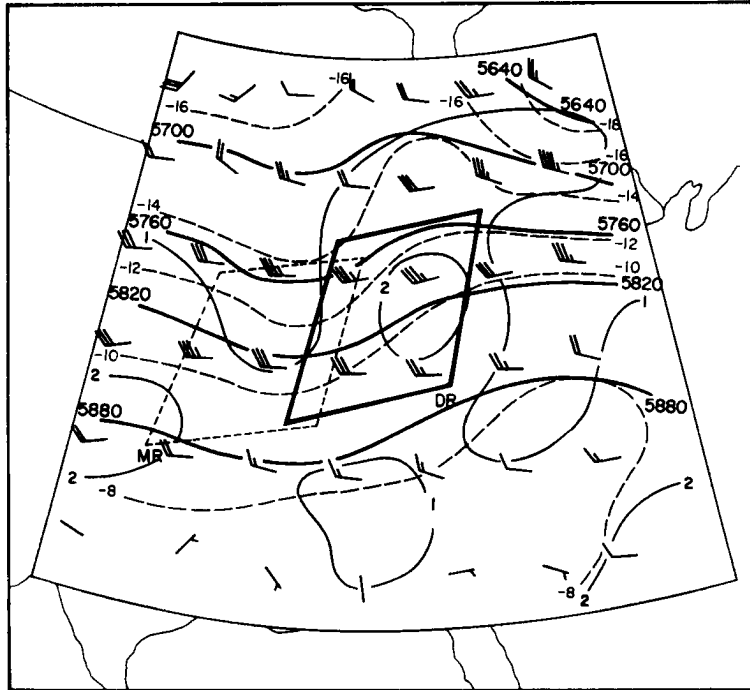


Fig. 32. Analysis of 500 mb level 12 h after the MCC. Details are similar to Fig. 16.

occurred over the MR as the MCC moved eastward). The entire MCC life-cycle has been linked to the eastward progression of the meso- α scale short-wave trough (wavelength approximately equal to twice the MCC diameter, or ~ 1500 km), but this short wave moved eastward through a larger scale pattern that changed little during the 24 h period considered.

The 300 mb analysis (Fig. 33) also indicates a well defined trough in the height and temperature fields and a pattern of marked up-gradient flow (i.e., kinetic energy being destroyed) over and downstream from the DR. The anticyclonic jetstreak apparent in Fig. 26 12 h earlier has moved eastward relative to the MCC, its curvature has become less pronounced and its speeds decreased. Moisture has moved with (and perhaps been advected downstream from) the MCC system.

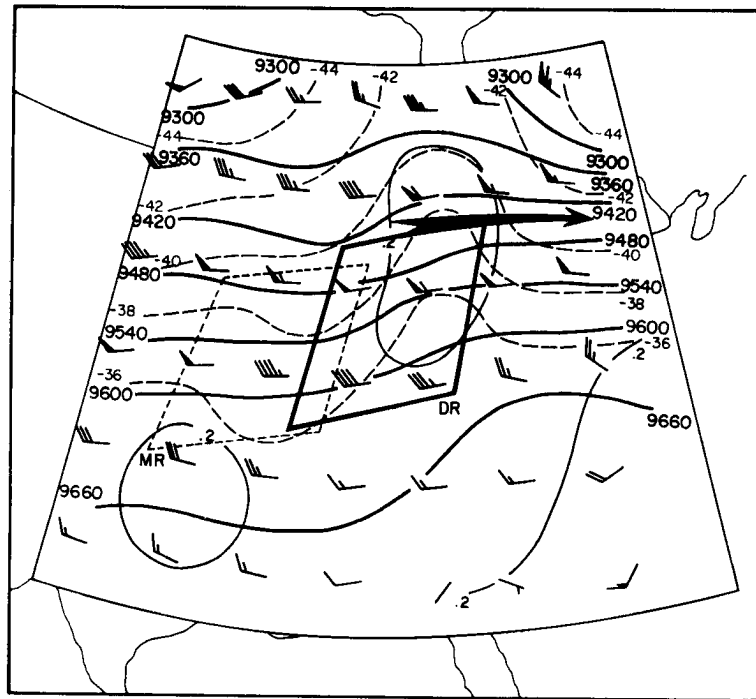


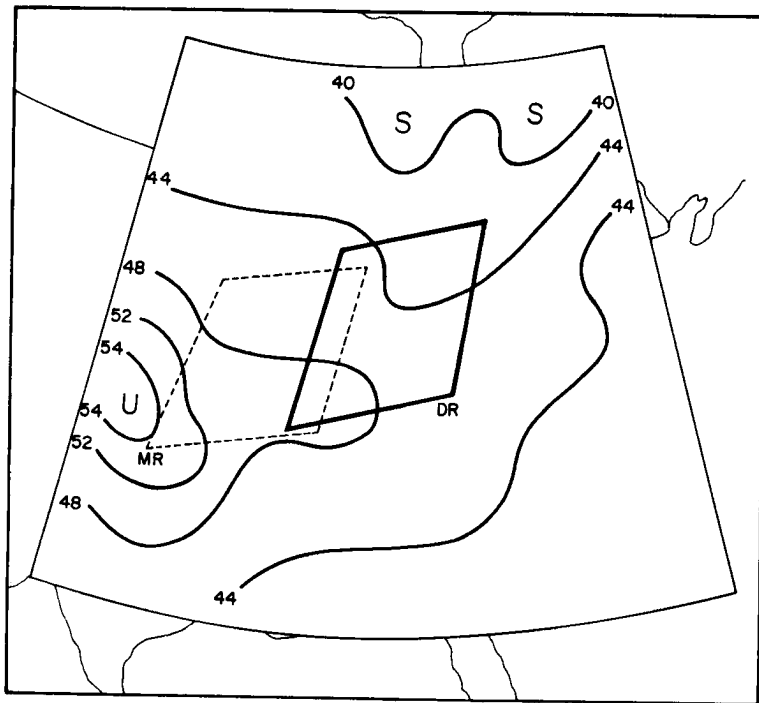
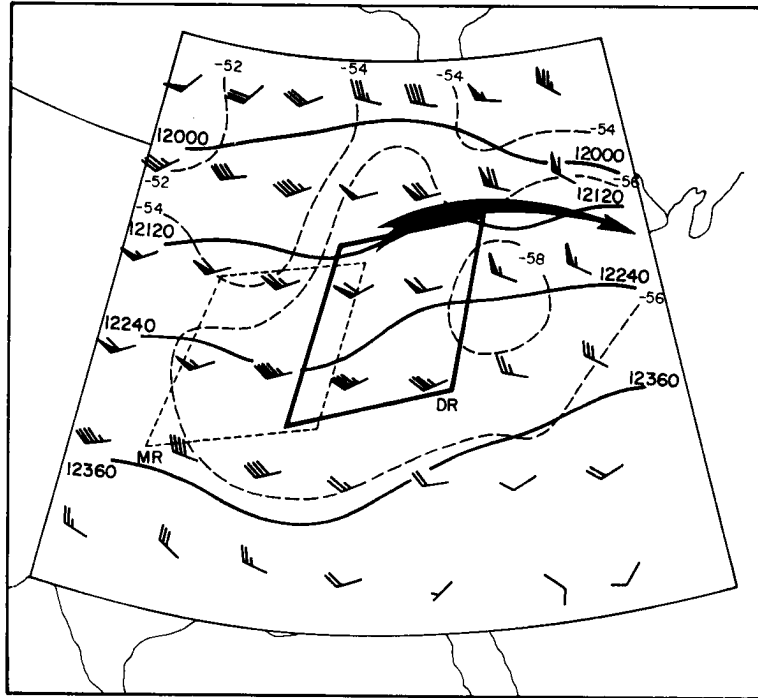
Fig. 33. Analysis of 300 mb level 12 h after the MCC. Details are similar to Fig. 16.

Overall, the conditions at 200 mb (Fig. 34) might be best described as chaotic. The height field exhibits a short-wave trough, ridge, trough pattern while the wind field presents a broad ridge. Once again the flow is strongly up-gradient downstream from the DR. The intense jetstreak that existed 12 h earlier (Fig. 27) has weakened, lost much of its anti-cyclonic curvature and moved downstream relative to the system. A large region of cooler temperatures is indicated and a small pocket of cooler air appears to have been advected downstream from the MCC.

The stability analysis (Fig. 35) shows that the MCC weather system has moved into a relatively stable region and that the most unstable conditions are now far to the west and southwest over the Plains. Comparison with Fig. 21 indicates that the stability pattern over the U.S. actually changed little during the entire period analyzed. Therefore, one of the most important factors in the decay of the composite system

Fig. 34. Analysis of 200 mb level 12 h after the MCC. Details are similar to Fig. 16.

Fig. 35. Analysis of the Totals stability index 12 h after the MCC.



is its eastward progression into an increasingly unfavorable environment for deep convection.

III.4 Relative Flow Fields

As discussed in Appendix B, the composite MCC moved to the east-northeast at $\sim 11 \text{ m s}^{-1}$. System-relative winds were computed for all of the objectively analyzed wind fields. The relative flow for the total wind at 850 mb before, during and after the MCC system is shown in Fig. 36 along with diagnosed vertical motions for the total wind (refer to Appendix B for an explanation of the vertical velocity calculations). During initial stages (Fig. 36a) relative flow at low levels is quite strong [$> 20 \text{ kt}$ ($\sim 10 \text{ m s}^{-1}$)] over the GR with inflow along the leading (east) and right (south) edges of the GR. The relative flow parallels the left

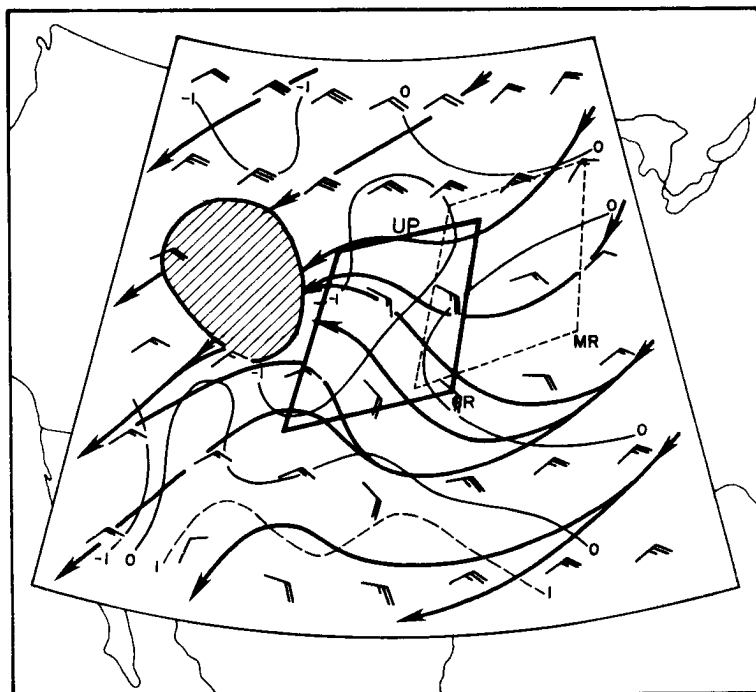


Fig. 36a. 850 mb relative flow 12 h before the MCC. Streamlines are shown with relative winds (full barb = 10 kt or $\sim 5 \text{ m s}^{-1}$) plotted at every other grid point. Contours of omega in $\mu\text{bar s}^{-1}$ (light solid and dashed lines) are shown for the total flow. Cross-hatched region is area where terrain elevation is above the 850 mb level.

(north) edge and exits the GR through the trailing (west) edge. Upward motion is occurring over almost all of the GR. (Note that ω of $1 \mu\text{bar s}^{-1}$ is approximately equal to 1 cm s^{-1} at 800 mb and to 2 cm s^{-1} at 350 mb.) At the time of the MCC (Fig. 36b) relative flow is much weaker [only on the order of 10 kt (5 m s^{-1})] over the MR. This is a result of the previously mentioned marked veering of the low-level flow that occurred during the night. Inflow continues along the leading and right edges of the system with outflow through the trailing edge. The stability analyses presented earlier indicate that the MCC feeds off the unstable air to the east and south of its track during its initial and mature stages. Relative inflow should maximize along the right edge of the system shortly after local midnight as the low-level wind undergoes its nocturnal oscillation (Bonner, 1968; Hoxit, 1975; and Thompson et al., 1976). Thus it is not surprising that satellite and radar data often



Fig. 36b. 850 mb relative flow at the time of the MCC. Details are similar to Fig. 36a.

indicate the most intense convective elements within the southern 1/3rd of the MCC system (refer back to Fig. 9a) although upward vertical motion is indicated over the entire MR region, with subsidence to the east and northwest.

The low-level relative flow fields shown in Figs. 36a and b are in some ways (easterly component of flow into the leading edge of the system and out of the trailing edge) quite similar to the relative flow fields found in both tropical and midlatitude squall lines (e.g., Houze, 1977; Zipser, 1977 and 1979; Moncrief and Miller, 1976; Betts et al., 1976; Riehl et al., 1974; Newton and Newton, 1959; and Newton, 1966). However, the three-dimensionality of the MCC situation is quite distinct. The fact that the most unstable air flows into the system from the right side makes it different than most of the squall systems studied by the researchers listed above (these squalls were considered as essentially two-dimensional systems with the unstable, low-level fuel supply lying directly ahead of the system). That lines of intense convective elements within MCC systems often are oriented parallel to their movement (and mid- to upper-tropospheric winds, refer to Figs. 9a and b) also distinguishes them from the other systems studied (the more typical convective line being oriented nearly orthogonal to the mid- and upper-level flow).

By the time the MCC system has decayed (Fig. 36c) the configuration of the relative low-level flow has changed markedly. Relative inflow now occurs on the leading and left edges with outflow continuing along the trailing edge. Subsidence is now diagnosed over much of the DR with upward motion indicated only in the northern portion. Comparison with Fig. 35 shows that the system is ingesting low θ_e , stable air -- a fact

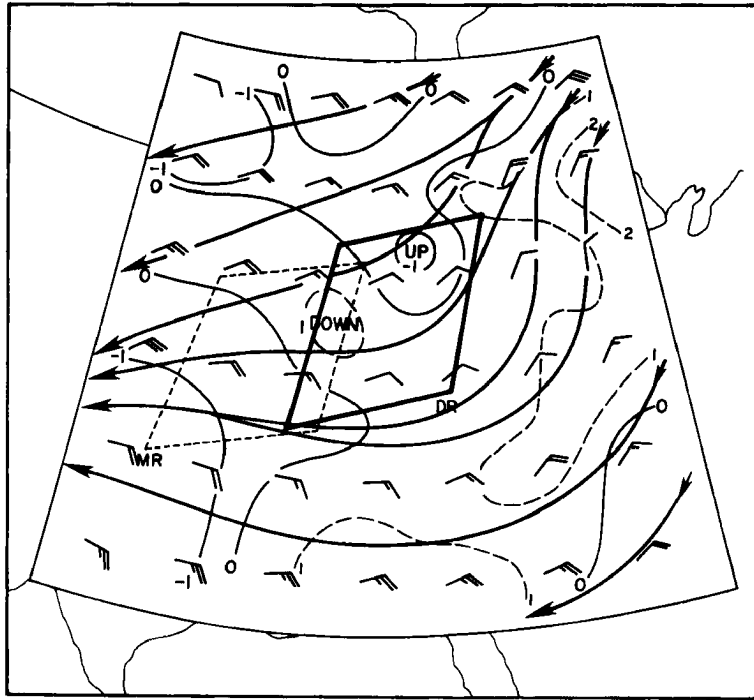


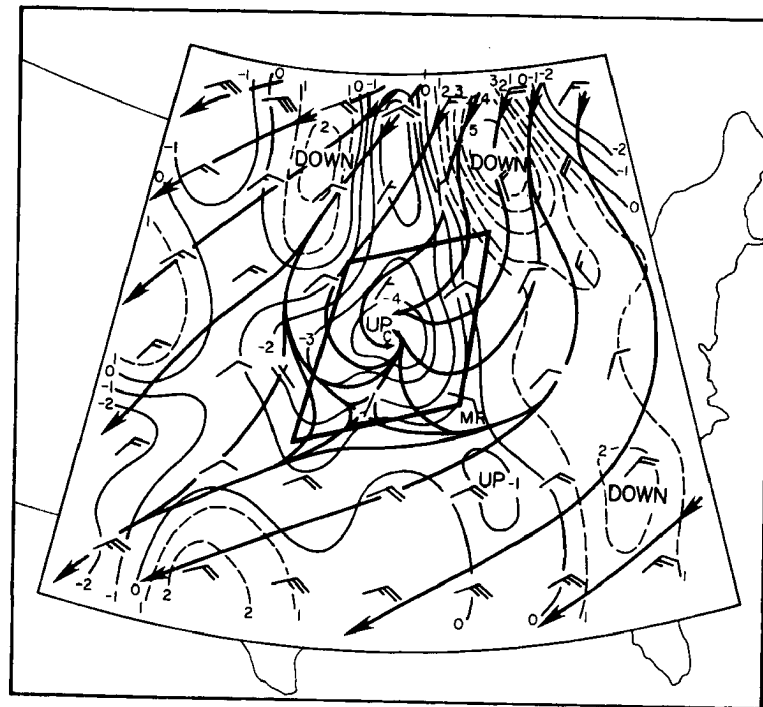
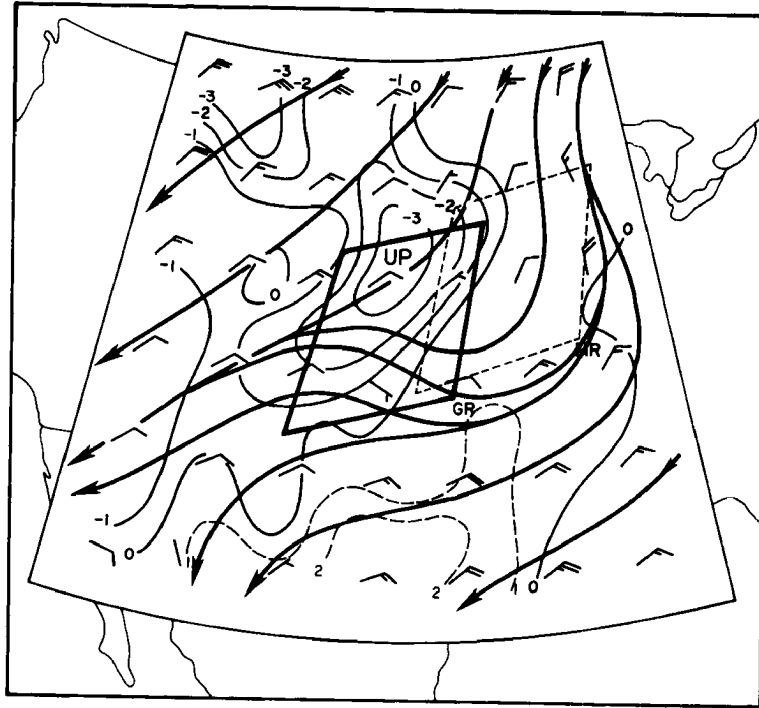
Fig. 36c. 850 mb relative flow 12 h after the MCC. Details are similar to Fig. 36a.

that undoubtedly contributes to its rapid demise between the times of Figs. 36b and 36c.

Corresponding relative flow fields at 700 mb are shown in Fig. 37. As the MCC system is initiating (Fig. 37a), weak relative inflow occurs primarily along the leading edge of the system with outflow along the trailing edge. This is similar to the tropical situation but somewhat different than midlatitude severe storm structure where relative 700 mb inflow occurs on the right or trailing edges (Maddox, 1976; and Darkow and McCann, 1977). Vertical motion over most of the GR region is upward with strongest vertical motion occurring over northern portions. Subsidence is occurring over the MR region to the east. At the time of the MCC (12 h later, Fig. 37b) the MR is characterized by significant upward motion centered within the MCC system. Strong subsidence is occurring NW and NE of the MR. The 700 mb relative flow has changed tremendously

Fig. 37a. 700 mb relative flow 12 h before the MCC. Details are similar to Fig. 36a.

Fig. 37b. 700 mb relative flow at the time of the MCC. Details are similar to Fig. 36a.



during this period with inflow now occurring through all sides of the system (contrast this with the relative flow over the MR in Fig. 37a). A closed cyclonic circulation is present at the center of the MCC system. This abrupt change in the flow field reflects a strong meso- α scale circulation that has developed in conjunction with the MCC.

Twelve hours later (Fig. 37c) the 700 mb relative flow fields have again changed dramatically. Weak inflow is now occurring along the left edge of the system with outflow along the right edge. Much of the DR exhibits subsidence, with upward motion only along northern portions. Comparison of Fig. 37c with Fig. 31 shows that very cool and dry 700 mb air is beginning to flow into the system.

Relative flow fields at 500 mb are presented in Fig. 38. During the initiation phase (Fig. 38a) of the MCC, relative flow at 500 mb is

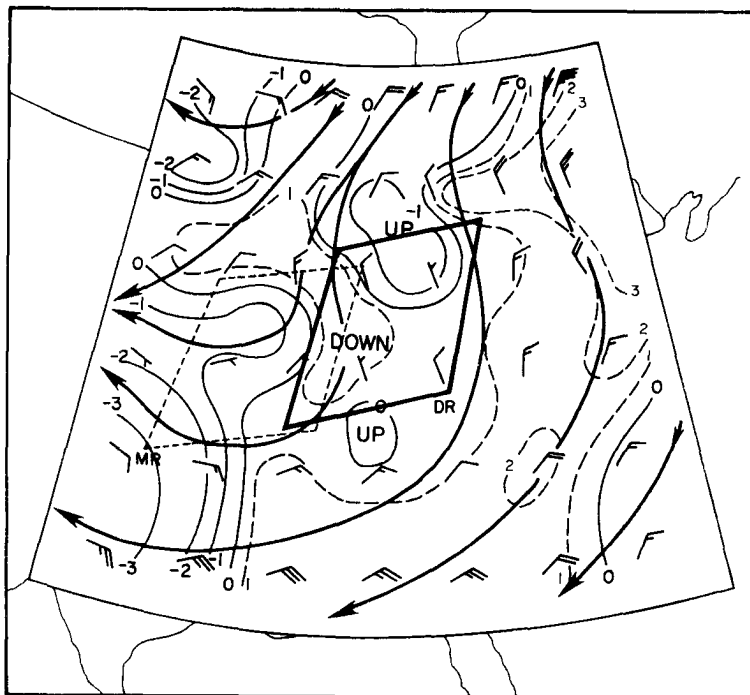


Fig. 37c. 700 mb relative flow 12 h after the MCC. Details are similar to Fig. 36a.

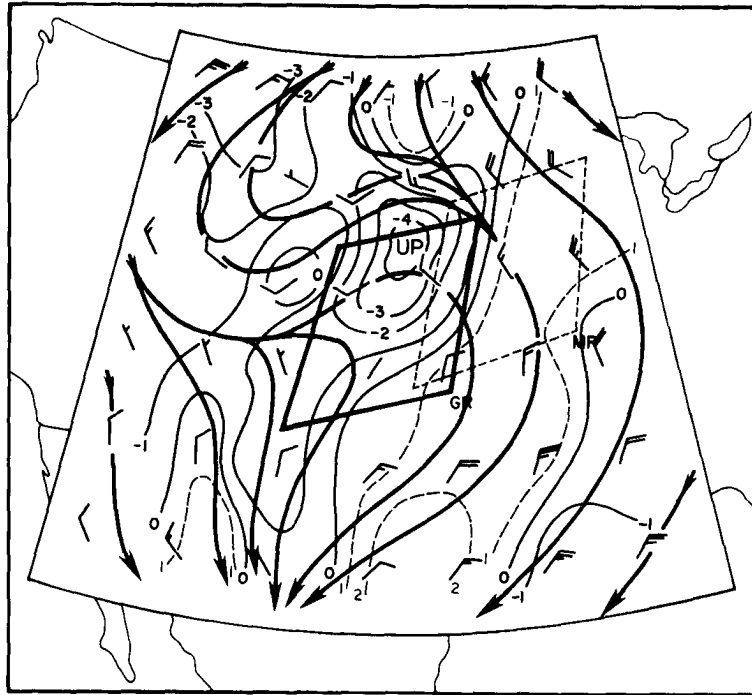


Fig. 38a. 500 mb relative flow 12 h before the MCC. Details are similar to Fig. 36a.

strongly diffluent over the GR. Weak inflow occurs along the trailing edge of the system with relative outflow along the leading and right edges. This pattern is considerably different than that usually associated with tropical systems. Significant upward motion is occurring over northern portions of the GR with subsidence over much of the MR. An important aspect of this precursor vertical motion field (presumably reflecting the approaching short-wave trough, the diurnal Plains-mountain orographic circulation and lifting along the east-west surface front) is that it is not directly advancing into the region of most unstable air (refer to Fig. 21) which is located to the south. Were this vertical motion field advancing directly into the very unstable air over the Plains a more typical severe squall line development might result.

At the time of the MCC system (Fig. 38b) the relative 500 mb flow is quite light (reflecting the fact that the system is moving nearly with

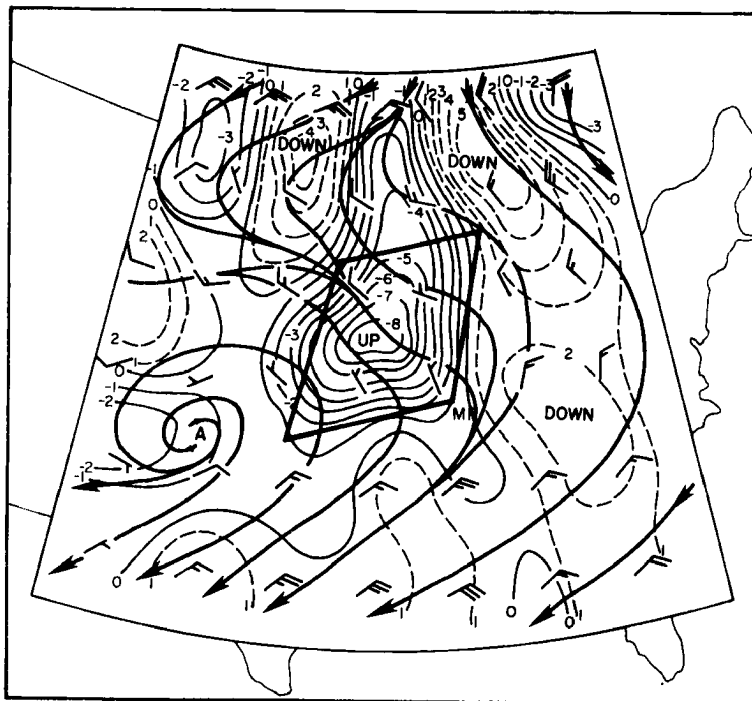


Fig. 38b. 500 mb relative flow at the time of the MCC. Details are similar to Fig. 36a.

the mean flow at this level). Weak inflow enters the trailing and left edges of the system and exits through the leading and right edges. An intense upward vertical circulation is centered within the MCC with strong subsidence to the northwest and northeast. Twelve hours later (Fig. 38c) the relative flow is stronger; however, it continues to enter the system from the northwest and exit to the southeast. The vertical motion field has lost its intense, highly organized character. Subsidence is occurring over much of the DR with pockets of upward motion to the north, south and west. Notice that the magnitude of the diagnosed motion has decreased fourfold as the system has continued to move into a convectively unfavorable environment.

The relative flow fields at 200 mb are shown in Fig. 39. As the MCC is developing (Fig. 39a) strong upper tropospheric flow enters the trailing edge of the GR and exits the leading right edges. This relative flow

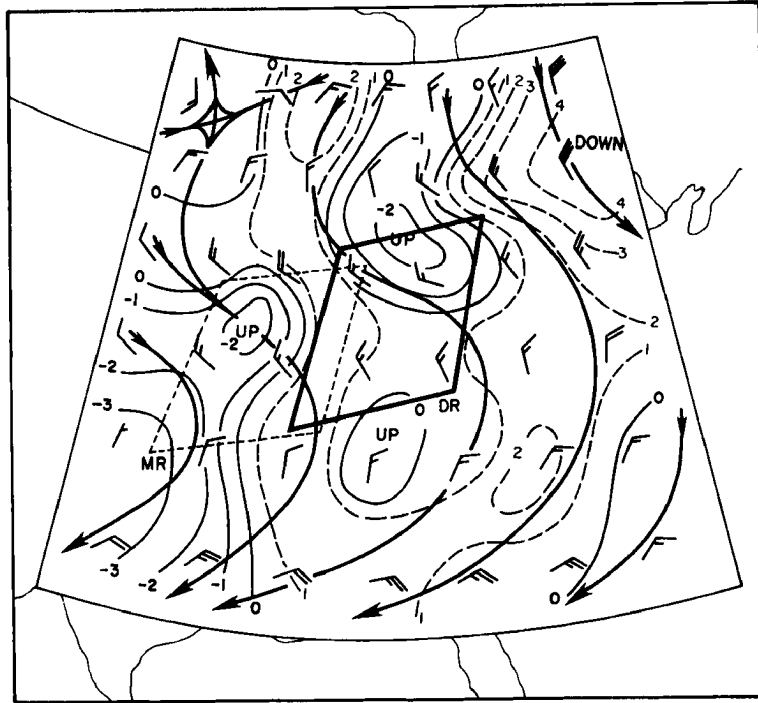


Fig. 38c. 500 mb relative flow 12 h after the MCC. Details are similar to Fig. 36a.

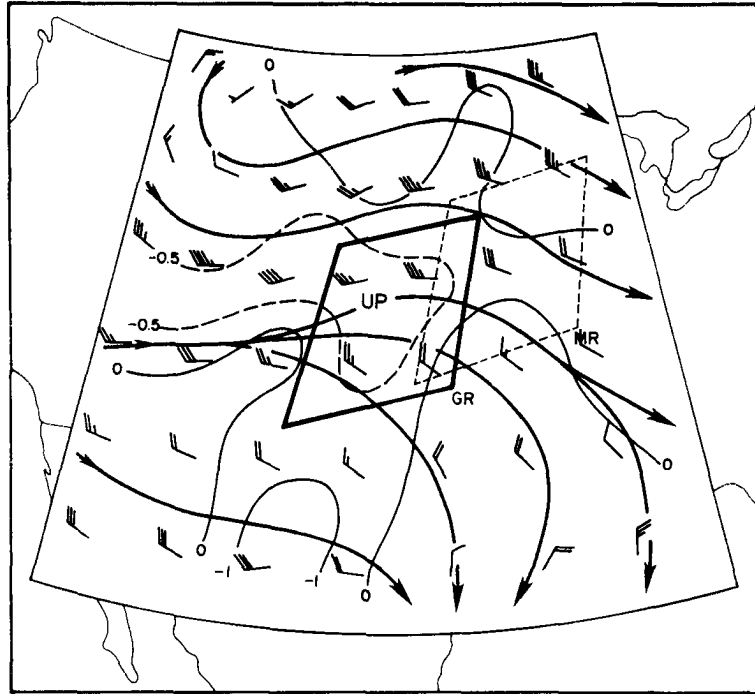


Fig. 39a. 200 mb relative flow 12 h before the MCC. Details are similar to Fig. 36a.

field is similar to those associated with midlatitude squall lines (e.g., Newton, 1966; and Browning and Ludlum, 1962) but much different than those often associated with tropical convective systems (e.g., Zipser, 1977 and 1979; Riehl et al., 1974). The tendency in the midlatitude convective system is for the anvil cloud and debris to spread out ahead of and to the right of the region of active convection. Since both tropical and midlatitude convective systems produce extensive regions of light precipitation [called "anvil precipitation" by Houze (1977) and Zipser (1977)] these important differences in anvil-level relative flow fields must be considered in developing physical explanations for the precipitation areas.

At the time of the MCC (Fig. 39b) tremendous changes are apparent in the relative flow aloft. Very weak inflow is present along the trailing edge of the MR with outflow across the other three boundaries. The strength of the relative outflow in the northeastern area of the MR is most impressive. The flow is extremely diffluent and is suggestive of upper-level

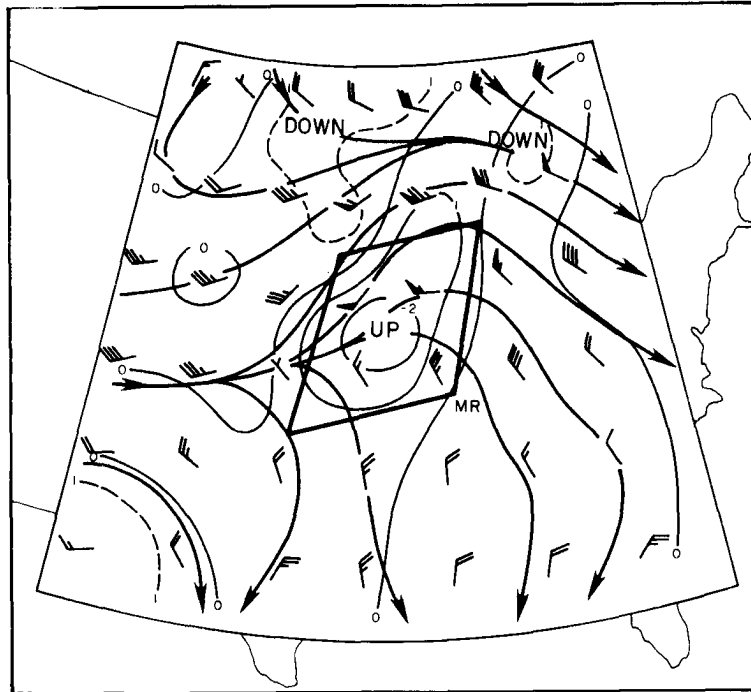


Fig. 39b. 200 mb relative flow at the time of the MCC. Details are similar to Fig. 36a.

outflow above hurricanes and typhoons. Strong upward motion is centered over the system. The strength and persistence of this upper tropospheric lifting is directly linked to the physical characteristics of the MCC system as seen in enhanced IR satellite views (i.e., the nearly circular, persistent, highly organized shield of very cold cloud). The relative flow field at the time of the system differs radically from those of either tropical or midlatitude squall lines.

Once the system has decayed (Fig. 39c) the upper tropospheric motion fields are more chaotic with both upward and downward motion over the DR. The relative flow is now somewhat similar to what it had been 24 h earlier with inflow across the trailing edge and outflow along the leading edge of the MR. Perhaps the most distinctive feature is the speed maximum in the relative flow moving away from the northeastern corner of the DR.

The MCC relative flow fields exhibit a number of characteristics that are qualitatively similar to the flows associated with both tropical

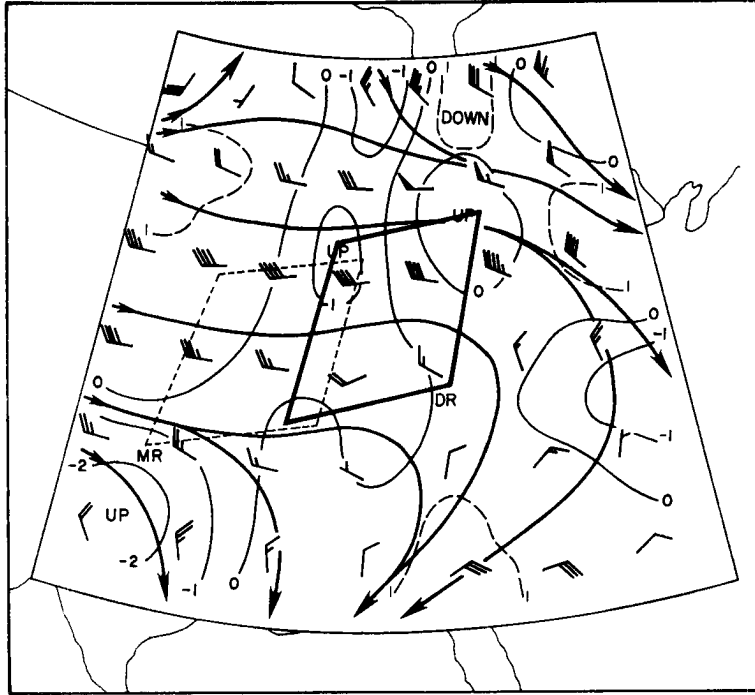


Fig. 39c. 200 mb relative flow 12 h after the MCC. Details are similar to Fig. 36a.

and midlatitude convective squall lines. However, the distinct three-dimensionality of the relative flows and their systematic changes in time distinguish the MCC system from other classes of convective weather systems. The precursor relative environmental wind hodographs shown in Fig. 40 illustrate, for three different types of convective systems, some

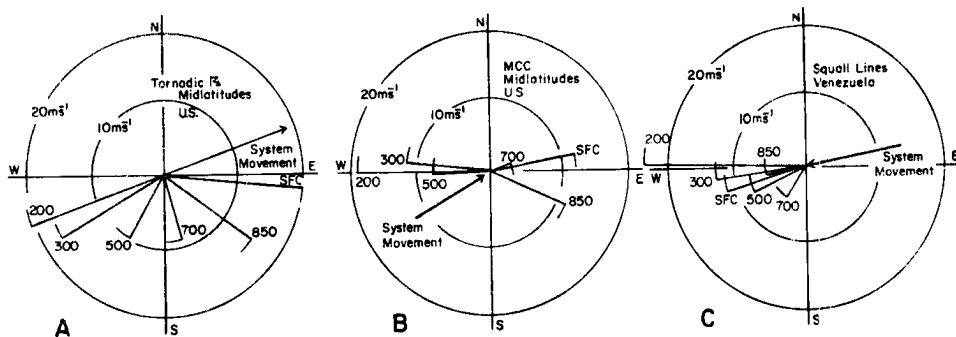


Fig. 40. Hodographs of the precursor relative wind fields for a) tornadoic thunderstorms central U.S. -- after Maddox, 1976; b) MCC central U.S.; c) tropical squalls in Venezuela -- after Betts, et al., 1976.

of the marked differences discussed above. Perhaps the most remarkable characteristic of the MCC is the marked change in the relative flow that occurs in time, apparently in response to the meso- α scale circulations associated with the mature system.

III.5 Vertical Profiles

Divergence and omega profiles have been averaged (following the MCC weather system) for the 12 interior grid points shown earlier in Fig. 14. The means obtained are representative of an area of $\sim 2.3 \times 10^5 \text{ km}^2$. The divergence profiles for before, during and after the MCC development are presented in Fig. 41. The profiles have been obtained from the

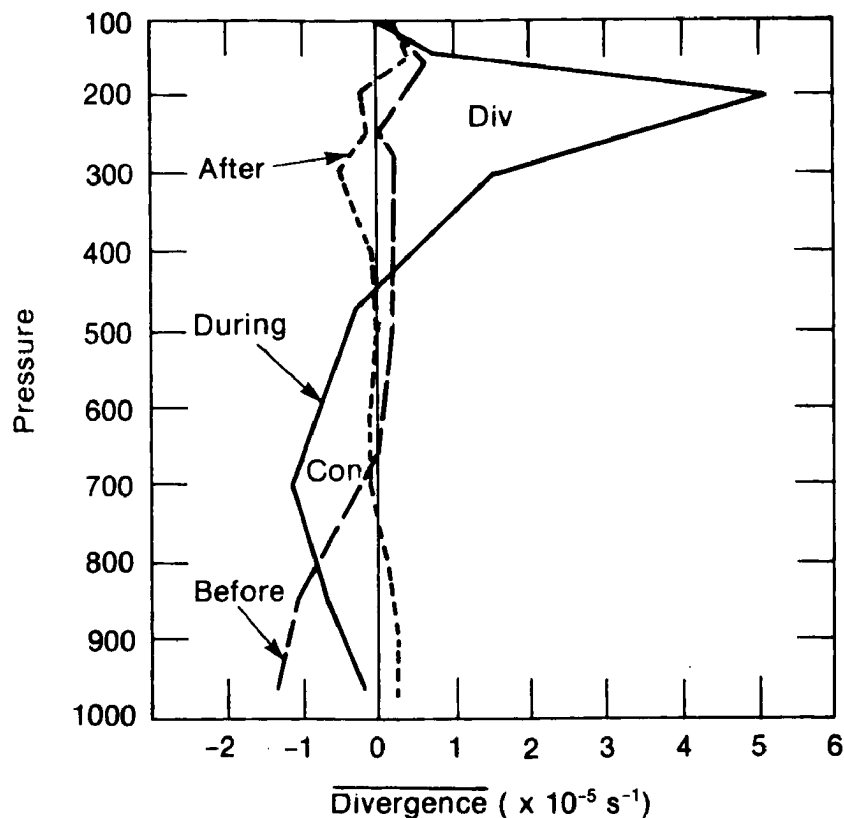


Fig. 41. Mean divergence (following the system) over 12 grid points within the MCC region -- see Fig. 14.

composited standard level analyses with no attempt made to impose mass balance. The GR (before profile) is characterized by strong low-level convergence (surface to ~ 750 mb) with a deep layer of weak divergence above. When the MCC has developed, the MR (during profile) is characterized by a deep layer of significant convergence (surface to ~ 500 mb) with a shallow layer (near 200 mb) of intense divergence above (maximum average $> 5 \times 10^{-5} \text{ s}^{-1}$). By the time the system has weakened (12 h later) the DR (after profile) is characterized by weak divergence near the surface (surface to 850 mb) and weak convergence aloft (near 300 mb). The evolution of these divergence profiles is similar to that found for tropical convective systems by Reed and Recker (1971), Riehl et al. (1974), Frank (1978) and Leary (1979) and for midlatitude systems by Nimomiya (1971a), Fankhauser (1974) and Bosart and Sanders (1981). The divergence profile at the time of the system is quite similar to that presented by Williams and Gray (1973) for intensifying tropical cloud clusters. Note that even though their average was computed over a smaller area ($\sim 1.9 \times 10^5 \text{ km}^2$) the MCC divergence values exceed those of the developing cloud cluster by more than a factor of two.

The resulting vertical motion fields (shown in $\mu\text{bars s}^{-1}$) are presented in Fig. 42 (refer to Appendix B for an explanation of the vertical velocity calculations). The pre-MCC average environment exhibits upward motion through the troposphere with a maximum occurring near 700 mb. At the time of the system the magnitude of the vertical circulation has increased fivefold with the maximum now in the vicinity of 500 mb. The upward flux through the mid-troposphere is comparable to that within the warm sector of a baroclinic cyclone (see for example Petterssen, 1956, chapter 17). Therefore, even though the summer months are relatively

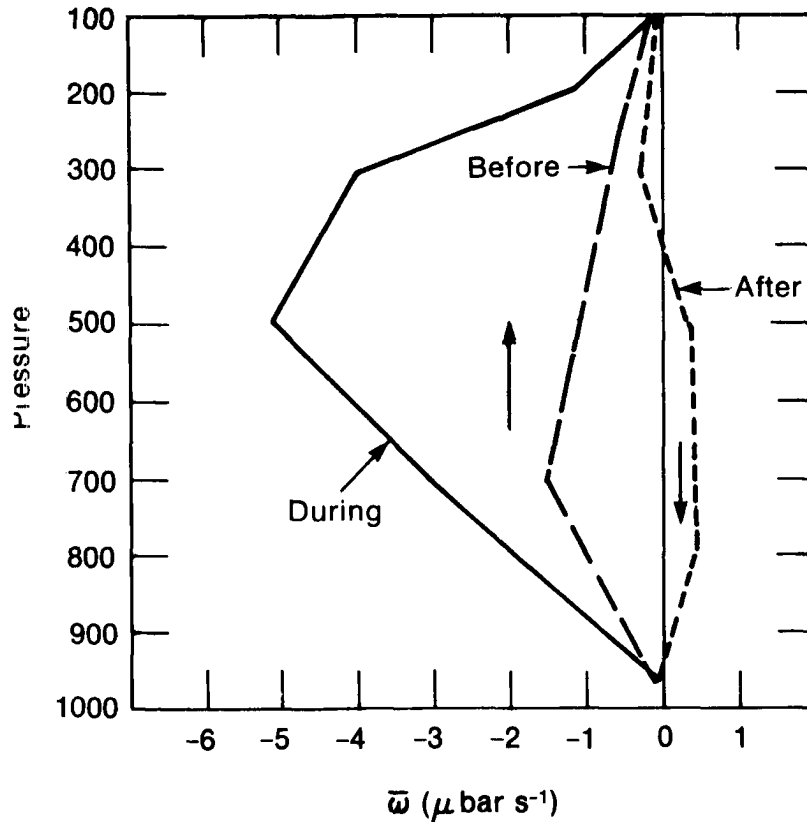


Fig. 42. Mean omega (following the system) over 12 grid points within the MCC region -- see Fig. 14.

quiet over the central U.S. in terms of intense baroclinic storms the frequent occurrence of MCCs and their associated large vertical circulations indicates that the summer months are certainly not tranquil. Once the system has weakened (after curve) a deep (surface to 500 mb) region of mesoscale subsidence is diagnosed with a shallow, residual layer of upward motion present in the upper troposphere.

The evolution of MCC vertical motion fields is also quite similar to tropical systems (see for example Frank, 1978 and Leary, 1979). However, there appears to be one significant difference. At the time of the MCC the system is characterized by a deep, mesoscale upward circulation that has its roots at low levels. This is in marked contrast to Zipser (1977) and Houze (1977) who found a region of lower tropospheric, mesoscale

descent beneath the region of "anvil rain" (i.e., immediately trailing the region of deep, active convection). A widespread and deep meso-downdraft appears not to develop in association with the MCC until it actually begins to decay. The vertical circulations diagnosed for the active MCC are thus somewhat similar to those attending the midlatitude, mesoscale, convective rainbands studied by Hobbs et al. (1980). The meso-updraft is apparently the mechanism responsible for maintaining the extensive shield of upper tropospheric cold cloud that characterizes the MCC in satellite images. Similar deep mesoscale updrafts associated with midlatitude convective systems have been diagnosed by Sanders and Paine (1975), Sanders and Emanuel (1977) and Ogura and Liou (1980). Ogura and Liou's results also indicate a mesoscale downdraft beneath a decaying system; however, their method of data compositing, coupled with rapid changes in the character of the convective system during the analysis period, makes interpretation of their results difficult. Numerical simulations of midlatitude convective systems by Krietzberg and Perkey (1977), Fritsch and Chappell (1980), Fritsch and Maddox (1981a), Maddox et al. (1981) and Chang et al. (1981) have produced similar mesoscale updrafts in response to parameterized convection. It is also important to note that Brown's (1977) two-dimensional simulation of a tropical system produced a deep, mesoscale updraft during the early stages of the system. It is proposed that, for the intense midlatitude MCC, the mature phase of the system is characterized by widespread precipitation produced within the mesoscale updraft region. Convective elements with varying intensity updrafts and downdrafts are embedded within this area; however, the general feature is a large meso-updraft. The decay of the MCC is marked by the development of mesoscale descent beneath the region of weakening

precipitation and residual cloud debris (note that a similar evolution has been numerically simulated by Chang *et al.*, 1981). The mesoscale downdraft may thus signal the abrupt demise of the MCC system; whereas, the organized tropical mesosystem may apparently persist for many hours after the meso-downdraft develops (see, for example, Houze, 1977; Brown, 1979; and Webster and Stevens, 1980).

Vertical profiles of the wind and θ_e at the grid points shown earlier in Fig. 14 (the five circles on the NW, SW, NE, SE corners and center of the MCC) are presented in Figs. 43a-e. The profiles are presented in an Eulerian framework (i.e., fixed points in space) and thus depict the evolution of θ_e and wind profiles as the MCC develops to the west, moves over and then east of the MR. The mean relative humidities and precipitable water from the surface to 300 mb are listed in Table 6 for each of the soundings shown in Fig. 43. At the NW corner of the MR (Fig. 43a) the θ_e profiles exhibit slight potential instability in middle levels.

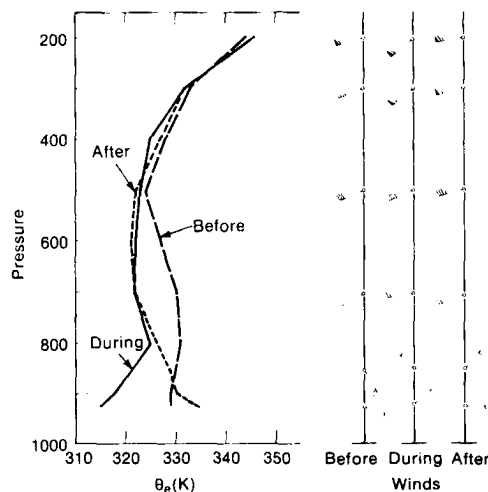
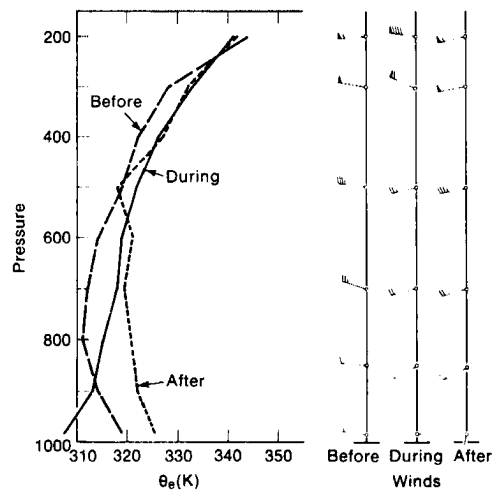
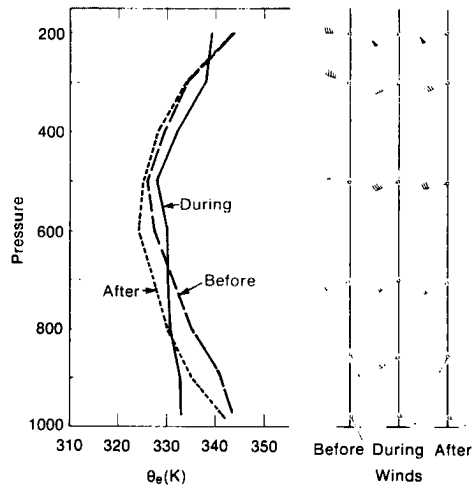
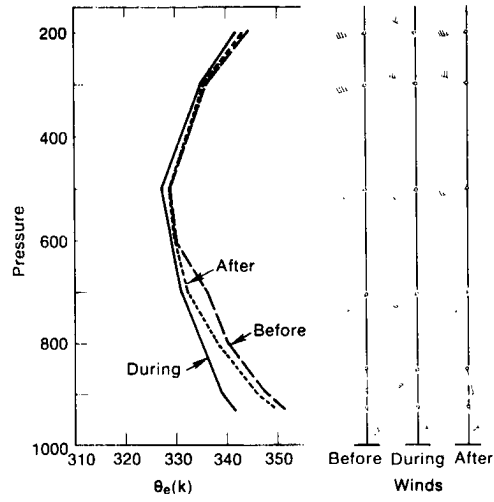


Fig. 43a. NW corner. Vertical profiles of winds aloft and θ_e before, during and after the MCC. Full wind barb is 10 kt^e or $\sim 5 \text{ m s}^{-1}$. Profile locations are indicated in Fig. 14.

Fig. 43b. SW corner

Fig. 43c. Center

Fig. 43d. NE corner



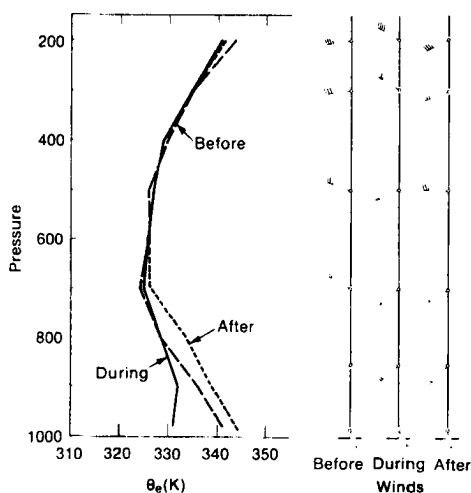


Fig. 43e. SE corner

The "during" and "after" profiles show pronounced decreases in θ_e . Slight cooling has occurred during the period along with considerable drying in middle levels (see Table 6). Strong diurnal cooling at low-levels is also evident (remember that the sounding times are 0000, 1200 and 0000 GMT). The wind profiles exhibit light winds at low-levels and west-southwesterly winds at mid-levels with little change through the analysis period. At upper-levels, however, the winds back and increase in speed at the time of the system. Moderate shear is indicated (850 - 200 mb) at all three times.

At the SW corner (Fig. 43b) the θ_e profiles change little with time and indicate that the atmosphere is potentially and convectively very unstable. Note that air lifted from as high as 600 - 700 mb is convectively unstable! The mean relative humidity and precipitable water (Table 6) do decrease slightly through the period; however, precipitable water contents remain greater than 3 cm through the period. This is the air mass that most likely fuels intense convective elements during the development and mature stages of the MCC system. Upper-troposphere winds veer and decrease in speed at the time of the system. In mid-levels, winds

Table 6

Mean Relative Humidities and Precipitable Water Surface to 300 mb

| | <u>Before</u> | <u>During</u> | <u>After</u> |
|-----------|---------------|---------------|--------------|
| NW corner | 58% | 50% | 47% |
| | 3.01 cm | 2.48 cm | 2.70 cm |
| SW corner | 45% | 42% | 40% |
| | 3.40 cm | 3.00 cm | 3.02 cm |
| Center | 50% | 76% | 46% |
| | 3.67 cm | 4.07 cm | 3.43 cm |
| NE corner | 42% | 53% | 55% |
| | 2.01 cm | 2.31 cm | 3.05 cm |
| SE corner | 47% | 52% | 46% |
| | 3.56 cm | 3.47 cm | 3.97 cm |

change little. At 850 mb the wind veers strongly and increases [from 25 to 30 kt (≈ 12 to 14 m s^{-1})]. The nocturnal increase in speed of the low-level jet has not been large but the change in direction has been substantial. Both before and during the system, winds are stronger at 850 mb than at 500 mb and, during the system, tropospheric winds are strongest at 850 mb. Wind profiles exhibiting similar "negative" shear profiles are often associated with heavy precipitation and flash flood events (Maddox *et al.*, 1978 and 1979). However, this is considerably different than the environment of the tropical squall which is characterized by a pronounced wind maximum at about the 700 mb level (see Mansfield, 1977 and Fernandez, 1980).

The θ_e profiles before and after the system at the central grid (Fig. 43c) are moderately unstable with the slight decrease in θ_e from before to after due primarily to slight drying (Table 6). The θ_e profile at the time of the system, however, shows the presence of a deep layer (surface to ~ 400 mb) of nearly uniform θ_e . This air is neutrally stable relative to its near environment. Winds at 850 mb veer and increase and vertical wind shear becomes quite small at the time of the system.

The sequential profiles of θ_e at the center grid convey the impression that the MCC system is cold core in the extreme upper and lower troposphere and warm core at mid-levels. Similar structure has been documented for both tropical and midlatitude convective systems, e.g., Riehl *et al.* (1973), Reed and Recker (1971), Ninomiya (1971a), Frank (1978), Ogura and Liou (1980), and Bosart and Sanders (1981). For the lower troposphere, however, this is in contrast to the picture conveyed by the two-dimensional analyses (see Fig. 22b) that indicate a warm core at the time of the system. Radiation, cloud cover and diurnal effects are probably responsible for this interesting paradox.

At the NE corner (Fig. 43d) the trend in θ_e in middle levels is reversed from that at the NW corner as θ_e increases (primarily due to moistening, see Table 6) markedly during the period. The vertical profiles are uniform and quite stable during and after the system. At the time of the system winds decrease in speed in mid-levels while veering slightly and increasing dramatically in speed [55 to 90 kt (~ 17 to 45 m s⁻¹) at 200 mb] in the upper troposphere. Vertical shear becomes quite strong at the time of the system [speed difference from 850 to 200 mb of 80 kt (~ 40 m s⁻¹) with most of this concentrated in the upper half of

the troposphere]. After the system passes the wind profile becomes quite like it was prior to the system.

The θ_e profiles at the SE corner (Fig. 43e) are moderately unstable and change little with time (some increase in lower levels from before and during to after). Winds aloft are generally light. Upper tropospheric winds veer while mid-level winds back at the time of the system. The 850 mb speed increases markedly from 10 to 25 kt (~ 5 to 12 m s^{-1}) as the MCC develops, with this low-level wind maximum being the most notable feature of the profiles.

The thermodynamic profile found at the center of the MCC system (during profile, Fig. 43c) must be the end result of many multi-scaled processes that ensued during the preceding 12 h. These would include, but certainly not be limited to, such things as meso- α scale ascent, both saturated and unsaturated; embedded within the upward motion field there are likely both meso- β and thunderstorm scale regions of ascent and descent (once again both saturated and unsaturated). Undoubtedly, turbulent mixing between these differing motion fields acts to mask characteristic signatures of particular circulations, especially by the time of the 1200 GMT composite system. (The complexities of each individual system's thermodynamic characteristics are dramatically illustrated by the case study soundings shown in Appendix C.) Additional complexity results from the distinct four-dimensional nature of the relative flow fields!

Note also that the lowest level of the composite soundings exhibits significant diurnal cooling which further complicates interpretation of the results. Early in the MCC's life-cycle both the background meso- α circulation and individual thunderstorms can tap the surface layer air;

however, by 1200 GMT, the time of the large complex, the system's circulations are strongly decoupled from the surface. The θ_e minimum (generally at 500 - 700 mb) for the four peripheral soundings ranges from 307 to 327 K. Thus, if widespread mid-level, mesoscale downdrafts were contributing significantly to the meso- α circulations at the time of the mature system considerably lower θ_e values might be expected at low-levels within the core of the system. Note also that precipitable water (Table 6) at the central grid is much greater, at the time of the MCC than at the peripheral locations and also greater than before or after the system. This is certainly consistent with the concept of net meso- α scale lifting, in conjunction with smaller scale mixing, distributing more moist air upward through the column.

III.6 Cross-Section Analyses

The analyses of the total meteorological fields shown in the preceding section illustrate a number of significant developments or changes during the MCC life-cycle. For example, upper tropospheric winds exhibited significant changes in direction and especially speed. A short-wave trough intensified along the trailing edge of the system within the upper half of the troposphere. An intense upward vertical motion field developed and then weakened during the period. The MCC life-cycle is now examined utilizing a series of west to east vertical sections along 40°N (the location of this cross-section was indicated earlier in Fig. 14).

Fig. 44 presents contours of the heights of the 850, 500, 250 and 150 mb pressure surfaces along the cross-section before, during, and after the time of the MCC. Before the MCC development a lee-trough at 850 mb and a more or less vertically stacked weak wave at 500 mb are present along the western edge of the GR. A broad trough at 250 and 150 mb is

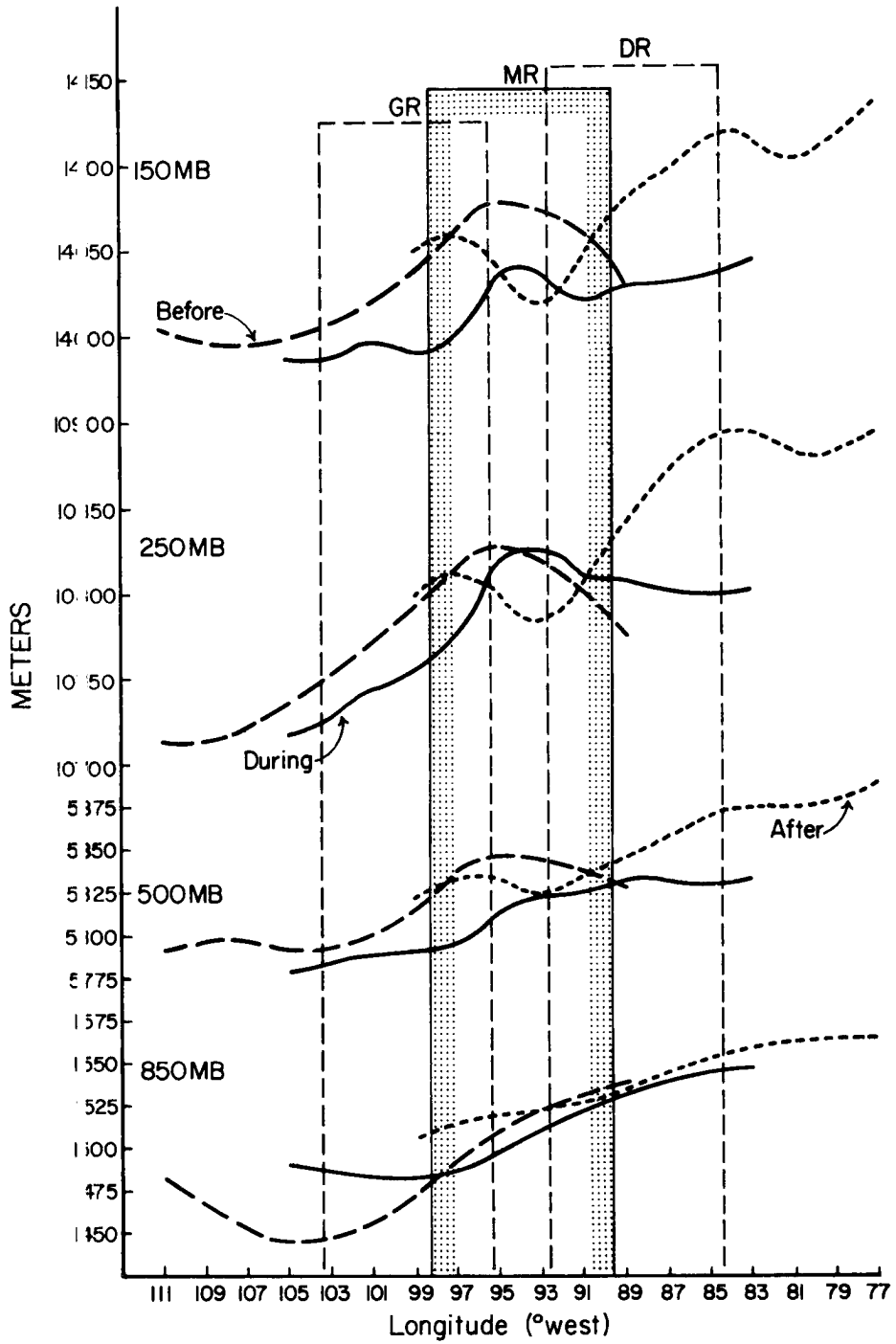


Fig. 44. Pressure surface heights along cross-section at 40°N (see Fig. 14). Locations of the GR, MR and DR are shown.

indicated west of the GR. At the time of the MCC 850 mb heights drop slightly over the MR and rise considerably to the west. At 500 mb heights fall 25-30 m over the western MR with a slight trough indicated along the western edge. At 250 mb heights fall over the western MR; however, the ridge position changes little with the net effect being a pronounced ridge directly over the MCC. At 150 mb the height falls over the MR but a pronounced ridge, with slight troughing to the west and east, is present over the MR. (Note that the normal diurnal tendency is for heights to fall from 0000 to 1200 GMT.) After the MCC has decayed, the 850 mb heights change little. At 500 mb a weak short-wave trough is clearly present along the western edge of the DR with the accompanying ridge just to the east. At 250 and 150 mb the short-wave trough has intensified and become very distinct. The ridge is again located just to the east of the DR. The pattern evolution has reasonable continuity if one considers the before and after fields; however, the pattern during the MCC does not have good continuity with either of the other times.

The before, during and after thickness contours for these pressure levels are displayed in Fig. 45. From before to during, the 850 - 500 mb thickness decreases -- 25 to 30 m (approximately equal to layer of cooling of 2°C) west of the MR (due to the southward push of the cold front and diurnal cooling). At the time of the MCC the thickness pattern indicates a slight warm core near the center of the MCC. The 500 - 250 mb thickness shows a marked ridge and warm core present within the system while the 250 - 150 mb thickness pattern shows pronounced cooling and a cold core over the MCC. The after patterns show little change in the 850 - 500 mb layer, the intensification of the short-wave trough in the upper troposphere, and slight warming in the 250 - 150 mb layer over the

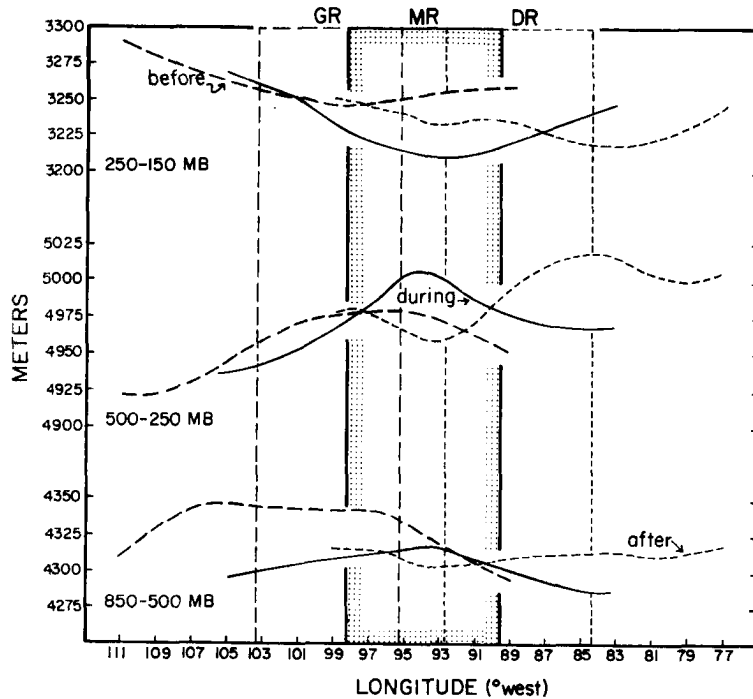


Fig. 45. Layer thicknesses along cross-section at 40°N.

MR as the cold core advects eastward. The mid-tropospheric warm core and upper tropospheric/lower stratospheric cold core appear to have moved eastward faster than the MCC system, which is certainly consistent with the upper winds.

The quasi-geostrophic equations (in particular the tendency and omega equations) provide one qualitative means of assessing the changes and causative mechanisms operating during the MCC life-cycle. Of particular interest is whether or not the MCC system occurs as a response to the evolving baroclinic large scale environment or if it develops as a convectively driven (quasi-tropical) weather system. The equations are clearly not quantitatively applicable in the MCC situation but Sanders (1976) has noted that one particularly valuable aspect of quasi-geostrophic theory is that it often elucidates situations in which its application is not precisely justified. Trenberth (1978) and Hoskins et al. (1978) have pointed out the difficulties inherent in qualitative

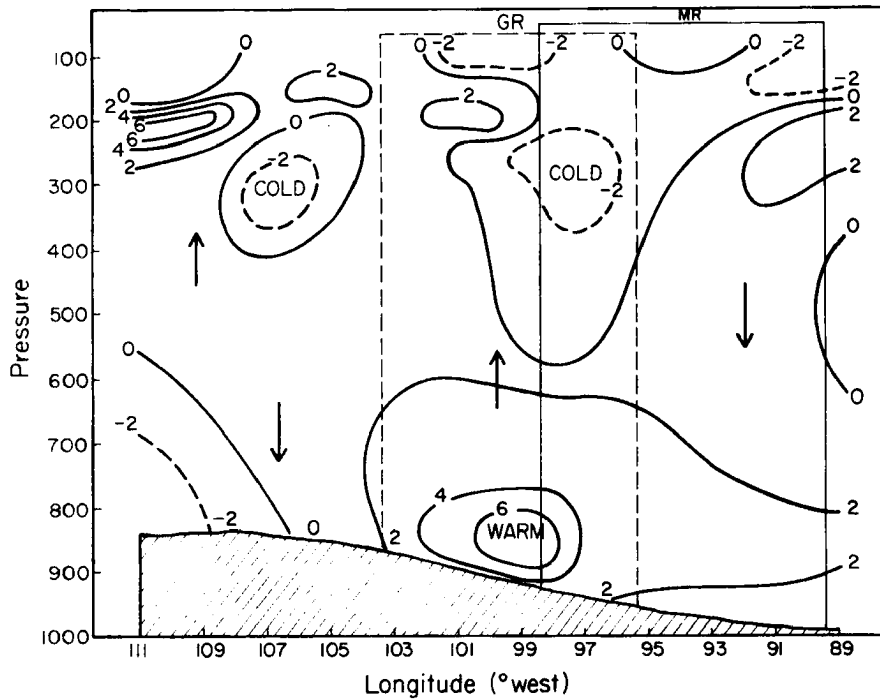
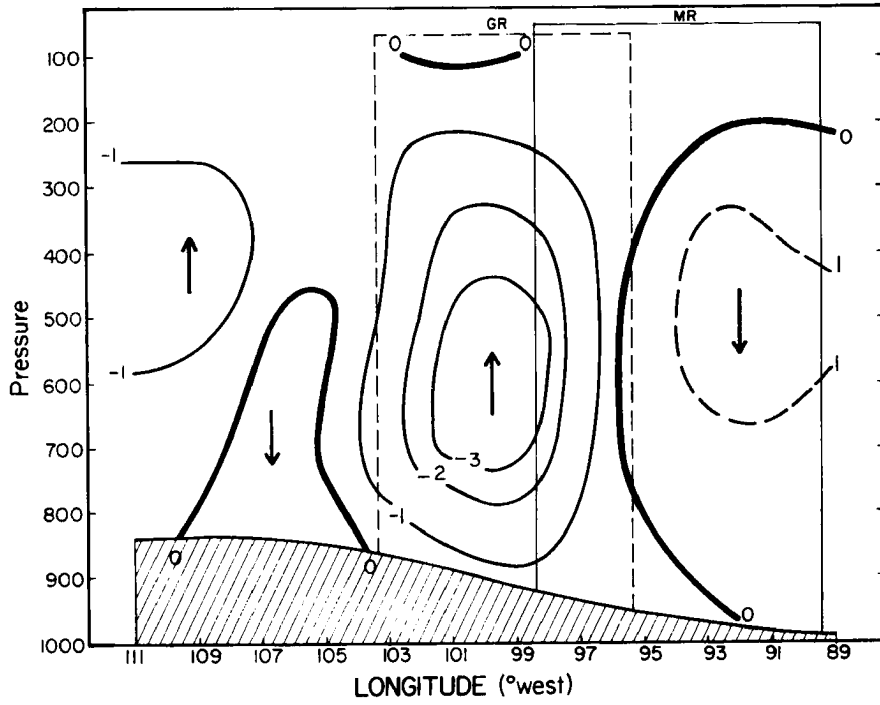
evaluation of the omega equation since the primary forcing functions (thermal advection and differential vorticity advection) often tend to partially cancel one another. However, since MCC situations have been found to be associated with very weak short-wave troughs and to occur during summer months, lower and middle tropospheric vorticity advection is likely to be weak, simplifying the problem of qualitative interpretation.

Figure 46a shows kinematically diagnosed omega along the west to east cross-section prior to MCC development. Significant upward motion is occurring in the lower half of the troposphere over the Plains (note that the maximum is at about 100°W , well to the east of the central Rocky Mountains which are at about $105\text{--}112^{\circ}\text{W}$). Weak subsidence is occurring further east over the Missouri and Mississippi River Basins. The GR is characterized by organized upward motion. The corresponding temperature advection is shown in Fig. 46b (advection by the total wind in $^{\circ}\text{C}$ per 12 h). The region of significant lower tropospheric upward motion appears directly coupled with a region of strong warm advection, as indeed it should (assuming that differential vorticity advection is weak, see Holton, 1972). The pattern also indicates destabilization through differential temperature advection over the eastern GR and western MR. Note that cold advection is occurring in much of the upper troposphere over the MR (the region in which the pronounced ridge develops by the time of the MCC).

Figure 46c shows analyses of the relative vorticity of the total wind and the u-component of the wind along the cross-section; regions of positive and negative vorticity advection (PVA and NVA) are indicated. [Comparison of point-by-point vertical profiles of relative vorticity

Fig. 46a. Omega ($\mu\text{bar s}^{-1}$) along cross-section at 40°N 12 h before the MCC.

Fig. 46b. Temperature advection ($^\circ\text{C}$ per 12 h) by the total wind along cross-section at 40°N 12 h before the MCC.



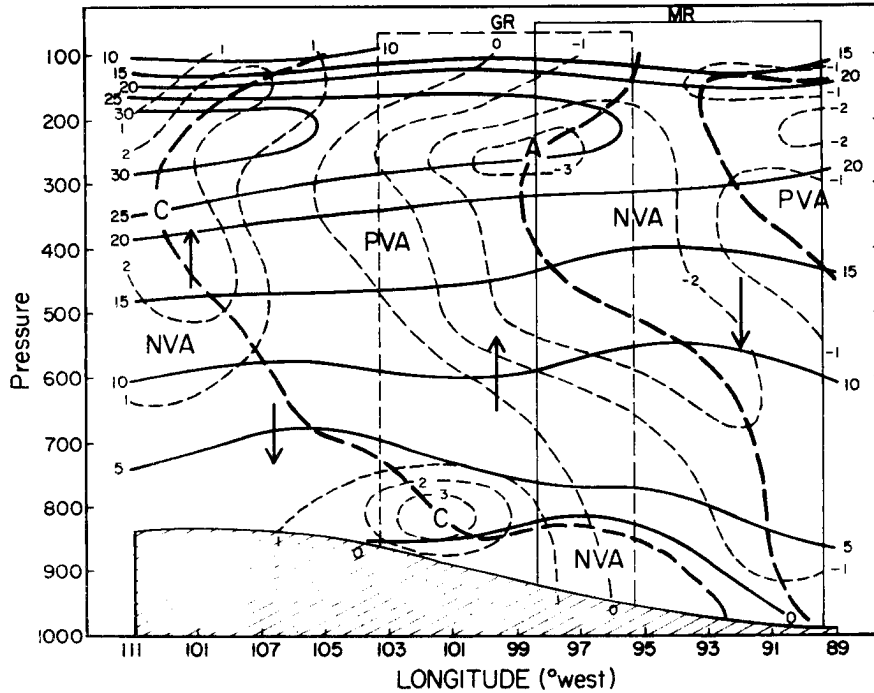


Fig. 46c. Relative vorticity ($\times 10^{-5} \text{ s}^{-1}$) of the total wind and the u-component of the wind (m s^{-1}) along cross-section at 40°N 12 h before the MCC. Regions of PVA and NVA by the u-component are indicated.

advection by the u-component with absolute vorticity advection by the total wind were qualitatively the same with only slight quantitative differences (on the order of 10%.) Vorticity advection is indeed weak in the lower troposphere (value of PVA on the order of $1\text{--}3 \times 10^{-11} \text{ s}^{-2}$, or $\sim 0.1 \times 10^{-5} \text{ s}^{-1}$ per 12 h, over the GR). The GR is, however, basically characterized by PVA although the warm advection pattern is much more pronounced. Note the upper tropospheric wind maximum to the west of the GR.

Figure 47a presents the diagnosed omega along the cross-section at the time of the MCC. The entire MR is now characterized by a deep and very strong upward circulation (note that maximum upward motion has more than doubled and has shifted upward into the middle troposphere). Subsidence is occurring both to the east and west. The corresponding

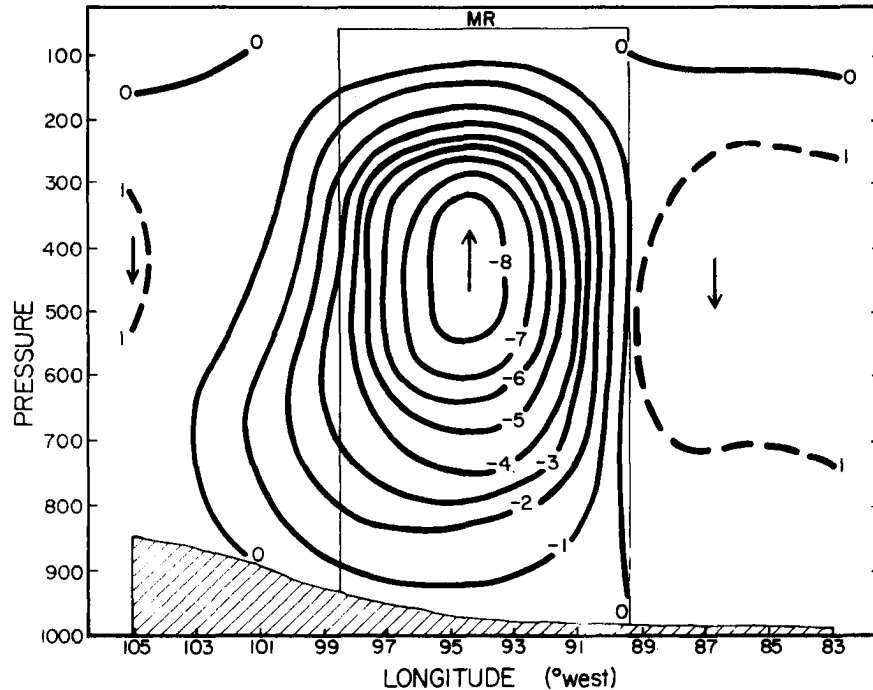


Fig. 47a. Omega ($\mu\text{bar s}^{-1}$) along cross-section at 40°N at the time of the MCC.

temperature advection pattern is presented in Fig. 47b. It is apparent that there is no time or space continuity of the advection patterns (compare Figs. 46b and 47b) except within the lower troposphere. The upward circulation remains rooted to the region of strong lower tropospheric warm advection, which has shifted eastward so that it is now centered in the MR region. Within the MCC region, the advection patterns (average from before to during) indicate that the 850 mb temperature should have increased about 4°C and the 700 mb temperature about $2\text{--}3^\circ\text{C}$ while in actuality the 850 temperature changed little and the 700 mb temperature decreased slightly. The average diagnosed vertical motion at 850 mb and the temperature advection approximately cancel one another. For dry adiabatic ascent, however, the average diagnosed vertical motion at 700 mb would produce a cooling on the order of 9°C . Thus, moist ascent is likely occurring at the 700 mb level. The temperature advection

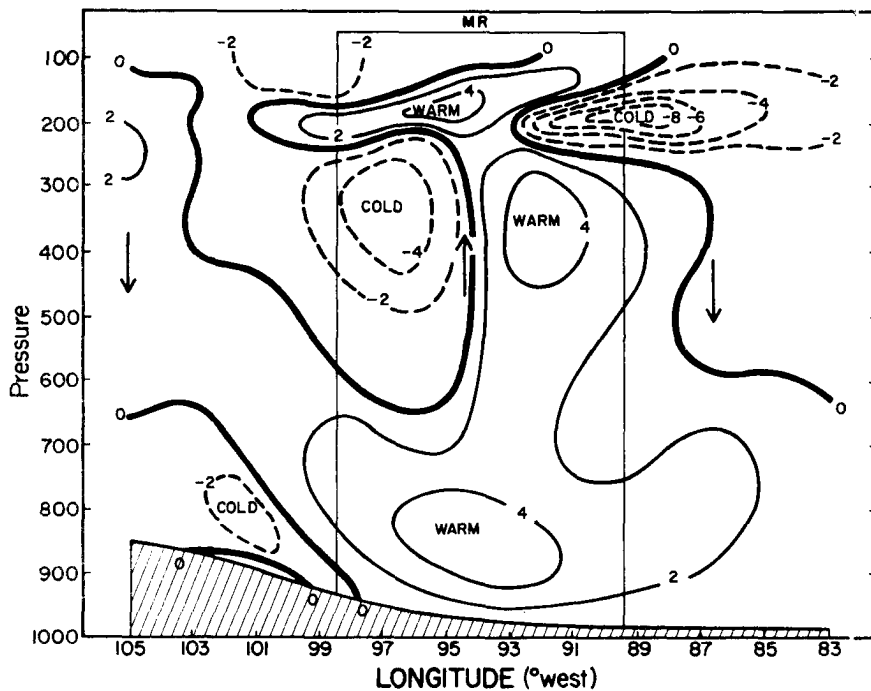


Fig. 47b. Temperature advection ($^{\circ}\text{C}$ per 12 h) by the total wind along cross-section at 40°N at the time of the MCC.

patterns in the middle and upper troposphere now reflect the strong diabatic effects of the MCC (note for example that at $\sim 94^{\circ}\text{W}$ the advection patterns indicate persistent cold advection in the 500 - 250 mb layer whereas in actuality a distinct warm core ridge develops (see Fig. 45). The warm core nature of the MCC circulation in the 500 - 250 mb layer results in diagnosed strong cold advection upstream and warm advection downstream. In the upper troposphere/lower stratosphere the cold core above the MCC produces the opposite pattern with cold advection downstream and warm advection upstream. It is most important to note the precursor large and medium scale vorticity and temperature advection patterns do not indicate that the vertical motion should increase markedly or that the mid-tropospheric ridge should amplify (Fig. 46).

The u-component of the wind and the relative vorticity fields at the time of the system are shown in Fig. 47c. The vorticity advection

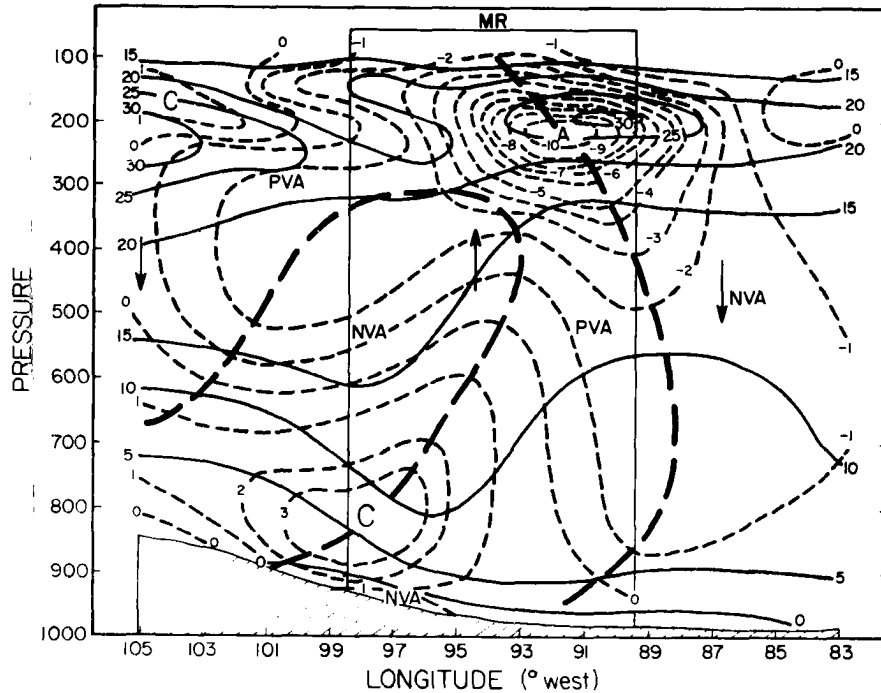


Fig. 47c. Relative vorticity ($\times 10^{-5} \text{ s}^{-1}$) of the total wind and the u-component of the wind (m s^{-1}) along cross-section at 40°N at the time of the MCC.

remains weak in the middle and lower troposphere but with little continuity apparent from the time of Figs. 46c to 47c. However, in the upper troposphere tremendous changes have occurred during the 12 h period. The upper-wind maximum to the west of the MCC retains its identity. But above and east of the system, a strong outflow jet has developed with an associated region of intense negative relative vorticity (note that at one grid point absolute vorticity has been driven to a slightly negative value). The upper tropospheric circulation is now much like the low absolute vorticity situations studied theoretically by Paegle (1978) and diagnostically by MacDonald (1977). However, the strongly divergent, low absolute vorticity circulation was not a feature of the precursor environment (see Fig. 46c) but rather was apparently forced and maintained by the organized MCC circulation. The rapid development of the outflow jet does agree well with the findings of Paegle (1978). The vorticity

advection fields are quite intense at upper-levels over and east of the MCC (NVA of $\sim -5 \times 10^{-9} \text{ s}^{-2}$ or approximately $-22 \times 10^{-5} \text{ s}^{-1}$ per 12 h).

The vertical motion fields 12 h later (Fig. 48a) have become both very chaotic and weak. The DR is characterized by weak subsidence in the upper troposphere. These motion fields bear almost no resemblance to those shown in Fig. 47a. The temperature advection pattern (Fig. 48b) does, however, somewhat resemble the field shown in Fig. 47b. The warm/cold advection couplet in the 250 to 150 mb layer appears to have moved eastward faster than the decaying MCC, with the warm advection now being stronger than the cold advection to the east. The cold/warm advection couplet in the middle troposphere remains; however, the warm advection has weakened (in fact it has vanished below 350 mb). The advection patterns in Fig. 48b seem reasonably consistent with the height and thickness patterns shown in Figs. 44 and 45. The vertical motion in the low

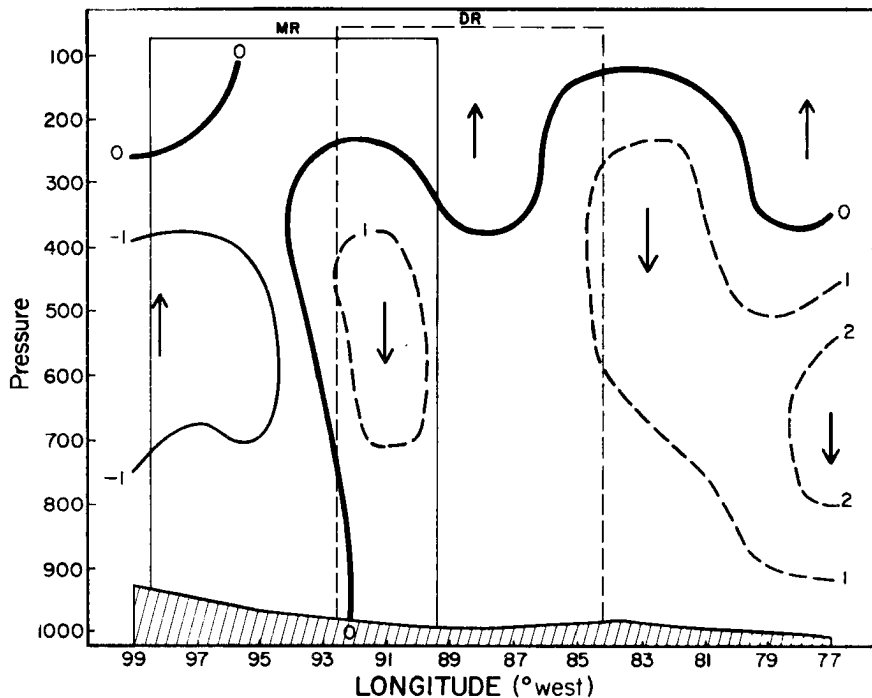


Fig. 48a. Omega ($\mu\text{bar s}^{-1}$) along cross-section at 40°N 12 h after the MCC.

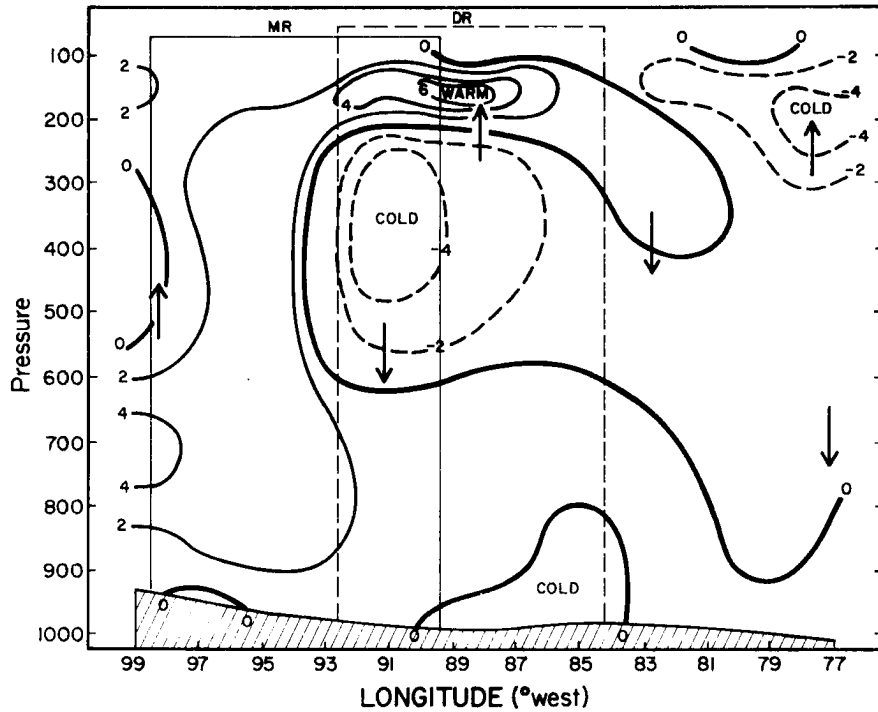


Fig. 48b. Temperature advection ($^{\circ}\text{C}$ per 12 h) by the total wind along cross-section at 40°N 12 h after the MCC.

and middle troposphere agree well with the thermal advection fields. Note that the region of strong low-level warm advection has not shifted eastward with the MCC and that very slight cold advection is now found at the surface in the DR. The u-component and relative vorticity fields are shown in Fig. 48c. The speed maximum in the westerly flow remains to the west of the MCC area; however, intense outflow is no longer found over and downstream from the system. The region of negative relative vorticity remains, with weak upper tropospheric subsidence in the region of strong NVA and weak upward motion in the PVA area. Note that the short-wave trough intensified in the region trailing the decaying MCC where cold advection was occurring and where this cold advection decreased with height.

These analyses indicate that the MCC develops and organizes within a precursor meso- α scale region of upward vertical motion over the

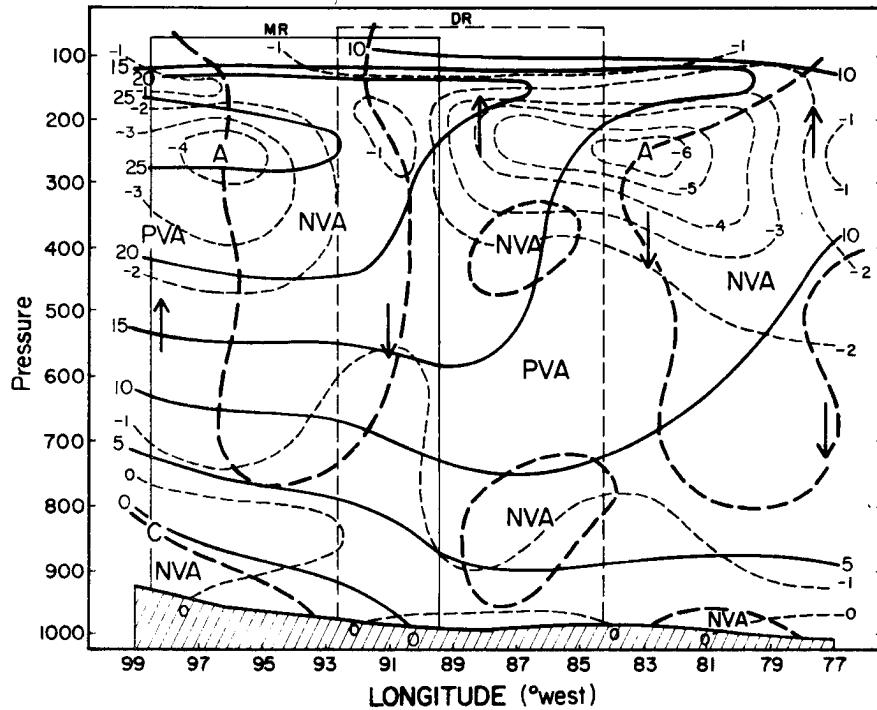


Fig. 48c. Relative vorticity ($\times 10^{-5} \text{ s}^{-1}$) of the total wind and the u-component of the wind (m s^{-1}) along cross-section at 40°N 12 h after the MCC.

Plains. This upward motion is primarily a reflection of strong low-level warm advection rather than of strong PVA in mid-levels (the advection pattern shifts rapidly eastward across the Plains as low-level winds increase and veer during the diurnal cycle). However, the medium scale environment responds strongly to the convection and a deep, warm core upward circulation develops. This circulation is overlain by a distinct cold core in the upper troposphere and lower stratosphere that is attended by an intense outflow jet. The evolution of events that transpire during the night cannot be inferred or interpreted in a quasi-geostrophic sense (other than the strong coupling of low-level warm advection and upward motion) which agrees with Wetzel *et al.* (1981) who found that the MCCs they studied did not act in the classic baroclinic sense and transport sensible heat northward. Once the MCC decays, the outflow jet rapidly weakens; however, the thermal perturbations appear

more persistent. The intensification of the middle and upper level short-wave trough and ridge (to the east) does agree qualitatively with quasi-geostrophic interpretations. Indeed, the intensification of this short wave often produces a well-defined "coma cloud" that is apparent in satellite images (see the images in Fig. 12, especially e). This sequence of events is somewhat similar to those associated with the development of "coma clouds" and associated polar lows (see Reed, 1979).

For the average case, the MCC interacts with its environment by moistening a deep tropospheric layer and by creating an upper tropospheric temperature perturbation to which the large scale must adjust (in this case by the intensification of a middle and upper level short wave that may persist and move eastward for several days). Because the time scale of development of this temperature perturbation is typically less than a half-pendulum day ($2\pi/f$), the meso- α flow becomes imbalanced in the quasi-geostrophic sense. Apparently the amplification of the short wave after 1200 GMT is a manifestation of this adjustment. The lower troposphere remains essentially decoupled from this adjustment process; however, in certain cases the MCC interactions and feedbacks may be self-perpetuating, resulting in a persistent, deep tropospheric wave and extended periods of significant weather (see Bosart and Sanders, 1981).

IV. THE MCC LIFE-CYCLE: A MODEL

The MCC climatology presented in Section II and analyses discussed in Section III lend considerable insight into the life-cycle of the "composite" MCC. These findings were utilized, in conjunction with detailed case analyses (Appendix C) and enhanced IR satellite depictions of the life-cycle of individual systems, to develop a conceptual model of the MCC life-cycle. The sequence of satellite images shown in Fig. 49 captures a 16 h period illustrating the life-cycle of a typical MCC system.

IV.1 Genesis

A number of individual thunderstorms develop within a region (most typically over the eastern slopes of the Rocky Mountains or the central Plains, see Section II) where large scale conditions favor convection. The approach of a weak mid-tropospheric short-wave trough is preceded by strong warm advection and organized meso- α scale upward motion in the lower troposphere. A conditionally unstable thermodynamic structure exists over a large area ahead of and to the right (usually south) of the short wave. An east-west oriented frontal zone frequently enhances low-level convergence. Small scale effects, such as topography and localized heat sources, may play important roles in initiating storm development. Latent heat release within the updrafts of the individual storms may combine with subsidence-induced warming in the storms' near environment to produce meso- β scale regions of anomalous warmth, much as hypothesized by Fritsch (1975). Some of the storms entrain potentially cold mid-level air so that strong, evaporationally driven downdrafts and cold air outflows with mesohigh pressure systems within the surface

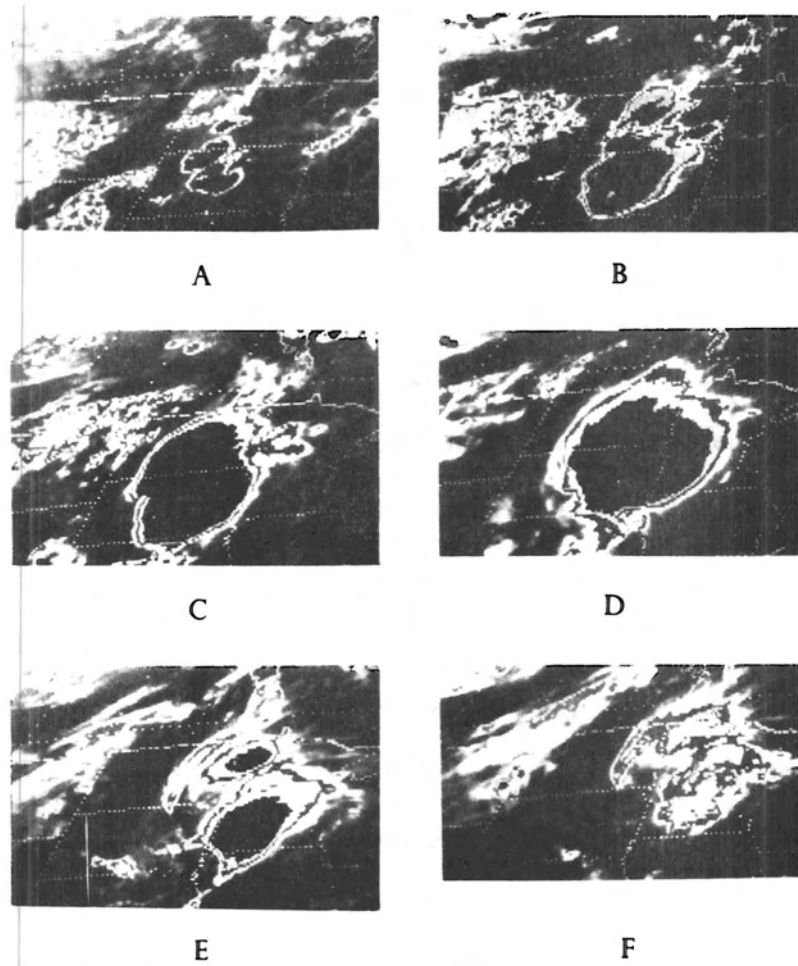


Fig. 49. Enhanced infrared satellite photographs documenting the life-cycle of an MCC mesoscale weather system during a 16 h period on 12 July 1979. The image times are A) 0030 GMT, B) 0300 GMT, C) 0600 GMT, D) 0900 GMT, E) 1430 GMT and F) 1630 GMT.

boundary layer develop; however, weak relative winds result in poor ventilation of the general storm area (see Gray, 1973). The thunderstorms often produce significant severe weather (tornadoes, hail and strong winds) during this period. The genesis phase of an MCC is illustrated in Figs. 49a and b.

IV.2 Organization

Individual thunderstorms intensify, grow and often merge as they move eastward into a more unstable and moist environment. Within the surface boundary layer, gust fronts and cold air outflows from the individual storms gradually merge to produce a meso- β and finally a meso- α scale high pressure region and convective cold front. The nocturnal increase in speed and significant veering of low-level winds amplifies both the warm advection and influx of moist unstable air. During this diurnal cycle, radiation cooling decouples the MCC from the surface layer with the roots of convective updrafts being aloft (say, in the layer $\sim 850 - 900$ mb). The meso- α scale background environment and the individual thunderstorms apparently interact synergistically, with the overall convective system growing rapidly, sometimes explosively, within the region of upward motion. Eventually the system reaches the size specified for MCCs in Table 2 (refer to Figs. 49b and c). The most intense convective elements occur along the convergence zone produced by the interaction of the outflow boundary and the low-level inflow air. If these developments occur in the vicinity of an east-west front, the thunderstorm outflows may strengthen the surface frontal zone, with the MCC developing and moving eastward on the cool side of the front. The nearby environment responds to the continued presence of an anomalously warm region with deep inflow that reaches the middle troposphere (e.g., from about 900 to 600 mb). The general mesoscale ascent, thunderstorm scale downdrafts and turbulent mixing from individual convective elements act to moisten a deep tropospheric layer and to slowly effect modifications of the local environment in which the system is occurring.

IV.3 Mature

During the mature stage (see Figs. 49c and d) flow in the lower half of the troposphere converges into the system (primarily from the southeast to southwest). Much of the inflow is incorporated into a central region of mean mesoscale ascent. Eventually this region exhibits a nearly moist adiabatic warm core structure relative to its surrounding environment. Intense convective elements continue to form where low-level inflow provides unstable fuel for the system. Severe thunderstorms may still occur; however, the primary type of significant weather is likely to be locally heavy rainfall. Convective elements occur within a deep moist environment that is now characterized by weak vertical wind shear so that they are very efficient precipitators (see Marwitz, 1972). Down-drafts are weak. Compensating subsidence occurs primarily within the nearby environment surrounding the meso-updraft. The dominant characteristic of the mature system is the meso- α scale upward circulation and its attendant area of widespread precipitation (see the 12 h rainfall maps in Appendix C). The satellite observed signature of this circulation is the large circular shield of continuously cold cloud top (see Fig. 49d). The warm core nature of the mid-tropospheric meso-circulation may generate a mesolow aloft, just above a shallow mesohigh at the surface, which further enhances convergence into the system (see Austin, 1951; Manabe, 1956; Aubert, 1957; and Bosart and Sanders, 1981). By this time a positive height perturbation (mesohigh) and anticyclonic outflow have developed within the upper-troposphere directly over the MCC (see Riehl and Burgner, 1950; Manabe, 1956; Aubert, 1957; Matsumoto and Ninomiya, 1967; Fankhanser, 1969; and Fritsch and Maddox, 1981a).

IV.4 Dissipation

The dissipation stage is marked by a rapid change in the character of the MCC. Dissipation commences as the system progresses eastward into a more stable and convectively unfavorable environment. Relative flow in the near environment changes so that the strongest influx of middle and lower tropospheric air occurs along the northwest and northern flanks of the system. This inflow is drier and potentially cool so that a deep meso-downdraft develops as the MCC decays. Although the system rapidly loses its meso- α scale organization, the cool air and boundary layer mesohigh, middle and high cloud debris and light showers may continue to move eastward and persist for many hours. If the large scale environment evolves so that an unstable air mass may be again tapped by the system, it can re-intensify (e.g., Wetzell et al., 1981; and Bosart and Sanders, 1981).

IV.5 Structure of the Mature System

A schematic diagram of the vertical structure of the MCC relative flow fields and mesoscale vertical motion fields is shown in Fig. 50. Note that the scale is greatly expanded in the vertical and that the area shown encompasses a large portion of the central United States (refer to Fig. 14). The surface patterns are not especially notable since the system is not well coupled with the near-surface air mass. However, at 850 mb the system is clearly feeding off of air from the east and south with weak subsidence indicated ahead of and behind the MCC. At 700 mb relative flow enters the system from all sides but the most significant inflow is again from the east and south. At 500 mb the flow moves slowly through the system (relative speeds are so weak that air entering the NW periphery of the system would only intrude about 150 km into the

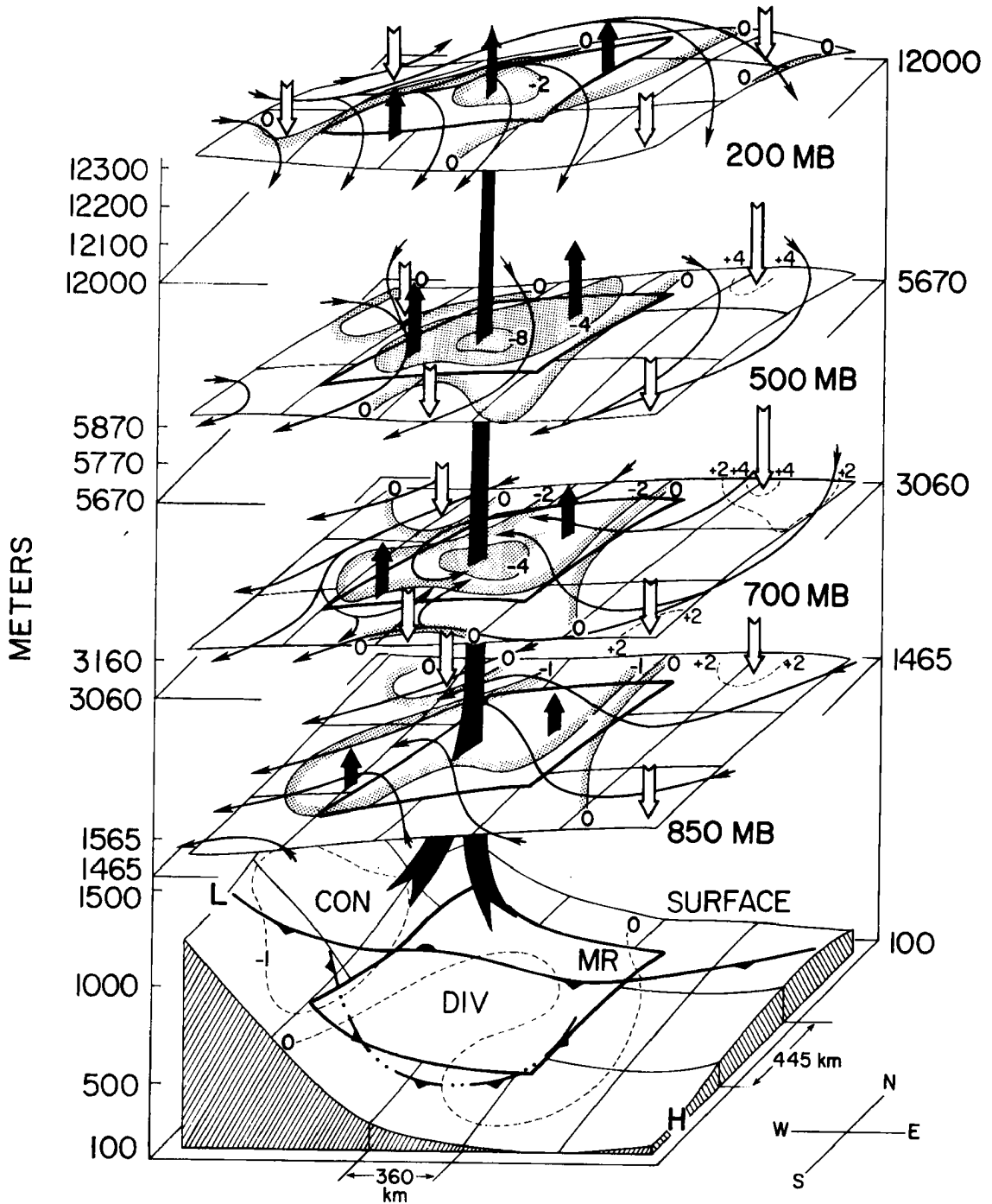


Fig. 50. Schematic drawing of the mature MCC and its near environment. Surface divergence ($\times 10^{-5} \text{ s}^{-1}$) is shown as are streamlines of relative flow on the pressure surfaces. Dark arrows illustrate regions of upward motion. Light arrows indicate regions of downward motion. Selected contours of ω ($\mu\text{bar s}^{-1}$) are shown. The vertical scale is greatly exaggerated.

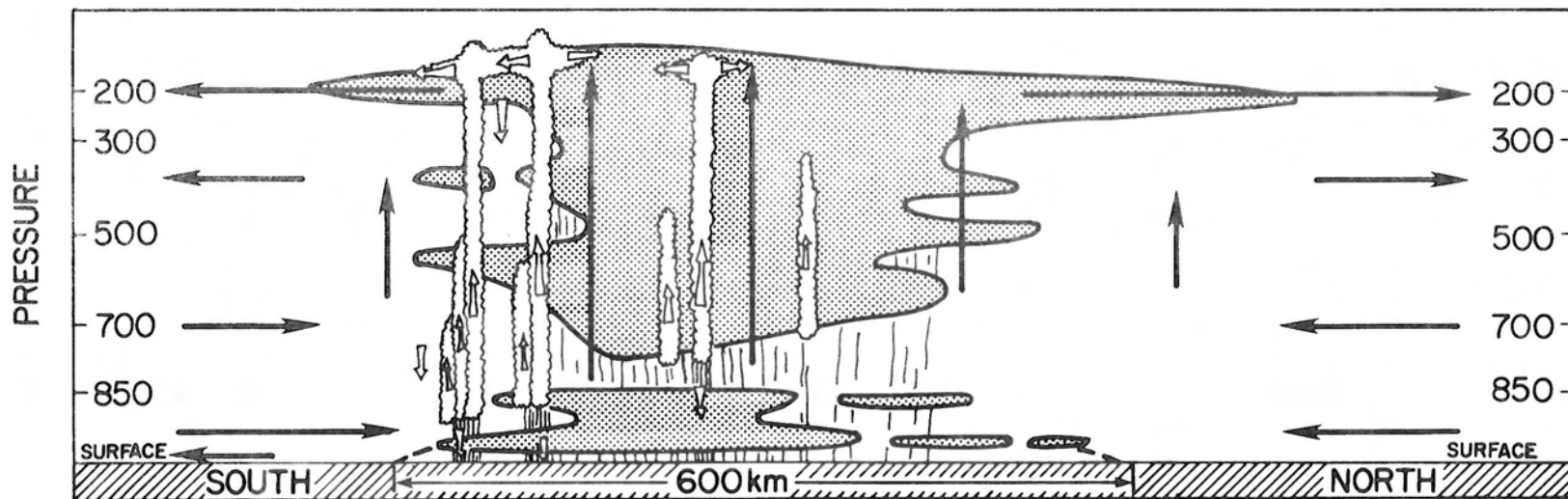


Fig. 51. South-to-north cross-section through a mature MCC and its near environment. Relative flow streamlines and shaded cloud areas illustrate the meso- α scale features of the MCC. Convective turrets and open arrows illustrate possible unresolved small scale interior structure. The vertical scale is greatly exaggerated.

interior during a 10 h period). At 200 mb the flow is strongly diffluent around the system and once again the relative speed of upper tropospheric air entering the rear of the system is very light. The 200 mb pressure surface exhibits upward bulging over the system with strong height gradients indicated along the northern and northwestern edges of the system.

A south to north cross-section through a mature system is shown in Fig. 51. The streamlines and shaded cloud structure represent the meso- α scale system and circulations revealed by the conventional sounding data that have been studied. However, radar, satellite and detailed surface observations (see Appendix C) indicate that considerable small scale internal structure is present within MCCs. Embedded convective elements and probable small scale circulations are indicated. The general cloud base of the system likely increases in height to the north where convective instability and moisture contents are less; however, the presence of widespread stratus and stratocumulus cloud decks within the saturated, near-surface air typically obscures details of the system's cloud structure. The diagram also indicates considerable small scale precipitation structure, with intense convective rain elements embedded within larger regions of steady light rain and/or showery precipitation.

V. MODEL VALIDATION

Certain characteristics of the MCC weather system should be detectable in the composite data set -- in particular, convectively induced meso- α scale temperature, height and horizontal wind perturbations. A quantitative objective analysis procedure is now utilized to examine both macroscale and meso- α scale aspects of the MCC composite data set. Macroscale fields essentially retain features associated with waves of length > 2500 km. Bandpass, or mesoscale, analyses were centered at wavelength 1500 km and extract medium scale features while suppressing both short and long wavelength "noise". The mesoscale fields are computed and presented as perturbations to the macroscale. The objective analysis and scale separation procedures are discussed in depth in Appendix A and the selection of the filter responses is explained in Appendix B.

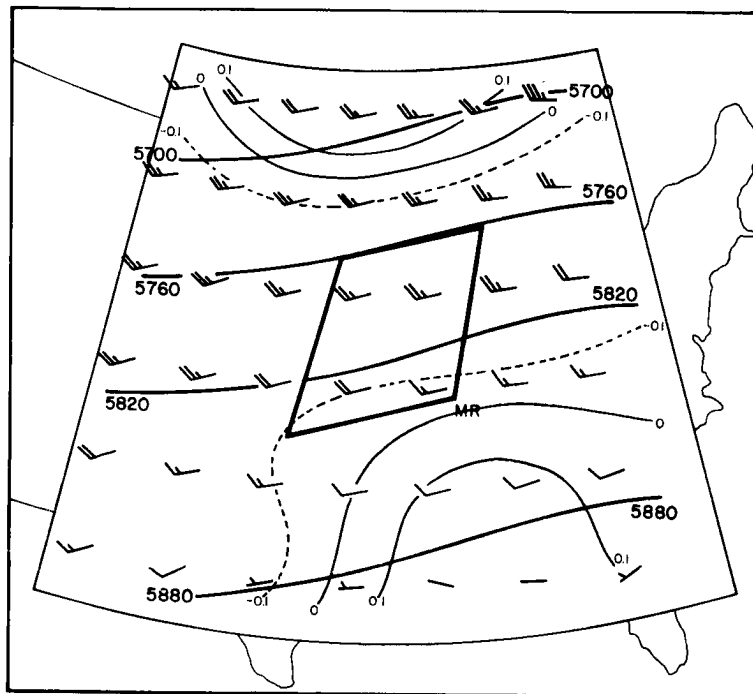
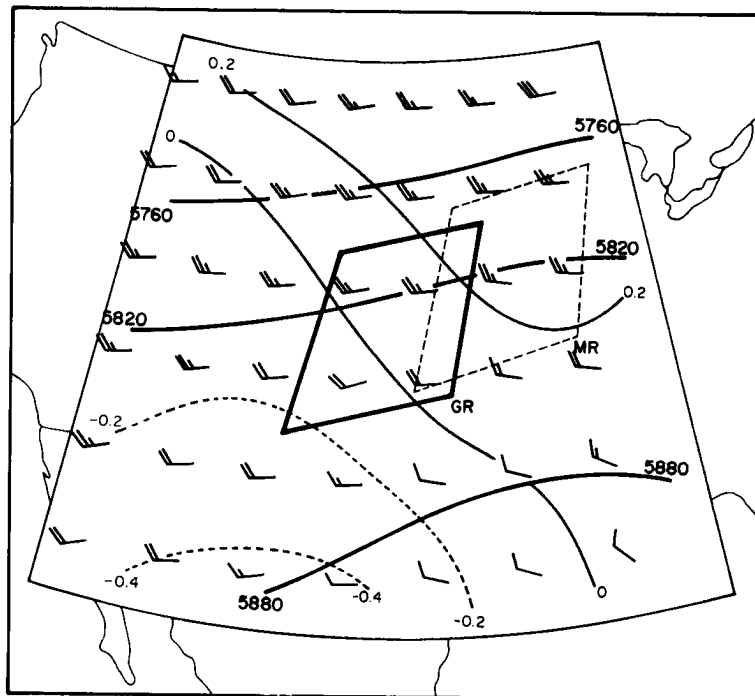
In addition to scale decomposition, the moisture and kinetic energy budgets of the MCC environment are also examined for model validation. It was felt that various aspects of the medium/large-scale interactions that were hypothesized to be occurring might be elucidated by a number of simple budget calculations.

V.1 Macroscale Setting

Macroscale height, wind and divergence analyses following the MCC system are shown for 500 mb. The analyses (Figs. 52a, b and c) show very little change in the large scale pattern during the course of the composite MCC's life-cycle. The ridge over the eastern U.S. weakens and shifts eastward slightly; however, a long-wave trough remains to the west of the domain throughout the analysis period with west-southwesterly flow over the MCC region. The appearance of the convergence maximum downstream

Fig. 52a. Macroscale analysis of the 500 mb level 12 h prior to the MCC. Winds (full barb = 10 kt or $\sim 5 \text{ m s}^{-1}$) are plotted at every other grid point. Height contours are heavy solid lines and divergence analysis ($\times 10^{-5} \text{ s}^{-1}$) is shown by light solid lines.

Fig. 52b. Macroscale analysis of the 500 mb level at the time of the MCC. Details are similar to Fig. 52a.



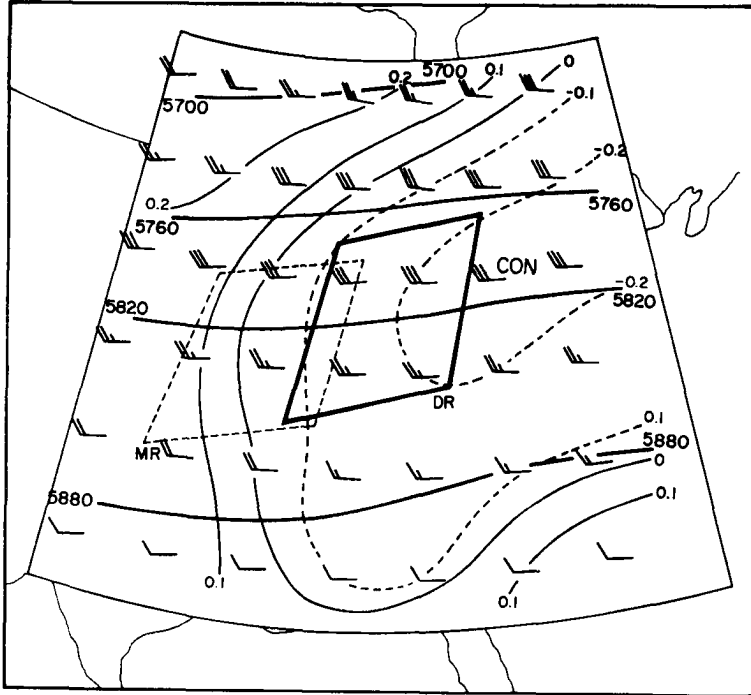


Fig. 52c. Macroscale analysis of the 500 mb level 12 h after the MCC. Details are similar to Fig. 52a.

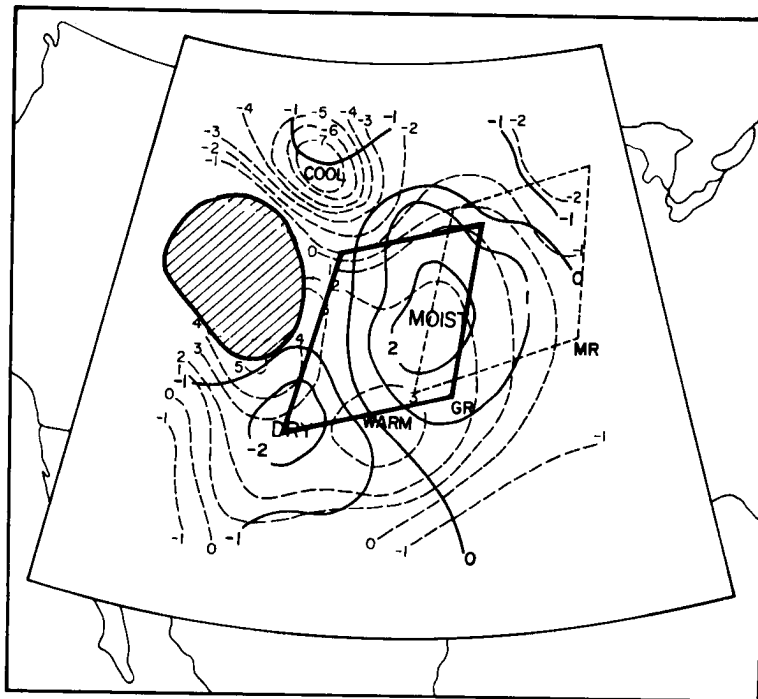
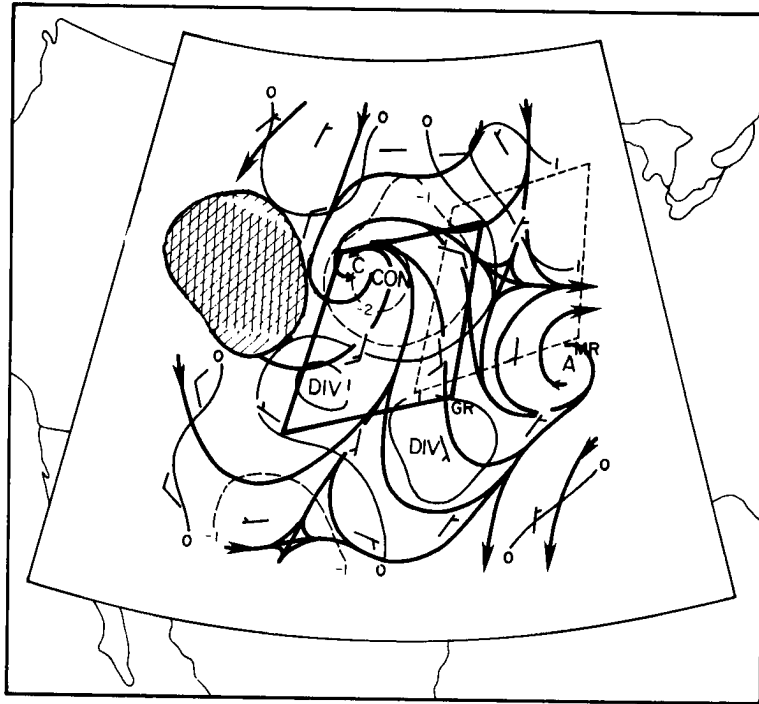
from the DR (Fig. 52c) seems to indicate that the net effect of the MCC has been to increase the speed of the large scale flow near the MCC.

V.2 Mesoscale Analyses

Analyses of the mesoscale perturbation wind (and its divergence), temperature and moisture fields at 850 mb are presented in Fig. 53. At the time the MCC is initially developing (Fig. 53a) a closed cyclonic flow perturbation is present over the northwest corner of the GR with significant south to southeast winds over the GR. Strong convergence is associated with this feature. Remembering that the most unstable airmass at this time is over the southeast corner of the GR, it is apparent that the perturbation flow is acting to advect and converge unstable air into the northern portion of the GR. The flow is confluent over the GR and diffluent (note the prominent col) over the MR at this time. The temperature and moisture perturbations (Fig. 53b) show cool air north of the GR with

Fig. 53a. Mesoscale analysis of the 850 mb level 12 h prior to the MCC. Streamlines are shown along with the divergence ($\times 10^{-5} \text{ s}^{-1}$) analysis. Cross-hatched region is area where terrain elevation is above 850 mb. Winds (full barb = 10 kt or $\sim 5 \text{ m s}^{-1}$) are plotted at every other grid point.

Fig. 53b. Mesoscale analysis of the 850 mb level 12 h prior to the MCC. Moisture perturbation (g/kg) are indicated by solid contours and temperature perturbations by dashed contours.



warm and dry air to the southwest. A distinct pocket of unusually high moisture content is centered over the eastern GR. The medium and large scale flow patterns have apparently preconditioned the Plains region for significant convection by providing a deep moist layer and a very unstable airmass. (Note that afternoon convection over the western Plains and Rocky Mountains may also help deepen the moist layer.)

At the time of the MCC (Fig. 53c) the perturbation flow has weakened somewhat while veering strongly over the MR. Since the total 850 mb jet speed increased during the period, the implication is that the diurnal wind increase occurred on a larger scale than was extracted here. The flow is now confluent over the MR with an elongated cyclonic circulation remaining on the northwest corner of the system. The col in the flow pattern has shifted to the northeast. Convergence is present over all of the MR, but its magnitude has decreased considerably from that present at 0000 GMT. The temperature and moisture analyses (Fig. 53d) show that strong warm and moist perturbations are present to the southwest of the MR. Notice that warm advection by the perturbation flow is now very evident (compare Figs 53a, b, c and d) and is occurring on the meso- α scale.

Twelve hours later (Fig. 53e) the perturbation flow has become very weak with westerly flow and divergence over much of the DR. The closed cyclonic circulation remains at the northwest corner showing that this weak system has advanced eastward. Moisture perturbations (Fig. 53f) have become weak while a noticeable cool and dry pocket has amplified over the MR and northwest DR region. Thermal advection by the perturbation flow is either neutral or cool over the entire DR.

Fig. 53c. Mesoscale analysis of the 850 mb level at the time of the MCC.
Details as in Fig. 54a.

Fig. 53d. Mesoscale analysis of the 850 mb level at the time of the MCC.
Details as in Fig. 54b.

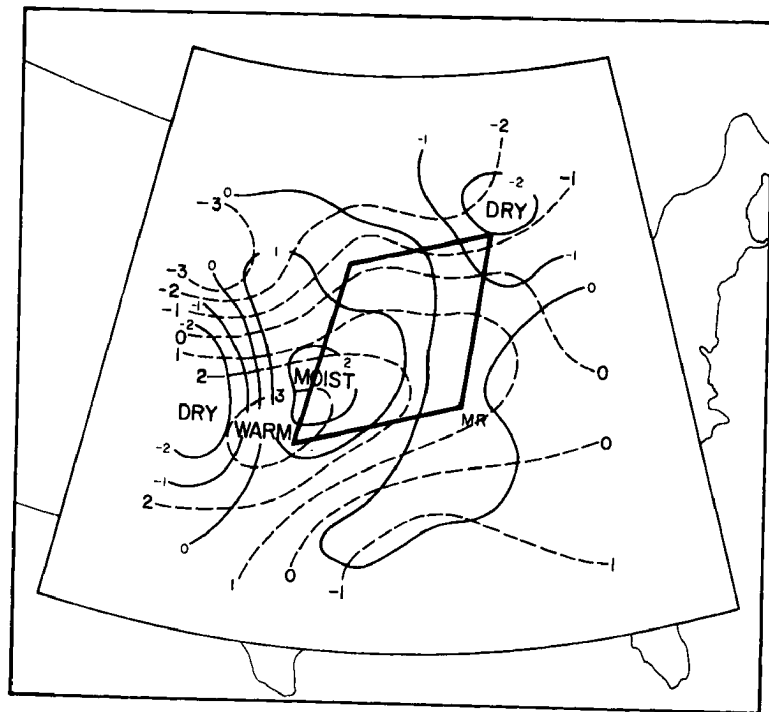
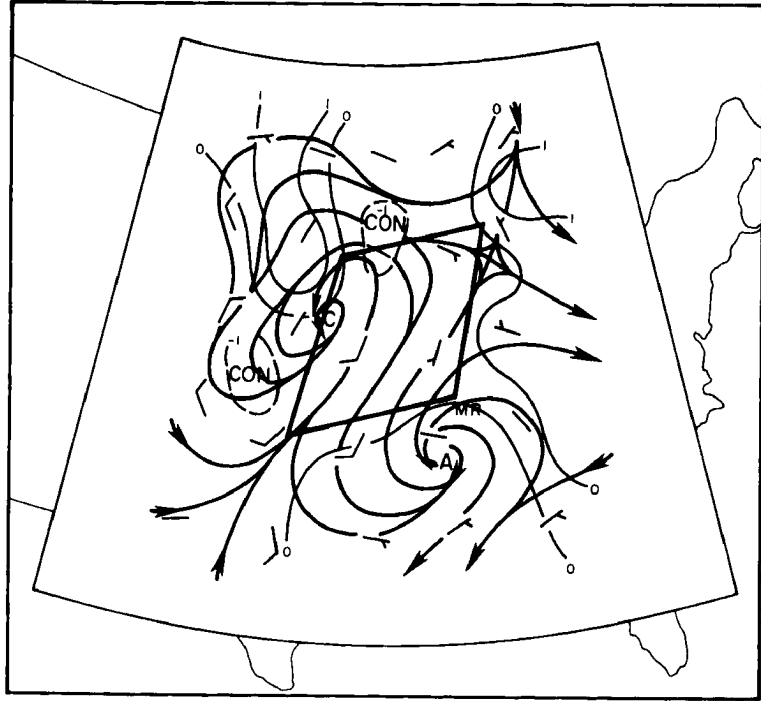
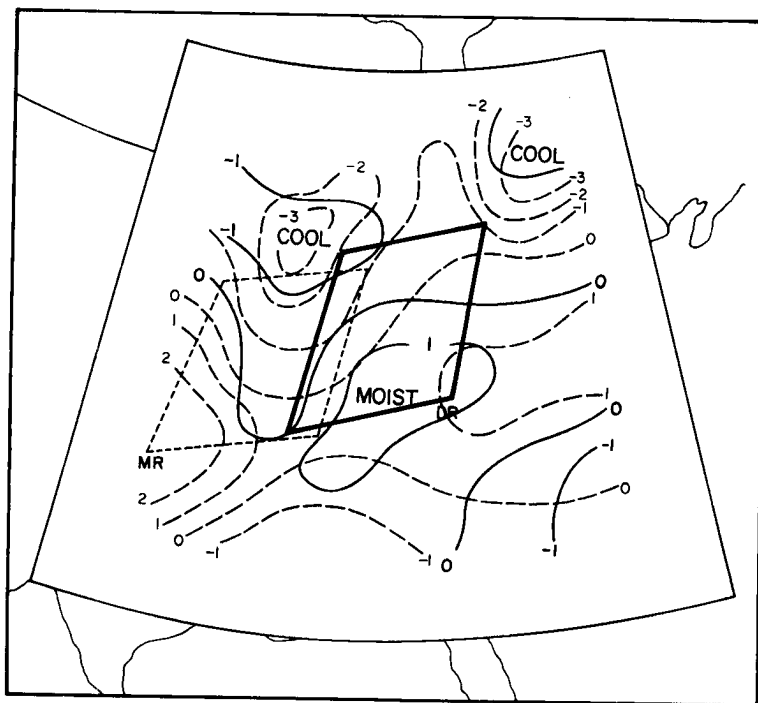
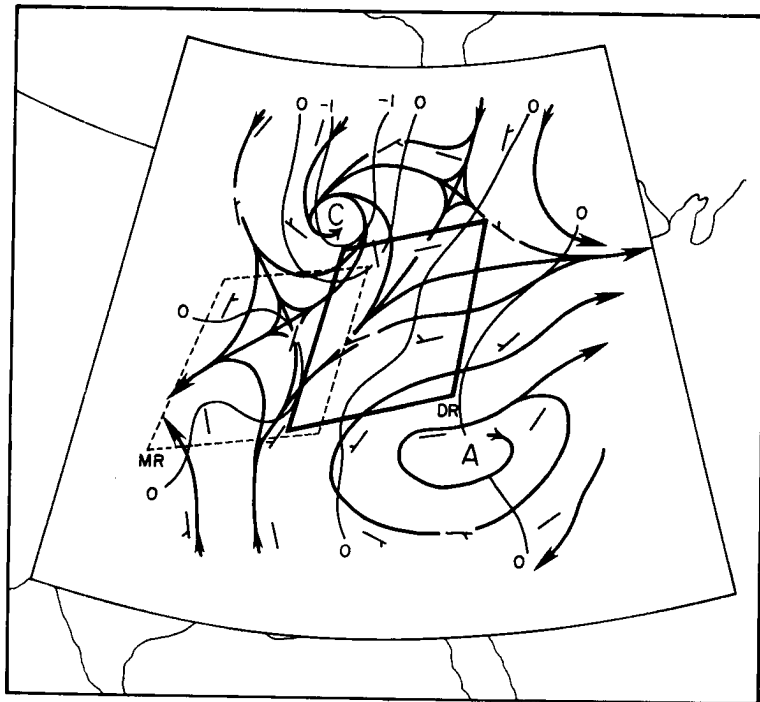


Fig. 53e. Mesoscale analysis of the 850 mb level 12 h after the MCC.
Details as in Fig. 54a.

Fig. 53f. Mesoscale analysis of the 850 mb level 12 h after the MCC.
Details as in Fig. 54b.



The perturbation flow at 500 mb prior to the MCC development (Fig. 54a) is generally light with weak divergence over much of the GR. The corresponding temperature and moisture perturbations (Fig. 54b) show slightly warmer and more moist air located over the GR and much of the MR. A pronounced cool anomaly is located to the northwest of the GR. The moist region does extend southwestward into northern Mexico, probably reflecting the mean southwest monsoon flow regime and accompanying thunderstorm activity over northern Mexico, New Mexico and Colorado.

At the time of the MCC (Fig. 54c), the MR is characterized by weak convergence and a short wave trough directly over the MR. There are marked moist (> 1 g/kg) and warm ($> 1^{\circ}\text{C}$) perturbations within the MCC region (Fig. 54d) indicating that the system is distinctly warm core. By the time the system has decayed (Fig. 54e) a closed cyclonic circulation has become apparent over the northwest corner of the DR. Strongest

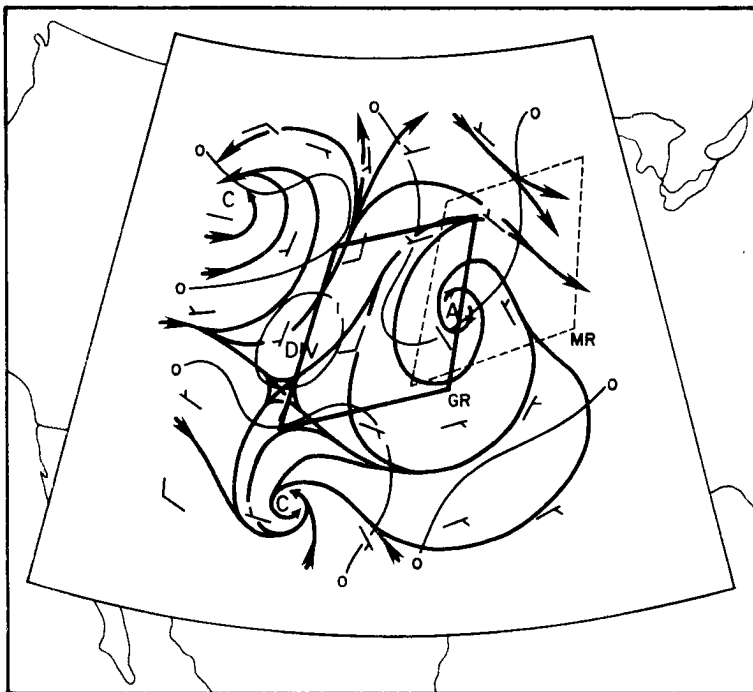


Fig. 54a. Mesoscale analysis of the 500 mb level 12 h prior to the MCC.

Fig. 54b. Mesoscale analysis of the 500 mb level 12 h prior to the MCC.

Fig. 54c. Mesoscale analysis of the 500 mb level at the time of the MCC.
Details at in Fig. 54a.

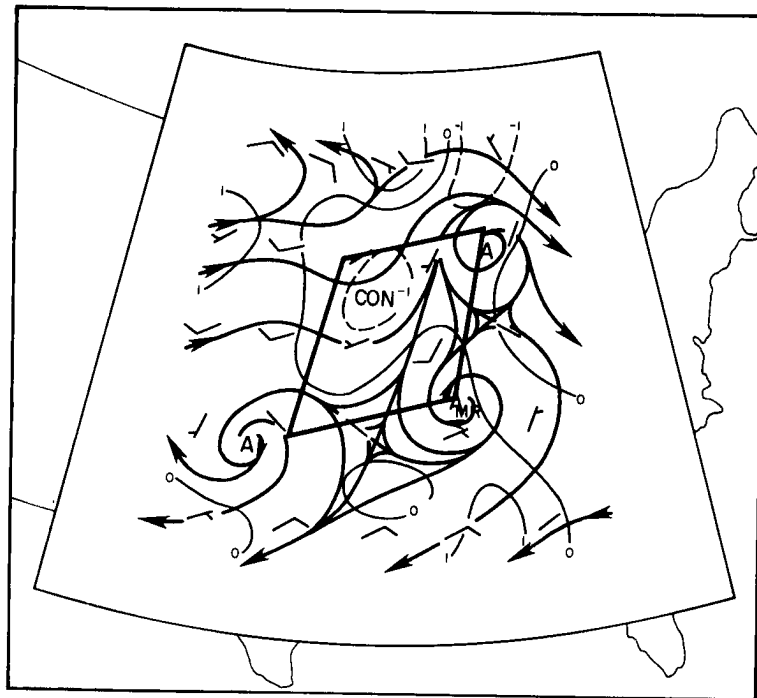
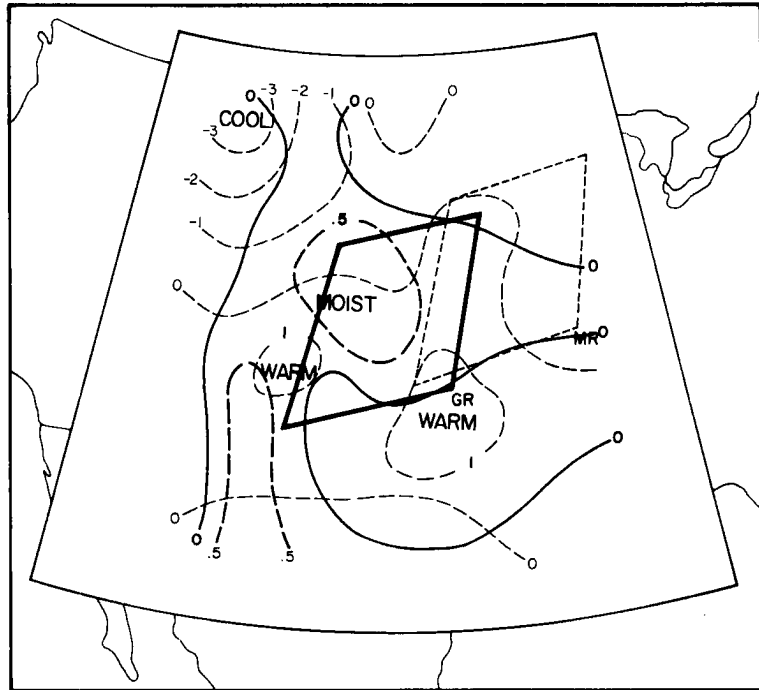
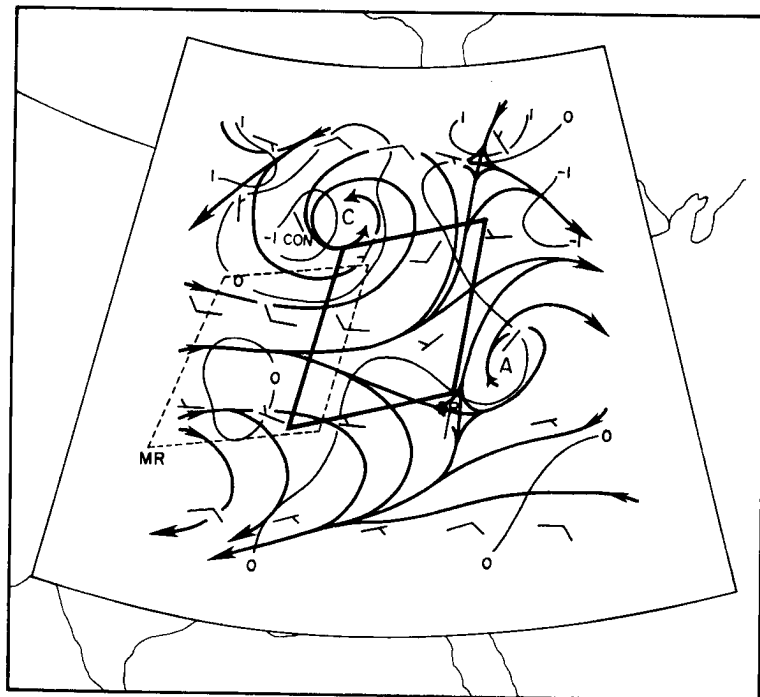
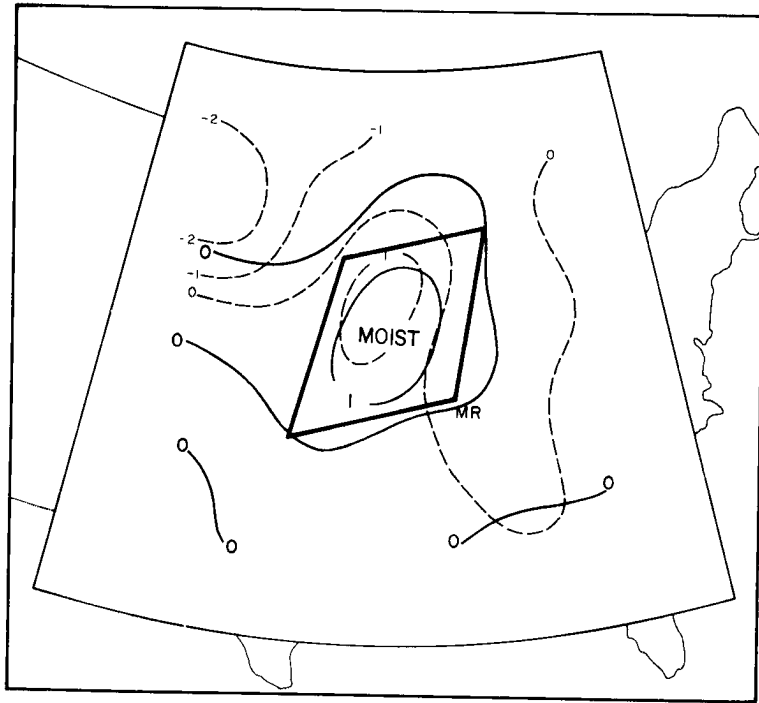


Fig. 54d. Mesoscale analysis of the 500 mb level at the time of the MCC.
Details as in Fig. 54b.

Fig. 54e. Mesoscale analysis of the 500 mb level 12 h after the MCC.
Details as in Fig. 54a.



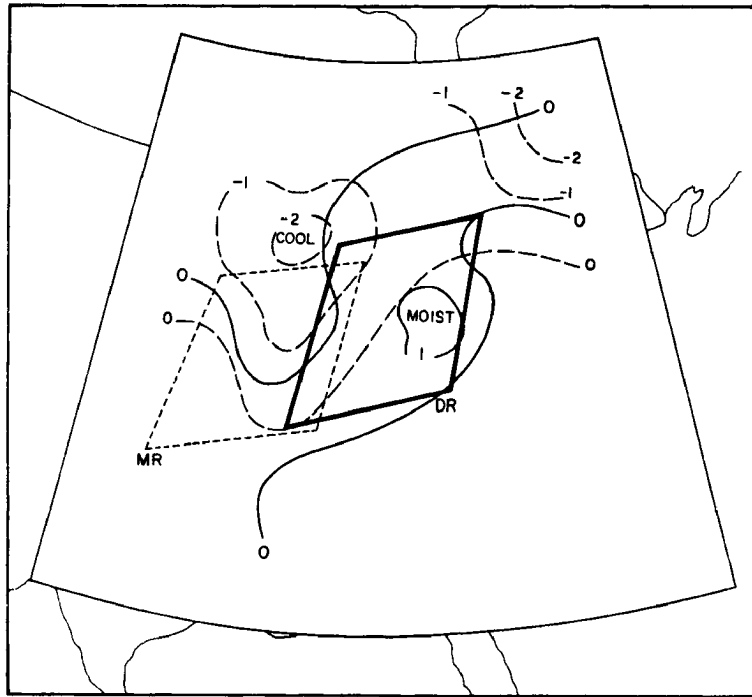


Fig. 54f. Mesoscale analysis of the 500 mb level 12 h after the MCC. Details as in Fig. 54b.

convergence is coincident with this circulation and the flow is weakly divergent over much of the DR. The temperature and moisture analyses (Fig. 54f) show that an unusually moist region has moved eastward and spread northeast from the system. There has been marked cooling and drying over the MR and DR regions and the cyclonic circulation is distinctly cold core.

Perturbation analyses in the upper troposphere (200 mb) are shown in Fig. 55. The perturbation flow prior to the MCC (Fig. 55a) is weakly divergent ($> 1 \times 10^{-5} \text{ s}^{-1}$) and generally less than 10 kt ($\sim 5 \text{ m s}^{-1}$). The temperature is cool over the GR (about 1°C , see Fig. 55b). Twelve hours later, tremendous changes are evident (see Fig. 55c). The perturbation flow depicts an intense anticyclone over the MR, with outflow on the order of 30 - 40 kt along the northern edge of the system. Divergence has increased with maximum values exceeding $7 \times 10^{-5} \text{ s}^{-1}$ centered over

Fig. 55a. Mesoscale analysis of the 200 mb level 12 h prior to the MCC.
Details as in Fig. 54a.

Fig. 55b. Mesoscale analysis of the 200 mb level temperature perturbations 12 h prior to the MCC.

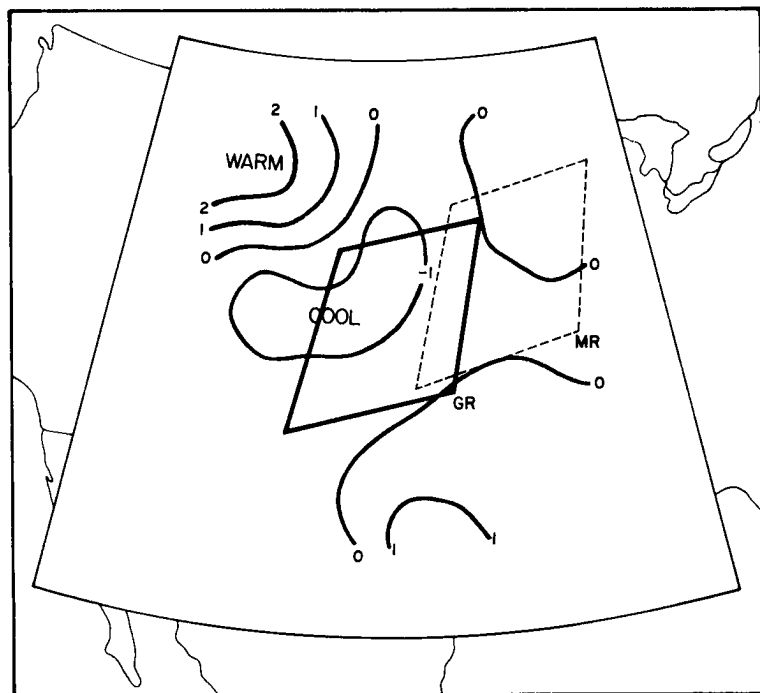
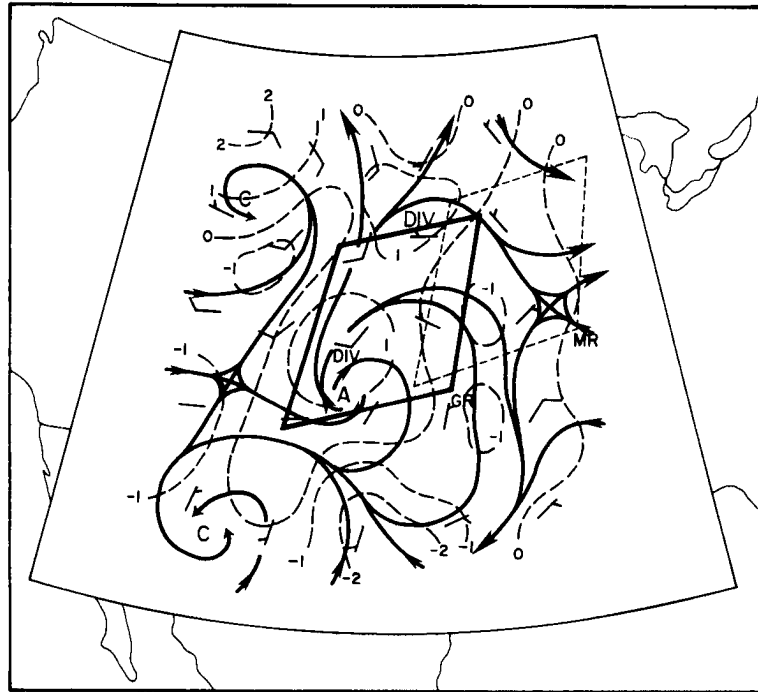
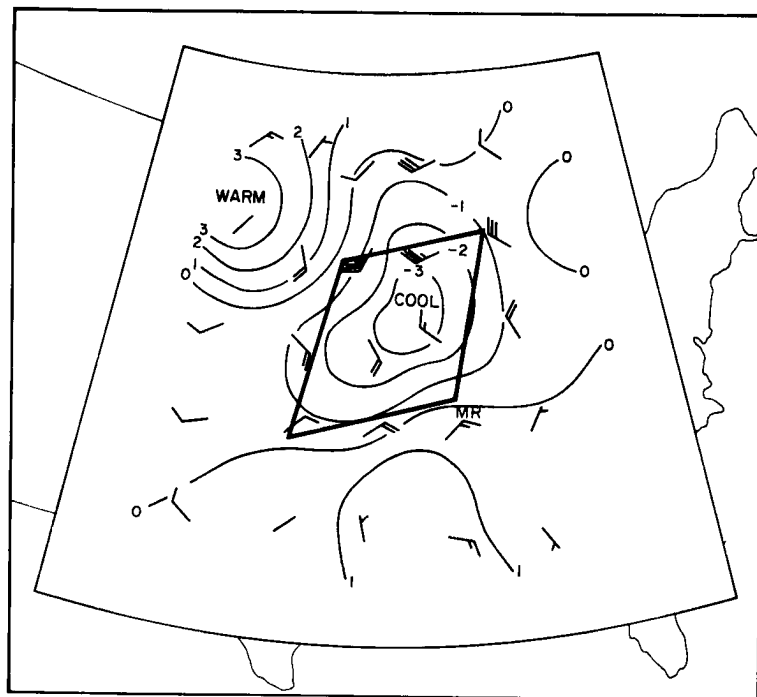
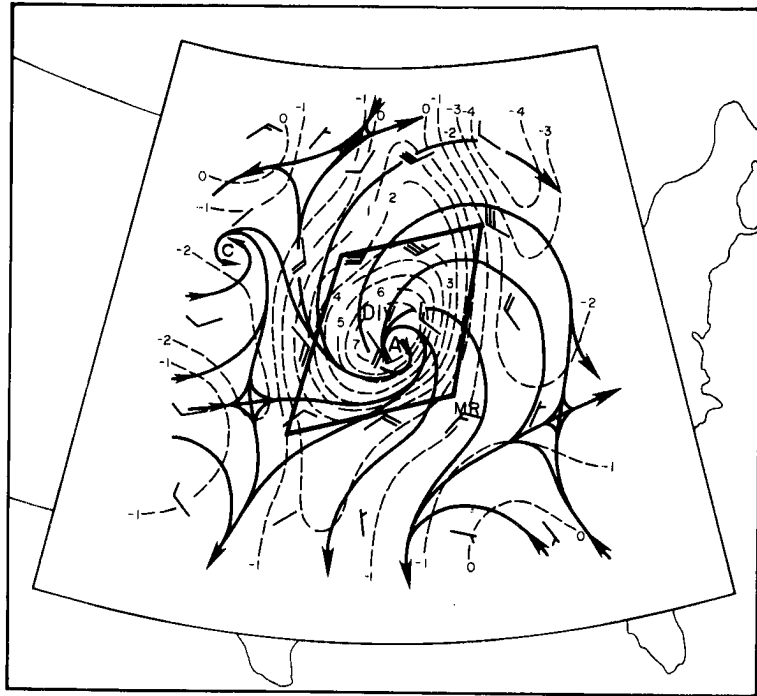


Fig. 55c. Mesoscale analysis of the 200 mb level at the time of the MCC.
Details as in Fig. 54a.

Fig. 55d. Mesoscale analysis of the 200 mb level at the time of the
MCC.



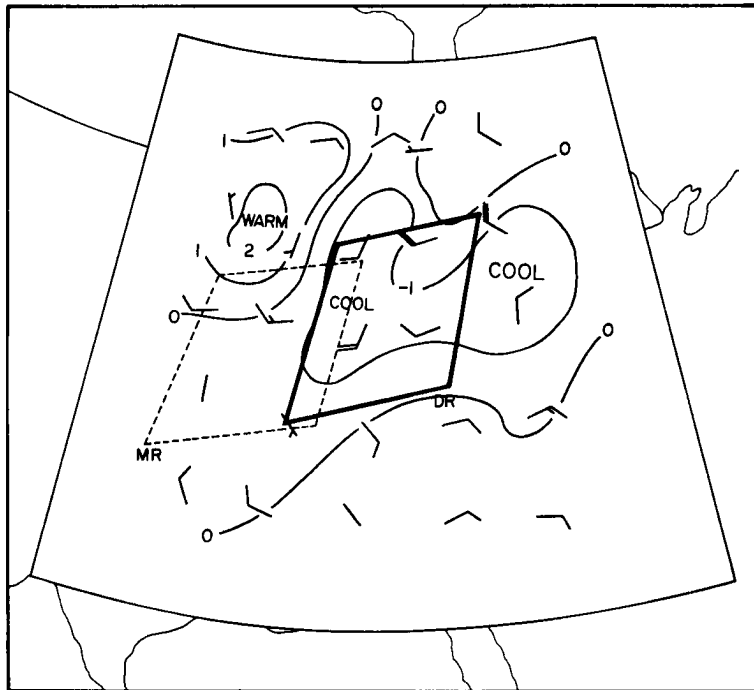
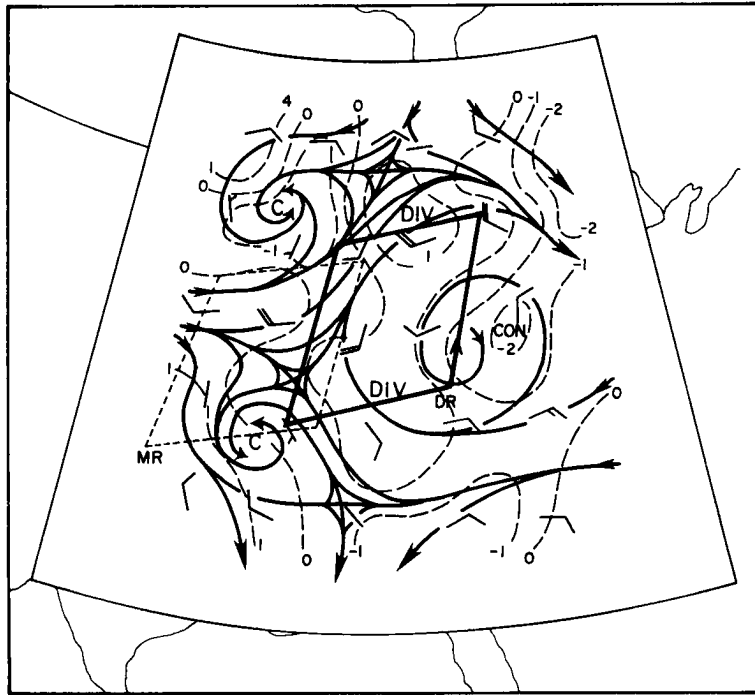
the MCC system. The temperature anomaly (Fig. 55d) has also changed markedly, with a distinct cold core now apparent at 200 mb over the system. There is virtually no continuity of mesoscale features during this 12 h period, reflecting the strength of the convectively-driven circulations (note that the divergent area is almost completely ringed by convergence). Twelve hours later (Fig. 55e), after the system has decayed, the mesoscale flow has become much less organized (once again there is little continuity between (Figs. 55c and 55e). There is weak divergence over much of the DR and the remnants of the once strong out-flow jet are present across the northern DR. The temperature perturbation field (Fig. 55f) has become quite chaotic.

Profiles of the average mesoscale temperature perturbation (for 12 interior grid points following the MCC system, see Fig. 14) are shown in Fig. 56. As the system is developing (before curve) the GR is distinctly warmer within the lower troposphere than its larger-scale environment. At the time of the system, the MR is warm core (relative to its environment) from the surface to 300 mb (the average mesoscale temperature perturbation is on the order of $+1^{\circ}\text{C}$ through this layer) and distinctly cold core at upper-levels. Note that the long-lived convective system studied by Bosart and Sanders (1981) was distinctly cold-core in low-levels. After the MCC has decayed the DR is slightly cool at the surface, weakly warm core at about 300 mb and cold core again at about 150 mb.

West to east vertical cross-sections of the mesoscale wind (in the plane of the section), height, temperature and moisture perturbations along 40°N (see again Fig. 14) are shown for 12 h prior to the MCC in Fig. 57a and b. The height perturbations reflect the lee-trough in low

Fig. 55e. Mesoscale analysis of the 200 mb level 12 h after the MCC.
Details as in Fig. 54a.

Fig. 55f. Mesoscale analysis of the 200 mb level temperature perturbations 12 h after the MCC.



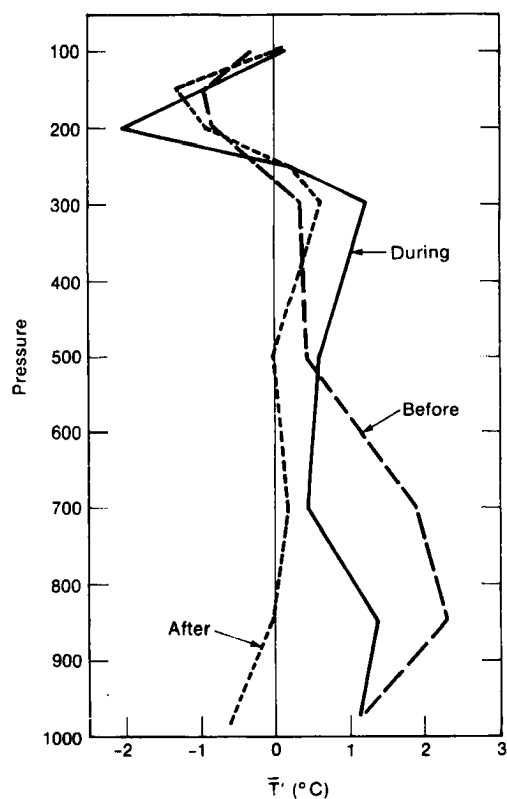


Fig. 56. Average mesoscale temperature perturbations for the 12 interior grid points following the MCC system.

levels (about 130°W) and the ridge over the Plains (about 95°W). The perturbation winds are generally quite light, with some indication of the upper tropospheric speed maximum to the west of the system. The most significant features of the temperature and moisture perturbations are the regions of anomalously warm and moist conditions in the lower levels over the Plains.

Similar west to east cross-sections at the time of the MCC are shown in Figs. 58a and b. Perturbation height and wind fields are significantly different than they were 12 h earlier. The winds now reflect the strong mesoscale (or secondary) circulation directly associated with the MCC. A region of maximum westerly flow in the lower troposphere (900 to 500 mb) is overlain by pronounced outflow at about 200 mb. The positive height perturbations (now > 40 m) aloft have remained centered at about 95°W and

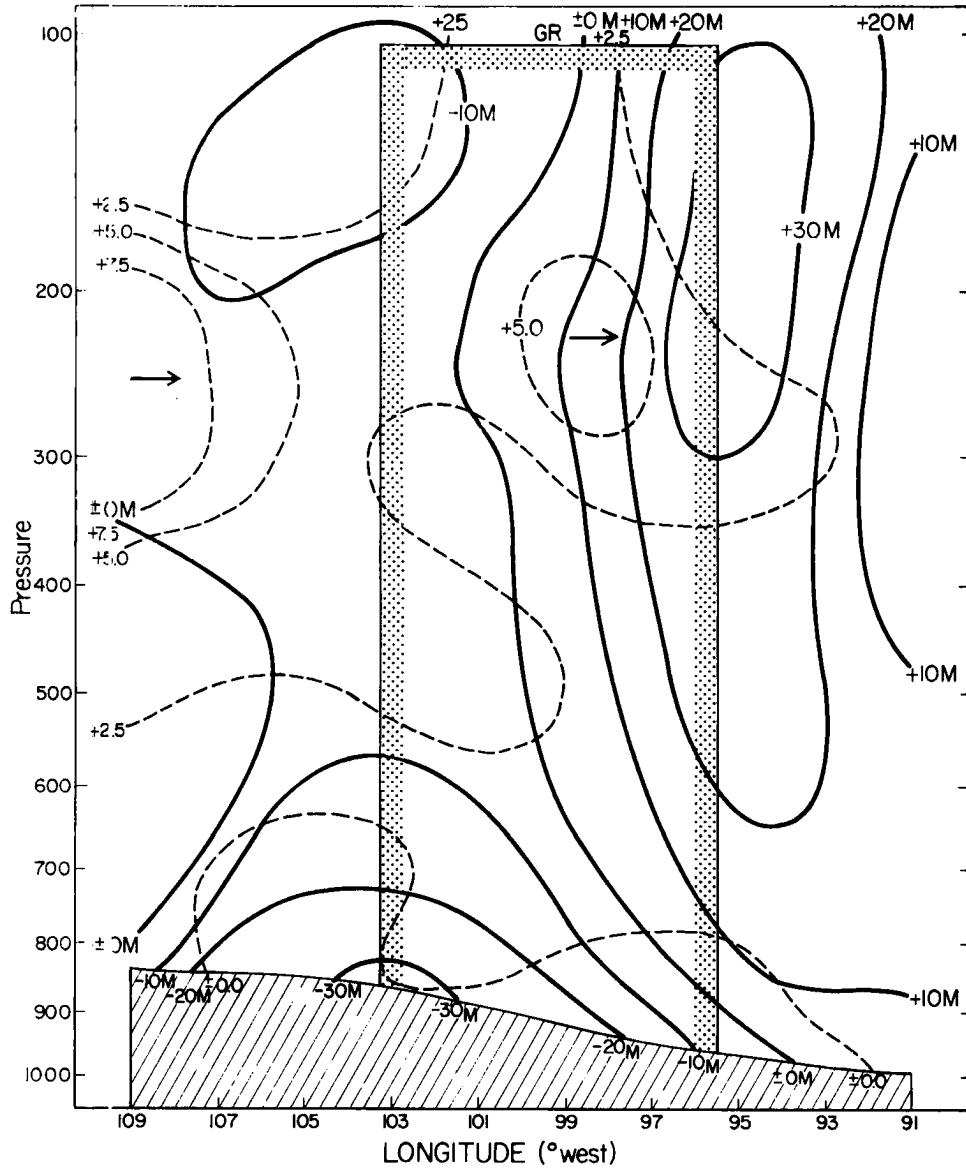


Fig. 57a. West to east cross-section of mesoscale height (solid lines, in m) and u-component (dashed lines, in m s^{-1}) perturbations 12 h prior to the MCC.

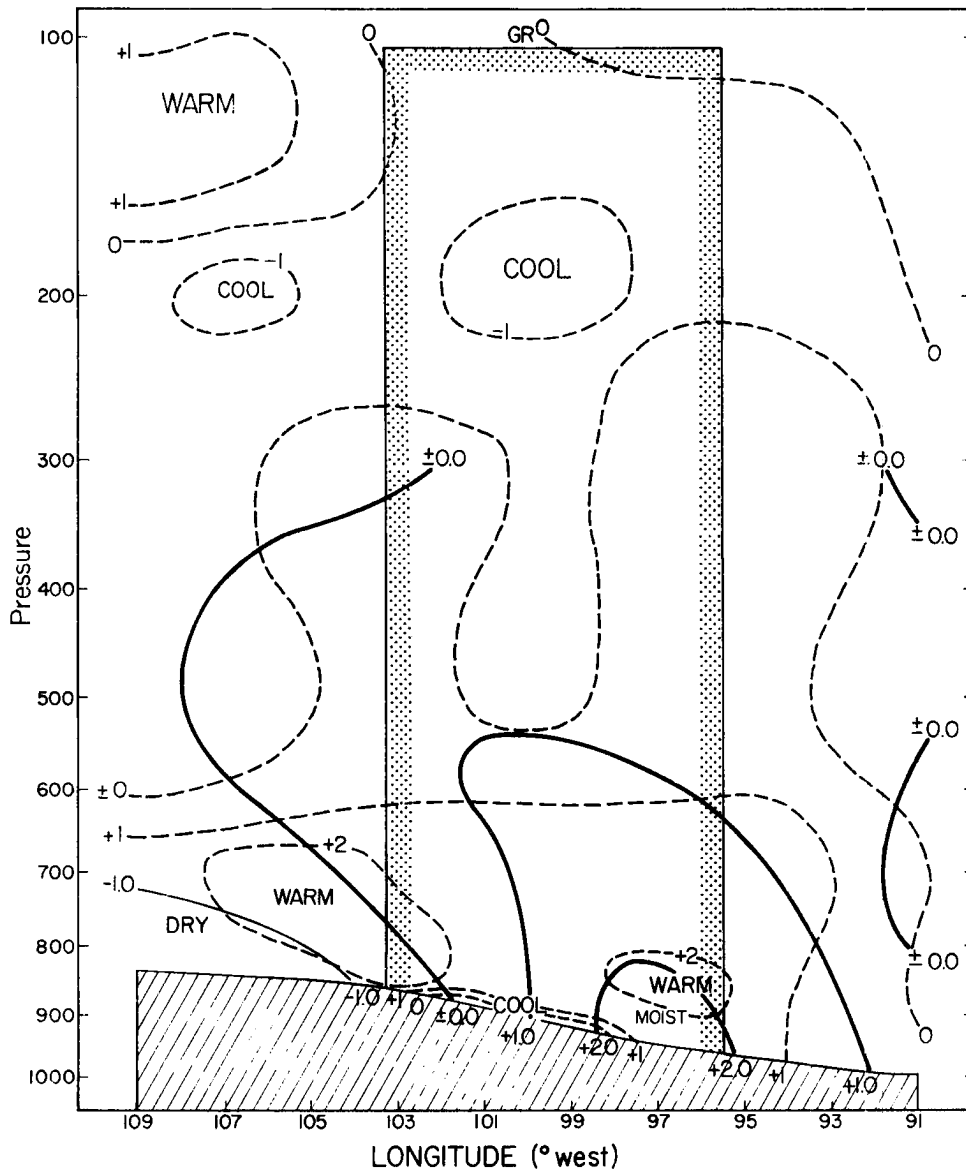


Fig. 57b. West to east cross-section of mesoscale temperature (dashed lines in °C) and moisture (solid lines, in g/kg) perturbations 12 h prior to the MCC.

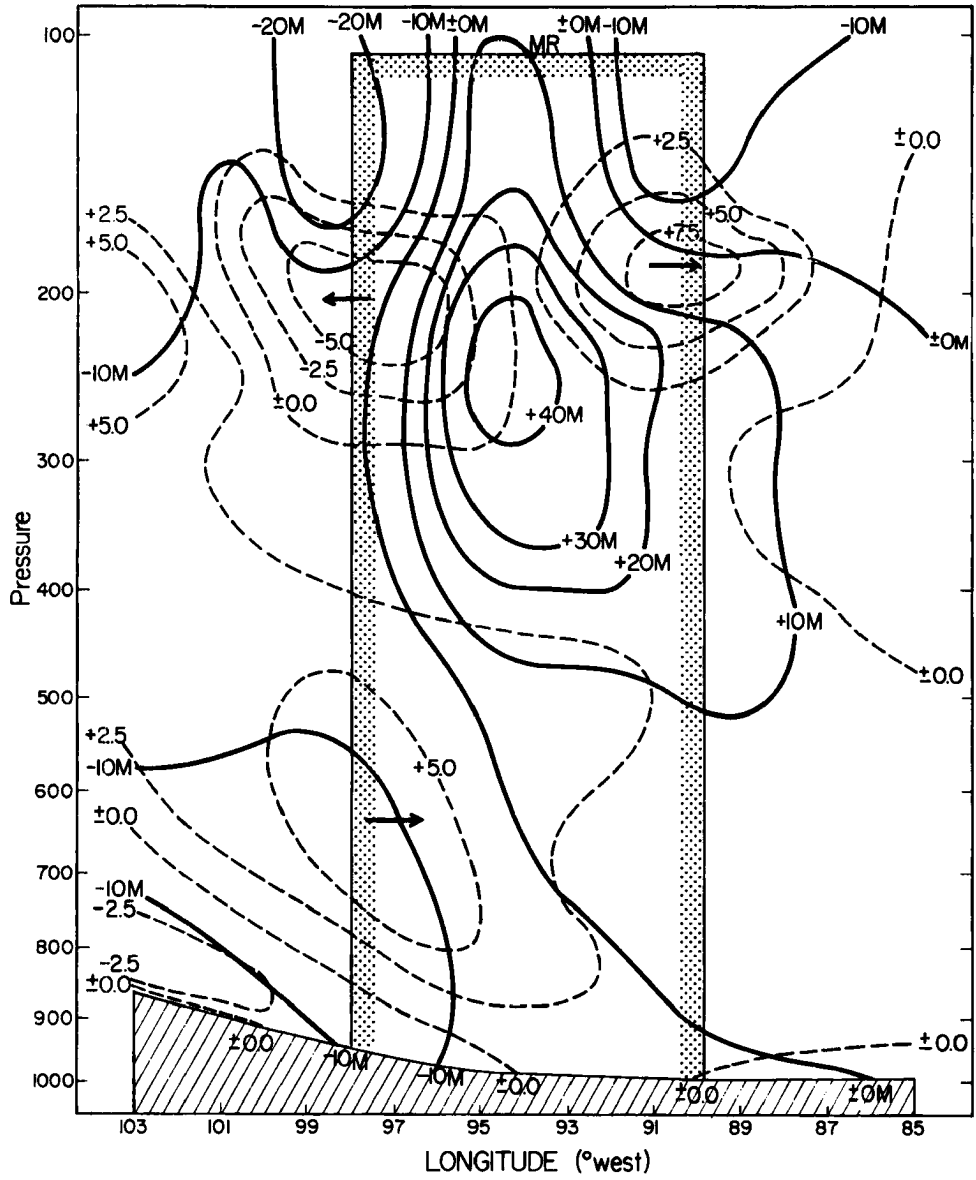


Fig. 58a. West to east cross-section of mesoscale height and u-component perturbation at the time of the MCC. Details similar to Fig. 57.

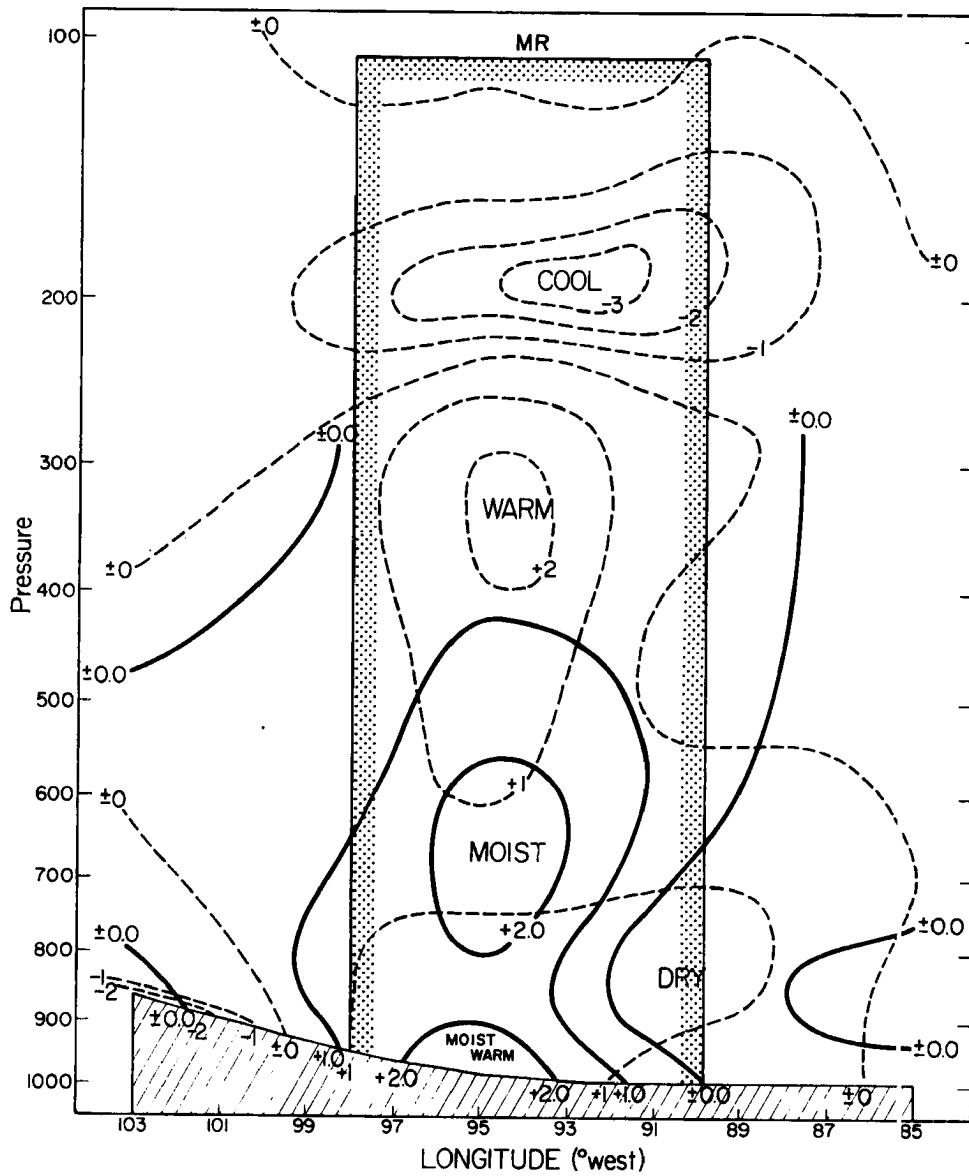


Fig. 58b. West to east cross-section of mesoscale temperature and moisture perturbations at the time of the MCC. Details similar to Fig. 57.

are directly above the MCC (note that the positive perturbation field has expanded eastward relative to that shown in Fig. 57a). The MCC region is distinctly warm relative to its environment up through 250 mb. The warm core is most pronounced between 500 and 300 mb and the upper troposphere above the MCC is much cooler than its near environment. Perturbations exceeding 1 g/kg through 500 mb indicate that the shallow layer of elevated mixing ratios found in Fig. 57b has been lifted through a deep layer. This region of anomalously high mixing ratio appears directly related to MCC mesoscale circulations. South to north sections (Figs. 59a and b) along 95°W at the time of the MCC depict the same general picture as do the west to east sections. The system does appear to slope slightly from south to north and regions to the south of the MCC are anomalously dry. Note the intensity of the mesoscale outflow on the north side of the MCC (speed > 17.5 m s⁻¹).

West to east sections after the organized MCC has decayed are shown in Figs. 60a and b, illustrating a number of interesting changes. The perturbation winds are again (as they were before the system developed) quite light and much less organized than at the time of the MCC. The maximum positive height perturbation continues to exceed 40 m; however, it is now centered at about 84°W. This is an eastward shift of > 900 km during a 12 h period. Comparison of the west to east sections suggests that, had the MCC not developed, the positive height perturbation (ridge) should have been located at about 89.5°W at the time of the MCC. Thus, the perturbing effect of the MCC system upon the upper tropospheric height fields is apparently even greater than explicitly depicted in Fig. 58a. Note that after the system has decayed the upper tropospheric trough has intensified resulting in a pronounced region of anomalously

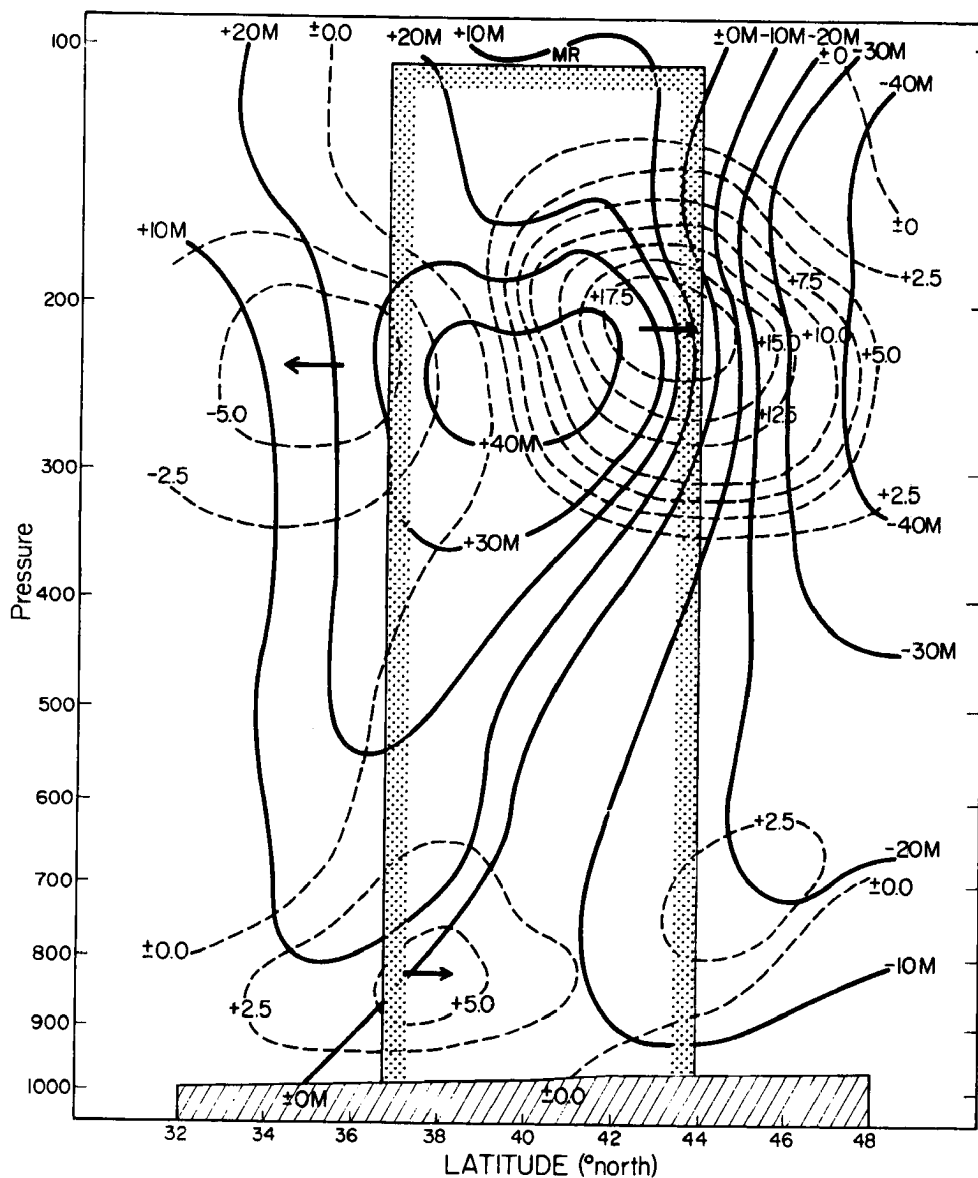


Fig. 59a. South to north cross-section of mesoscale height u-component perturbations at the time of the MCC. Details similar to Fig. 57.

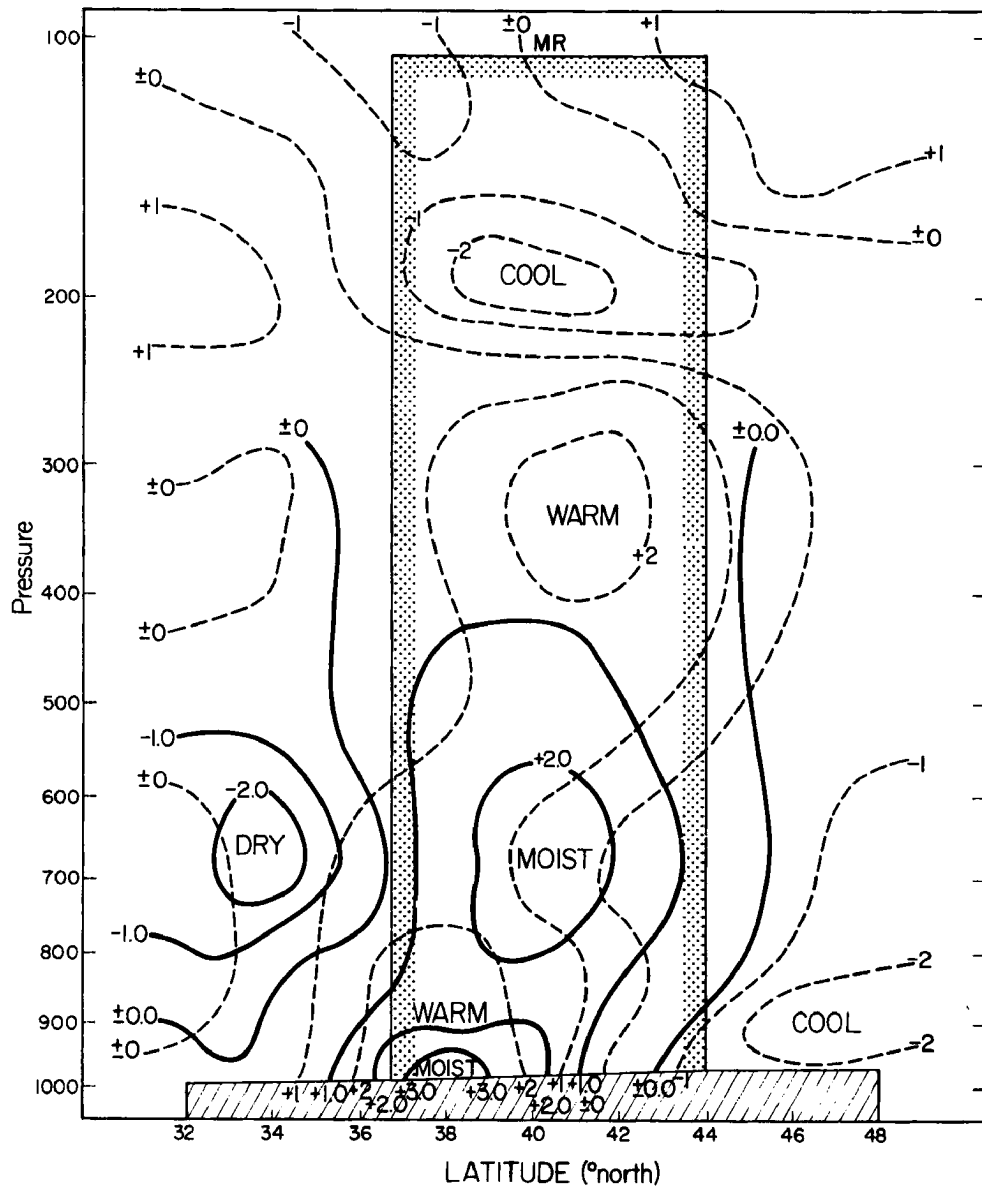


Fig. 59b. South to north cross-section of mesoscale temperature and moisture perturbations at the time of the MCC. Details similar to Fig. 57.

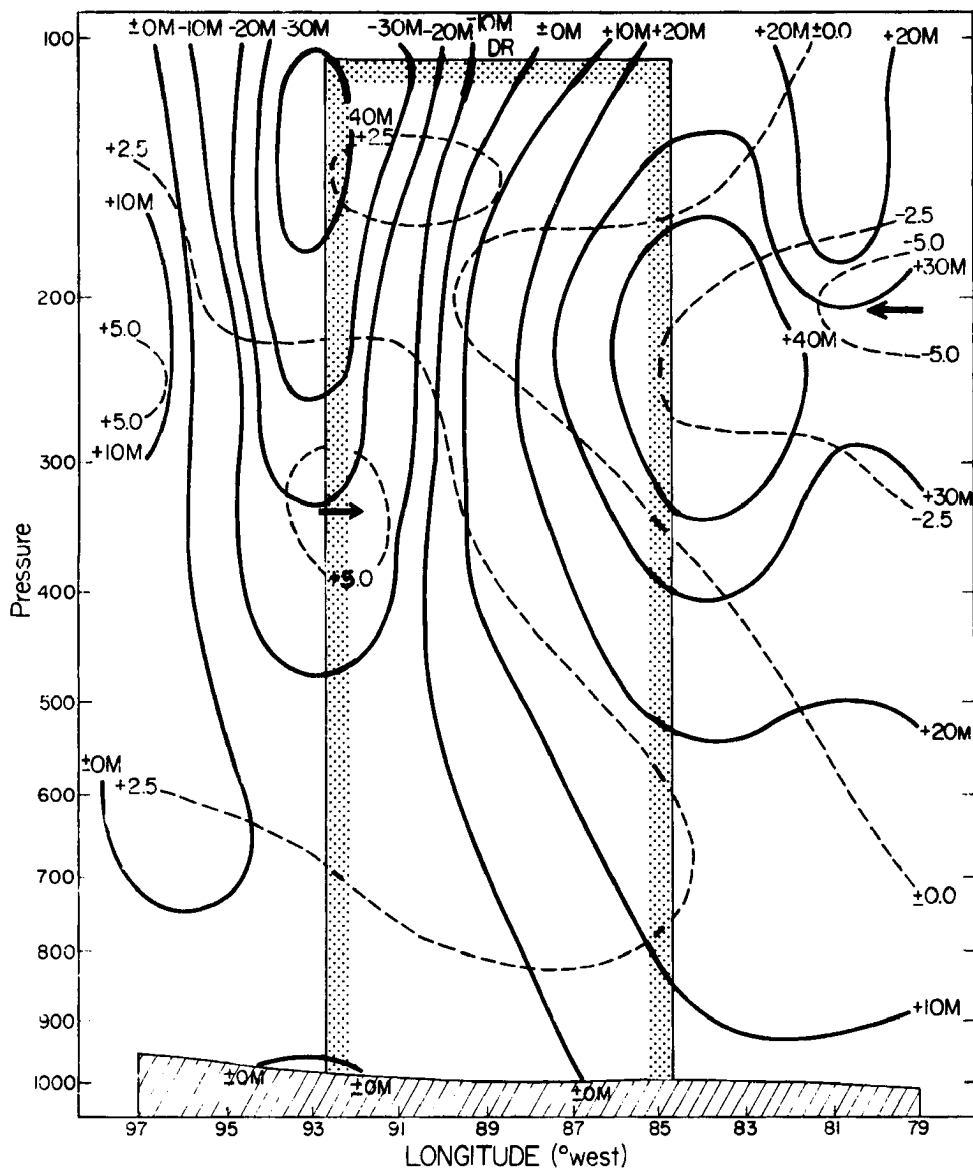


Fig. 60a. West to east cross-section of mesoscale height and u-component perturbations 12 h after the MCC. Details similar to Fig. 57.

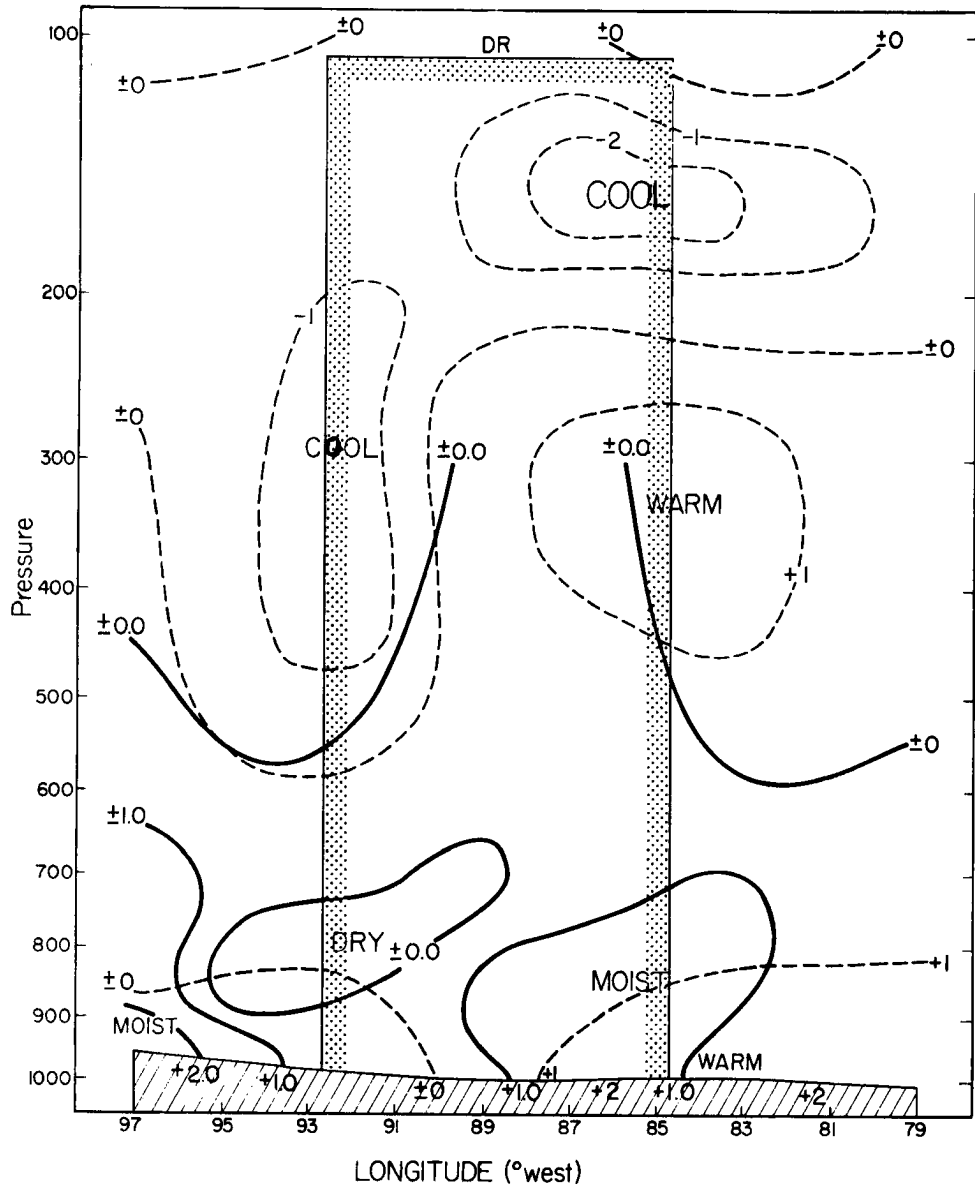


Fig. 60b. West to east cross-section of mesoscale temperature and moisture perturbations 12 h after the MCC. Details similar to Fig. 57.

low heights trailing the DR. Moisture perturbations are now quite weak and suggest that a region of enhanced moisture (and probably cloudiness) has continued to move eastward as the MCC decayed. The warm/cool couplet centered at 300/150 mb has moved eastward slightly faster than the MCC and is not as pronounced as it was 12 h earlier. The trough trailing the MCC now exhibits an upper tropospheric cold core structure that is consistent with the analyses discussed in the previous section.

Indeed, the analyses discussed above (both macroscale and mesoscale) serve to substantiate many aspects of the meso- α scale conceptual model of Section IV that was developed after an examination of the total meteorological fields. It has been shown that an intense, meso- α scale atmospheric circulation (accompanied by pronounced modifications of atmospheric thermal structure and moisture distribution) develops in conjunction with the MCC weather system. When the intense convection that is driving the system can no longer continue (i.e., early to midmorning when the inflow air is no longer unstable and when the boundary-layer flow decreases and backs as surface heating begins) the typical MCC system decays rapidly; however, the atmosphere is left in a highly unbalanced state (i.e., strongly ageostrophic outflow and jet streak along the northern periphery of the system and significant thermal perturbations). The analyses indicate that the jet streak weakens rapidly and becomes less anticyclonic and that the advection patterns associated with the temperature perturbations result in an intensified upper tropospheric short-wave trough. The lower troposphere seems to be unaffected by these upper level adjustments.

The figures shown in Appendix C indicate that the NWS operational forecast model (the LFM) does not adequately forecast the precipitation produced by MCC weather systems. Fritsch and Maddox (1981b) have shown

that the LFM does not forecast the development of the upper tropospheric MCC circulation. Thus the LFM often does not forecast the adjustments described above. Not only do MCCs significantly affect the evolution of tropospheric features and sensible weather over large portions of the eastern U.S. for periods exceeding 24 h but attendant atmospheric developments and responses are not forecast by operational numerical models.

V.3 The MCC Moisture Budget

The characteristics of the MCC life-cycle indicate that the system not only intensifies and grows in extent quite rapidly during the late afternoon and evening but that it also decays rapidly during early to midmorning. The composite system grew to maximum extent several hours prior to 1200 GMT sounding time. Thus the likelihood of deriving quantitatively accurate MCC moisture budgets utilizing the coarse data sets available is not great. Nevertheless a number of such calculations were made so that the energetics of MCCs could be considered in a qualitative manner.

Precipitation isohyets for the 12 h period ending at 1200 GMT are shown in Appendix C for each of the 10 MCCs studied. These data were used to calculate 12 h precipitation for the composite, "typical" MCC and the results are shown in Table 7. During the 12 h considered the composite system produced measurable rainfall across an area of 306,580 km² (for comparison note that the area of the state of Iowa is \sim 129,000 km²). The data of Table 7 indicates that the composite system produced an area average precipitation of 0.79 in. over the rainfall area (or 19.9 mm/12 h or an average rain rate of 1.66 mm/h). This results in the truly prodigious amount of water on the ground of 6.1×10^{12} kg during only 12 h. Since average July precipitation across Iowa is \sim 3 to 4 in.

Table 7

Composite MCC Rainfall

| <u>Amount (in.)</u> | <u>Amount (mm)</u> | <u>Area Affected (km²)</u> | <u>% of MCC Rain Area</u> |
|---------------------|--------------------|---------------------------------------|---------------------------|
| T - 0.5 | T - 12.7 | 138,870 | 45.3 |
| 0.5 - 1.0 | 12.7 - 25.4 | 85,560 | 27.9 |
| 1.0 - 1.5 | 25.4 - 38.1 | 38,590 | 12.6 |
| 1.5 - 2.0 | 38.1 - 50.8 | 17,930 | 5.8 |
| 2.0 - 2.5 | 50.8 - 63.5 | 11,670 | 3.8 |
| 2.5 - 3.0 | 63.5 - 76.2 | 4,380 | 1.4 |
| 3.0 - 3.5 | 76.2 - 88.9 | 3,840 | 1.3 |
| 3.5 - 4.0 | 88.9 - 101.6 | 2,430 | 0.8 |
| 4.0 - 4.5 | 101.6 - 114.3 | 1,810 | 0.6 |
| 4.5 - 5.0 | 114.3 - 127.0 | 890 | 0.3 |
| 5.0 - 5.5 | 127.0 - 139.7 | <u>610</u> | <u>0.2</u> |
| Total Rain Area | | 306,580 | 100% |

(76 to 102 mm) it is apparent from Table 7 that only 2-3 MCC systems could easily account for much of a typical July's rainfall.

Figure 61 shows the vertical profile of average mixing ratio (again over the 12 grid points shown earlier in Fig. 14) following the MCC system and Fig. 62 shows vertical profiles of horizontal moisture advection, moisture divergence and total horizontal moisture flux divergence for the three analysis times. During the genesis period (Fig. 62a) a significant increase in water vapor is indicated in the lower 100 - 150 mb layer. This increase is almost totally a result of vapor convergence. However, at the time of the MCC (Fig. 62b) a significant rate of increase is indicated from the surface through 500 mb. In lower levels this

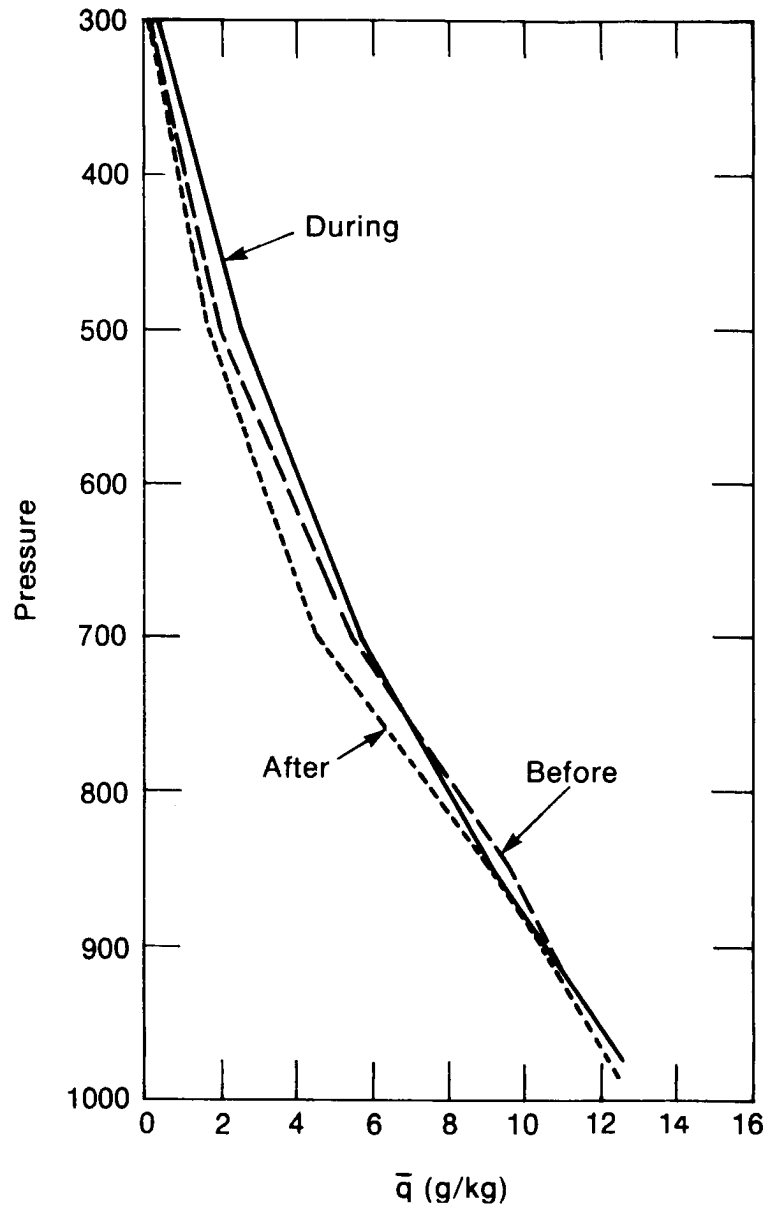
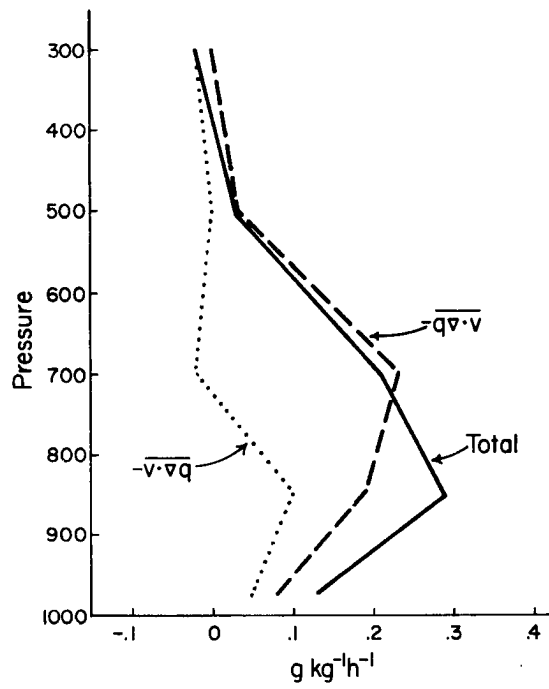
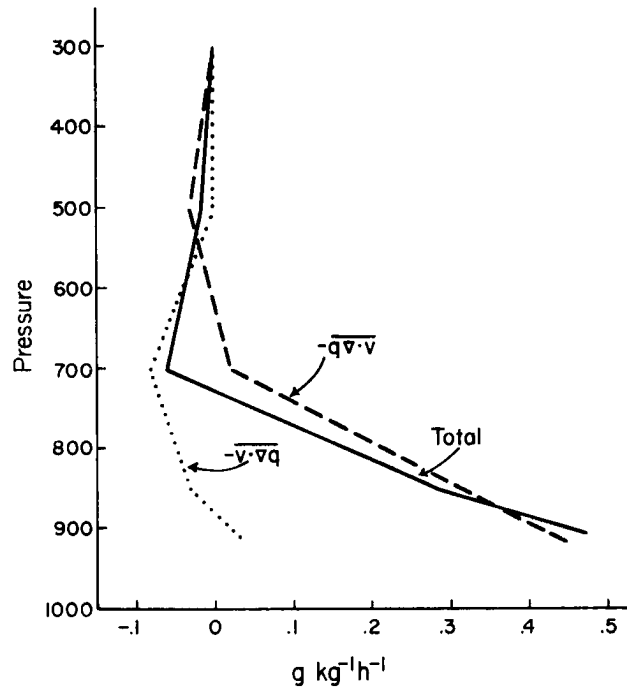


Fig. 61. Vertical profiles of mean mixing ratio following the MCC.

Fig. 62a. Total horizontal flux divergence of water vapor into the Genesis Region (before the MCC) is shown by solid line. Moisture advection is indicated by dotted line and moisture divergence by dashed line.

Fig. 62b. Total horizontal flux divergence of water vapor into the MCC Region (during the MCC). Details as in Fig. 62a.



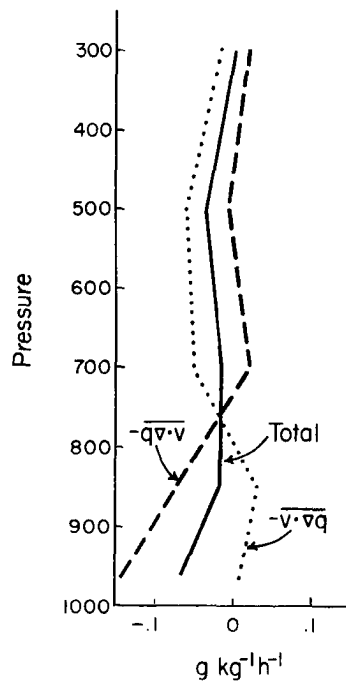


Fig. 62c. Total horizontal flux divergence of water vapor into the Decay Region (after the MCC). Details as in Fig. 62a.

tendency is due to both significant advection and convergence; whereas in mid-levels it is a result of convergence. After the system has decayed (Fig. 62c) a tendency for decreasing vapor content is indicated. At low-levels there is slight positive advection that is counteracted by strong moisture divergence; whereas, in mid-levels there is slight moisture convergence that is counteracted by negative advection.

With the vagaries of accurately specifying areal coverage of convective precipitation in mind, the approach used in considering the moisture budget was extremely simple. All forms of water substance were ignored. Evaporation was not considered and the vertical flux of vapor through the 300 mb surface was ignored. The average mixing ratio and horizontal flux divergence were computed for 16 fixed grid points that covered an area almost exactly equal to the rainfall area of the composite MCC (see Table 7). The 16 points were chosen, considering system movement

and the rainfall maps of Appendix C, as representative of the region that actually experienced rain during the period 0000 to 1200 GMT. The means of the before and during composite data were considered representative of conditions during the precipitation event. Assuming that the total horizontal flux divergence of vapor (.056 g/h) into the system (minus atmospheric storage of .018 g/h) was realized as precipitation, a rain-rate of 0.97 mm/h was indicated. However, the calculated rain rate (from Table 7) was 1.66 mm/h. Thus the large and meso- α scale environment did not supply ample water vapor to the convective system to explain the observed rain amounts. Although the deficit can not be precisely determined from composite data, it is clear that the system processed nearly twice as much water vapor than was supplied by its larger scale environment. This is certainly consistent with similar findings for both tropical and midlatitude convective systems by Gray (1973), Ogura and Cho (1973), Newton (1966) and Fritsch et al. (1976).

The deficit may be explained by considering two aspects of the data studied here. Convective and small-scale features have been filtered from the analyses. Much of the undetected vapor influx undoubtedly occurs within localized regions of strong low-level inflow associated with intense convective elements (especially along the right flank of the system). The vertical resolution of the composite data set is coarse and the time scale of the observations is not sufficient for detailed budget calculations. Since the MCCs grew to largest extent several hours prior to observation time (about the time of the local diurnal low-level wind maximum) it is reasonable to assume that the large and meso- α scale environments supply vapor to the system (from late evening through early morning) at a rate greater than that inferred using only 0000 and 1200 GMT standard level data.

V.4 Kinetic Energy Budgets in the MCC Region

The simple kinetic energy equation considered in this study (similar to that developed by Smith, 1969) is given by:

$$\frac{\partial k}{\partial t} = - \underset{(a)}{V \cdot \nabla \phi} - \underset{(b)}{\nabla \cdot kV} - \underset{(c)}{\frac{\partial \omega k}{\partial p}} + \underset{(d)}{V \cdot F} \quad (1)$$

(a) (b) (c) (d) (e)

V = horizontal wind vector

ω = vertical motion in pressure coordinates

k = horizontal energy per unit mass $[(u^2 + v^2)/2]$

F = frictional force per unit mass

Local changes in k (a) are a result of four processes: kinetic energy generation (b), horizontal flux divergence (c), vertical flux divergence (d) and friction (e). In kinetic energy studies [see for example Robertson and Smith (1980)] term (a) is usually computed as the difference in kinetic energy for two consecutive sounding times with terms (b), (c) and (d) computed at both sounding times and averaged to yield a 12 h mean. Term (e) is then computed as the residual required to balance eq. (1). Term (e) thus includes all subgrid effects including friction. Implicit in this methodology is the assumption that the atmosphere is well-behaved so that kinetic energy and terms (b), (c) and (d) change linearly in time. However, the analyses of Section III indicate that this is probably not the case for MCC situations. In fact, analyses by Maddox (1979) for a single MCC situation showed significant changes in upper-level winds occurring during periods of less than 6 h.

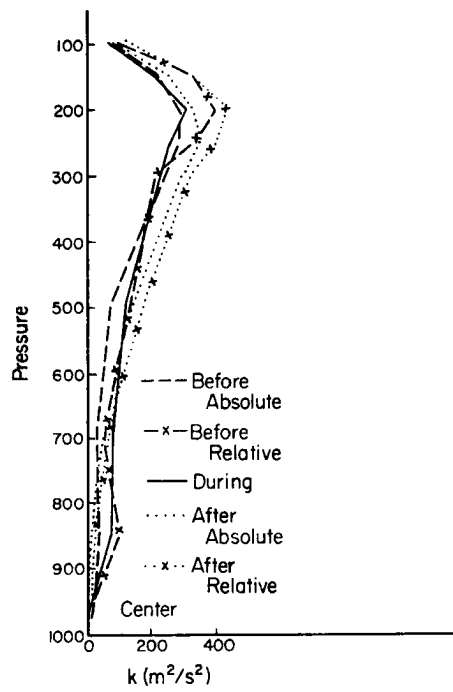
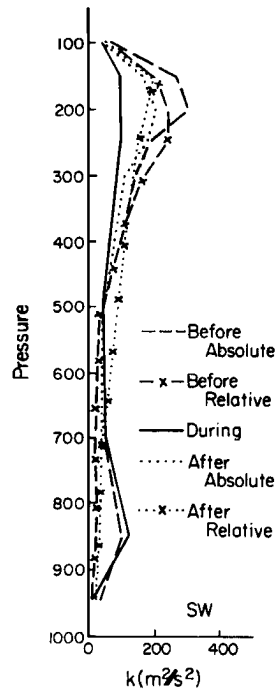
A number of researchers have, nevertheless, studied kinetic energy budgets during intense convective situations employing the basic approach described above. Robertson and Smith (1980) found that the greatest

rates of kinetic energy increase were occurring in regions with deep convection and that horizontal flux convergence constituted the major source of kinetic energy (this reflects the presence of major jet streams in the two springtime cases used). Fuelberg and Scoggins (1978) utilized 3 to 6 h synoptic scale soundings and found that large generation of kinetic energy was associated with areas of convection and that major transport of kinetic energy out of the storm area occurred near the jet stream level. They also found that, even though generation and advection terms were large in the vicinity of active storms, total kinetic energy changed little -- this finding may be an artifact of their use of centered in time differences to compute $\partial k / \partial t$ in eq. (1). McGinley (1975) studied severe thunderstorm situations in and near the NSSL sounding network in Oklahoma and found that storms remained active and intense as long as kinetic energy was transferred from mid-levels into the boundary layer (presumably by storm scale cold downdrafts). Kung and Tsui (1975) and Tsui and Kung (1977) also studied kinetic balances during severe thunderstorm conditions utilizing mesoscale soundings from the NSSL network. They found that net energy changes were very small and that large generation and dissipation were occurring in the lower and upper troposphere. The energetics of the composite MCC system are considered within a very general framework since it is felt that the energetic changes which occur during the MCC life-cycle are most definitely non-steady.

Vertical profiles of kinetic energy (k) are shown in Fig. 63 for the SW, center and NE grid points (see Fig. 14). (Note that k of $100 \text{ m}^2 \text{ s}^{-2}$ within a 100 mb layer over a horizontal area of 1 m^2 is equivalent to approximately $1 \times 10^5 \text{ J m}^{-2}$.) These profiles are shown in both fixed and

Fig. 63a. Vertical profiles (both in relative and fixed coordinates) of kinetic energy at the SW grid point.

Fig. 63b. Vertical profiles (both in relative and fixed coordinates) of kinetic energy at the center grid point.



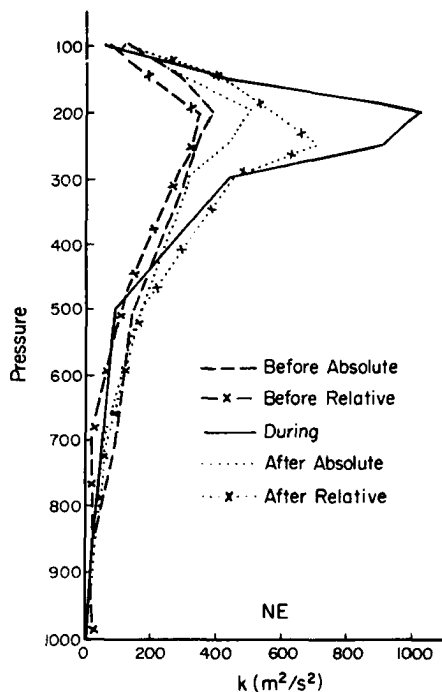


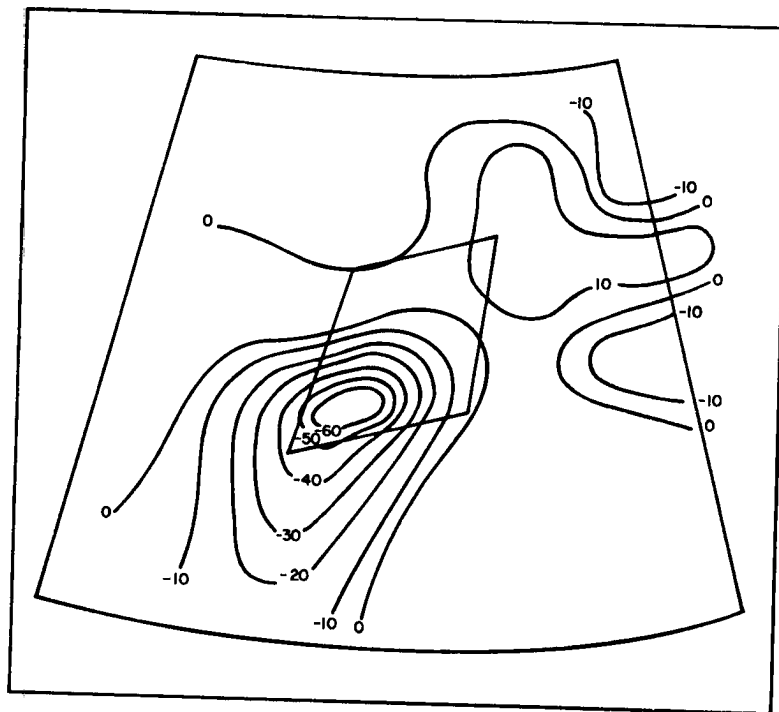
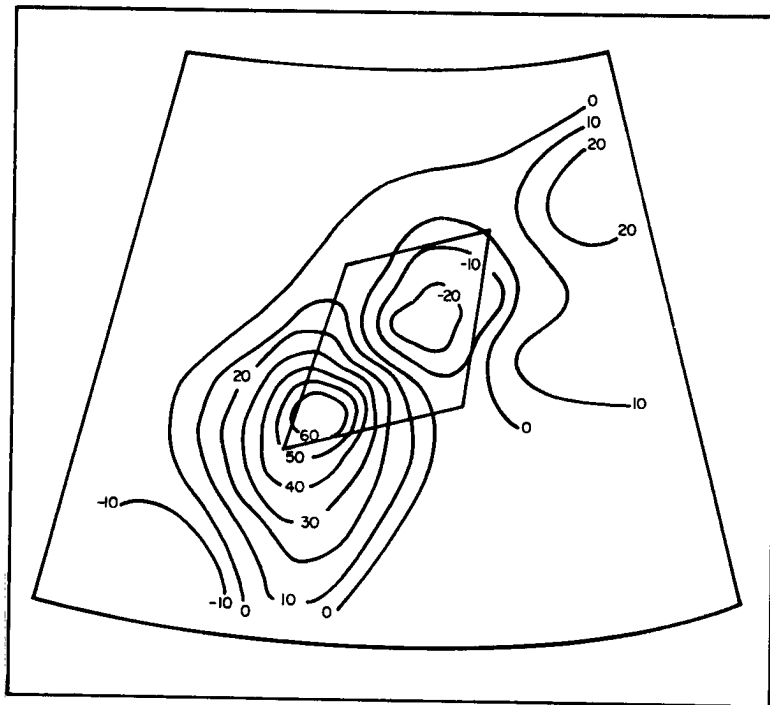
Fig. 63c. Vertical profiles (both in relative and fixed coordinates) of kinetic energy at the NE grid point.

MCC relative coordinates. At the SW corner (Fig. 63a) the increase in the low-level jet is most pronounced in the relative system. The decay of the low-level jet is apparent in both coordinate systems. At upper levels the prominent feature is the decrease in k at the time of the system that is apparent in both reference frames. The center grid point (Fig. 63b) is rather inactive as far as changes in k content are concerned. There is some slight indication of increases in the lower troposphere and decreases in the upper troposphere. However, the NE grid profiles (Fig. 63c) show a strong increase in k at the time of the MCC that is apparent in either coordinate system. Notice the extreme changes in the vertical distribution of k across the MCC region from the SW to the NE corner.

The changes in k within the 850 - 700 mb layer relative to the moving MCC system are illustrated in Fig. 64. From before to during (Fig. 64a) a strong increase in k occurs at the southwestern corner of

Fig. 64a. Change in k ($\text{m}^2 \text{s}^{-2}$) before-during the MCC within the 850 - 700 mb layer following the system.

Fig. 64b. Change in k ($\text{m}^2 \text{s}^{-2}$) during-after the MCC within the 850 - 700 mb layer following the system.



the system with an accompanying, but weaker, decrease over the northeast corner. From during to after (Fig. 64b) k decreases over the southwestern corner while increasing slightly to the northeast of the system. At 500 mb (Figs. 65a and b) the changes are slight with the most prominent characteristic being an increase in k over and to the east of the system with a corresponding decrease to the northwest from during to after. The relative changes in k at 200 mb are depicted in Figs. 66a and b. The change in jet stream structure from before to during is reflected by the strong increase in k over the northeastern portion of the MCC area and the accompanying decrease over the southwestern portion of the area. Comparison with Fig. 39b shows the major k changes occurring directly southwest (for the decrease) and considerably northeast (for the increase) of the upward mass circulation associated with the MCC. From during to after (Fig. 66b) the k pattern tends toward its undisturbed configuration with increases over the SW portion and decreases over the northeast portions of the MCC region.

Tables 8, 9 and 10 present budget tabulations for the three corners in both a fixed and relative sense. Term (a) $[\partial k / \partial t]$ of eq. (1) is computed as the difference between two sequential composite analyses (i.e., 12 h apart) with terms (b), (c) and (d) averaged and then summed (Σ RHS). The residual (R) is computed as $\frac{\partial k}{\partial t} - \Sigma$ RHS so that negative values indicate unresolved destruction of k . The residuals are so great, along with changes in sign depending upon the coordinate system considered, that physical interpretation is difficult. Perhaps the Tables best illustrate that the assumption of steady evolution is totally unrealistic when large convective systems are present and that data with better

Fig. 65a. Change in k ($\text{m}^2 \text{s}^{-2}$) before-during the MCC at 500 mb following the system.

Fig. 65b. Change in ($\text{m}^2 \text{s}^{-2}$) during-after the MCC at 500 mb following the system.

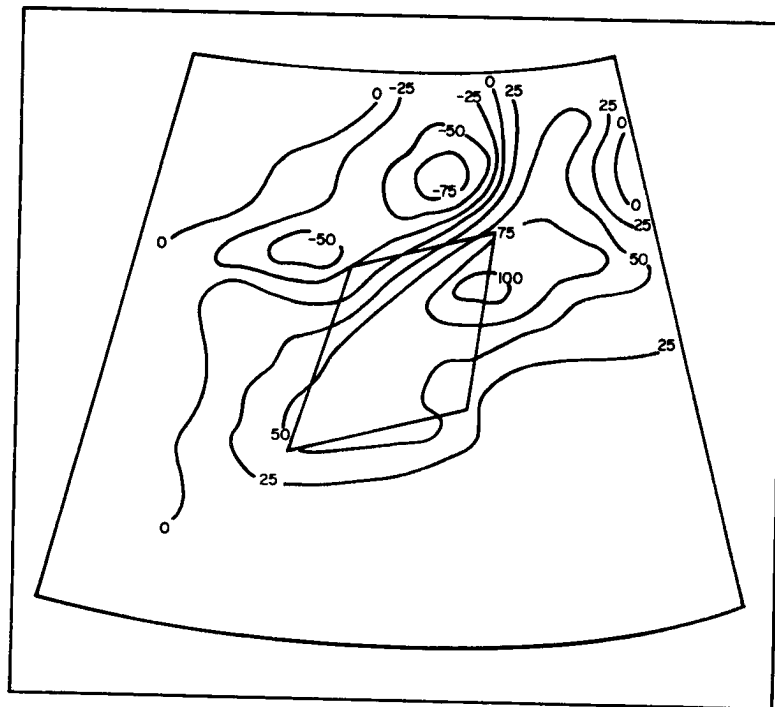
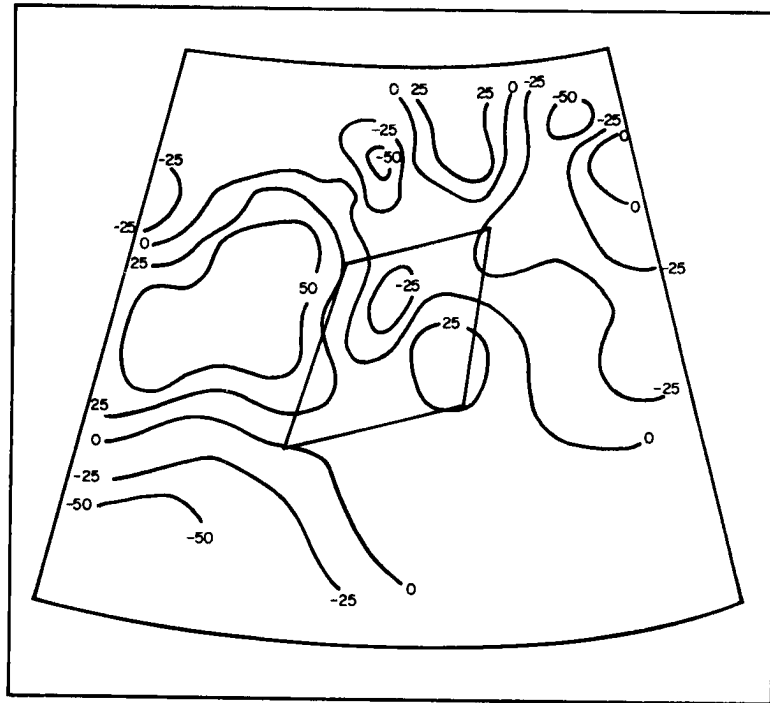


Fig. 66a. Change in k ($\text{m}^2 \text{s}^{-2}$) before-during the MCC at 200 mb following the system.

Fig. 66b. Change in k ($\text{m}^2 \text{s}^{-2}$) during-after the MCC at 200 mb following the system.

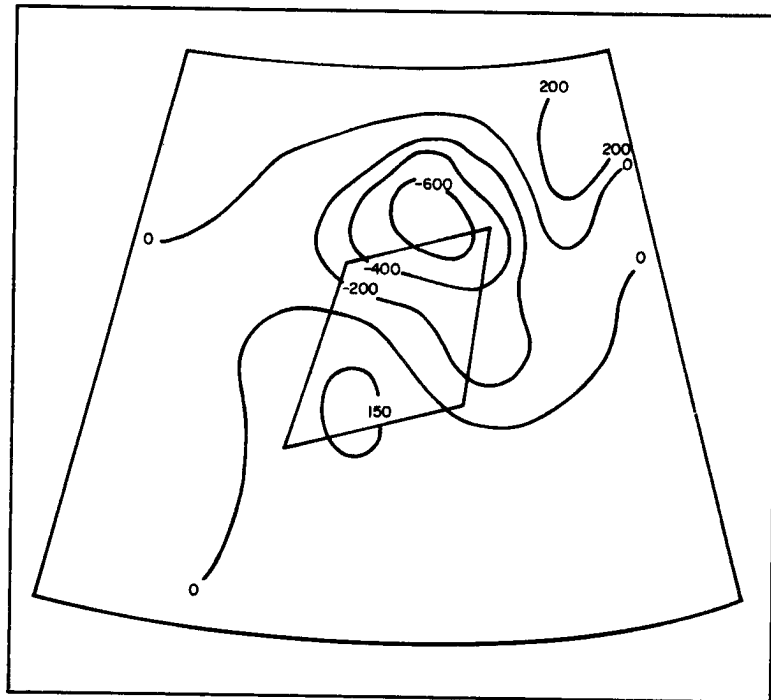
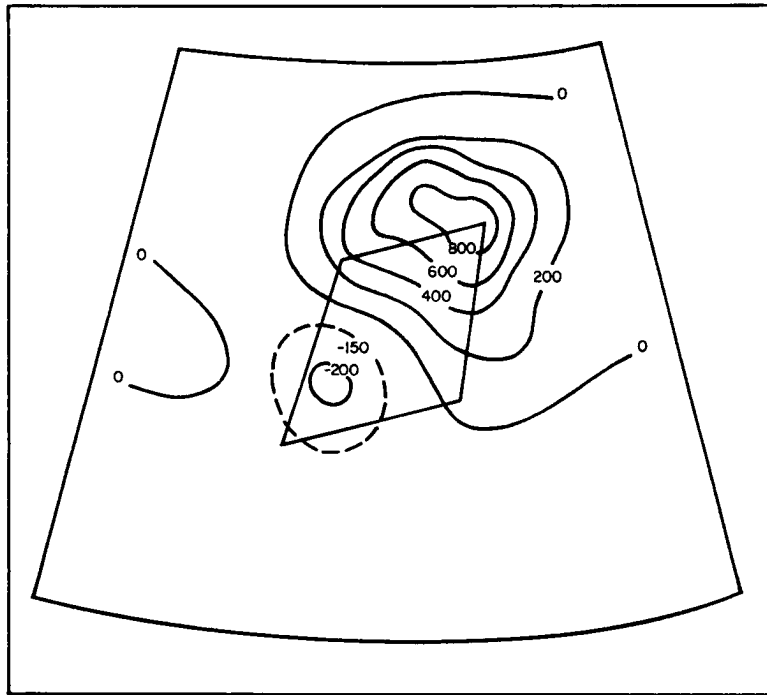


Table 8

Kinetic Energy Budget SW Corner

Relative Coordinates

| | Before to During ($\text{m}^2 \text{s}^{-2}$) | | | During to After ($\text{m}^2 \text{s}^{-2}$) | | |
|---------|---|--------------------------------------|----------|--|--------------------------------------|----------|
| | <u>$\partial k/\partial t$</u> | <u>ΣRHS</u> | <u>R</u> | <u>$\partial k/\partial t$</u> | <u>ΣRHS</u> | <u>R</u> |
| Surface | -3.6 | -37.2 | 33.6 | -4.6 | -12.8 | 8.2 |
| 850 | 88.8 | 30.7 | 59.1 | -81.5 | 12.2 | -83.7 |
| 700 | 37.0 | -35.4 | 72.4 | -10.0 | -62.1 | 52.1 |
| 500 | -2.0 | -21.6 | 19.6 | 39.3 | -39.3 | 78.6 |
| 300 | -81.0 | -119.8 | 38.9 | 50.0 | -48.6 | -98.6 |
| 250 | -142.0 | -50.4 | -91.6 | 60.0 | 10.9 | 49.1 |
| 200 | -153.0 | 64.4 | -217.4 | 101.0 | 262.3 | -161.3 |
| 150 | -103.0 | 101.4 | -204.4 | 101.0 | -38.3 | 139.3 |
| 100 | -34.0 | -67.4 | 33.4 | 11.7 | -90.0 | 111.7 |

Fixed Coordinates

| | Before to During ($\text{m}^2 \text{s}^{-2}$) | | | During to After ($\text{m}^2 \text{s}^{-2}$) | | |
|---------|---|--------------------------------------|----------|--|--------------------------------------|----------|
| | <u>$\partial k/\partial t$</u> | <u>ΣRHS</u> | <u>R</u> | <u>$\partial k/\partial t$</u> | <u>ΣRHS</u> | <u>R</u> |
| Surface | -22.1 | 54.4 | -76.1 | 0.1 | -29.4 | 29.5 |
| 850 | 9.3 | 120.8 | -111.5 | -82.7 | 31.3 | -114.0 |
| 700 | -1.2 | -66.9 | 65.7 | -14.6 | -60.1 | 45.5 |
| 500 | +8 | -97.0 | 96.2 | -2.6 | -20.0 | 17.4 |
| 300 | -57.2 | -693.7 | 636.5 | 32.3 | -14.4 | 46.7 |
| 250 | -93.7 | -610.2 | 516.5 | 78.2 | 29.7 | 48.5 |
| 200 | -200.1 | -719.5 | 519.5 | 107.1 | 127.6 | -20.5 |
| 150 | -166.7 | -330.8 | 164.1 | 67.8 | 17.0 | 50.8 |
| 100 | -17.8 | -143.9 | 126.1 | 2.8 | 7.8 | -5.0 |

Table 9

Kinetic Energy Budget Center Grid Point

Relative Coordinates

| | Before to During ($\text{m}^2 \text{s}^{-2}$) | | | During to After ($\text{m}^2 \text{s}^{-2}$) | | |
|---------|---|--------------------------------------|----------|--|--------------------------------------|----------|
| | <u>$\partial k/\partial t$</u> | <u>ΣRHS</u> | <u>R</u> | <u>$\partial k/\partial t$</u> | <u>ΣRHS</u> | <u>R</u> |
| Surface | -16.8 | 31.5 | -48.3 | -1.6 | 19.9 | -21.5 |
| 850 | 26.6 | 114.9 | -88.3 | -47.2 | -49.5 | 2.3 |
| 700 | 24.8 | -48.6 | 73.4 | -12.7 | -142.8 | -130.1 |
| 500 | 11.6 | -125.9 | 137.5 | 57.9 | -421.5 | 479.4 |
| 300 | 6.7 | -551.7 | 558.4 | 92.3 | -908.5 | 1000.8 |
| 250 | -68.3 | -1521.3 | 1453.0 | 135.7 | -1052.9 | 1188.6 |
| 200 | -82.0 | -2844.6 | 2762.6 | 115.0 | -1289.2 | 1404.2 |
| 150 | -114.3 | -506.8 | 392.5 | 105.7 | -1068.9 | 1174.6 |
| 100 | -36.8 | -287.0 | 250.2 | 15.2 | -453.9 | 467.7 |

Fixed Coordinates

| | Before to During ($\text{m}^2 \text{s}^{-2}$) | | | During to After ($\text{m}^2 \text{s}^{-2}$) | | |
|---------|---|--------------------------------------|----------|--|--------------------------------------|----------|
| | <u>$\partial k/\partial t$</u> | <u>ΣRHS</u> | <u>R</u> | <u>$\partial k/\partial t$</u> | <u>ΣRHS</u> | <u>R</u> |
| Surface | -10.7 | 30.6 | -41.3 | 0.2 | 30.3 | -30.1 |
| 850 | 35.2 | 48.8 | -13.6 | -62.2 | -4.3 | -57.9 |
| 700 | 50.3 | -136.9 | 187.2 | -35.8 | -9.3 | -26.5 |
| 500 | 47.0 | -224.7 | 271.7 | 19.1 | -58.3 | 77.4 |
| 300 | -5.3 | -498.0 | 492.7 | 56.7 | 2.7 | 54.0 |
| 250 | -19.1 | -338.0 | 318.9 | 8.4 | 390.8 | -309.4 |
| 200 | 22.4 | -350.7 | 328.3 | 10.5 | 753.7 | -743.2 |
| 150 | -5.3 | -206.8 | 201.5 | 34.2 | 927.9 | -893.7 |
| 100 | -10.3 | -229.0 | 218.7 | 2.1 | 243.1 | -241.0 |

Table 10

Kinetic Energy Budget NE Corner

Relative Coordinates

| | Before to During ($\text{m}^2 \text{s}^{-2}$) | | | During to After ($\text{m}^2 \text{s}^{-2}$) | | |
|---------|---|--------------------------------------|----------|--|--------------------------------------|----------|
| | <u>$\partial k/\partial t$</u> | <u>ΣRHS</u> | <u>R</u> | <u>$\partial k/\partial t$</u> | <u>ΣRHS</u> | <u>R</u> |
| Surface | -5.3 | 28.3 | -33.6 | 0.8 | 10.8 | -10.0 |
| 850 | 2.0 | 30.3 | -28.3 | 10.7 | -23.5 | 34.2 |
| 700 | 27.4 | -127.2 | 154.6 | 4.5 | -46.4 | 50.9 |
| 500 | -14.7 | -213.3 | 198.6 | 74.7 | 241.7 | -167.0 |
| 300 | 203.8 | -136.4 | 340.2 | -36.1 | 1313.7 | -1349.8 |
| 250 | 581.0 | 340.0 | 24.0 | -200.8 | 2267.9 | -2467.9 |
| 200 | 688.0 | 419.5 | 268.5 | -473.3 | 1530.3 | -2003.6 |
| 150 | 252.0 | -349.8 | 601.8 | -45.8 | 788.3 | -834.1 |
| 100 | -19.2 | -121.5 | 102.3 | 65.6 | 214.2 | -148.6 |

Fixed Coordinates

| | Before to During ($\text{m}^2 \text{s}^{-2}$) | | | During to After ($\text{m}^2 \text{s}^{-2}$) | | |
|---------|---|--------------------------------------|----------|--|--------------------------------------|----------|
| | <u>$\partial k/\partial t$</u> | <u>ΣRHS</u> | <u>R</u> | <u>$\partial k/\partial t$</u> | <u>ΣRHS</u> | <u>R</u> |
| Surface | -0.4 | 6.6 | -7.0 | -0.2 | 11.5 | -11.5 |
| 850 | -4.0 | -17.9 | 13.9 | 9.2 | -44.8 | 54.0 |
| 700 | -37.1 | 32.1 | -69.2 | 14.4 | -167.7 | 172.1 |
| 500 | -55.1 | 115.0 | -170.1 | 77.3 | -300.9 | 378.2 |
| 300 | 172.8 | 137.9 | 34.9 | -171.0 | -488.1 | 317.1 |
| 250 | 584.0 | 535.8 | 48.2 | -479.0 | -238.2 | -240.8 |
| 200 | 649.6 | 573.2 | 76.4 | -543.0 | -32.8 | -510.8 |
| 150 | 166.9 | -52.0 | 218.9 | -143.8 | -1172.1 | 1028.3 |
| 100 | -75.2 | -39.7 | -35.5 | 15.4 | -327.0 | 342.4 |

resolution (especially in time) is required before the energetic processes attending the MCC can be meaningfully described.

Figures 67a, b and c present horizontal distributions of term (b) [k generation] at the time of the MCC for the 850, 500 and 200 mb levels respectively. At 850 mb significant destruction of k is occurring. This is presumably a reflection that the nocturnal low-level jet remains out of balance with the mass field at this time and is blowing slightly up-gradient. The 500 mb pattern indicates weak destruction of k north and northwest of the MCC. The 200 mb field shows intense generation of k over the northwestern portion of the MCC due to down-gradient flow in the system's outflow. The generation area is almost entirely surrounded by a region of upgradient destruction of k. Wilson (1980) computed parcel accelerations along three-dimensional trajectories in the vicinity of a

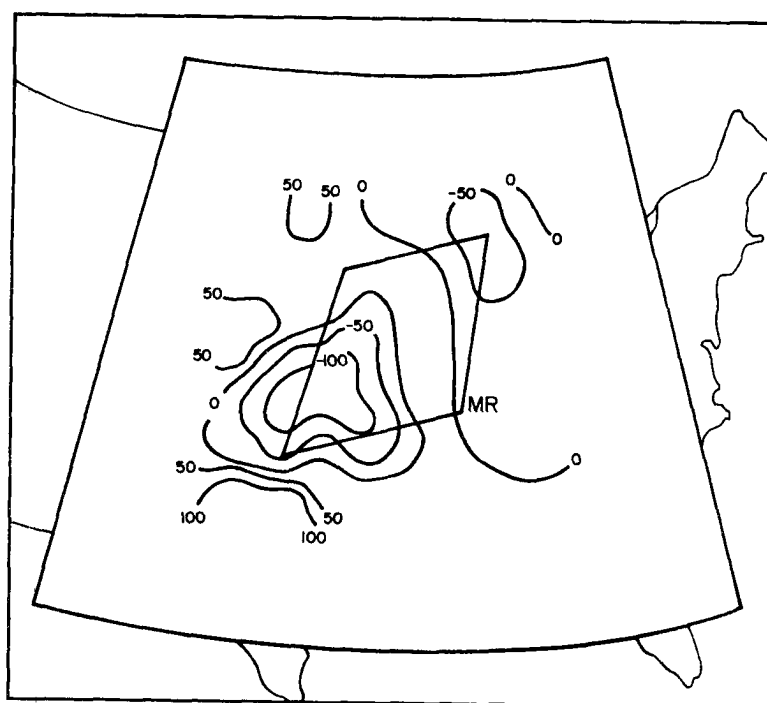


Fig. 67a. Generation of k ($\text{m}^2 \text{s}^{-2}$ per 12 h) at 850 mb at the time of the MCC.

Fig. 67b. Generation of k ($\text{m}^2 \text{s}^{-2}$ per 12 h) at 500 mb at the time of the MCC.

Fig. 67c. Generation of k ($\text{m}^2 \text{s}^{-2}$ per 12 h) at 200 mb at the time of the MCC.

large MCC type convective system and his results were quite similar to those shown here (see for example his Fig. 34). The 200 mb k generation field is entirely consistent with the observed development of the intense jet streak along the northern periphery of the MCC.

VI. SUMMARY AND CONCLUSIONS

Satellite imagery was utilized to identify and study the physical characteristics of large convective weather systems that occurred over the central and eastern United States. Synoptic upper-air sounding data were composited relative to ten of these systems so that meteorological aspects of both the convective weather system and its background environment could be considered. The results of this study are briefly summarized below:

1. An important type of convective weather system, the Mesoscale Convective Complex (MCC), has been identified and quantitatively defined. Their organization, size and attendant mass circulations distinguish MCCs from other types of convective systems.
2. These systems frequently affect the central U.S. and it is felt that MCCs strongly influence the precipitation and convection climatologies for much of the growing season over the corn and wheat belts.
3. Composite analyses of upper-air data show that MCCs interact with and modify their larger-scale environment and thereby affect the evolution of meteorological features over much of the eastern U.S.
4. The weather phenomena, especially heavy precipitation and scale interactions, attending MCC weather systems are not accurately forecast by operational numerical models.
5. A conceptual model of the life-cycle of MCC convective weather systems has been developed and partially substantiated by a

quantitative isolation of mesoscale features. The following list presents important aspects of the MCC life-cycle:

- i) The development and movement of the MCC is closely tied to the eastward progression of a middle tropospheric short-wave trough.
- ii) The initial storm developments occur within a region of organized meso- α scale upward vertical motion that is primarily forced by strong lower-tropospheric warm advection.
- iii) The large-scale setting provides a conditionally very unstable thermodynamic structure over a large region ahead of and to the right of the advancing short-wave.
- iv) Weak relative winds result in poor ventilation of the general storm area.
- v) The nocturnal increase in speed and significant veering of the low-level winds enhances both the warm advection and influx of moist unstable air; while radiative cooling decouples the entire system from the near surface layer.
- vi) Individual storms, clusters of storms and features of their nearby environment interact synergistically, allowing the convective system to grow explosively.
- vii) The nearby environment responds to the continued presence of anomalous diabatic warming in the convective region and a deep inflow develops that reaches to the mid-troposphere.
- viii) Much of the inflow is probably incorporated into a central region of mean mesoscale ascent.

- ix) Convective elements occur within an environment that is characterized by deep moisture and weak or even negative vertical wind shear. Thus, downdrafts are not intense but precipitation efficiency is high.
 - x) Differential radiational cooling beneath the MCC's dense cloud shield and surrounding clear areas acts to enhance the meso-circulations and to prolong the life of the system.
 - xi) The MCC weather system eventually moves into a more stable and convectively less favorable environment, thus initiating its demise.
 - xii) As potentially cool air flows into the system, a deep meso-downdraft develops and the MCC decays.
6. The data studied were of sufficient detail to detect a number of important aspects of the structure of the mature MCC weather system. These are summarized below:
- i) Relative inflow enters the system from all sides within the lower half of the troposphere (especially near 700 mb); however, the system is not directly coupled to the surface layer.
 - ii) Relative flow in mid-levels is quite weak, since the system is moving nearly with the mid-tropospheric flow. In the upper troposphere relative flow diverges around the system and is much stronger downwind than upwind.
 - iii) Strongest convective elements often occur within the right rear quadrant of the system, occasionally assuming line orientations parallel to the system's direction of movement.

- iv) A large region of lighter precipitation and showers also occurs, usually to the left of the region of intense convection, within the area of mean mesoscale ascent.
 - v) The MCC occurs within a region of strong warm advection and significant convergence at the nose of a southerly low-level wind maximum.
 - vi) The system is probably cold core within a shallow surface layer, warm core through much of the mid-troposphere and then cold core again in the upper troposphere and lower troposphere.
 - vii) The thermal structure produces a mesohigh within the boundary layer, a mesolow just above the mesohigh and an upper tropospheric mesohigh capping the system. The mesolow acts to enhance inflow into the system, while the upper mesohigh tightens the height gradient along the northern edge of the system and an intense, anticyclonically curved outflow jet streak forms.
7. Brief examination of the kinetic energy budget indicates that detailed studies of this type must await more comprehensive data sets. This is not because certain MCC systems are not large enough to be considered with synoptic observations but, rather, because the temporal evolution of these systems is extremely non-steady.
8. Moisture budget relationships indicate that the MCC produces considerably more precipitation than can be explained by large and medium scale rates of vapor supply as defined by 12 h synoptic data.

9. The MCC might best be described as a hybrid baroclinic/tropical weather system since it exhibits the following characteristics:

i) Baroclinic aspects

- a. The system develops and moves eastward in conjunction with a weak short-wave trough in the westerlies.
- b. Strong warm advection forces a meso- α scale vertical motion field in which the system grows.
- c. The typical MCC moves eastward within a baroclinic environment; however, pronounced baroclinicity exists primarily within the lower troposphere.
- d. Large scale baroclinic response to thermal perturbations that remain after the system decays produces an intensification of the short-wave trough, especially within the upper troposphere.

ii) Tropical aspects

- a. The system develops within a larger scale environment that is characterized by very weak mid-tropospheric vorticity advection.
- b. The mature system is primarily driven by persistent latent heating associated with intense embedded convective elements.
- c. The system develops wind field and thermal characteristics that are similar to those of tropical convective systems.
- d. The system does not transport sensible heat northward to reduce the pre-existent baroclinicity (i.e., the

system does not develop strong east-west temperature gradients).

It should be emphasized that not all MCCs behave exactly as the ten cases considered here in detail. Some systems may remain nearly stationary, or move quite slowly, even though environmental flows may be very strong. Other systems may actually move against the mean tropospheric flow. Midlatitude MCCs with an arc of intense convective activity along the leading edge of the system were occasionally observed. In such cases it is hypothesized that low-level convergence along the leading edge becomes the dominant forcing mechanism and that the entire system moves along with this mechanism. The environmental relative flows associated with these systems may be quite similar to those of tropical convective systems.

Although this study has provided answers to many basic questions concerning midlatitude Mesoscale Convective Complexes and documented their specific large and medium scale meteorological aspects, a number of important scientific questions remain that were beyond the scope of this initial study. Some of the more important considerations include the following:

1. Are there small scale controls that govern initial thunderstorm formation in the MCC precursor environment?
2. What is the role of storm scale downdrafts and downdraft interactions within a nascent MCC?
3. Precisely how do individual convective storms interact to initiate and drive meso- α or large meso- β scale circulations?
4. What are the small scale characteristics and structure of the diagnosed region of mesoscale upward circulation (e.g., does

the upward mass flux occur primarily within intense storm-scale updrafts?)?

5. What are the details of the precipitation structure of the system?
6. What are the relative contributions of convective and stratiform precipitation?
7. What are the dynamic and thermodynamic constraints that determine the size of a given MCC?
8. What is the longer term (greater than 12 h) impact of MCCs on the evolution of meso- α scale and synoptic scale flow?
9. Are there other controls on dissipation above and beyond the system's progression into a convectively favorable regime?
10. What is the quantitative impact of MCCs on the precipitation climatology of areas east of the Rocky Mountains?
11. What are the dynamic and thermodynamic controls responsible for the distinct nocturnal character of MCCs?
12. What are the quantitative effects of differential radiational cooling upon the evolution of MCC systems?
13. Can the location, timing and intensity of MCC development be accurately forecast?
14. How frequently and in what specific locales do MCC type weather systems affect other parts of the globe?

Midlatitude MCCs, by virtue of their frequent occurrence over the central United States and their large areal extent, should be quite amenable to the more detailed study required to answer these important questions. Existing data sets would initially be of value. For example, the climatologies presented in this work must be considered only a preliminary

effort. Satellite data archives should be utilized to effect a more comprehensive documentation of the types and characteristics of convective weather systems that affect the United States. Detailed precipitation data (such as that available from NOAA EDIS in Hourly Precipitation Data) could be incorporated into the climatology so that the impact of MCC systems upon the precipitation distributions over U.S. agriculture regions could be quantified. In addition the importance of these systems in the climatology of severe thunderstorms could also be determined.

The work reported in this dissertation is essentially of a large and medium scale nature. Detailed study of synoptic network 10 cm radar data, hourly precipitation data, hourly and special surface observations, etc. could help elucidate smaller scale aspects of MCC structure and evolution (e.g., precipitation intensities and distributions, spatial distributions and temporal evolution of intense thunderstorm outflows) allowing more detailed comparison and contrasts of tropical and midlatitude convective systems. The use of high resolution (time and space) satellite data processed upon an interactive system, such as CSU's ADVISAR, would be invaluable in such studies.

The eventual specification of the energetics and detailed structure of MCC systems requires additional data sets that can only be gathered during intensive field efforts designed to probe the life-cycle of a number of systems. Required would be dense surface observations, extensive radar data (5 and 10 cm conventional and Doppler) special sounding networks and high frequency visible, infrared, and satellite sounder data. [Note that soundings from the new geosynchronous satellite sounders (VAS) should be especially useful for studying the MCC's near environment.]

More succinctly, a SESAME-type field effort could be designed to study the development and evolution of MCC weather systems. It would seem most logical to center such a program over the Plains of the United States; however, other regions could be considered (e.g., the northwestern Mexican Provinces experience a high frequency of MCCs that are not only large and intense but quite slow moving). Once such special data sets are gathered, numerical simulations of MCC systems and their near environment (with convective effects either parameterized or explicitly predicted) will provide the ultimate tool for studying and isolating the mechanisms and processes that effect such profound interactions between convective, mesoscale and macroscale features within the MCC environment.

VII. REFERENCES

- Aubert, E. J., 1957: On the release of latent heat as a factor in large scale atmospheric motions. J. Meteor., 14, 527-542.
- Austin, J. M., 1951: Mechanism of Pressure Change. Compendium of Meteorology, T. F. Malone (Editor), AMS, Boston, 630-638.
- Barnes, S. L., 1964: A technique for maximizing details in numerical weather map analysis. J. Appl. Meteor., 3, 396-409.
- _____, 1973: Mesoscale objective map analysis using weighted time series observations. NOAA Tech. Memo. ERL NSSL-62, 60 pp. [NTIS COM-73-10781].
- _____ and D. K. Lilly, 1975: Covariance analysis of severe storm environments. Preprints Ninth Conf. Severe Local Storms (Norman), AMS, Boston, 201-306.
- Bates, F. C., 1961: The Great Plains squall line thunderstorm -- A model. Ph.D. Dissertation, St. Louis University, St. Louis, MO, 161 pp.
- Beebe, R. G. and F. C. Bates, 1955: A mechanism for assisting in the release of convective instability. Mon. Wea. Rev., 83, 1-10.
- Bermowitz, R. J. and E. A. Zurndorfer, 1979: Automated guidance for predicting quantitative precipitation. Mon. Wea. Rev., 107, 122-128.
- Betts, A. K., R. W. Grover and M. W. Moncrieff, 1976: Structure and motion of tropical squall-lines over Venezuela. Quart. J. Roy. Meteor. Soc., 102, 395-404.
- Bleeker, W. and M. J. Andre, 1951: On the diurnal variation of precipitation, particularly over central U.S.A., and its relation to large-scale orographic circulation systems. Quart. J. Roy. Meteor. Soc., 77, 260-271.
- Bonner, W. D., 1966: Case study of thunderstorm activity in relation to the low-level jet. Mon. Wea. Rev., 94, 167-178.
- _____, 1968: Climatology of the low-level jet. Mon. Wea. Rev., 96, 833-850.
- Bosart, L. F. and F. Sanders, 1981: The Johnstown flood of July 1977: A long-lived convective storm. Submitted to J. Atmos. Sci.
- Brown, J. M., 1979: Mesoscale unsaturated downdrafts driven by rainfall evaporation: A numerical study. J. Atmos. Sci., 36, 313-338.
- Browning, K. A. and F. H. Ludlum, 1962: Airflow in convective storms. Quart. J. Roy. Meteor. Soc., 88, 117-135.

- Brunk, I. W., 1953: Squall lines. Bull. Amer. Meteor. Soc., 34, 1-9.
- Byers, H. R. et al., 1949: The thunderstorm. Govt. Printing Office, Washington, D. C., 287 pp. (NTIS #PB234515).
- Chang, C. E., D. J. Perkey and C. W. Kreitzberg, 1981: A numerical case study of the squall line of 6 May 1975. Submitted to J. Atmos. Sci.
- Charba, J. P., 1979: Recent performance of operational two-six hour objective forecasts of severe local storms on outbreak days. Preprints 11th Conf. on Severe Local Storms (Kansas City), AMS, Boston, 600-607.
- Charney, J. G. and A. Eliassen, 1964: On the growth of the hurricane depression. J. Atmos. Sci., 21, 68-75.
- Clark, J. D., A. J. Lindner, R. Borneman and R. E. Bell, 1980: Satellite observed cloud patterns associated with excessive precipitation outbreaks. Preprints Eighth Conf. on Weather Forecasting and Analysis (Denver), AMS, Boston, 463-473.
- Cotton, W. R., R. L. George and P. J. Wetzel, 1981: A long-lived meso-scale convective complex. Part I: The mountain generated component. Submitted to Mon. Wea. Rev.
- Cryslar, K. A., R. A. Maddox, B. M. Muller and L. R. Hoxit, 1980: Climatology of heavy precipitation and flash flooding for various regions of the United States. Submitted to Mon. Wea. Rev.
- Darkow, G. L., V. E. Suomi and P. M. Kuhn, 1958: Surface thermal patterns as a tornado forecast aid. Bull. Amer. Meteor. Soc., 10, 532-537.
- _____ and D. W. McCann, 1977: Relative environmental winds for 121 tornado bearing storms. Preprints Tenth Conf. on Severe Local Storms (Omaha), AMS, Boston, 413-417.
- Dirks, R. A., 1969: A climatology of central Great Plains mesoscale convective systems. Final Contract Report ESSA Grant E-10-68G, Atmospheric Science Dept., Colorado State Univ., Ft. Collins, CO, 60 pp.
- Doswell, C. A., III, 1977: Obtaining meteorologically significant surface divergence fields through the filtering property of objective analysis. Mon. Wea. Rev., 105, 885-892.
- Emanuel, K. A., 1979: Inertial stability and mesoscale convective systems. Preprints Eleventh Conf. on Severe Local Storms (Kansas City), AMS, Boston, 421-426.
- Fankhauser, J. C., 1969: Convective processes resolved by a mesoscale rawinsonde network. J. Appl. Meteor., 8, 778-798.

- Fankhauser, J. C., 1974: The derivation of consistent fields of wind and geopotential height from mesoscale rawinsonde data. J. Appl. Meteor., 13, 637-464.
- Fernandiz, W., 1980: Environmental conditions and structure of some types of convective mesosystems observed over Venezuela. Arch. Met. Geoph. Biokl., Ser. A, 29, 249-267.
- Follansbee, W. A. and V. J. Oliver, 1975: A comparison of infrared imagery and video pictures in the estimation of daily rainfall from satellite data. NOAA Tech. Memo. NESS 62, Washington, D.C., 14 pp.
- Frank, W. M., 1977: Convective fluxes in tropical cyclones. J. Atmos. Sci., 34, 1554-1568.
- _____, 1978: The life-cycles of GATE convective systems. J. Atmos. Sci., 35, 1256-1264.
- Fritsch, J. M., 1975: Cumulus dynamics: Local compensating subsidence and its implications for cumulus parameterization. Pageoph., 113, 851-867.
- _____, C. F. Chappell and L. R. Hoxit, 1976: The use of large-scale budgets for convective parameterization. Mon. Wea. Rev., 104, 1408-1418.
- _____, R. A. Maddox, L. R. Hoxit and C. F. Chappell, 1979: Convectively driven mesoscale pressure systems aloft. Preprints Fourth Conf. on Numerical Weather Prediction (Silver Spring), AMS, Boston, 398-406.
- _____ and C. F. Chappell, 1980: Numerical prediction of convectively driven mesoscale pressure systems, Part II: Mesoscale model. To be published in J. Atmos. Sci.
- _____ and R. A. Maddox, 1981a: Convectively driven mesoscale weather systems aloft. Part I: Observations. J. Appl. Meteor., 20, No. 1.
- _____ and R. A. Maddox, 1981b: Convectively driven mesoscale weather systems aloft. Part II: Numerical simulations. J. Appl. Meteor., 20, No. 1.
- Fuelberg, H. E. and J. R. Scoggins, 1978: Kinetic energy budgets during the life cycle of intense convective activity. Mon. Wea. Rev., 106, 637-653.
- Fujita, T., 1955: Results of detailed synoptic studies of squall lines. Tellus, 4, 405-436.
- _____, 1959a: Precipitation and cold air production in mesoscale thunderstorm systems. J. Meteor., 16, 454-466.
- _____, 1959b: Study of mesosystems associated with stationary radar echoes. J. Meteor., 16, 38-52.

- Fujita, T., and H. A. Brown, 1958: A study of mesosystems and their radar echoes. Bull. Amer. Meteor. Soc., 39, 538-554.
- Gandin, L. S., 1963: Objective Analysis of Meteorological Fields. Hydrometeor. Publ. House, Leningrad, USSR (English version, Israel Program for Scientific Translations, 1965), 242 pp.
- George, R. L., 1979: Evolution of mesoscale convective systems over mountainous terrain. Colorado State Univ. Atm. Sci. Paper No. 318, Ft. Collins, 160 pp.
- Glahn, H. R. and D. A. Lowry, 1972: The use of Model Output Statistics (MOS) in objective weather forecasting. J. Appl. Meteor., 11, 1203-1211.
- Gray, W. M., 1968: Global view of the origin of tropical disturbances and storms. Mon. Wea. Rev., 96, 669-700.
- _____, 1973: Cumulus convection and larger scale circulations, I. Broadscale and mesoscale considerations. Mon. Wea. Rev., 101, 839-855.
- Griffith, C. G., W. L. Woodley, P. G. Grube, D. W. Martin, J. Stout, and D. N. Sikdar, 1978: Rain estimation from geosynchronous satellite imagery -- visible and infrared studies. Mon. Wea. Rev., 1153-1171.
- Griffith, K. T., S. K. Cox and R. G. Knollenberg, 1980: Infrared radiative properties of tropical cirrus clouds inferred from aircraft measurements. J. Atmos. Sci., 37, 1077-1087.
- Grover, R. W., 1974: Characteristics of tropical squall-lines over Venezuela. Atm. Sci. Paper No. 228, Colorado State University, Ft. Collins, 79 pp.
- Hamilton, R. A. and J. W. Archbold, 1945: Meteorology of Nigeria and adjacent territory. Quart. J. Roy. Meteor. Soc., 71, 231-262.
- Hane, C. E., 1972: Squall line structure and maintenance: Numerical experimentation. Florida State University. Report No. 72-5, Dept. of Meteorology, Tallahassee, FL, 190 pp.
- _____, 1973: The squall line thunderstorm: Numerical experimentation. J. Atmos. Sci., 30, 1672-1690.
- Hobbs, P. V., T. J. Matejka, P. H. Herzegh, J. D. Locatelli, and R. A. Houze, Jr., 1980: The mesoscale and microscale structure and organization of clouds and precipitation in midlatitude cyclones. I: A case study of a cold front. J. Atmos. Sci., 37, 568-596.
- Holloway, J. L., Jr., 1958: Smoothing and filtering of time series and space fields. Advance in Geophysics, Vol. 4, Academic Press, 351-389.

- Holton, J. R., 1972: An introduction to dynamic meteorology. Academic Press, New York, 319 pp.
- Hoskins, B. J., I. Draghici and H. C. Davies, 1978: A new look at the ω -equation. Quart. J. Roy. Meteor. Soc., 104, 31-38.
- Houze, R. A., Jr., 1977: Structure and dynamics of a tropical squall-line system. Mon. Wea. Rev., 105, 1541-1567.
- Hoxit, L. R., 1975: Diurnal variations in planetary boundary-layer winds over land. Boundary-Layer Meteor., 8, 21-38.
- _____, C. F. Chappell and J. M. Fritsch, 1976: Formation of meso-lows or pressure troughs in advance of cumulonimbus clouds. Mon. Wea. Rev., 104, 1419-1428.
- Kasahara, A., 1961: A numerical experiment on the development of a tropical cyclone. J. Meteor., 18, 259-282.
- Kincer, J. B., 1916: Daytime and nighttime precipitations and their economic significance. Mon. Wea. Rev., 44, 628-633.
- Klein, W. H. and H. R. Glahn, 1974: Forecasting local weather by means of model output statistics. Bull. Amer. Meteor. Soc., 55, 1217-1227.
- Krietzberg, C. W. and D. J. Perkey, 1977: Release of potential instability: Part II. The mechanism of convective/mesoscale interaction. J. Atmos. Sci., 34, 1569-1595.
- Kung, E. C. and T. L. Tusi, 1975: Subsynoptic-scale kinetic energy balance in the storm area. J. Atmos. Sci., 32, 729-740.
- La Seur, N., 1974: Middle latitude convective systems -- an introduction. Subsynoptic Extratropical Weather Systems: Observation, Analysis, Modeling and Prediction: Volume I, Principal Lectures, 46-52. Available from National Center for Atmospheric Research, Boulder, CO.
- Leary, C. A., 1979: Behavior of the wind field in the vicinity of a cloud cluster in the intertropical convergence zone. J. Atmos. Sci., 36, 631-639.
- _____ and R. A. Houze, Jr., 1979: The structure and evolution of convection in a tropical cloud cluster. J. Atmos. Sci., 36, 437-457.
- Lilly, D. K., 1979: The dynamical structure and evolution of thunderstorms and squall lines. Ann. Rev. Earth Planet. Sci., 7, 117-161.
- Ludlum, F. H., 1966: Cumulus and cumulonimbus convection. Tellus, 18, 687-698.
- Ludwig, G. H., 1974: The NOAA operational environmental satellite system - status and plans. Preprints Sixth Conf. on Aerospace and Aeronautical Meteorology (El Paso), AMS, Boston, 137-145.

- MacDonald, A. E., 1977: On a type of strongly divergent steady state. Mon. Wea. Rev., 105, 771-785.
- Maddox, R. A., 1976: An evaluation of tornado proximity wind and stability data. Mon. Wea. Rev., 104, 133-142.
- _____, 1979: The evolution of middle and upper tropospheric features during a period of intense convective storms. Preprints Eleventh Conf. on Severe Local Storms (Kansas City), AMS, Boston, 41-48.
- _____, 1980: An objective technique for separating macroscale and mesoscale features in meteorological data. Mon. Wea. Rev., 108, 1108-1121.
- _____, L. R. Hoxit, C. F. Chappell and F. Caracena, 1978: Comparison of meteorological aspects of the Big Thompson and Rapid City flash floods. Mon. Wea. Rev., 106, 375-389.
- _____, C. F. Chappell and L. R. Hoxit, 1979a: Synoptic and meso- α scale aspects of flash flood events. Bull. Amer. Meteor. Soc., 60, 115-123.
- _____, L. R. Hoxit and C. F. Chappell, 1979b: Interactions between convective storms and their environment. Final Project Report NASA Contract No. S-40336B, 96 pp.
- _____, D. J. Perkey and J. M. Fritsch, 1980: Evolution of upper-tropospheric features during the development of a Mesoscale Convective Complex. Submitted to J. Atmos. Sci.
- Magor, B. W., 1959: Mesoanalysis: Some operational analysis technique utilized in tornado forecasting. Bull. Amer. Meteor. Soc., 40, 499-511.
- Malkus, J. S. and H. Riehl, 1960: On the dynamics and energy transformations in steady-state hurricanes. Tellus, 12, 1-20.
- Manabe, S., 1956: On the contribution of heat released by condensation to the change in pressure pattern. J. Meteor. Soc. Japan, 34, No. 6, 12-24.
- Mansfield, D. A., 1977: Squall lines observed in GATE. Quart. J. Roy. Meteor. Soc., 103, 569-574.
- Martin, D. W. and D. N. Sikdar, 1975: A case study of Atlantic cloud clusters: Part I. Morphology and thermodynamic structure. Mon. Wea. Rev., 103, 691-708.
- Marwitz, J. D., 1972: Precipitation efficiency of thunderstorms. Proc. Third Conf. on Wea. Mod. (Rapid City), AMS, Boston, 245-247.

- Matsumoto, S. and K. Ninomiya, 1967: On the mesoscale warm core above the condensation level related to convective activities under the influence of dome shaped cold air. J. Meteor. Soc. Japan, 45, 306-314.
- McBride, J. L. and W. M. Gray, 1980a: Mass divergence in tropical weather systems Paper I: Diurnal variation. Quart. J. Roy. Meteor. Soc., 106, 501-516.
- _____ and _____, 1980b: Mass divergence in tropical weather systems Paper II: Large-scale controls on convection. Quart. J. Roy. Meteor. Soc., 106, 517-538.
- McGinley, J. A., 1975: Environmental energy fields associated with severe storms. WEAT Report No. 13, Univ. of Oklahoma Atmospheric Research Laboratory, Norman, OK, 129 pp.
- McNulty, R. P., 1978: On upper tropospheric kinematics and severe weather occurrence. Mon. Wea. Rev., 106, 662-672.
- Means, L. L., 1944: The nocturnal maximum occurrence of thunderstorms in the midwestern states. Misc. Report No. 16, The Univ. of Chicago, 38 pp.
- _____, 1952: On thunderstorm forecasting in the central United States. Mon. Wea. Rev., 80, 165-189.
- _____, 1954: A study of the mean southerly wind-maximum in low levels associated with a period of summer precipitation in the Middle West. Bull. Amer. Meteor. Soc., 35, 166-170.
- Miller, R. C., 1967: Notes on analysis and severe storm forecasting procedures of the Military Weather Warning Center. AWS Tech. Report 200 (available from Headquarters Air Weather Service, Scott AFB, IL), 94 pp.
- Moncrieff, M. W. and M. J. Miller, 1976: The dynamics and simulation of tropical cumulonimbus and squall lines. Quart. J. Roy. Meteor. Soc., 102, 373-394.
- Neumann, J., 1951: Land breezes and nocturnal thunderstorms. J. Meteor., 8, 60-67.
- Newton, C. W., 1950: Structure and mechanism of the prefrontal squall line. J. Meteor., 7, 210-222.
- _____, 1962: Dynamics of severe convective storms. NSSP Report No. 9, Washington, D. C., 44 pp.
- _____, 1966: Circulations in large sheared cumulonimbus. Tellus, 18, 699-713.
- _____ and S. Katz, 1958: Movement of large convective rainstorms in relation to winds aloft. Bull. Amer. Meteor. Soc., 32, 129-136.

- _____ and H. R. Newton, 1959: Dynamical interaction between large convective clouds and environment with vertical shear. J. Meteor., 16, 483-496.
- Ninomiya, K., 1971a: Dynamical analysis of outflow from tornado-producing thunderstorms as revealed by ATS III pictures. J. Appl. Meteor., 10, 275-294.
- _____, 1971b: Mesoscale modification of synoptic situations from thunderstorm development as revealed by ATS III and aerological data. J. Appl. Meteor., 10, 1103-1121.
- O'Brien, J. J., 1970: Alternative solutions to the classical vertical velocity problem. J. Appl. Meteor., 9, 197-203.
- Ogura, Y., 1964: Frictionally controlled, thermally driven circulations in a circular vortex with application to tropical cyclones. J. Atmos. Sci., 21, 610-621.
- _____ and H. R. Cho, 1973: Diagnostic determination of cumulus cloud populations from observed large-scale variables. J. Atmos. Sci., 30, 1276-1286.
- _____ and Y. L. Chen, 1977: A life history of an intense mesoscale convective storm in Oklahoma. J. Atmos. Sci., 33, 1458-1476.
- _____, Y. L. Chen, J. Russell and S. T. Soong, 1979: On the formation of organized convective systems observed over the eastern Atlantic. Mon. Wea. Rev., 107, 426-441.
- _____ and M. Liou, 1980: The structure of a mid-latitude squall line: a case study. J. Atmos. Sci., 37, 553-567.
- Ooyama, K., 1964: A dynamical model for the study of tropical cyclone development. Geofisica International Mexico, 4, 187-198.
- Orlanski, I., 1975: A rational subdivision of scales for atmospheric processes. Bull. Amer. Meteor. Soc., 56, 527-530.
- Paegle, J., 1978a: A linearized analysis of diurnal boundary layer convergences over the topography of the United States. Mon. Wea. Rev., 106, 492-502.
- _____, 1978b: The transient mass-flow adjustment of heated atmospheric circulations. J. Atmos. Sci., 35, 1678-1688.
- _____ and D. W. McLawhorn, 1973: Correlation of nocturnal thunderstorms and boundary-layer convergence. Mon. Wea. Rev., 101, 877-883.
- Palmén, E. H., 1948: On the formation and structure of tropical cyclones. Geophysica, 31, 26-38.
- _____ and H. Riehl, 1957: Budget of angular momentum and energy in tropical storms. J. Meteor., 14, 150-159.

- Pedgley, D. E., 1962: A meso-synoptic analysis of the thunderstorms on 28 August 1958. Geophysical Memour No. 106, Meteorological Office 711 (available from Her Majesty's Stationary Office, London, England), 74 pp.
- Petterssen, S., 1956: Weather Analysis and Forecasting, Second Edition, Volume I, Motion and Motion Systems. McGraw-Hill, New York, 428 pp.
- Philipp, C. B., 1979: Observations of progressive convective interactions from the Rocky Mountain slopes to the plains. Atmos. Sci. Paper No. 316, Colorado State Univ., Fort Collins, 100 pp.
- Pitchford, K. L. and J. London, 1962: The low-level jet as related to nocturnal thunderstorms over midwest United States. J. Appl. Meteor., 1, 43-47.
- Porter, J. M., L. L. Means, J. E. Hovde and W. B. Chappell, 1955: A synoptic study on the formation of squall lines in the north central United States. Bull. Amer. Meteor. Soc., 36, 390-396.
- Purdom, J. F. W., 1979: The development and evolution of deep convection. Preprints Eleventh Conf. on Severe Local Storms (Kansas City), AMS, Boston, 143-150.
- _____, 1976: Some uses of high-resolution GOES imagery in the meso-scale forecasting of convection and its behavior. Mon. Wea. Rev., 104, 1474-1483.
- Reap, R. M. and D. S. Foster, 1979: On producing categorical forecasts from operational probability forecasts of thunderstorms and severe local storms. Preprints Eleventh Conf. on Severe Local Storms (Kansas City), AMS, Boston, 619-624.
- Reed, R. J., 1979: Cyclogenesis in polar air streams. Mon. Wea. Rev., 107, 38-52.
- _____ and E. E. Recker, 1971: Structure and properties of synoptic scale wave disturbances in the equatorial western Pacific. J. Atmos. Sci., 28, 1117-1133.
- Reiter, E. R., 1963: Jet-stream Meteorology. The University of Chicago Press, Chicago (Chapter 3), 515 pp.
- Reynolds, D. W. and E. A. Smith, 1979: Detailed analysis of composited digital radar and satellite data. Bull. Amer. Meteor. Soc., 60, 1024-1037.
- _____ and T. H. Vonder Haar, 1979: Satellite support to HIPLEX: Summary of results 1976-1978. Final Report, Bureau of Reclamation Contract #6-07-DR-20020 Dept. of Atmospheric Science, Colorado State Univ., Ft. Collins, 89 pp.
- Riehl, H., 1954: Tropical Meteorology. McGraw-Hill, New York, 392 pp.

- Riehl, H., 1978: Recent tropical experiments in the general context of tropical meteorology. Meteorology over the Tropical Oceans, D. B. Shaw (Editor), Roy. Meteor. Soc., Bracknell, England, 9-30.
- _____ and N. M. Burgner, 1950: Further studies of the movement and formation of hurricanes and their forecasting. Bull. Amer. Meteor. Soc., 31, 244-253.
- _____ et al., 1952: Forecasting in the middle latitudes. Meteor. Monogr. No. 5, Amer. Meteor. Soc., Boston, 80 pp.
- _____ and J. S. Malkus, 1961: Some aspects of hurricane Daisy. Tellus, 13, 181-213.
- _____, L. Cruz, M. Mata and C. Muster, 1973: Precipitation characteristics during the Venezuela rainy season. Quart. J. Roy. Meteor. Soc., 99, 746-757.
- _____, D. Rossignol and W. Lückeferdt, 1974: On the structure and maintenance of west African squall lines. Report for: De L'Exploitation Meteorologique, ASECNA B. P. 3144, Dakar (Available from Institut Für Meteorologie, Freie Universität Berlin, Podbielski Allee 62, Berlin 33), 29 pp.
- Robertson, F. R. and P. J. Smith, 1980: The kinetic energy budgets of two severe storm producing extra-tropical cyclones. Mon. Wea. Rev., 108, 127-143.
- Rosenthal, S. L., 1970: A circularly symmetric primitive equation model of tropical cyclone development containing an explicit water vapor cycle. Mon. Wea. Rev., 98, 643-663.
- Ruprecht, E. and W. M. Gray, 1976: Analysis of satellite observed tropical cloud clusters, Papers I and II. Tellus, 28, 391-426.
- Sanders, F., 1976: The quasi-geostrophic prediction equations and their qualitative application. Lecture Notes, MIT, Cambridge, 39 pp. (Unpublished Manuscript)
- _____ and R. J. Paine, 1975: The structure and thermodynamics of an intense mesoscale convective storm in Oklahoma. J. Atmos. Sci., 32, 1563-1579.
- _____ and K. A. Emanuel, 1977: The momentum budget and temporal evolution of a mesoscale convective system. J. Atmos. Sci., 34, 322-330.
- Scofield, R. A. and V. J. Oliver, 1977: A scheme for estimating convective rainfall from satellite imagery. NOAA Tech. Memo. NESS 86, Washington, D. C., 47 pp.

- Shmeter, S. M., 1969: Structure of fields of meteorological elements in a cumulonimbus zone. Transaction of the Central Aerological Observatory No. 88 (Translated from Russian, Israel Program for Scientific Translations Cat. No. 5696), 117 pp.
- Sikdar, D. N., V. E. Suomi and C. E. Anderson, 1970: Convective transports of mass and energy in severe storms over the United States -- an estimate from a geostationary altitude. Tellus, 22, 5.
- Simpson, J. S., M. Garstang, E. J. Zipser and G. A. Dean, 1967: A study of a non-deepening tropical disturbance. J. Appl. Meteor., 6, 237-254.
- Smith, P. J., 1969: On the contribution of a limited region of the global energy budget. Tellus, 21, 202-207.
- Thompson, O. E., P. A. Arkin and W. D. Bonner, 1976: Diurnal variations of the summertime wind and force field at three midwestern locations. Mon. Wea. Rev., 104, 1012-1022.
- Trenberth, K. E., 1978: On the interpretation of the diagnostic quasi-geostrophic omega equation. Mon. Wea. Rev., 106, 131-137.
- Tsui, T. L. and E. C. Kung, 1977: Subsynoptic-scale energy transformations in various severe storm situations. J. Atmos. Sci., 34, 98-110.
- Uccellini, L. W., 1980: On the role of upper tropospheric jet streaks and leeside cyclogenesis in the development of low-level jets in the Great Plains. Mon. Wea. Rev., 108, 1689-1696.
- _____ and D. R. Johnson, 1979: The coupling of upper and lower tropospheric jet streaks and implications for the development of severe convective storms. Mon. Wea. Rev., 107, 682-703.
- Vonder Haar, T. H., 1969: Meteorological applications of reflected radiance measurements from ATS 1 and ATS 3. J. Geophysical Res., 74, 5404-5412.
- Wallace, J. M., 1975: Diurnal variations in precipitation and thunderstorm frequency over the conterminous United States. Mon. Wea. Rev., 103, 406-419.
- Webster, P. J. and G. L. Stephens, 1980: Tropical upper-troposphere extended clouds: Inferences from winter MONEX. J. Atmos. Sci., 37, 1521-1541.
- Wetzel, P. J., W. R. Cotton and R. L. McAnelly, 1981: A long-lived meso-scale convective complex. Part II: Morphology of the mature complex. Submitted to Mon. Wea. Rev.
- Whiting, R. M., 1957: The surface chart as a synoptic aid to tornado forecasting. Bull. Amer. Meteor. Soc., 38, 353-356.

- Whiting, R. M. and R. E. Bailey, 1957: Some meteorological relationships in the prediction of tornadoes. Mon. Wea. Rev., 85, 141-150.
- Williams, D. T., 1948: A surface micro-study of squall line thunderstorms. Mon Wea. Rev., 76, 239-246.
- Williams, K. T. and W. M. Gray, 1973: Statistical analysis of satellite observed cloud clusters in the western North Pacific. Tellus, 25, 178-201.
- Wilson, G. S., 1980: Thunderstorm -- environment interactions determined with three-dimensional trajectories. NASA Ref. Pub. 1054, NASA Scientific and Technical Infor. Office, Washington, D. C., 153 pp.
- Woodley, W. L., B. Sancho and A. H. Miller, 1972: Rainfall estimation from satellite cloud photographs. NOAA Tech. Memo. ERL OD-11, Boulder, CO, 43 pp.
- Yanai, M., 1961: A detailed analysis of typhoon formation. J. Meteor. Soc. Japan, 39, 187-214.
- Zipser, E. J., 1969: The role of unsaturated convective downdrafts in the structure and rapid decay of an equatorial disturbance. J. Appl. Meteor., 8, 799-814.
- _____, 1977: Mesoscale and convective-scale downdrafts as distinct components of squall-line circulation. Mon. Wea. Rev., 105, 1568-1589.
- _____, 1979: Kinematic and thermodynamic structure of mesoscale systems in GATE. Presented at the National Academy of Science Seminar: The impact of GATE on Large-Scale Numerical Modeling, Woods Hole, MA, August 1979 (available from National Center for Atmospheric Research, Boulder, CO), 10 pp.
- _____ and C. Gautier, 1978: Mesoscale events within a GATE tropical depression. Mon. Wea. Rev., 106, 789-805.

APPENDIX A

A SCALE SEPARATION TECHNIQUE BASED ON NUMERICAL FILTERING

Holloway (1958) reviewed the use of lowpass, highpass, and bandpass filtering to detect and evaluate various wavelength signals within geophysical time-series data. Barnes (1964), using a Gaussian weight function, developed an objective analysis/filtering technique for application to two-dimensional meteorological fields. Barnes' (1973) revised scheme is utilized as the basic tool for scale separation. The technique first functions as a lowpass filter, smoothing the observed data field to a known response to define the macroscale field. A bandpass filter then extracts the mesoscale signal using a modification of the analysis scheme developed by Doswell (1977). Finally an objective analysis of the total meteorological field is recovered as the sum of the mesoscale and macroscale components. Short wavelength noise is suppressed throughout the analyses.

1. Lowpass objective analysis

Two-dimensional meteorological data are interpolated to a cartesian grid and simultaneously filtered. The first estimate of the gridded values of some parameter, f , is given by:

$$f_o(i,j) = \frac{\sum_{n=1}^N w_n f_n(x,y)}{\sum_{n=1}^N w_n}, \quad (A1)$$

where the weight function, w_n , is:

$$w_n = \exp(-d_n^2/4c). \quad (A2)$$

The weight function constant, c , is arbitrarily chosen to fit a particular application of the scheme. The distance from the (i,j) grid point to the

location of the observed data, $f_n(x,y)$ is denoted by d_n and N is the number of observations that fall within a specified radius of influence.

Barnes' (1973) modification requires only a single correction pass through the first estimate field to achieve the desired response for specific wavelengths. This procedure significantly reduces computation time compared to the earlier use of several successive iterations. To accomplish this the value of the weight function constant is reduced for the correction pass and the final grid point values are given by:

$$f(i,j) = f_o(i,j) + \frac{\sum_{n=1}^N w'_n D_n}{\sum_{n=1}^N w'_n} \quad (A3)$$

where the modified weight function, w'_n , is:

$$w'_n = \exp(-d_n^2/4gc), \quad 0 < g < 1, \quad \text{and} \quad (A4)$$

$$D_n = f_n(x,y) - f_o(x,y). \quad (A5)$$

D_n is the difference between an observed data value and the first estimate value at the same point. A simple biquadratic interpolation between the values of $f_o(i,j)$ at the nearest grid points is used to estimate $f_o(x,y)$. The radius of influence is set so that once the observation weight becomes very small (i.e., $w'_n < 5 \times 10^{-3}$) further computations are terminated. Barnes has shown that final response, as a function of wavelength λ , is given by:

$$R = R_o (1 + R_o^{g-1} - R_o^g), \quad \text{where:} \quad (A6)$$

$$R_o = \exp(-\pi^2/4c/\lambda^2). \quad (A7)$$

Advantages of this Gaussian weighting, objective analysis and filtering technique listed by Barnes (1973) include:

- 1) The weight function constants c and g are chosen prior to the analysis so that pattern scales resolvable by the data distribution will be revealed to a known response amplitude.
- 2) Since (A2) approaches zero asymptotically, the influence of data may be extended to any distance without changing the weight function and response characteristics.
- 3) Small scale noise is suppressed so that further smoothing with numerical filters is not necessary.
- 4) Desired scale resolution is achieved with only one iteration.

Barnes also listed a number of practical guidelines to be used in specifying the values of c and g to fit particular applications. The density and distribution of observations is the most critical factor affecting the analyses. The analyses produced with this technique are referred to as lowpass fields.

2. Bandpass objective analysis

Doswell (1977) utilized Barnes' (1964) original technique for a bandpass filter, objective analysis process. He developed a non-dimensionalized equation set (in wavenumber space) that could be solved simultaneously (by iteration) to yield analysis constants that were utilized in two lowpass analyses. The difference between these two analyses defined the bandpass field which had peak response at a predetermined, mesoscale wavelength. The bandpass analysis suppresses both short and long wavelength features so that the filter response is peaked at a specific wavelength. The bandpass field is defined by the difference of two lowpass analyses.

Let $F1(i,j)$ and $F2(i,j)$ be two lowpass analyses defined by A3 with weight function constants $C1, G1, C2$ and $G2$. The bandpass field is then given by:

$$B(i,j) = r [F1(i,j) - F2(i,j)], \quad (A8)$$

and the bandpass filter response is:

$$BR = r(R1 - R2). \quad (A9)$$

The inverse of the maximum response difference is denoted by r . Bandpass response is arbitrarily restored to 100% at the wavelength (λ_{\max}) where maximum response difference occurs.

Design of the bandpass filter proceeds as follows. The weight function constants $C1, G1, C2$ and $G2$ are chosen so that λ_{\max} occurs near to some desired wavelength. The choice of this mesoscale wavelength is based upon supplemental information concerning the scale of the phenomena to be considered. The analysis constants are subjectively determined from graphs of A6 for a range of values c and g under the constraint that response difference at λ_{\max} be approximately 0.8. Thus r is prevented from being unduly large and very small difference fields are not greatly amplified. Weight function constants $C1, G1$, and $C2$ are then held constant and $G2$ is iteratively adjusted in A9 until λ_{\max} occurs at, or very near, the desired wavelength.

3. Scale separation

Scale separation is accomplished by choosing $C2$ and $G2$ such that the $F2(i,j)$ lowpass field may be considered to represent the macroscale environment. The bandpass field, $B(i,j)$, is an analysis of mesoscale features. (Macroscale is thus defined to include all features whose wavelengths are longer than those extracted by the bandpass analysis.) An objective analysis of the total meteorological field (with short

wavelength noise suppressed) is recovered by summing the $B(i,j)$ and $F2(i,j)$ analyses.

A set of filter response curves (from equations A6 and A9) for this scale separation scheme is depicted in Fig. A1 while typical observation weight curves (from equation A2 with $C1 = 40,000$ and $C2 = 300,000$) are illustrated in Fig. A2. The analysis constants in Fig. A1 were chosen (values are shown on the figure) so that λ_{\max} occurs at 500 km (see the bandpass response curve BR). The $F1(i,j)$ lowpass field is used only in the bandpass procedure and the three resultant analysis fields [$B(i,j)$, $F2(i,j)$, and $T(i,j)$] respectively depict mesoscale, macroscale, and total meteorological fields. (In this example "macroscale" includes all features of wavelength greater than about 900 km.) The filter response for the total field (curve TR) exceeds 100% for some wavelengths because of the artificial amplification imposed upon the bandpass field; however the amplification does not appear to significantly affect analysis results (i.e., analysis patterns are not affected and analyzed magnitudes rarely exceed observed values). As indicated by response curves BR and F2, neither the mesoscale nor macroscale analyses respond strongly to features of wavelength 700 to 900 km because the cutoff between mesoscale and macroscale response is not sharp. Thus, the scale separation technique is most effective if the amplitudes of features whose wavelengths lie within this overlap region are weak or non-existent.

The analysis procedures may produce unrealistic results near the boundaries of the data domain where the observation distribution about a grid point is highly asymmetrical. Because of this limitation, only features lying wholly within the data domain are considered.

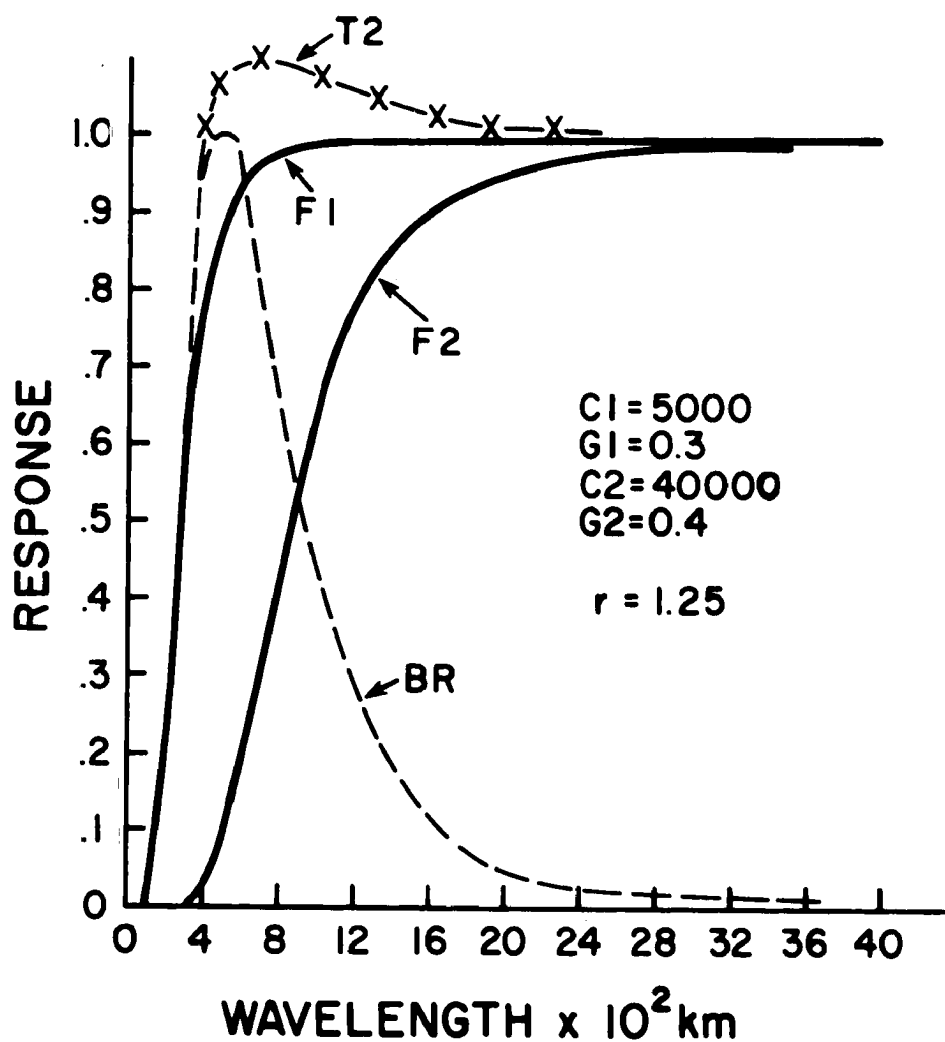


Fig. A1. Response curves for filters used for objective scale separation. Curves F1 and F2 are lowpass filters used to define the band-pass (mesoscale) filter, curve BR. Response F2 also defines the macroscale field and curve TR is response for the analysis of the total meteorological field.

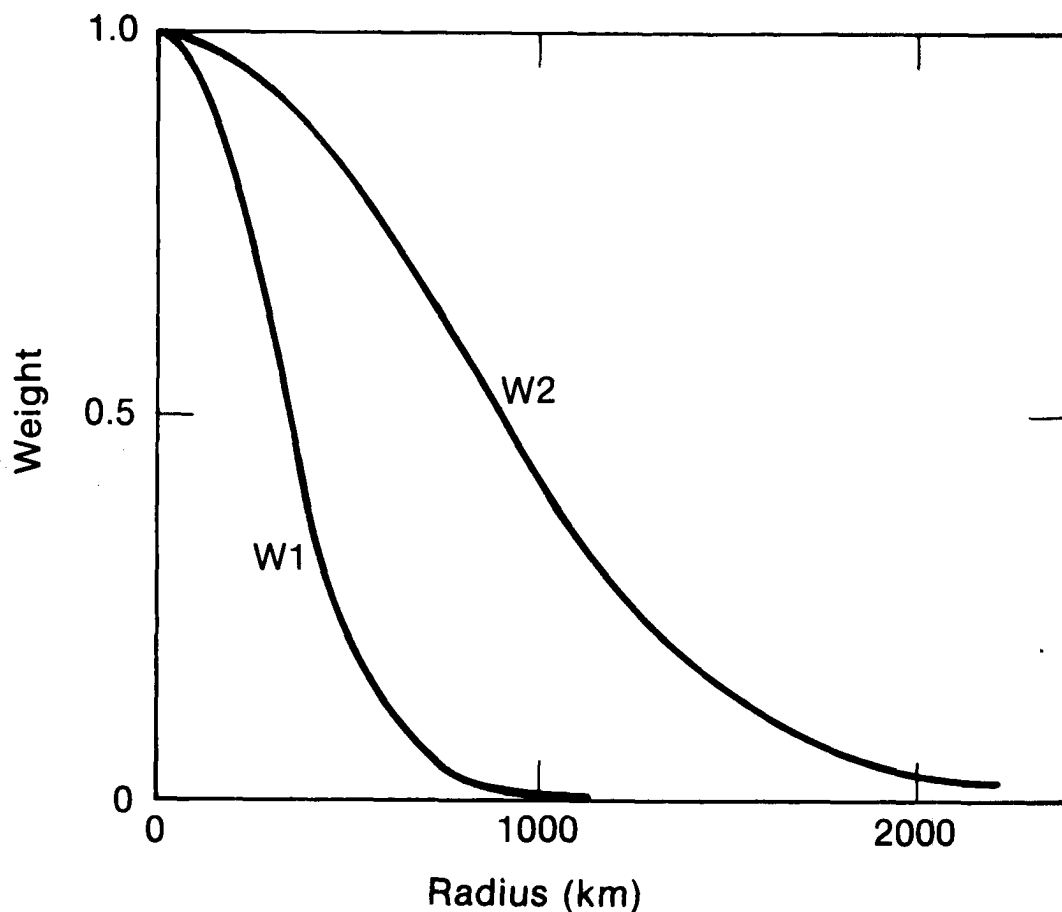


Fig. A2. Observation weight curves from equation A2 with $C = 40,000$ (curve W1) and with $C = 300,000$ (curve W2).

4. Determination of λ_{\max}

For a specific meteorological situation and parameter of interest the wavelength band of important mesoscale features must be determined from supplementary analyses. Two methods are used in this paper: one is subjective and the other is a statistical analog to variance spectrum analysis. For example, consider the subjectively analyzed surface temperature field in Fig. A3. The meteorological situation is quite complex with a number of mesoscale features present. Several thermal features of wavelength ~ 500 km are indicated by this subjective analysis (e.g., the

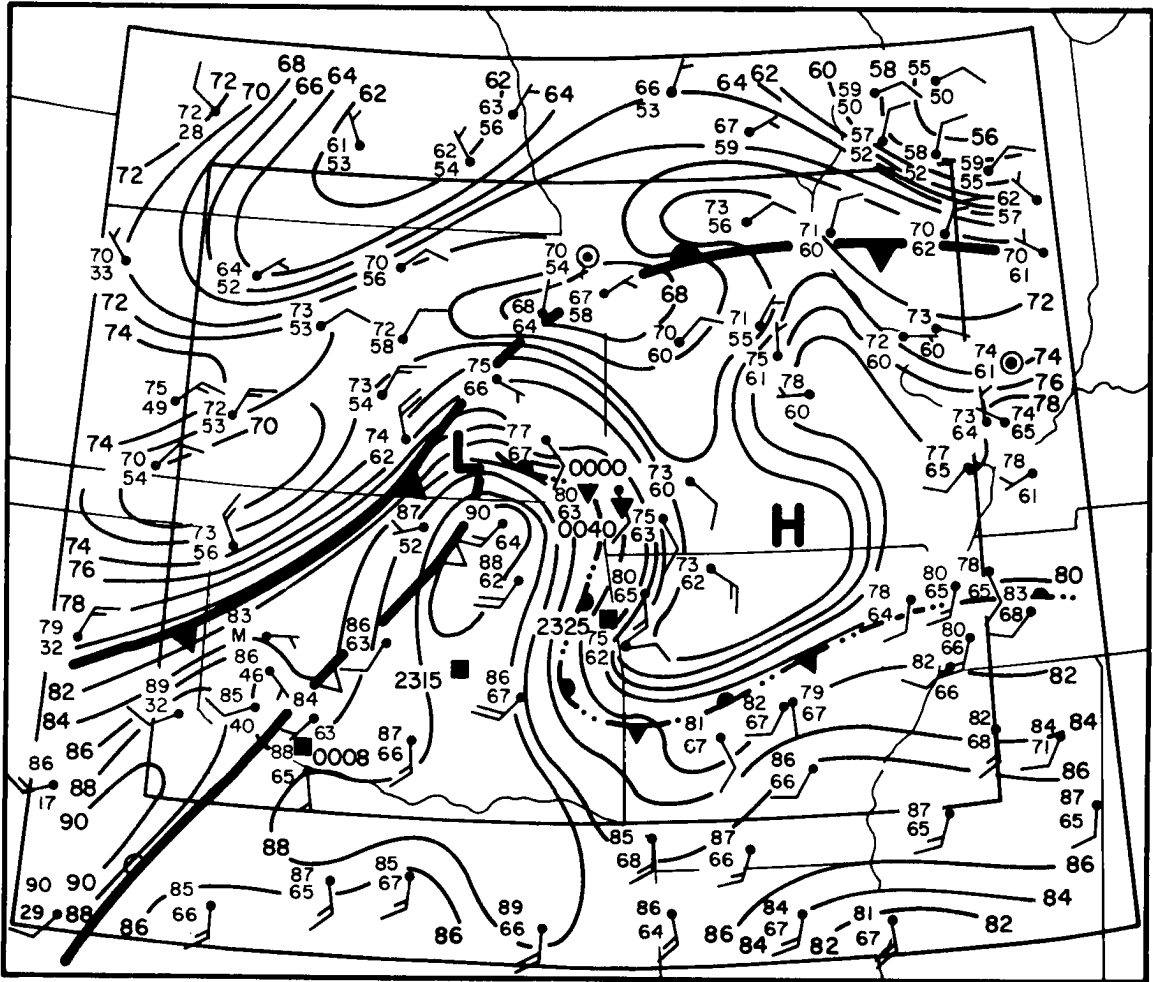


Fig. A3. Surface analysis for 2100 GMT 24 April 1975. Isotherms are drawn for 2°F intervals with fronts and pressure centers shown. Thunderstorm cool air outflow boundary is shown as squall symbol with barbs. Open barbs denote a surface dryline. The locations and times (GMT) of tornadic storms (triangles) and hailstorms (squares) are indicated. The analysis domain is shown as a large quadrilateral and an inner domain (first two analysis grids excluded), over which results of the objective analysis are shown, is indicated by the smaller quadrilateral.

thermal wave that extends from southwest Kansas eastward to southeast Missouri), suggesting that the bandpass filter be centered at 500 km.

Generation of a subjective analysis prior to the scale separation analysis might be inconvenient for applications in a near real-time mode. Furthermore, one might wish to confirm the importance of various scales

apparent in a subjective analysis. Evaluation of the two-dimensional structure function from the observed data might also be used to determine the mesoscale wavelength of interest. [Gandin (1963) and Barnes and Lilly (1975) have discussed the physical characteristics of the structure function.] Classically, researchers have available data sets taken at a number of fixed observing sites for some specific period of time. The structure function computed from such a data base represents "climatological" conditions over the observing network. This characteristic had to be considered in formulating an instantaneous expression for the structure function, which is defined here as:

$$B(R) = \frac{1}{N} \sum_1^N [f'(r_i) - f'(r_j)]^2. \quad (A10)$$

The separation interval R is defined to be a specific distance interval, e.g., $50 \text{ km} \leq R < 100 \text{ km}$. N is the number of data pairs $f(r_i)$, $f(r_j)$ whose separation distances $|r_i - r_j|$ fall within interval R , and $f'(r_i) = f(r_i) - \bar{f}$, with \bar{f} defined as the spatial mean of the particular data set. The vectors r_i and r_j are position vectors of the observation sites. Implicit in these calculations are assumptions of homogeneity and isotropy.

A plot of structure function versus data separation distance is shown in Fig. A4 for the 2100 GMT, 24 April 1975 temperature observations. The structure values were averaged and plotted for 50 km increments of observation separation distance. In the absence of significant small scale variance, the structure function should be a smooth, concave (upward) curve and should asymptotically approach twice the variance of uncorrelated data obtained at points large distances apart. The hump in the structure curve (fitted subjectively) at 250 km indicates that mesoscale thermal

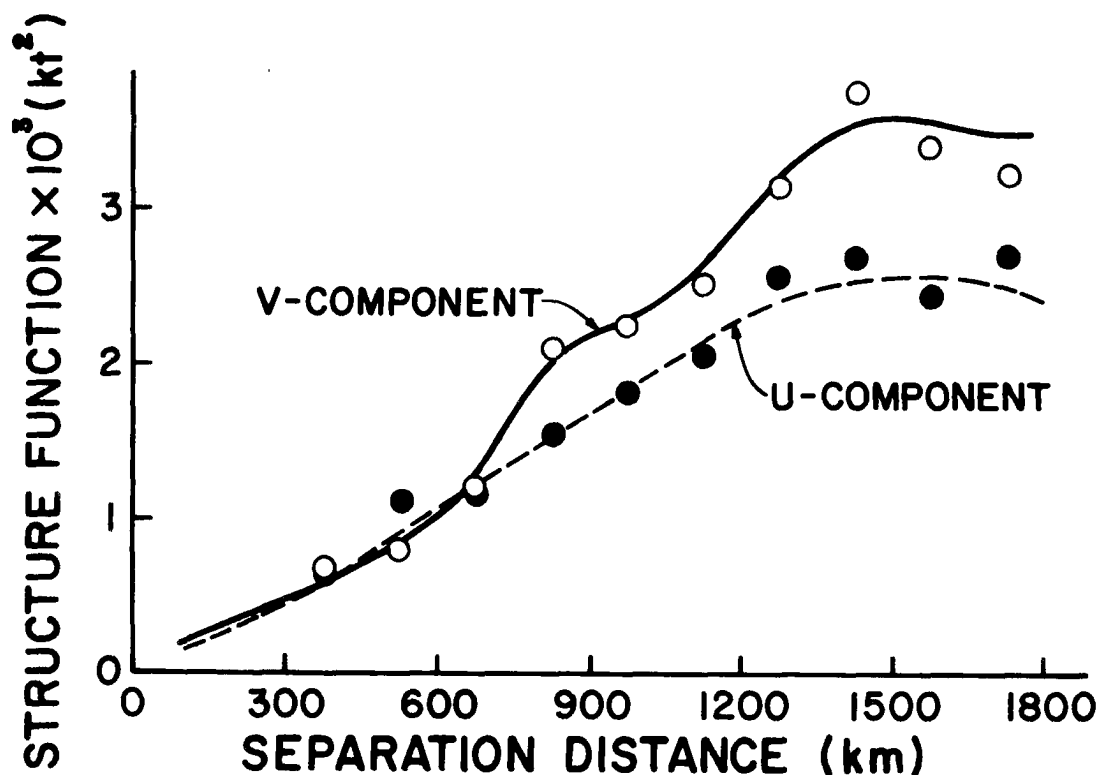


Fig. A4. Structure function for the observed temperature field at 2100 GMT 24 April 1975. Curve is fit to data points (circles) subjectively. Dashed line shows expected structure function in the absence of mesoscale perturbations.

features of ~ 500 km wavelength are present. This analysis confirms the subjective appraisal that the bandpass filter should be centered at about 500 km. Other important features appear to be of much longer wavelengths.

5. Analysis example

Results from the 24 April 1975 case are presented to demonstrate the usefulness of this objective scale separation technique in diagnosing conditions associated with the development of intense convective storm systems. The analysis procedure, utilizing the constants and response curves shown in Fig. A1, was run on the temperature data that are subjectively analyzed in Fig. A3. Mesoscale temperature perturbations (see

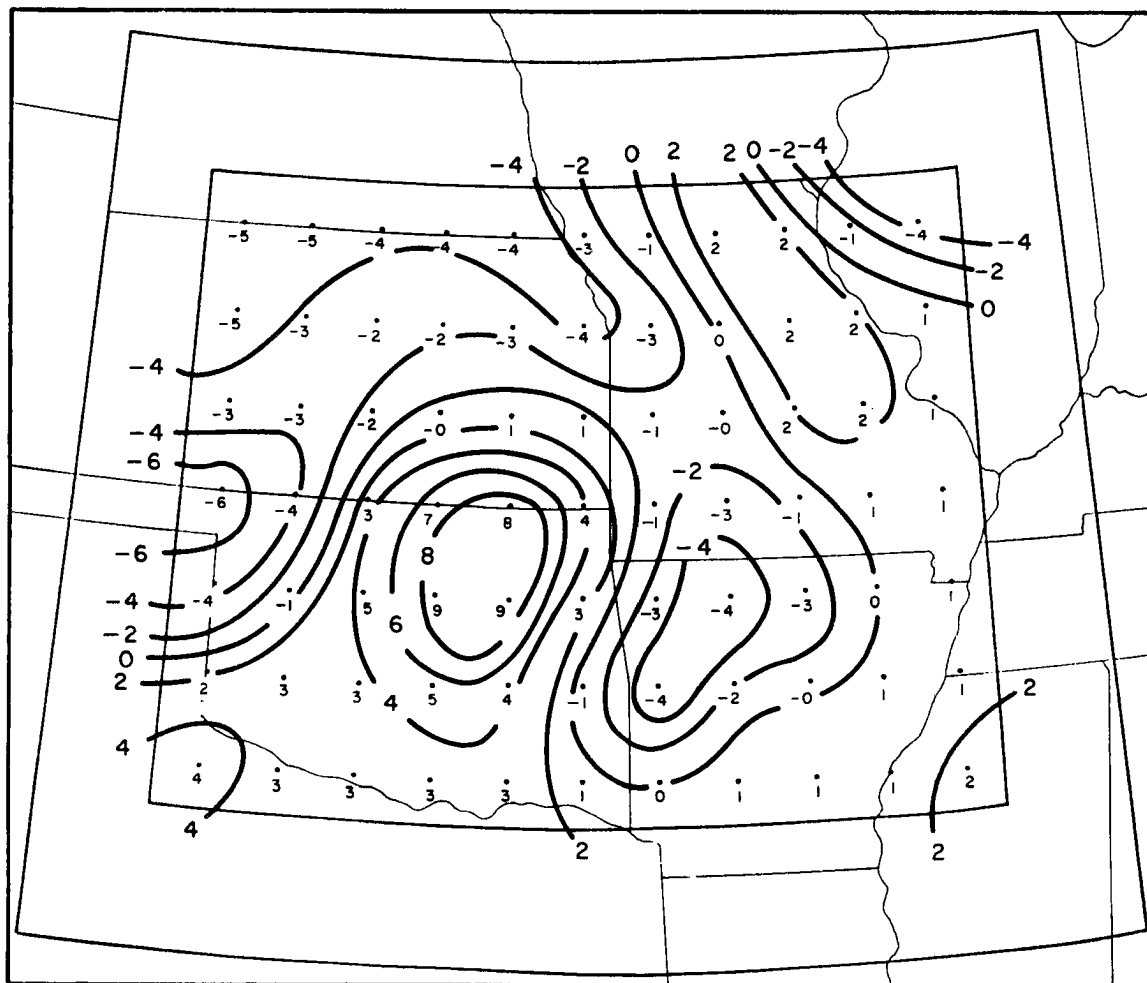


Fig. A5. Mesoscale temperature perturbations ($^{\circ}\text{F}$) for 2100 GMT 24 April 1975. The bandpass filter response center at wavelength 500 km (see Fig. A1). Grid length is 1° of latitude or longitude.

response curve BR in Fig. A1) are shown in Fig. A5. The warm/cool air couplet in northeastern Oklahoma and northwestern Arkansas is clearly depicted. Most of the severe thunderstorms during the subsequent four hours (refer to Fig. A3) occurred in a region of strong temperature gradient associated with this mesoscale thermal wave. The macroscale temperature field (response curve F2 in Fig. A1) is presented in Fig. A6. This analysis depicts the general south to north decrease in temperature and also indicates the presence of a low-amplitude thermal wave of

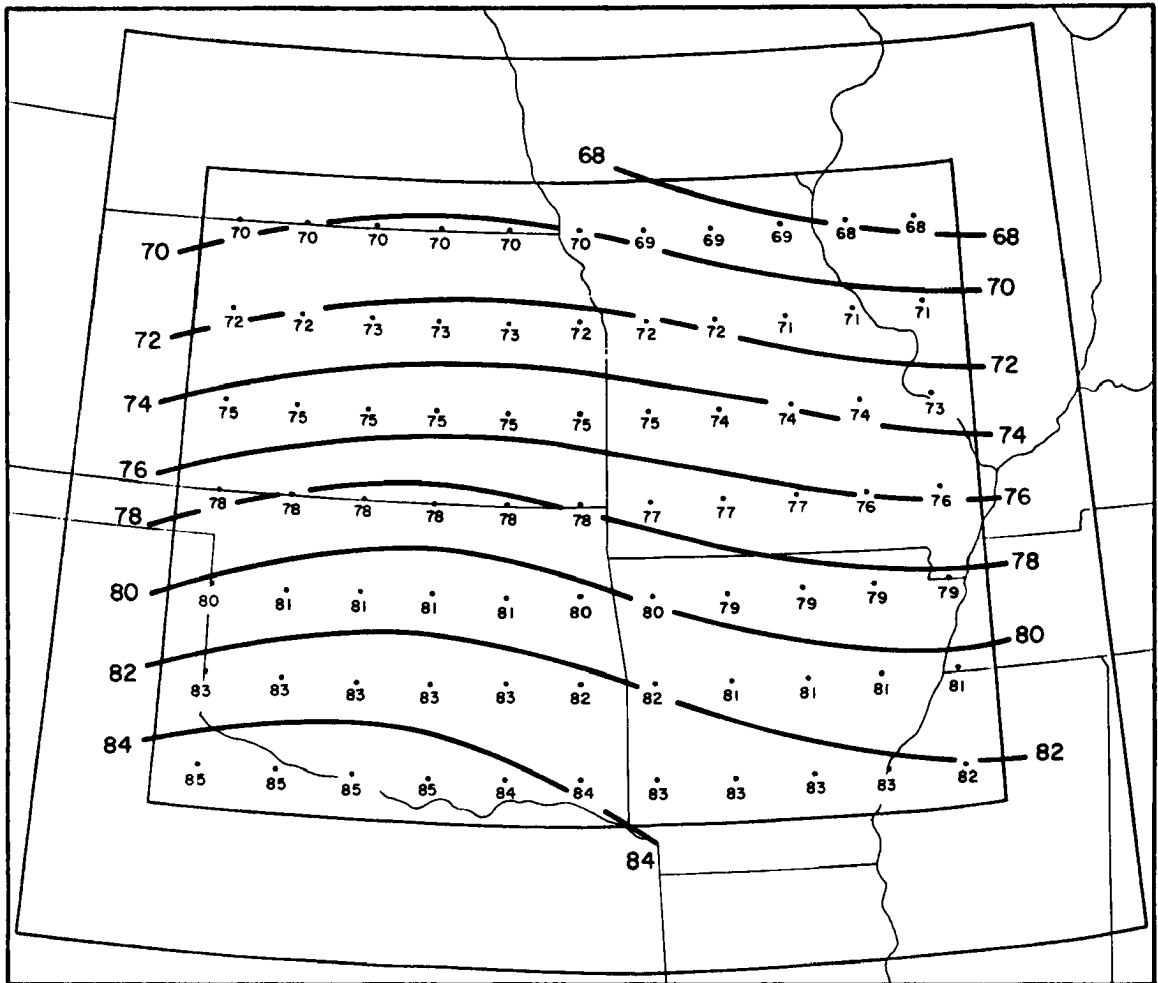


Fig. A6. Macroscale temperature analysis ($^{\circ}\text{F}$) for 2100 GMT 24 April 1975, utilizing filter F2 (see Fig. A1).

approximately 1000 km length. The objective analysis of the total temperature (Fig. A7, see response curve TR in Fig. A1), obtained by summing the mesoscale and macroscale fields, retains much of the detail of the subjective analysis, but undesired, very short wave features have been filtered.

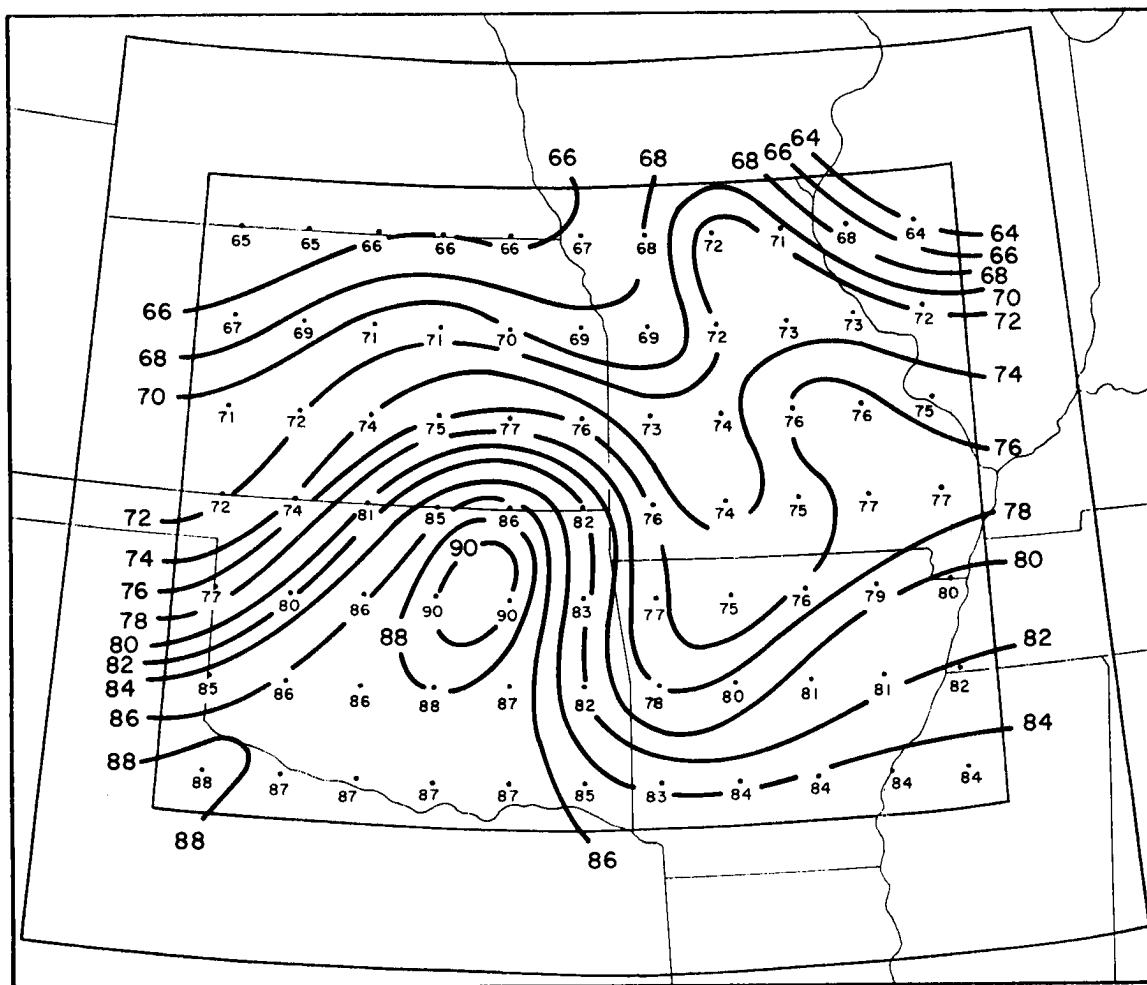


Fig. A7. Total temperature analysis ($^{\circ}\text{F}$) for 2100 GMT 24 April 1975, resulting from addition of mesoscale and macroscale fields shown in Figs. A5 and A6.

APPENDIX B

OBJECTIVE ANALYSIS OF THE COMPOSITE DATA SETS

The objective analysis and scale separation techniques described in Appendix A have been used to analyze standard-level rawinsonde data upon a common grid for ten MCC cases. Mesoscale, macroscale and total meteorological fields have been obtained for three consecutive data times (0000, 1200, and 0000 GMT) spanning the life-cycles of the MCCs studied. The 1200 GMT sounding data were positioned upon a two-dimensional latitude/longitude analysis grid with the MCC located at the center. Quadrilaterals were subjectively fit to each cloud shield (using enhanced IR satellite images) and the shape and size of the "average" system is indicated in Fig. B-1 which also shows the composite analysis domain. The analysis domain is shown not only at the time of the system (central grid) but also for 12 h before and after the time of the system. The analysis grid was moved at the average velocity of the ten systems. System movement was determined by tracking the centroid of the $\leq -32^{\circ}\text{C}$ cloud shield during a 6 h period centered upon the time of the MCC's maximum extent. The average velocity thus obtained was 240° at 11.8 m s^{-1} (23 kt). Therefore the data were composited about the region where the system was developing at 0000 GMT (the Genesis Region or GR), the region occupied by the MCC at 1200 GMT (the MCC Region or MR) and the region where the system might have moved by 0000 GMT (the Decay Region or DR) the next evening. (Specific details and meteorological analyses for the ten cases studied are presented in Appendix C.) There is considerable overlap of the three analysis domains (before, during and after the MCC) so that the results may be interpreted within either a Lagrangian or Eulerian context. The analysis mesh was 16×13 with a grid length of two degrees latitude or longitude so that

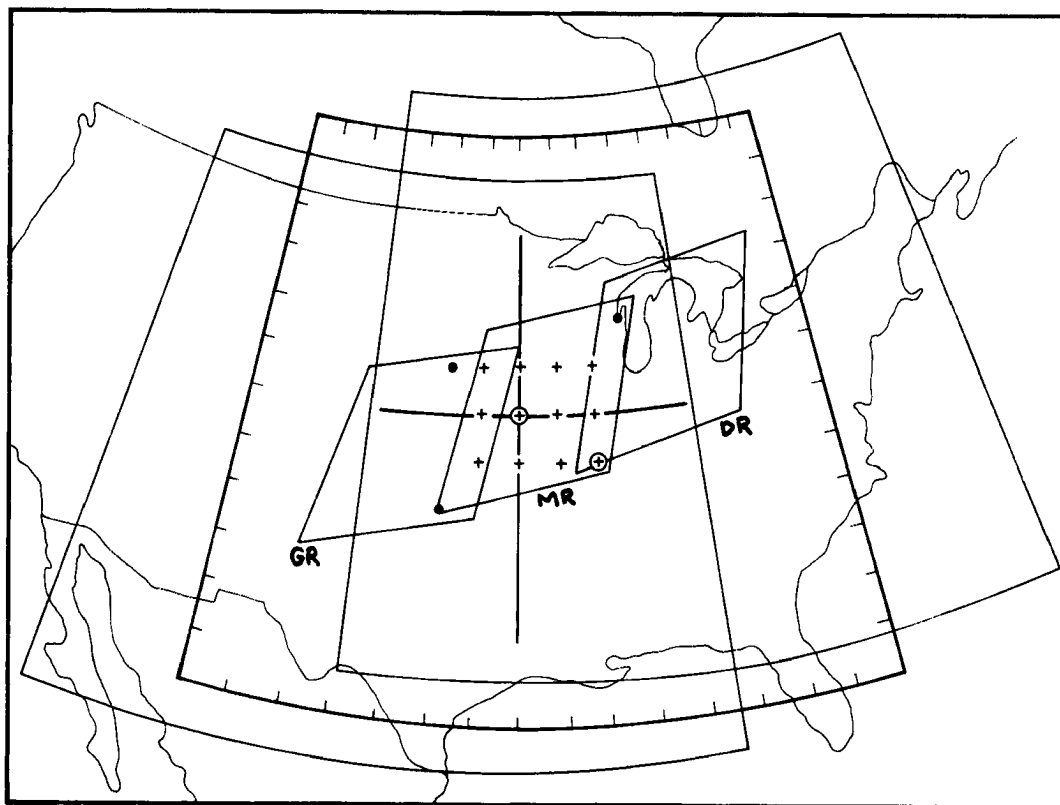


Fig. B1. Composite analysis grids before, during and after (0000, 1200, 0000 GMT) the MCC. Map background scales the domain and indicates the track of the "average" MCC studied.

the Δx grid length was ~ 170 km at the center of the domain while the Δy grid was everywhere ~ 222 km. Analysis software accounts for the varying Δx grid length.

Some of the systems were larger or smaller than the average and a few (~ 30) observations were subjectively repositioned so that the observation's position relative to the MCC was maintained. This repositioning introduces noise into the composite data set. Likewise, repositioning the observations upon the composite analysis grid generates noise, owing to spatial distortions (i.e., the actual separation distance of a pair of observations may be different than that computed when they are shifted into the common grid). Spatial distortion introduced during compositing

ranged from 0 to as much as 250 km. The resultant noise produced in the observation set would be significant if short wavelength features were of interest. Varying meteorological environments attending the ten MCCs (see Appendix C) studied also introduce noise into the composite data set as do spurious soundings (such as those entering thunderstorm updrafts). Therefore, meaningful results can be obtained only if the analysis scheme filters the short wavelength noise generated by the vagaries of data compositing, random and non-random errors and non-representative soundings. A subjective check for gross errors was applied during the extraction of the standard-level data from complete sounding listings.

The "average" MCC studied had horizontal dimensions on the order of 700 - 800 km. This indicates -- if we consider the organized cloud system observed from GOES to be the visible manifestation of the half-wavelength of a circulation system -- that the bandpass, or mesoscale, analysis be centered about ~ 1500 km. The structure function (refer to Appendix A) for u- and v-components of the composite 500 mb wind field (at the time of the MCC) is shown in Fig. B-2 and there does appear to be some mesoscale signature at this wavelength as indicated by the humps in the curves at ~ 750 km. The increase in structure value at separations less than 350 km is due to noise introduced by compositing procedures. Thus the amplitude of features with wavelengths < 700 km should be strongly filtered from the analyses. With these characteristics in mind, the filters whose response curves are shown in Fig. B3 were designed and utilized in all of the composite, objective analyses. Note that all of the analyses retain $< \sim 25\%$ of the amplitude of 700 km wavelength features and that they are virtually unaffected by waves of < 300 km. The noise generated by the composite procedures has been filtered, along

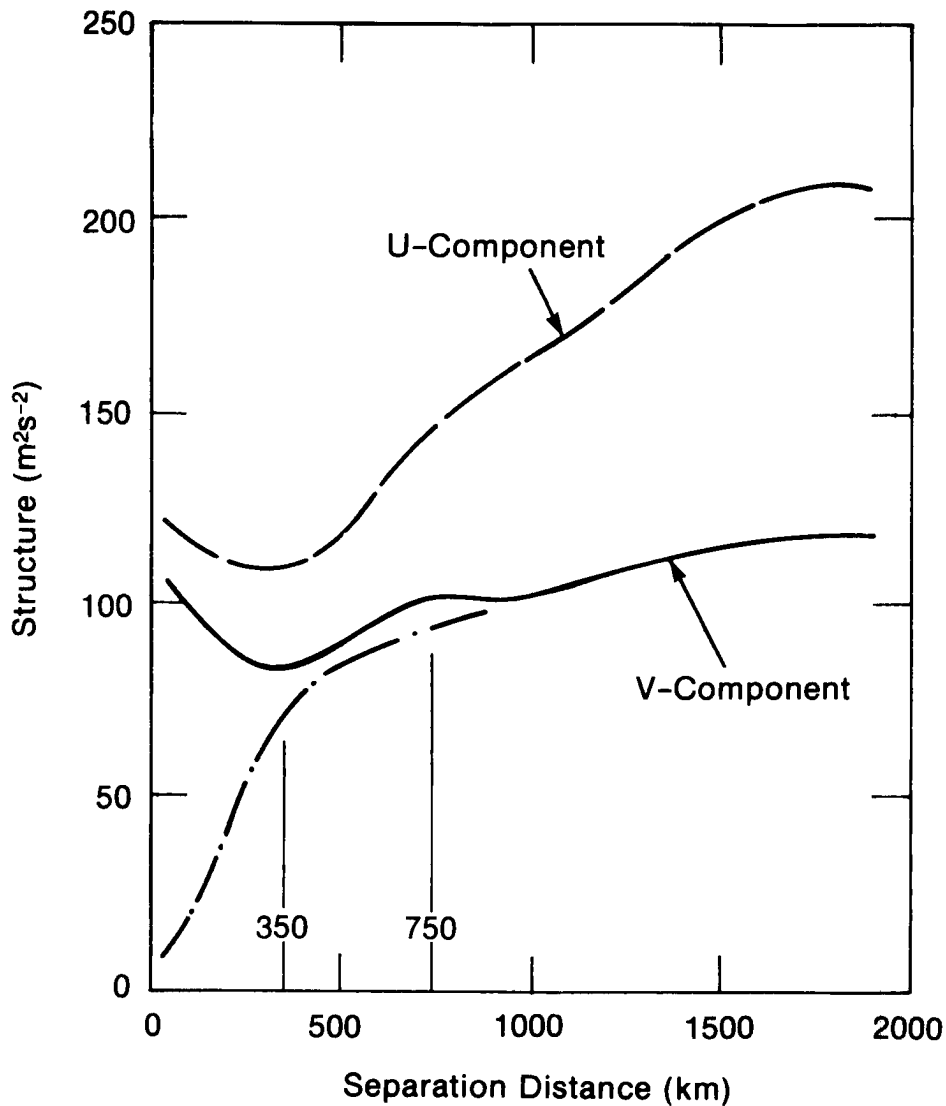


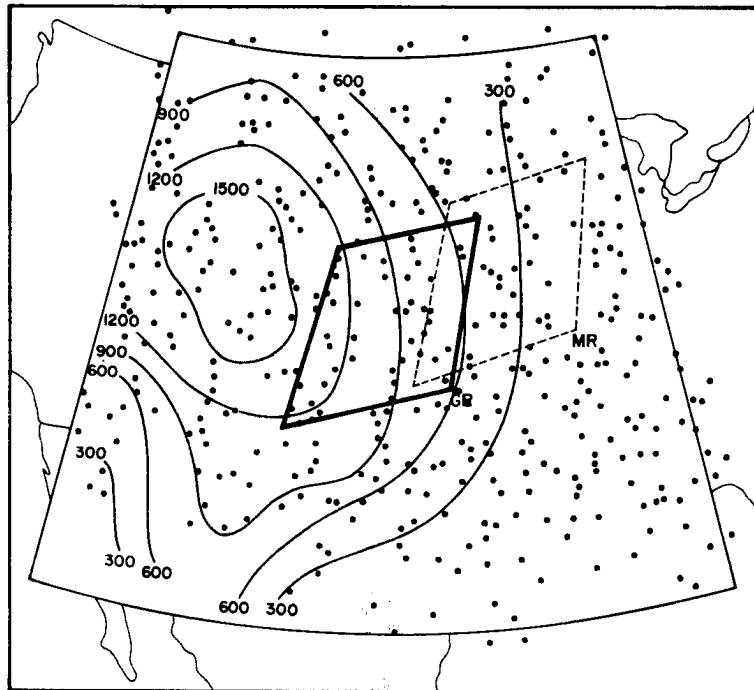
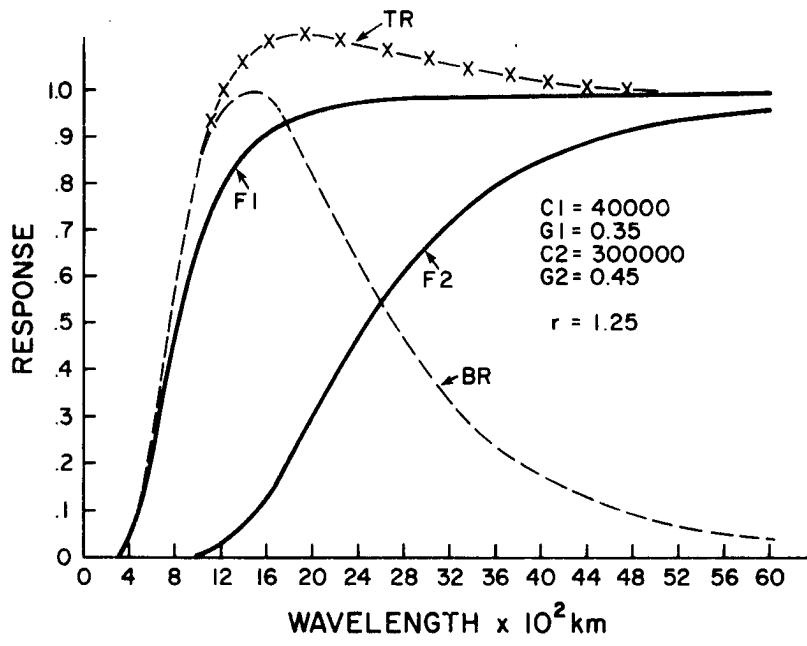
Fig. B2. Structure function versus distance for composite 500 mb winds at the time of the MCC.

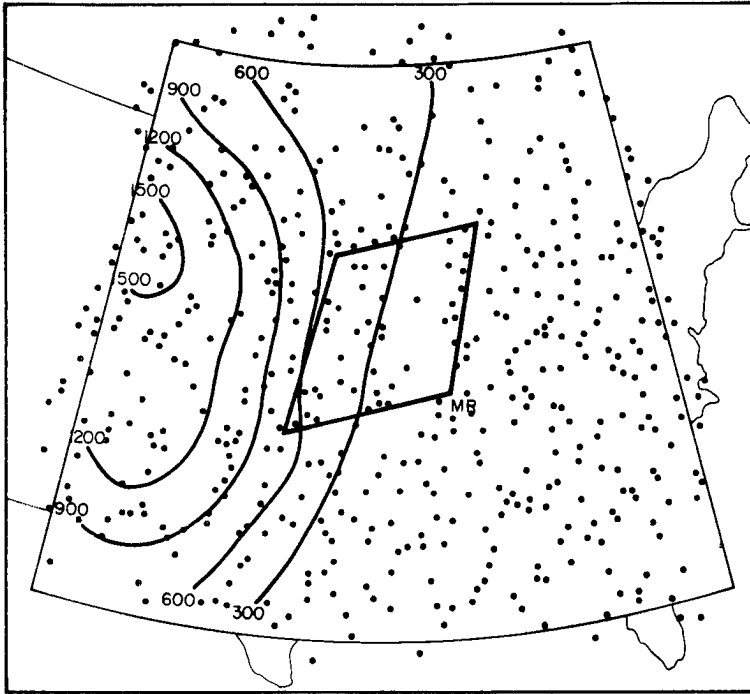
with other short wavelength noise, so that the final fields represent a meaningful objective analysis of medium and large scale meteorological features associated with MCCs.

Distributions of composite sounding locations for the three time periods analyzed are shown in Fig. B4. Compositing even as few as ten cases over the United States yields a large number of observations for each time period (428 soundings before, 489 soundings during the MCC and

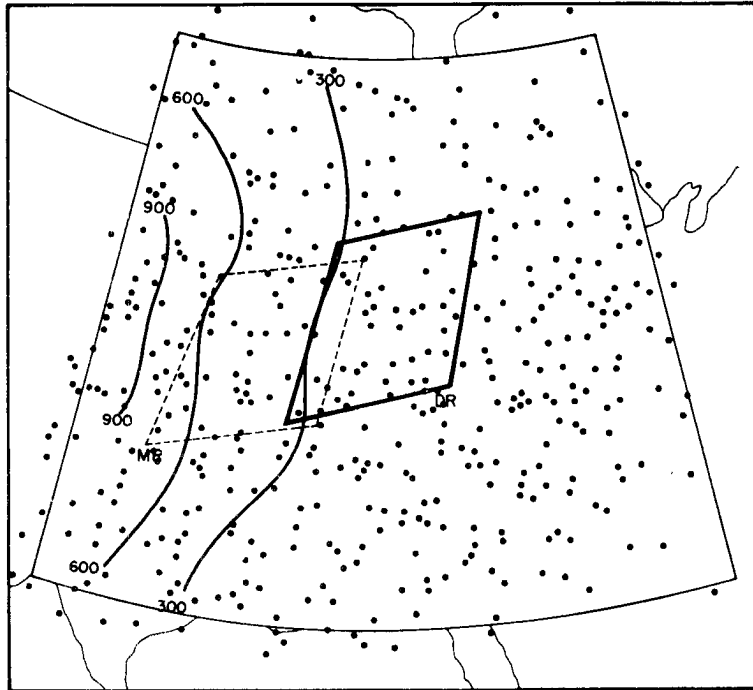
Fig. B3. Response curves and analysis constants utilized in the objective analyses of the composite data fields (refer to Appendix A for complete details).

Fig. B4. Locations of the soundings used in the composite analyses and the smoothed terrain elevations (in meters) for each of the analysis grids (a, before; b, during; and c, after the MCC).





b



c

431 soundings after). The objectively analyzed terrain contours for each analysis domain are also shown. No additional data (i.e., additional surface observations, aircraft or satellite winds, etc.) other than synoptic-net rawinsonde observations are used in the objective analyses. Thus the data set had essentially the same density and distribution characteristics at all levels. Levels analyzed in detail were: surface, 850, 700, 500, 300, 250, 200, 150 and 100 mb. The radius of influence for the F1 and F2 analyses was set to 750 and 2200 km respectively (refer to Figs. B3 and A2). All computations (vorticity, divergence, etc.) were made using centered finite differences. Vertical motion calculations were kinematic and were adjusted following O'Brien (1970, see his equation 19); however, because of the MCC's low shear environment it was not assumed that the composited wind fields were more representative at low-levels. Vertical motion was computed and adjusted twice, once from the surface to 100 mb and once from 100 mb to the surface. Final values were the average of the two calculations. Boundary conditions imposed were that ω at the surface was equal to that induced by the slope of the terrain and that ω at 100 mb was zero.

APPENDIX C

OVERVIEW OF THE CASES COMPOSITED

Specific details documenting the life-cycles of the ten convective systems that were composited are presented in Table C1. The systems studied occurred from late spring through late summer and within a variety of large scale meteorological patterns. All but three of the systems considered had grown to maximum extent (as depicted in the satellite imagery) several hours prior to synoptic data time. Thus, the composite analyses represent a time in the MCC life-cycle that occurs after the most intense phase (assuming that the large, continuously cold IR cloud shield at maximum extent occurs about the same time that MCC associated circulations are most intense). However, the systems were indeed still active

Table C1

The Composite MCC Systems

| <u>No.</u> | <u>Date</u> | <u>Max. Extent</u> | <u>Terminate</u> | <u>Area $\leq -32^{\circ}\text{C}$ at Max. Extent (km²)</u> | <u>Eccentricity</u> |
|------------|----------------|--------------------|------------------|---|---------------------|
| 1 | 23/24 April 75 | 0900 | 1500 | 518,500 | ~ .75 |
| 2 | 6/7 May 78 | 1200 | 2230 | 924,000 | ~ .80 |
| 3 | 18 May 78 | 1330 | 1600 | 223,600 | ~ 1.00 |
| 4 | 30/31 May 78 | 0900 | 1500 | 405,400 | ~ .85 |
| 5 | 3/4 June 78 | 1230 | 1430 | 174,200 | ~ .70 |
| 6 | 19/20 June 78 | 0630 | 1430 | 545,700 | ~ .70 |
| 7 | 19/20 July 78 | 0800 | 1430 | 237,900 | ~ .75 |
| 8 | 20/21 July 78 | 0930 | 1300 | 243,000 | ~ .80 |
| 9 | 3/4 August 77 | 1000 | 1300 | 353,900 | ~ .75 |
| 10 | 4/5 August 77 | 0900 | 1600 | 299,500 | ~ .75 |

and producing significant weather at the time of the 1200 GMT composite analyses. The systems composited are quite typical of the larger sample of MCCs discussed in Section II. Individual meteorological analyses and satellite images are shown for each of these ten systems in the following subsections.

C.1 MCC of 23/24 April 1975

Severe thunderstorms developed over south-central Iowa and northern Missouri about 2200 GMT on the 23rd. These storms grew rapidly and organized into a large mesosystem. Other storms that had developed over northeastern Colorado early in the afternoon moved rapidly eastward and merged with the complex about the same time that an area of activity broke off from the eastern portion of the complex, weakened and moved rapidly eastward across Indiana and Ohio. After 1000 GMT the system split (as indicated by the cold and presumably active areas depicted by satellite) as it weakened. The western-most region of convective activity briefly re-intensified over Kentucky and Tennessee during the afternoon.

Figure C1 presents an enhanced IR image showing the MCC at 0900 GMT while Figs. C2 and C3 show analyses of the maximum winds aloft for 0000 and 1200 GMT on the 24th. Note the pronounced increase in anticyclonic curvature and speeds in the jet stream north and northeast of the convective complex. Upper-level diffluence had also increased markedly.

A stability, precipitable water and 850 mb wind chart for 0000 GMT (Fig. C4) shows that the system developed in a region of large conditional instability (LI -4 to -8 and KI 27-38), strong low-level southwesterly flow and just south of a col in the 850 mb flow. Precipitable water contents were slightly more than an inch. Figure C5 is an analysis of 12 h precipitation (from NOAA, EDIS Hourly Precipitation Data) for the

Fig. C1. Enhanced IR image for 0900 GMT 24 April 1975.

Fig. C2. Maximum observed winds aloft for 0000 GMT 24 April 1975. Isotachs are in knots with axis of wind maxima indicated by heavy streamlines. Dashed contours show height of the maximum wind in km. The track of the MCC is also shown (dash-dot is region of initial storm development, triangle indicates location at initiation, circle with system number from Table C1 shows MCC location at maximum extent and heavy "X" shows location at termination).

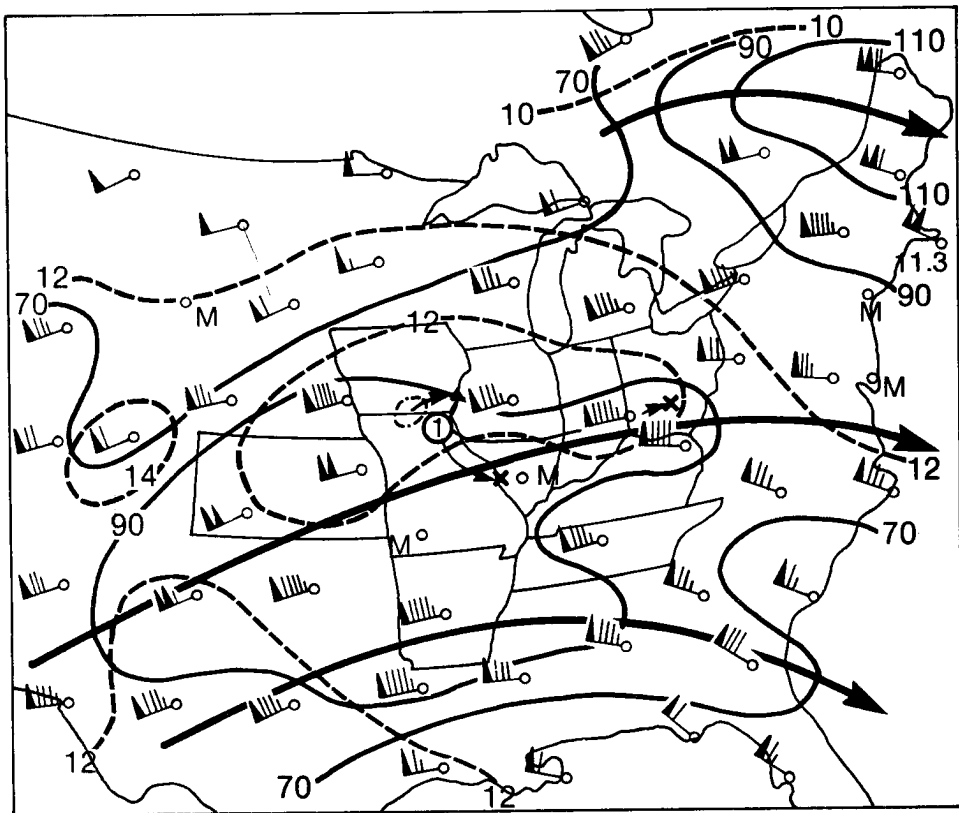
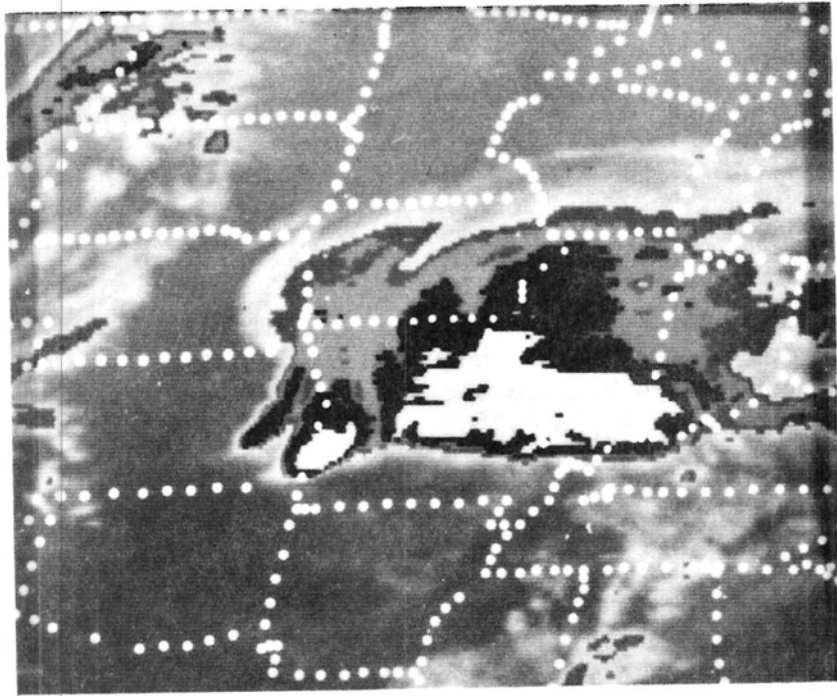


Fig. C3. Maximum observed winds aloft for 12 GMT 24 April 1975. The location of the MCC as indicated by satellite data at 12 GMT is shown (cross-hatched region is $IR T_{BB} \leq -32^{\circ}C$ and stippled regions are $IR T_{BB} \leq -52^{\circ}C$).

Fig. C4. Stability chart for 0000 GMT 24 April 1975. Lifted Index is shown over the K-Index with the Lifted Index values contoured. Winds (kt) at 850 mb are plotted with low-level wind maxima indicated by the heavy arrows. Precipitable water (surface to 500 mb) is also plotted at selected locations.

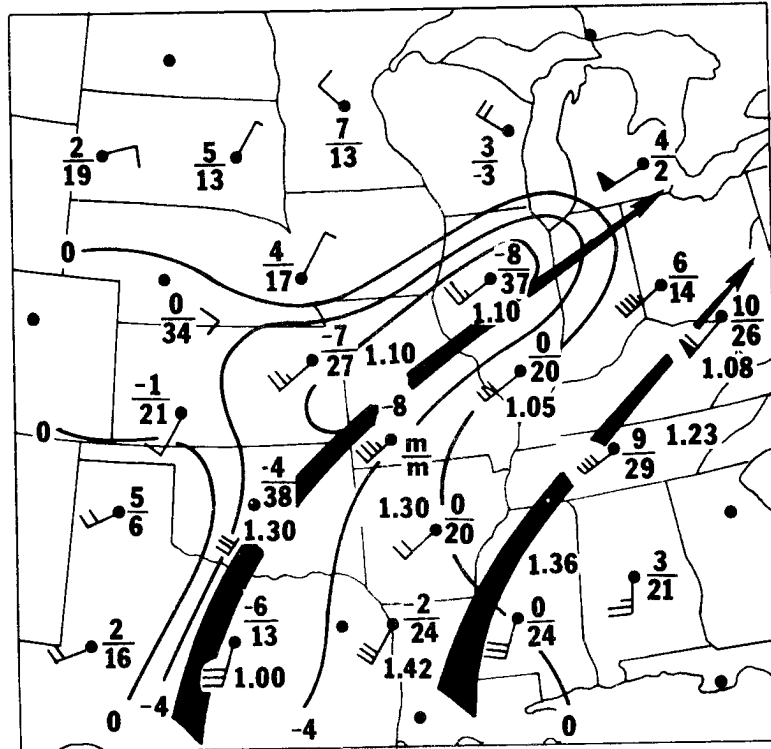
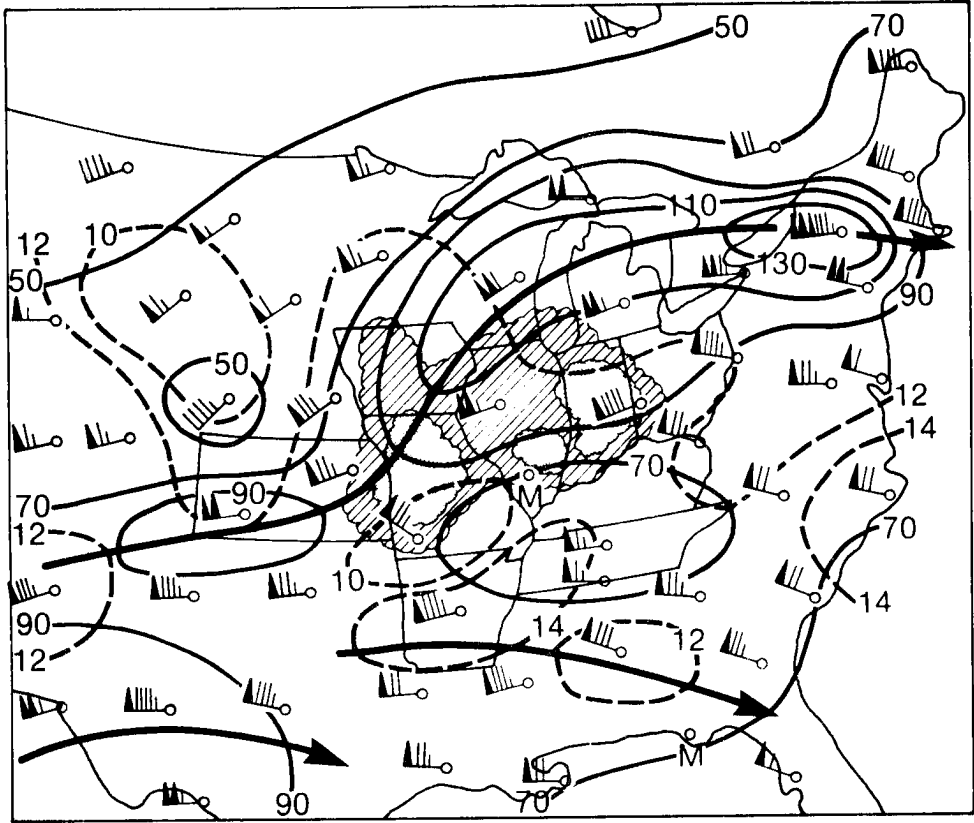
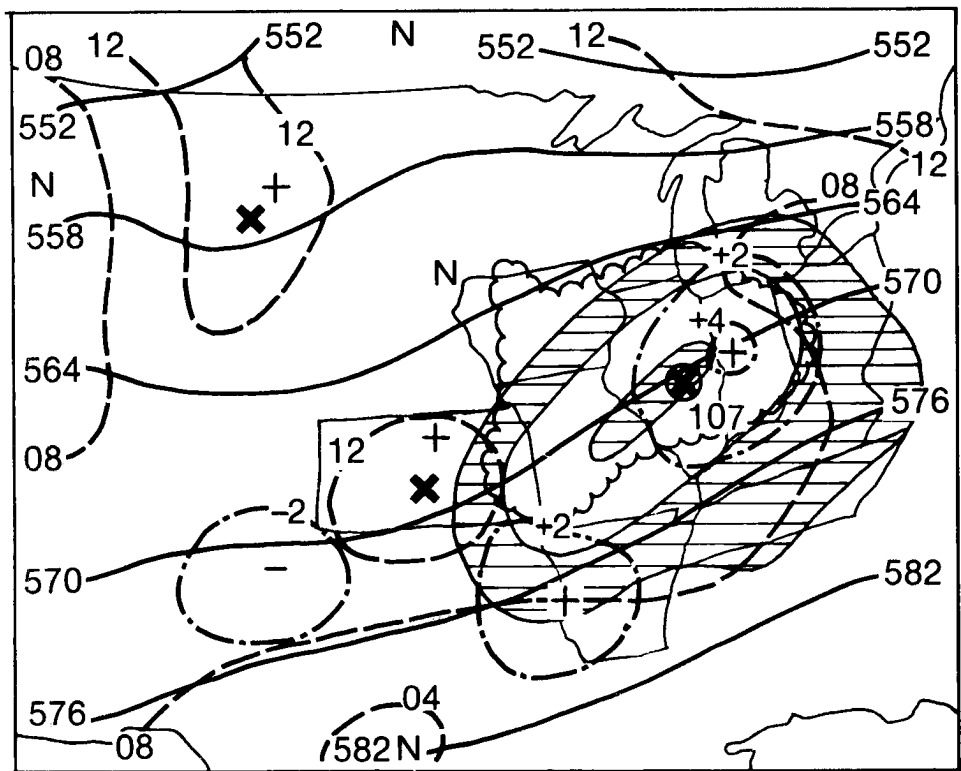
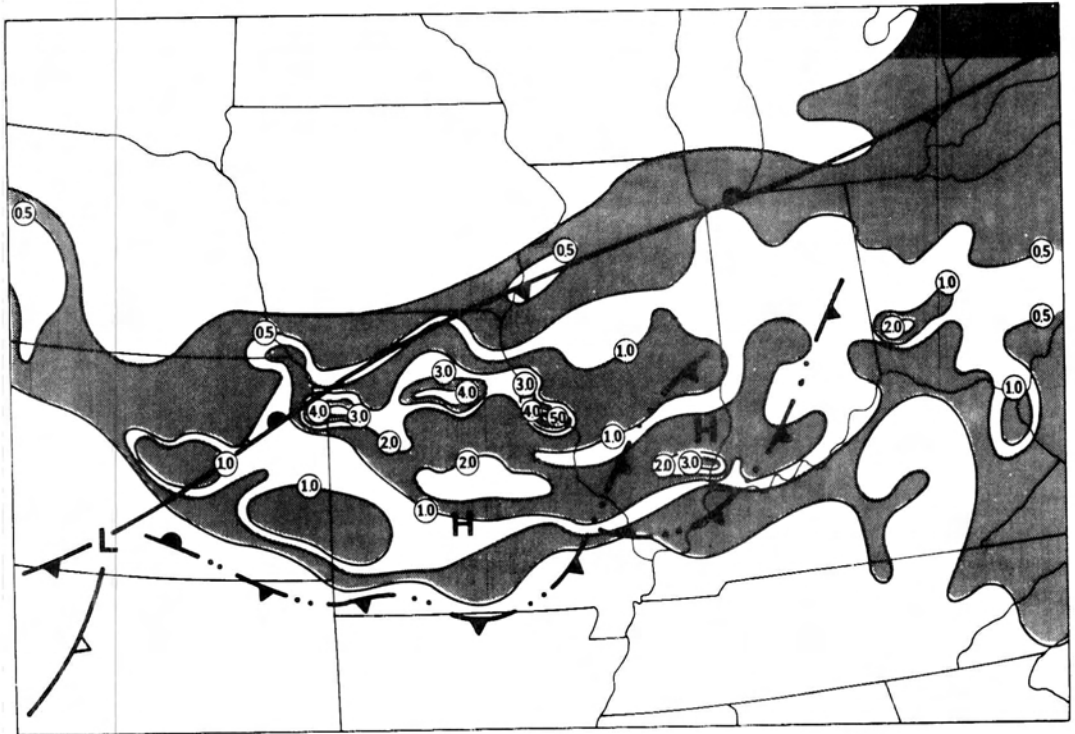


Fig. C5. Accumulated precipitation (in inches) from 0000 to 1200 GMT on 24 April 1975. Surface features at 12 GMT are also shown.

Fig. C6. Twelve hour Limited Fine Mesh (LFM) numerical forecast valid at 1200 GMT 24 April 1975. Shown are 500 mb heights (solid), vorticity contours (dashed), 700 mb vertical (dash-dot), and forecasted 12 h accumulated precipitation (cross-hatched). The MCC's satellite indicated cloud shield is also indicated.



period ending 1200 GMT on the 24th. Heavy rains were widespread during the night with amounts of 3 to 5 in. (75 to 125 mm) common. The 12 h LFM forecast is shown in Fig. C6. The MCC apparently developed just ahead of a weak, mid-level short-wave trough. The model forecasted the areal extent of precipitation quite well (missing only the band of convective precipitation across Kansas); however, the amounts of precipitation were considerably underforecast (note the forecasted region of .5 to 1.0 in.) with the center of activity occurring considerably further west than forecast. Additional details concerning large scale conditions and the evolution and severity of this particular convective system are available in Maddox (1979) and Maddox et al. (1979b).

C.2 MCC of 6/7 May 1978

Severe thunderstorms developed over northern Arkansas at about 2230 GMT on the 6th and rapidly developed into an intense mesosystem. Other thunderstorm systems developed over eastern and northeastern Texas between 0200 and 0300 GMT. These clusters intensified, grew large and merged with the original system. During its life-cycle, which extended well into the afternoon of the 7th, this MCC became one of the largest systems documented to date and produced tremendous amounts of damage due to severe thunderstorms and flash flooding.

Figure C7 is a satellite photograph of this MCC at 1200 GMT 7 May showing the system covering a large portion of the south-central U.S. Maximum winds aloft for 0000 and 1200 GMT on the 7th are presented in Figs. C8 and C9. Once again the anticyclonic curvature and speed of the jet stream increased dramatically north and northeast of the MCC with a tremendous increase in diffluence apparent over the system. At the time of the system (1200 GMT) strongest tropospheric winds were occurring in

Fig. C7. Enhanced IR image for 1200 GMT 7 May 1978.

Fig. C8. Maximum observed winds aloft for 0000 GMT 7 May 1978. Regions where maximum winds occurred below 8 km are cross-hatched.

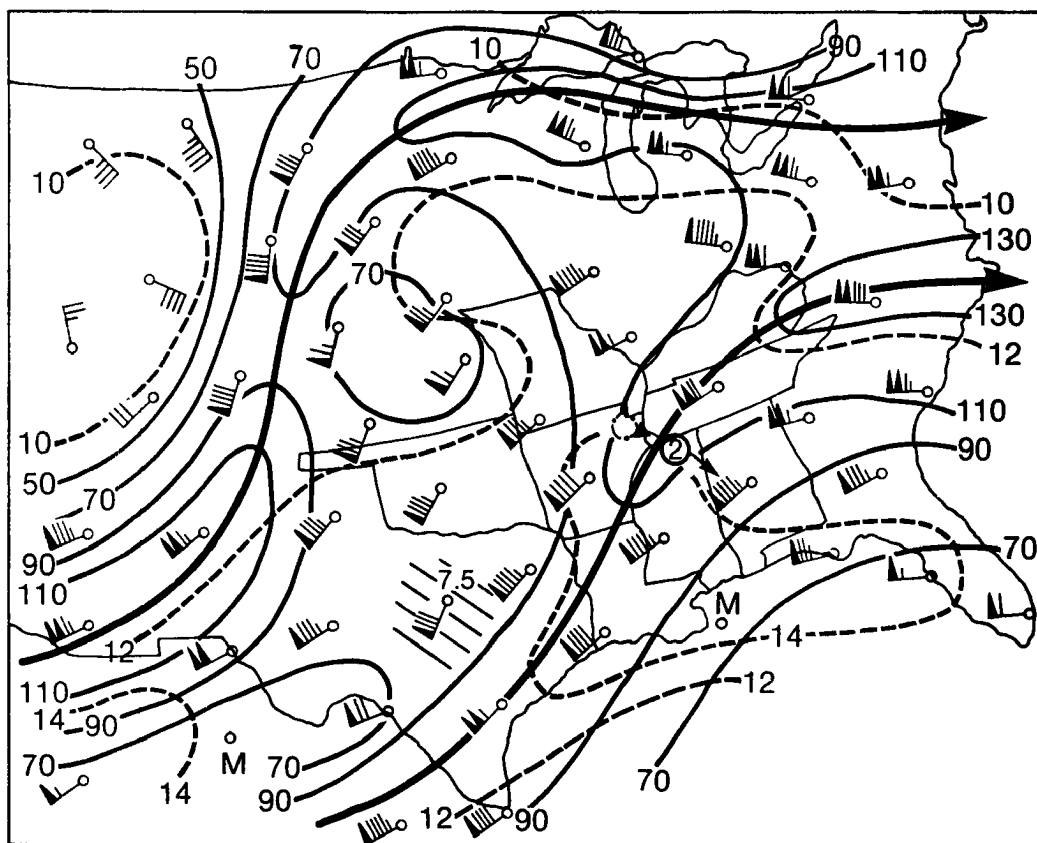
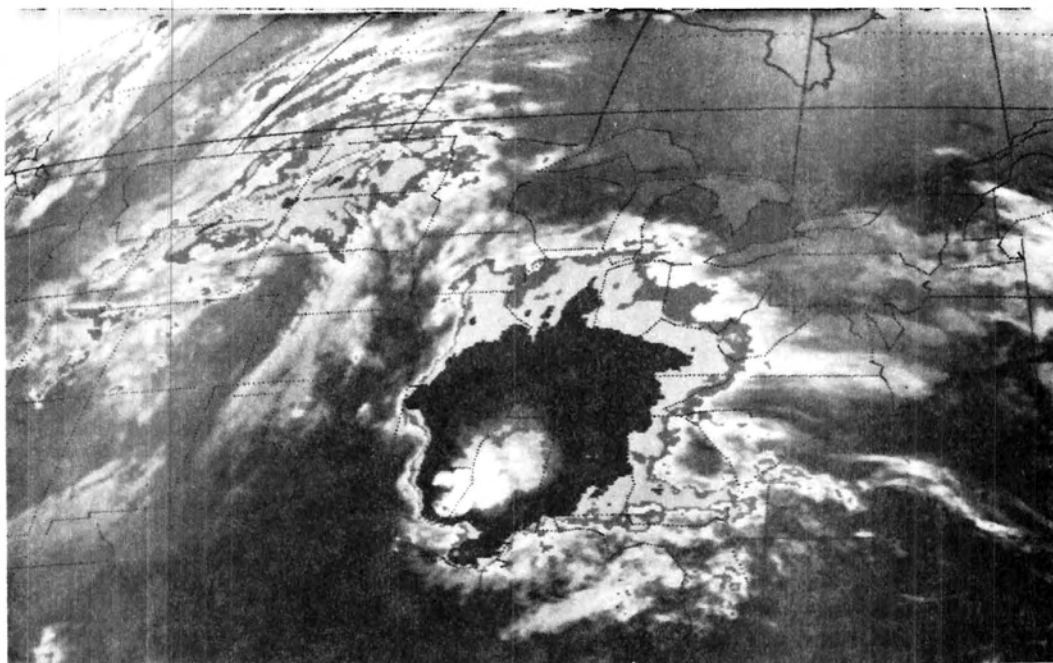
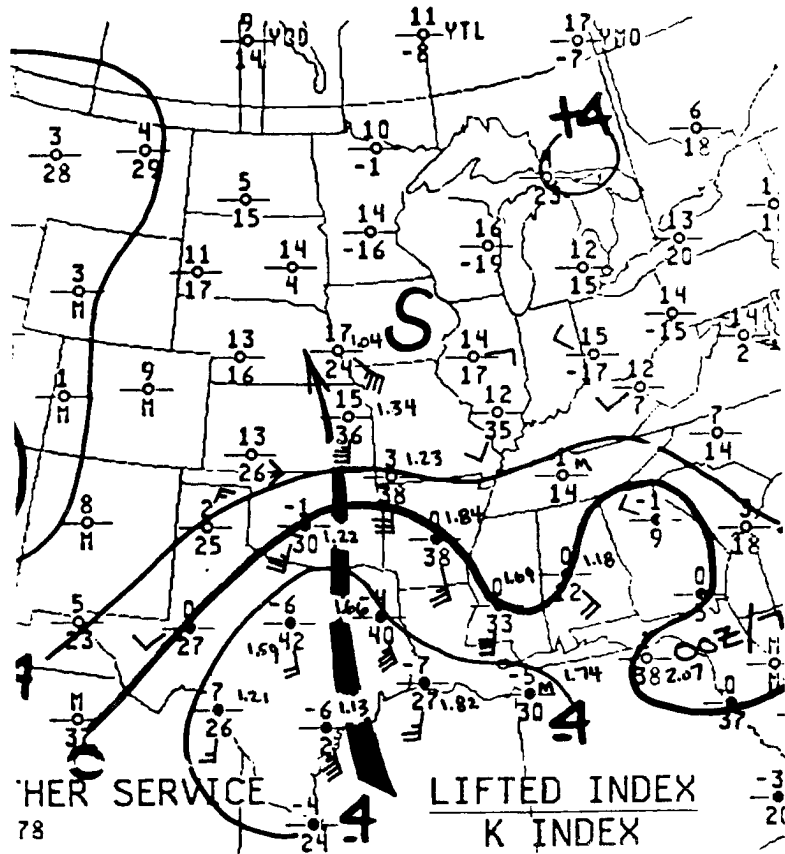
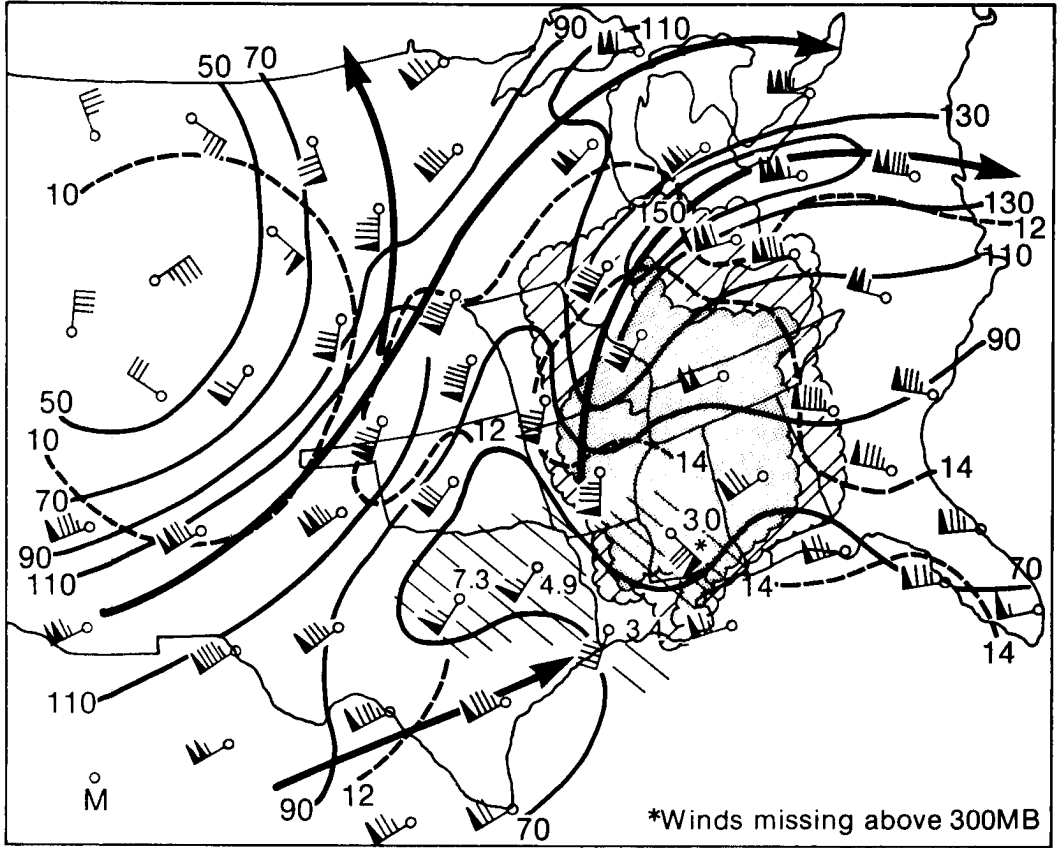


Fig. C9. Maximum observed winds aloft for 1200 GMT 7 May 1978.

Fig. C10. Stability chart for 0000 GMT 7 May 1978.



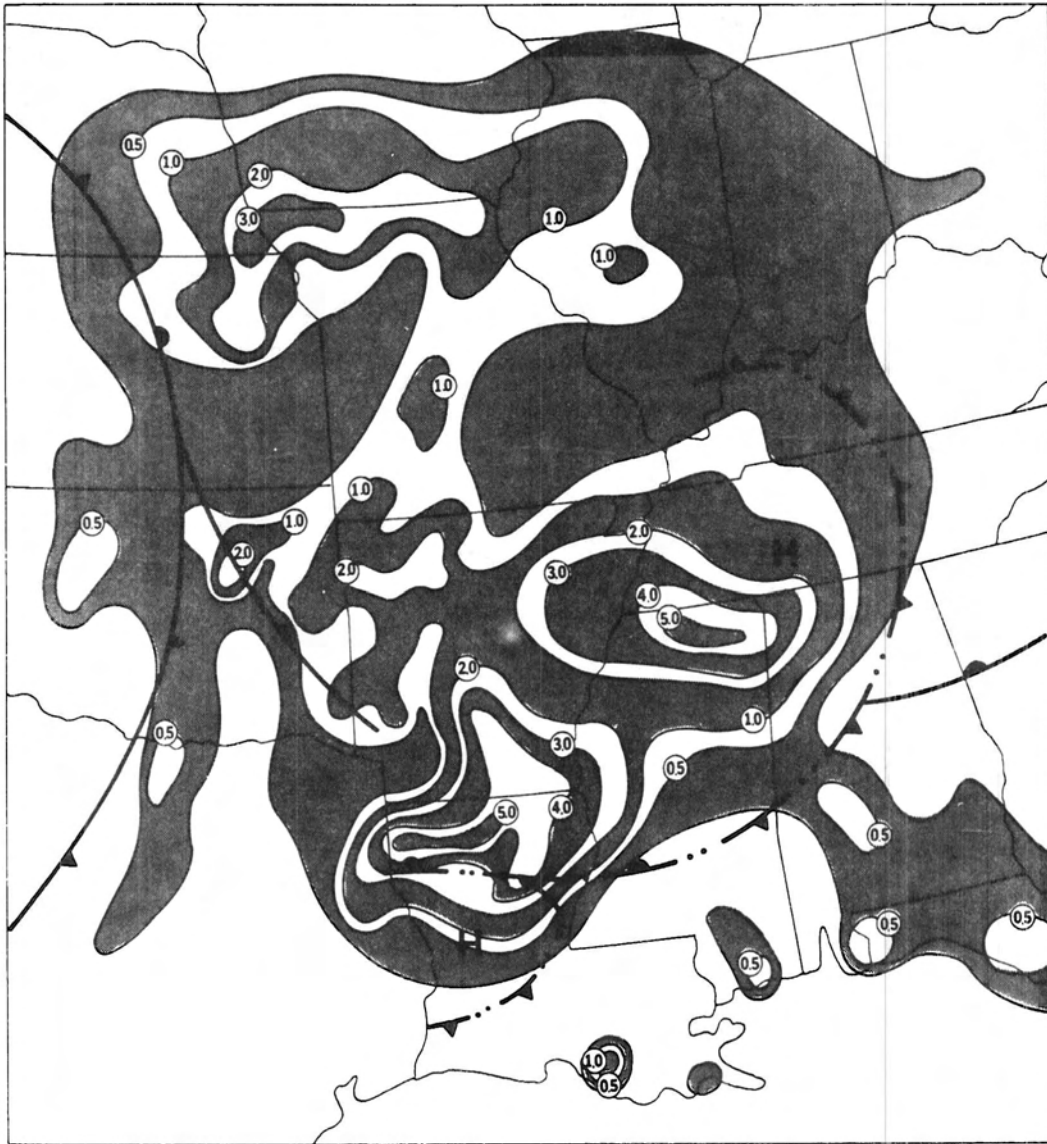


Fig. C11. Accumulated precipitation (in inches) from 0000 to 1200 GMT on 7 May 1978. Surface features at 1200 GMT are also shown.

the lower troposphere south and southwest of the system. The stability, precipitable water and 850 mb winds for 0000 GMT are shown in Fig. C10. This MCC also developed within a region characterized by a very unstable air mass with strong southerly low-level flow and very high moisture contents. The 12 h precipitation chart (Fig. C11) illustrates the significant, widespread heavy precipitation produced by this system (the

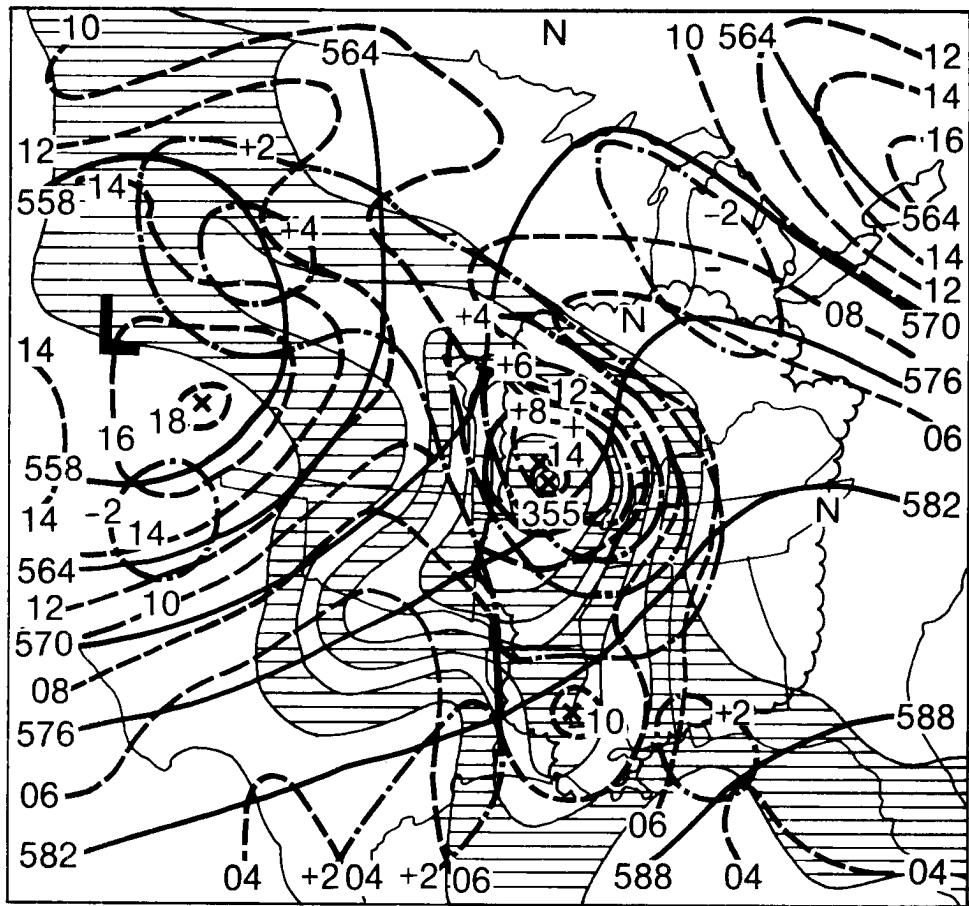


Fig. C12. Twelve hour LFM numerical forecast valid at 1200 GMT 7 May 1978.

precipitation maximum over northwest Missouri was produced by a separate convective system that dissipated rapidly during the early nighttime hours). The LFM 12 h forecast (Fig. C12) showed that the model forecasted widespread precipitation with a very significant (for the LFM) maximum of over 3.5 in. over southern Missouri just ahead of a weak short-wave swinging out of the broad trough to the west. The observed precipitation considerably exceeded the numerical forecast with the region of heaviest rains shifted southward toward the convectively unstable air mass (see Figs. C11 and C10). Additional analyses of upper tropospheric features attending this MCC may be found in Fritsch *et al.* (1979) and Maddox (1980).

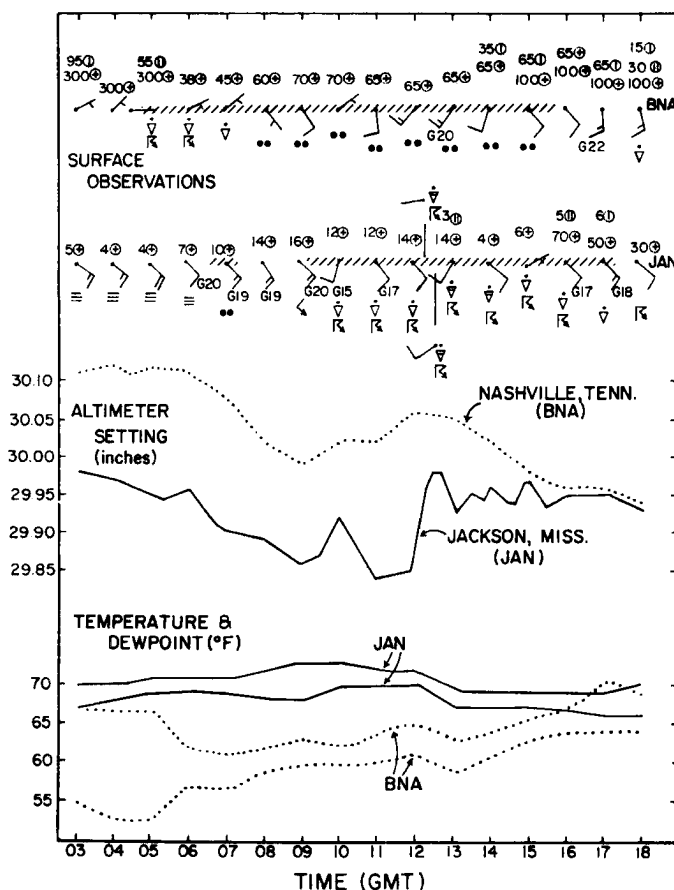


Fig. C13. Surface observation time-series for Jackson, Mississippi, and Nashville, Tennessee. Winds are in knots and are plotted with north to the top of the page. Cross-hatching indicates periods of reported rainfall.

A time series of surface observations taken at Nashville, Tennessee (beneath the northern portion of the system) and at Jackson, Mississippi (beneath the southern portion of the MCC) is depicted in Fig. C13. The temperature at Nashville dropped rapidly and the dewpoint increased as the initial thunderstorm activity moved over the station at 0500 GMT. However, the general tendency during the night was one of slowly increasing temperatures at both stations. The most important characteristic illustrated here is the persistence of the weather phenomena attending the MCC. Precipitation fell steadily for a 10 h period at Nashville from an overcast cloud deck that gradually lifts from 3800 ft. to 10000 ft. AGL. At Jackson

thunder and rain persisted continuously for more than 8 h with the low stratus breaking to an overcast at 5-8000 ft. AGL near the end of the event. Various windshifts and pressure jumps/falls illustrate embedded small (thunderstorm) scale features within the overall MCC weather system.

Figure C14 is a map showing surface weather reports for 1100 GMT on the 7th (approximately the time of release of the 1200 GMT upper-air soundings), the locations of eight upper-air soundings taken within or near this system and the approximate position of 3 selected IR T_{BB} isotherms from the 1100 GMT satellite image. Precipitation is reported beneath most of the cold cloud shield with the major exception being the eastern quarter of the system -- the cold cloud shield in this region might be considered high-level, thick cirrus "blowoff".

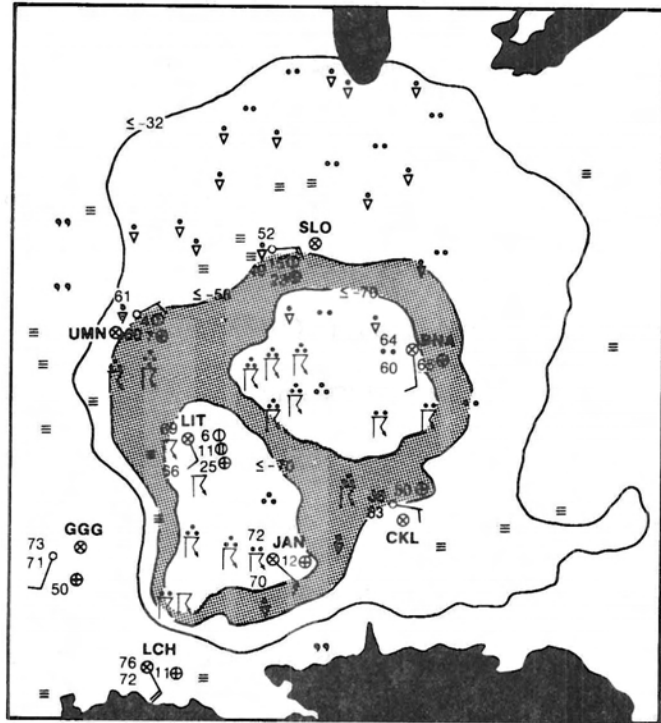


Fig. C14. Surface weather reports for 1100 GMT 7 May 1978. Eight upper-air sounding locations are indicated as are selected (-32 , -58 and -70°C) IR T_{BB} contours.

Vertical profiles of the wind, θ_e and θ_{e_s} are presented in Figs. C15 through C22 for the sounding locations indicated on Fig. C14. The GGG sounding indicates a conditionally unstable profile with apparent strong flow of high θ_e air in the 750 - 900 mb layer toward the MCC. The LCH profiles are similar except that the high θ_e layer is much deeper (> 345 K from the surface to 700 mb) and the entire column is much nearer saturation (less lifting required to release the instability than required in the GGG air mass). The CKL and JAN soundings (Figs. C17 and C18) -- taken near the leading edge of the precipitation and thunderstorm region -- are quite interesting. Both display a lower layer of cool, moist low θ_e air with a deep layer of slowly decreasing θ_e air above. This air mass is very dry near its lower base (800 - 850 mb) but is increasingly moist above. These two soundings are very similar to Zipser's (1977) composite sounding just to the rear of the precipitation area of tropical convective systems. They are suggestive of unsaturated downdrafts and precipitation falling from cloud based between 700 and 600 mb. This cloud mass and precipitation is presumably being ejected from the approaching region of very intense convection so that it may be quite similar to the "anvil rain" areas documented by Houze (1977) and Zipser (1977).

The soundings from LIT, BNA, UMN and SLO (taken within northern and western portions of the MCC system) all appear to indicate deep layers of moist or nearly moist ascent based at 800 - 900 mb. The UMN sounding may have sampled undilute ascent within a convective element in mid-levels. The SLO sounding is most remarkable because of the extreme difference in the characteristics of the very cool surface layer and the layer of moist, high θ_e air that overlays it. The source of this over-running air mass is most certainly well to the south and southwest of SLO.

Fig. C15. Vertical profiles of wind, θ_e and θ_{e_s} for Longview, Texas (GGG) at 1200 GMT 7 May 1978. Winds are in knots.

Fig. C16. Vertical profiles of wind, θ_e and θ_{e_s} for Lake Charles, Louisiana (LCH) at 1200 GMT 7 May 1978.

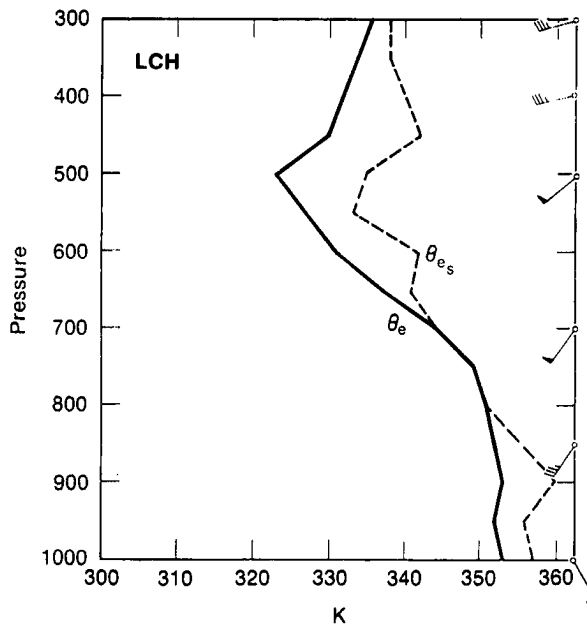
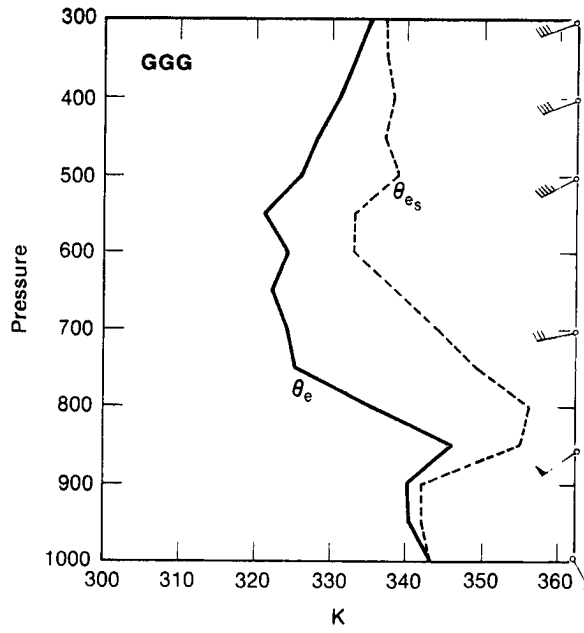


Fig. C17. Vertical profiles of wind, θ_e and θ_{e_s} for Centerville, Alabama (CKL) at 1200 GMT 7 May 1978.

Fig. C18. Vertical profiles of wind, θ_e and θ_{e_s} for Jackson, Mississippi (JAN) at 1200 GMT 7 May 1978.

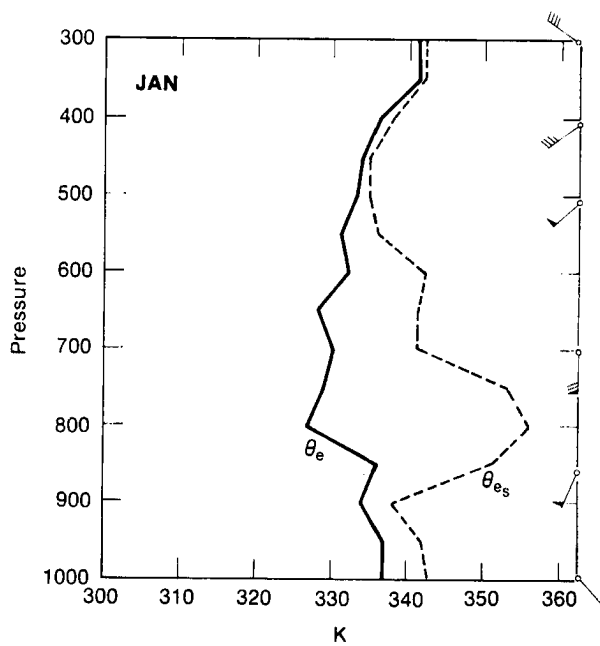
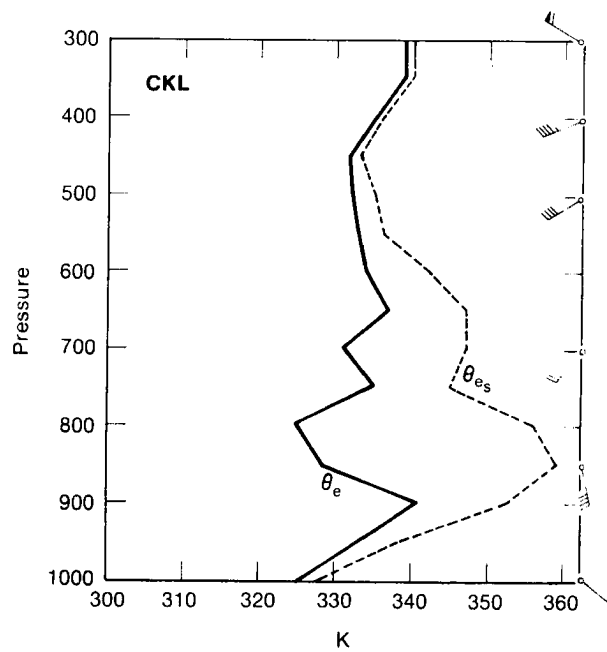


Fig. C19. Vertical profiles of wind, θ_e and θ_{e_s} for Little Rock, Arkansas (LIT) at 1200 GMT 7 May 1978.

Fig. C20. Vertical profiles of wind, θ_e and θ_{e_s} for Nashville, Tennessee (BNA) at 1200 GMT 7 May 1978.

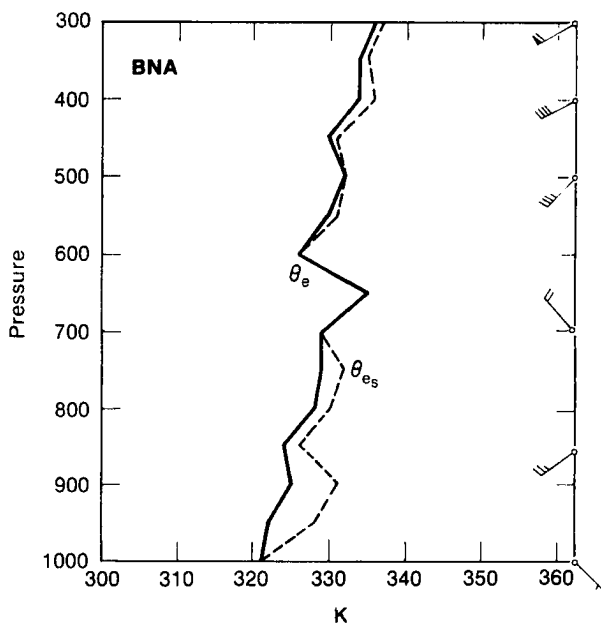
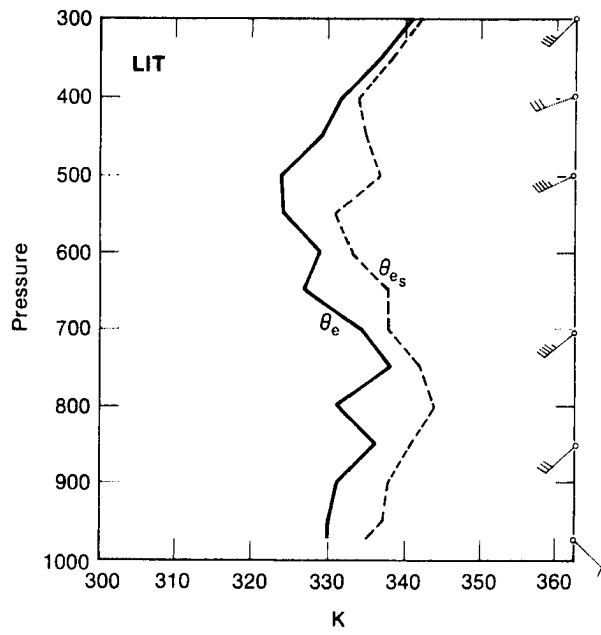
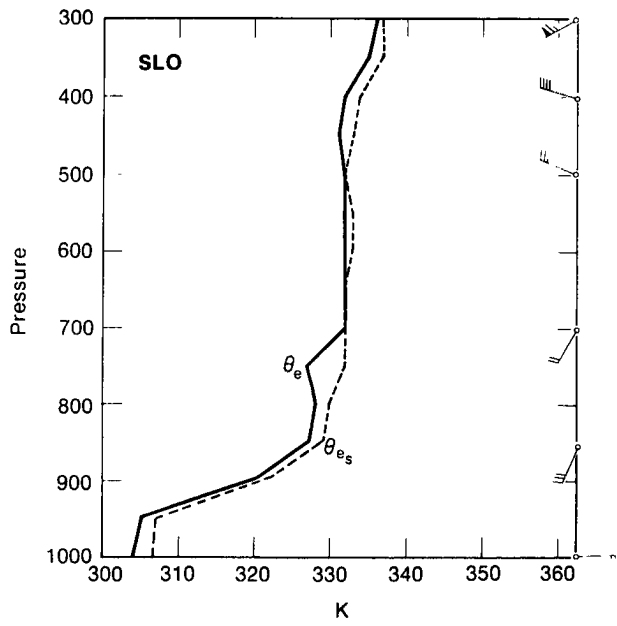
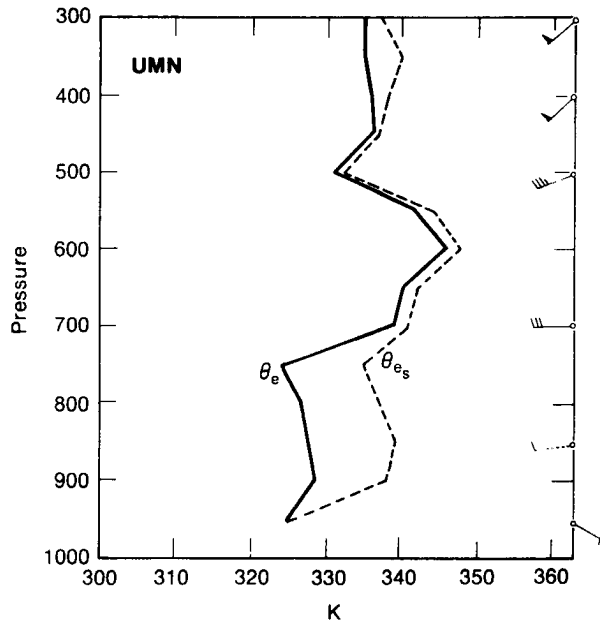


Fig. C21. Vertical profiles of wind, θ_e and θ_{e_s} for Monett, Missouri (UMN) at 1200 GMT 7 May 1978.

Fig. C22. Vertical profiles of wind, θ_e and θ_{e_s} for Salem, Illinois (SLO) at 1200 GMT 7 May 1978.



C.3 MCC of 18 May 1978

The initial thunderstorms that developed into this system formed between 0300 and 0330 GMT over southwestern Kansas and grew steadily during the night into a large, nearly circular complex. Two storm clusters developed south of the main system and then merged into it. Figure C23 shows the system at 1330 GMT. Figures C24 and C25 show tropospheric maximum wind charts that indicate again that upper-level winds became more anticyclonic and much stronger north and northeast of the system. At the time of the system strongest winds were in the lower troposphere to its south and southwest.

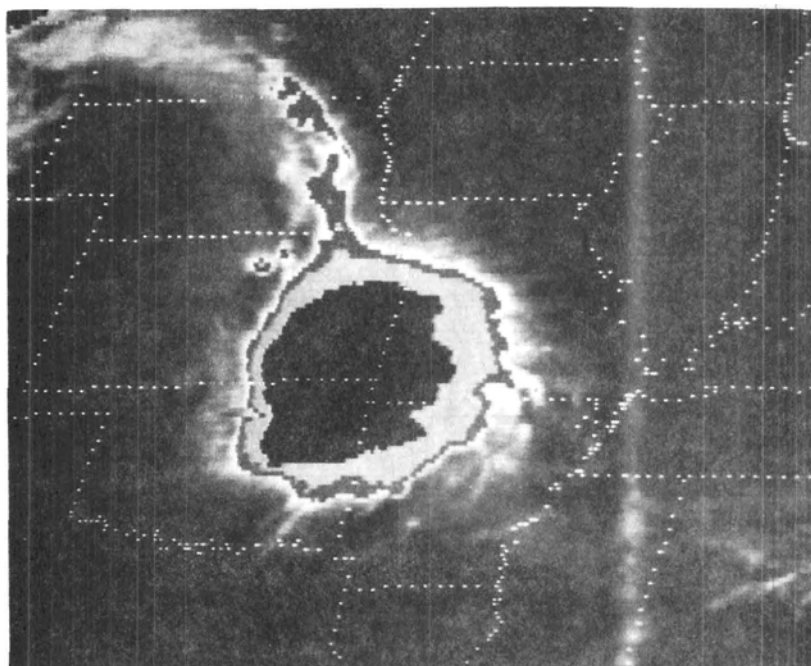
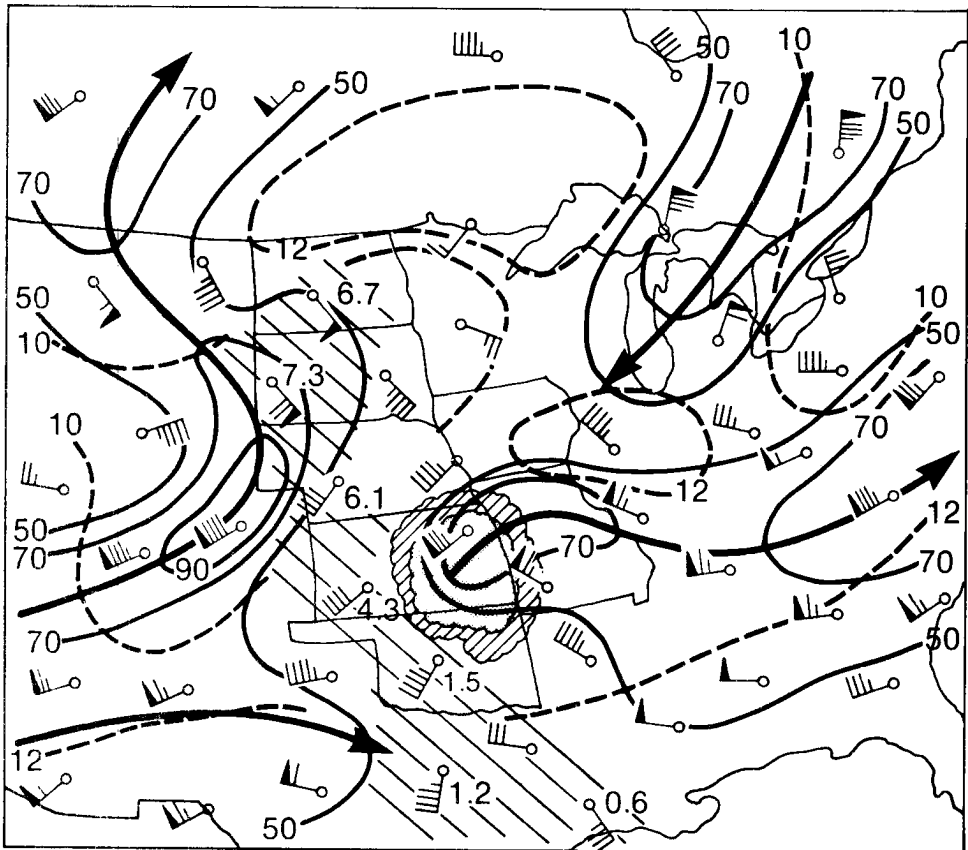
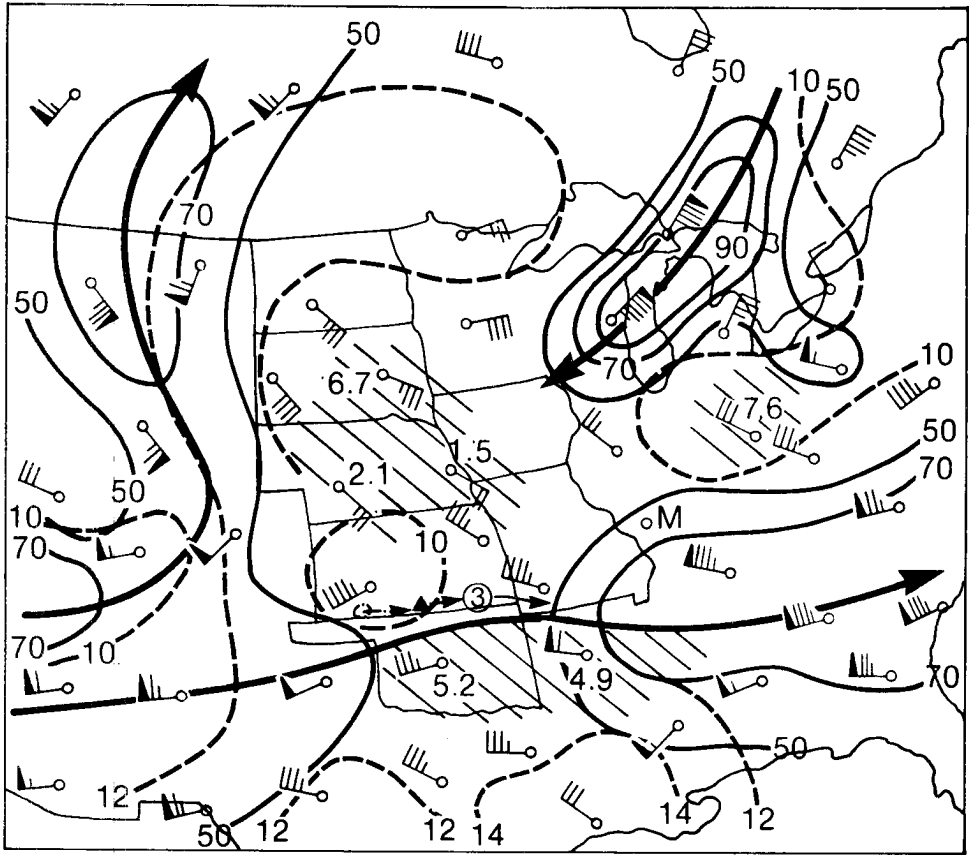


Fig. C23. Enhanced IR image for 1330 GMT 18 May 1978.

Fig. C24. Maximum observed winds aloft for 0000 GMT 18 May 1978.

Fig. C25. Maximum observed winds aloft for 1200 GMT 18 May 1978.



The 0000 GMT precipitable water, stability analysis and 850 mb winds (Fig. C26) show that the MCC developed in a region of moderate instability (LI-2 to -4) with moisture contents of 1 to 1.25 inches and south-southeasterly low-level flow of 20-25 knots. The accumulated precipitation map (Fig. C27) shows a swath of rainfall across Kansas and northern Oklahoma with maximum amounts exceeding 2.5 inches. The LFM forecast for this period (Fig. C28) indicated a broad, large scale precipitation region along the frontal zone with a maximum over western Oklahoma and northern Texas. The actual precipitation event was dominated by the MCC which

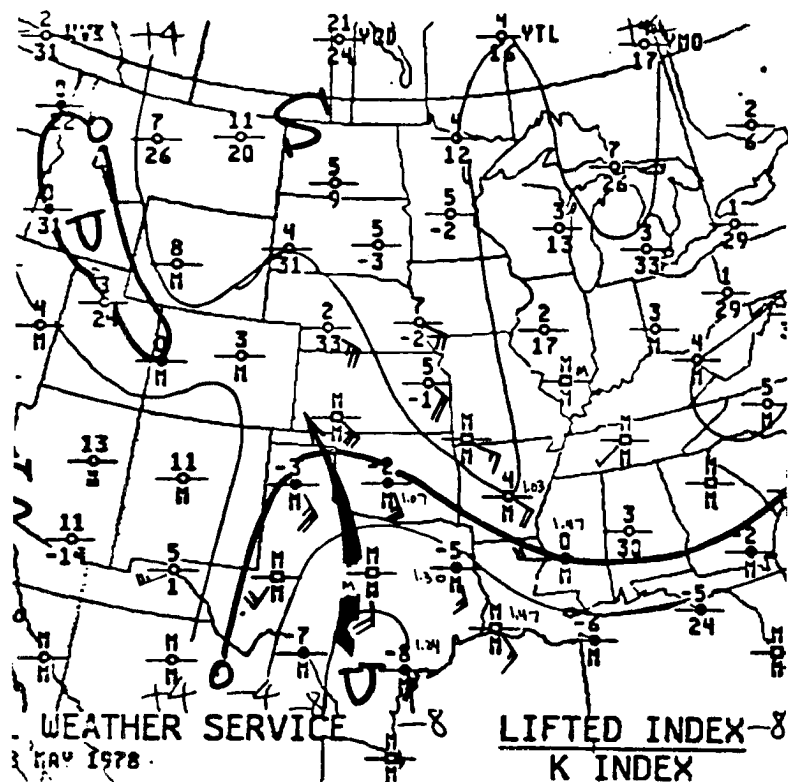
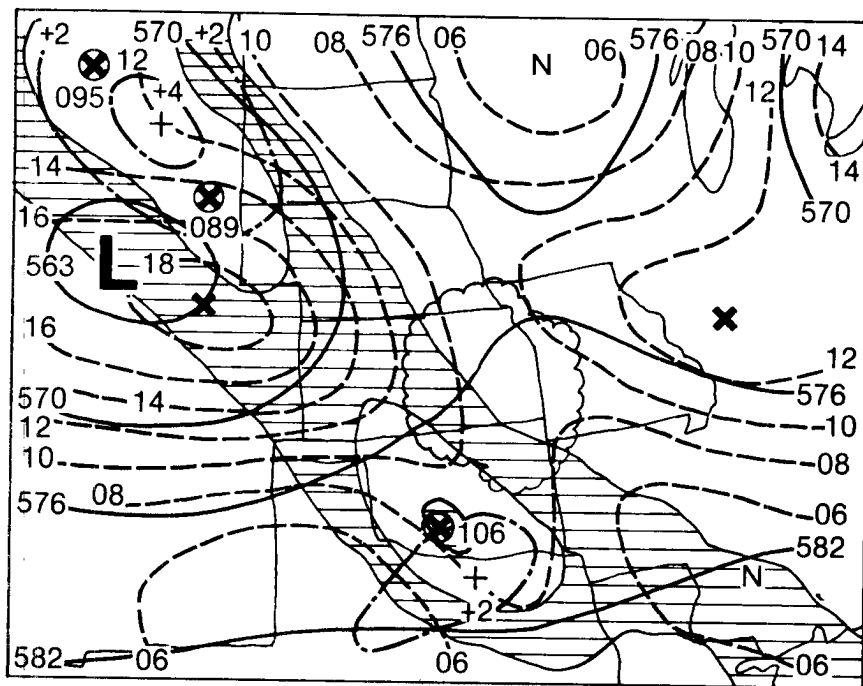
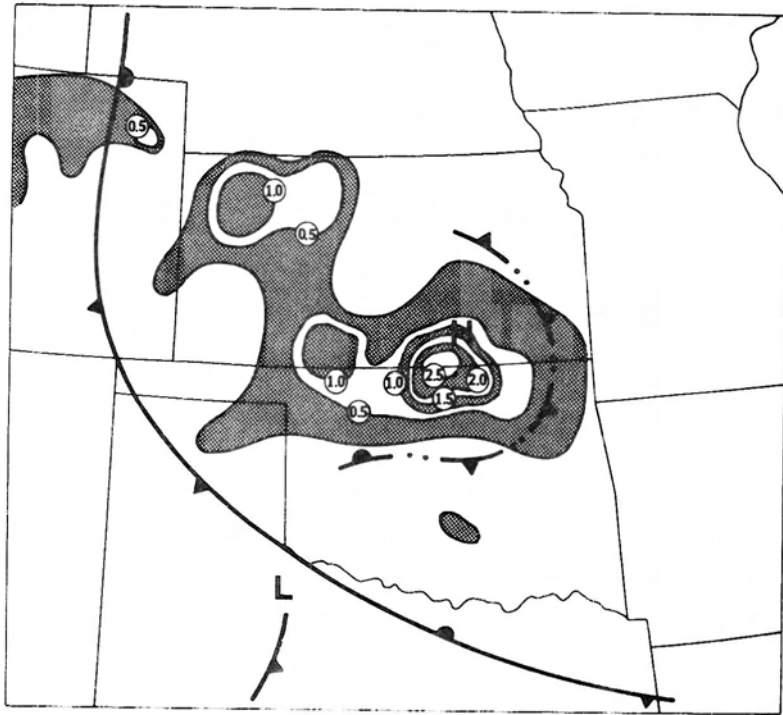


Fig. C26. Stability chart for 0000 GMT 18 May 1978.

Fig. C27. Accumulated precipitation (in inches) from 0000 to 1200 GMT on 18 May 1978. Surface features at 1200 GMT are also shown.

Fig. C28. Twelve hour LFM numerical forecast valid at 1200 GMT 18 May 1978.



moved eastward just ahead of a weak short-wave trough (see Fig. C28), beneath a large scale blocking high.

C.4 MCC of 30/31 May 1978

Thunderstorms developed over western Kansas between 2030 and 2130 GMT on the 30th and grew into a complex. The system merged with other storm activity that developed over southeastern Nebraska and eastern Kansas. Abundant thunderstorm activity over Colorado, southeastern Wyoming and the Nebraska Panhandle weakened as it moved eastward and did not merge with the MCC. This system is pictured in Fig. C29. Jet stream analyses for 0000 and 1200 GMT on the 31st are shown in Figs. C30 and C31. The changes in upper-level flow during this 12 h period are quite similar to those accompanying the other systems. The 0000 GMT analysis does indicate a pronounced precursor jet streak over southern Wyoming. The

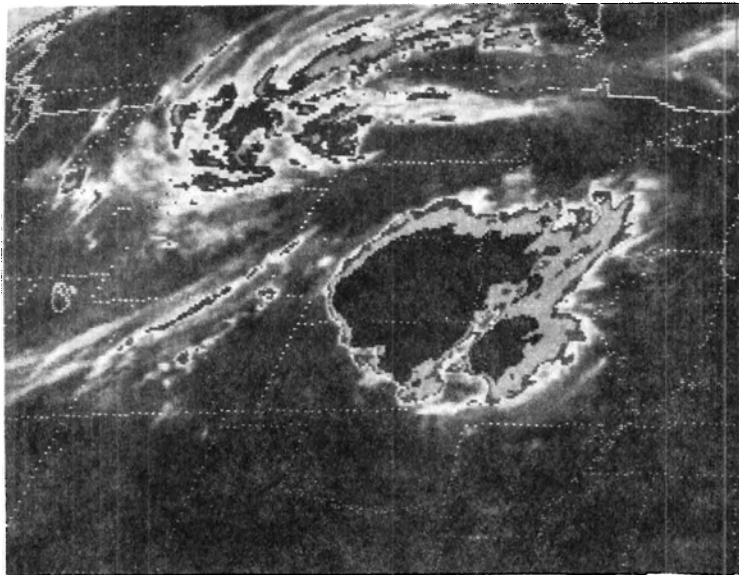
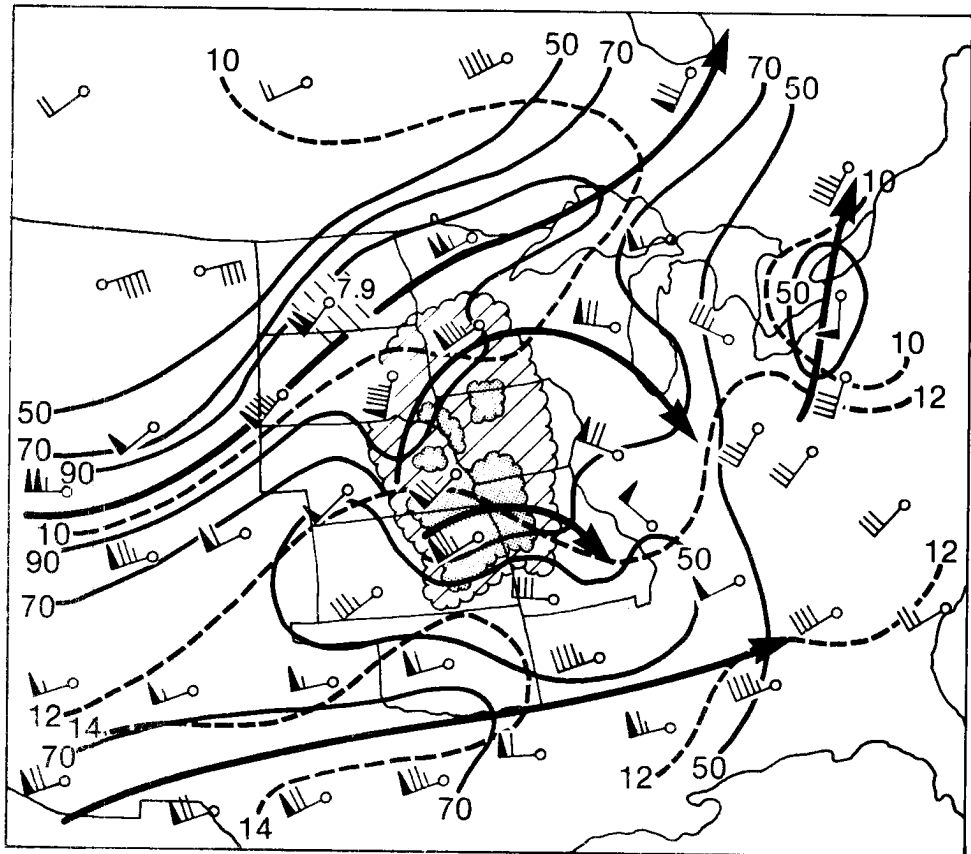
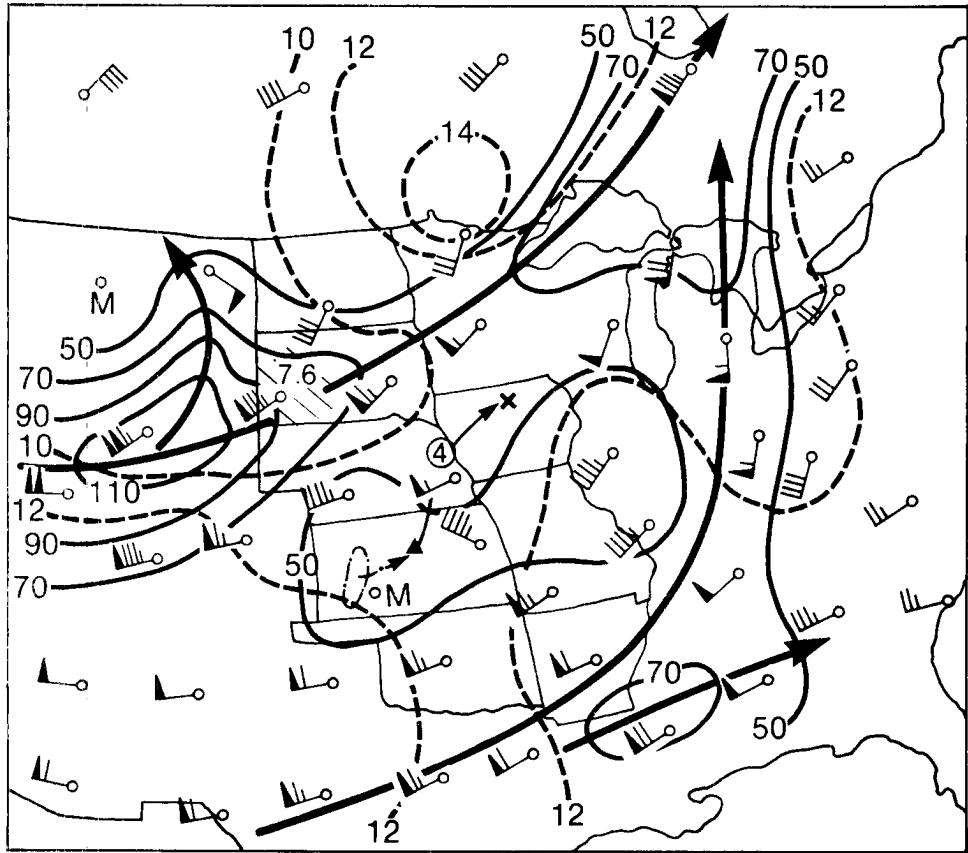


Fig. C29. Enhanced IR image for 0900 GMT 31 May 1978.

Fig. C30. Maximum observed winds aloft for 0000 GMT 31 May 1978.

Fig. C31. Maximum observed winds aloft for 1200 GMT 31 May 1978.



early stages of the development of this MCC occurred within the right exit zone of this jet or within a region usually not considered favorable for intense storm development (see Riehl *et al.*, 1952; Beebe and Bates, 1955; Reiter, 1963; McNulty, 1978; and Uccellini and Johnson, 1979).

The precipitable water, stability and 850 mb wind analysis (Fig. C32) show that the system again developed in a very unstable region (LI -6 to -7). Precipitable water contents exceeded an inch and a south-southwesterly low-level jet was present. Once again the MCC developed just south and southwest of a pronounced col in the low-level streamlines. The accumulated precipitation map (Fig. C33) indicates that this system produced widespread general rains with amounts of 1 to 2 inches common.

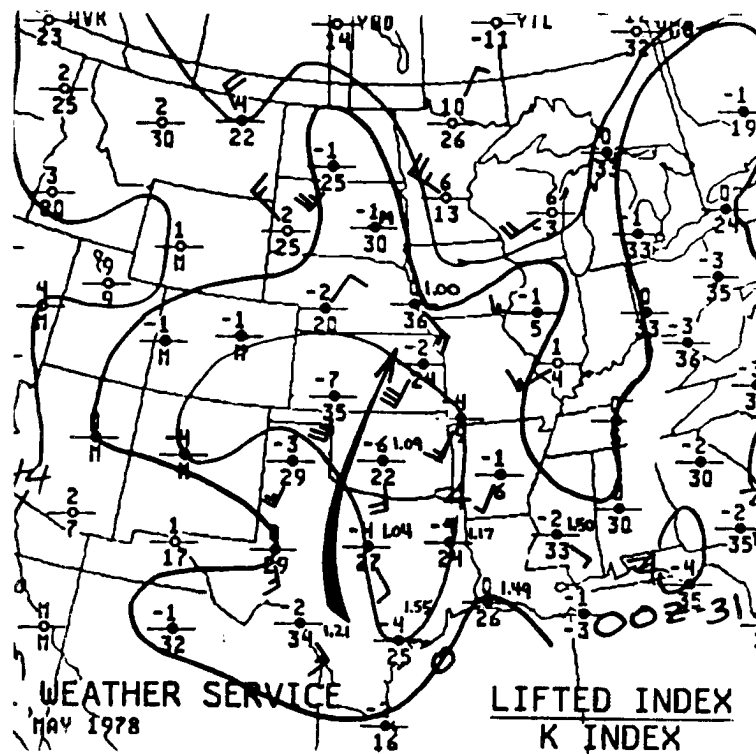


Fig. C32. Stability chart for 0000 GMT 31 May 1978.

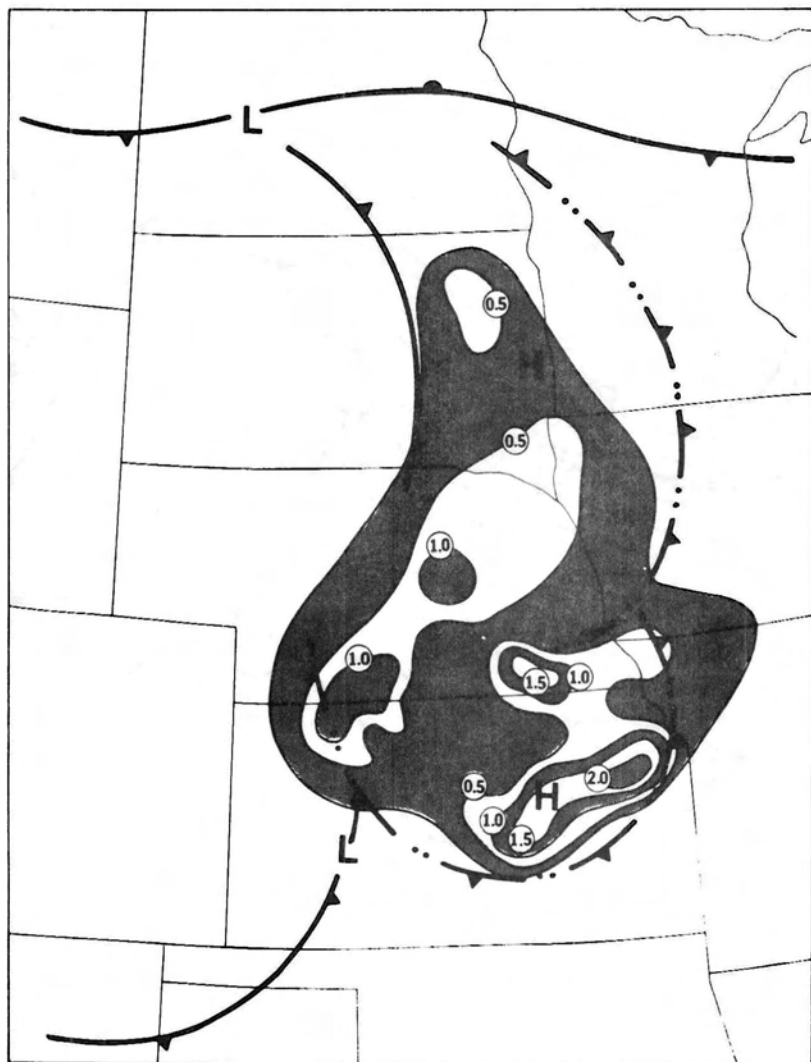


Fig. C33. Accumulated precipitation (in inches) from 0000 to 1200 GMT on 31 May 1978. Surface features at 1200 GMT are also shown.

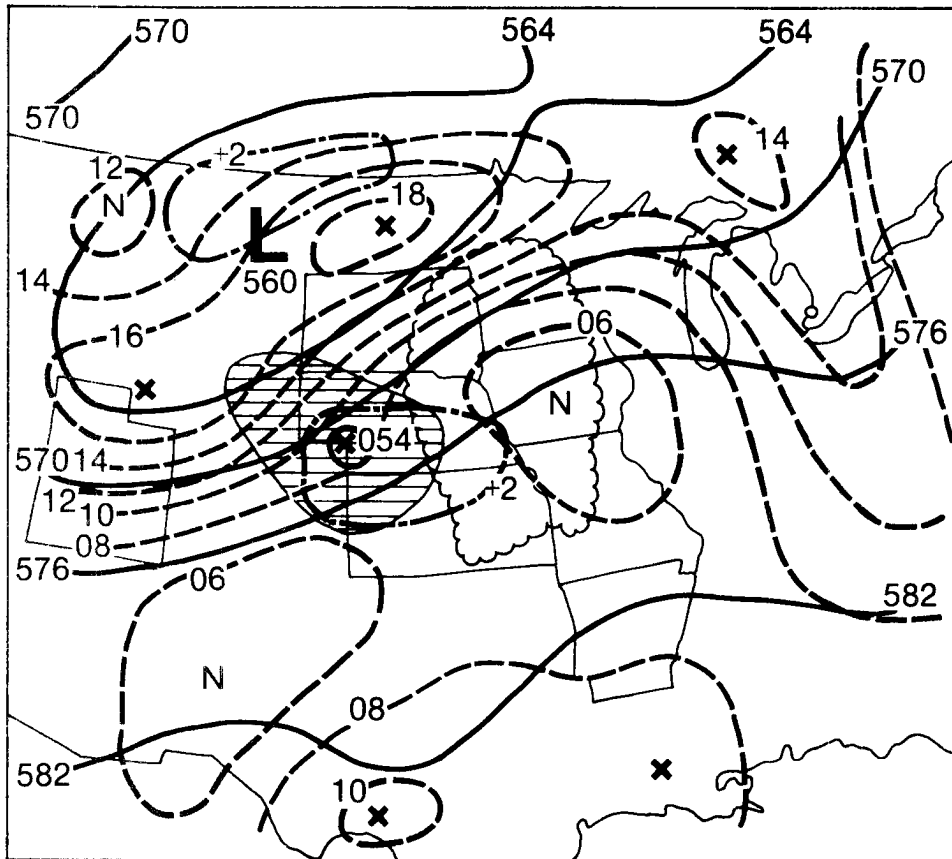


Fig. C34. Twelve hour LFM numerical forecast valid at 1200 GMT 31 May 1978.

The LFM 12 h forecast (Fig. C34) had indicated no precipitation over most of this region; however, the height, vorticity and vertical motion fields indicate that this MCC did develop just ahead of a very weak short-wave trough that was moving northeastward out of the trough over Wyoming and Utah.

C.5 MCC of 3/4 June 1978

A cluster of thunderstorms formed over northeast Colorado about 2200 GMT on the 3rd and slowly grew into the MCC system. A smaller cluster that developed over southeastern Colorado merged with the main system. Another smaller system over the Texas Panhandle merged with the MCC during

the final stages of its life-cycle. The MCC system is shown in the satellite image of Fig. C35. The jet stream analyses before and during the MCC (Figs. C36 and C37) again illustrate the increase in anticyclonic curvature and in speed north and northeast of the system.

The precipitable water, stability and 850 mb wind chart (Fig. C38) shows that this system developed within a more stable air mass (LI only 0 to -2), precipitable water contents of about 1.25 inch and with no low-level jet apparent. It is thus not surprising that this was the smallest

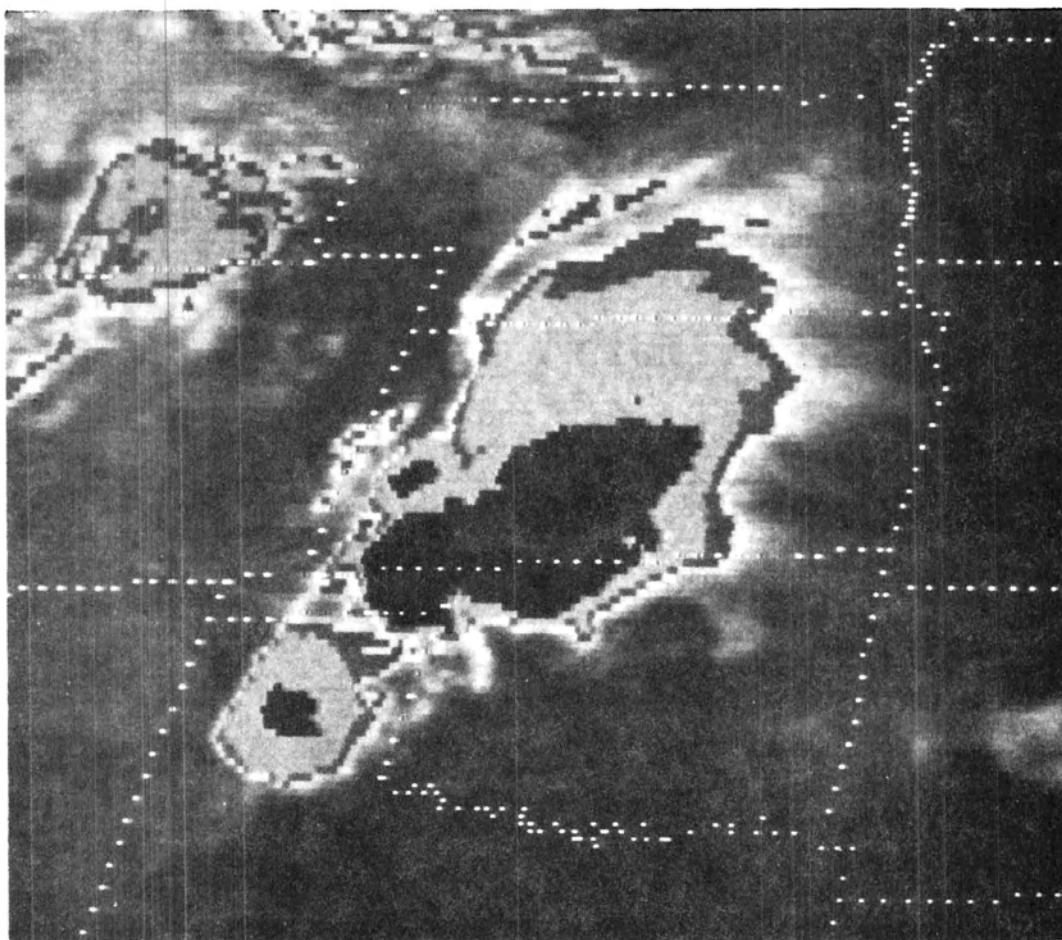


Fig. C35. Enhanced IR image for 1200 GMT 4 June 1978.

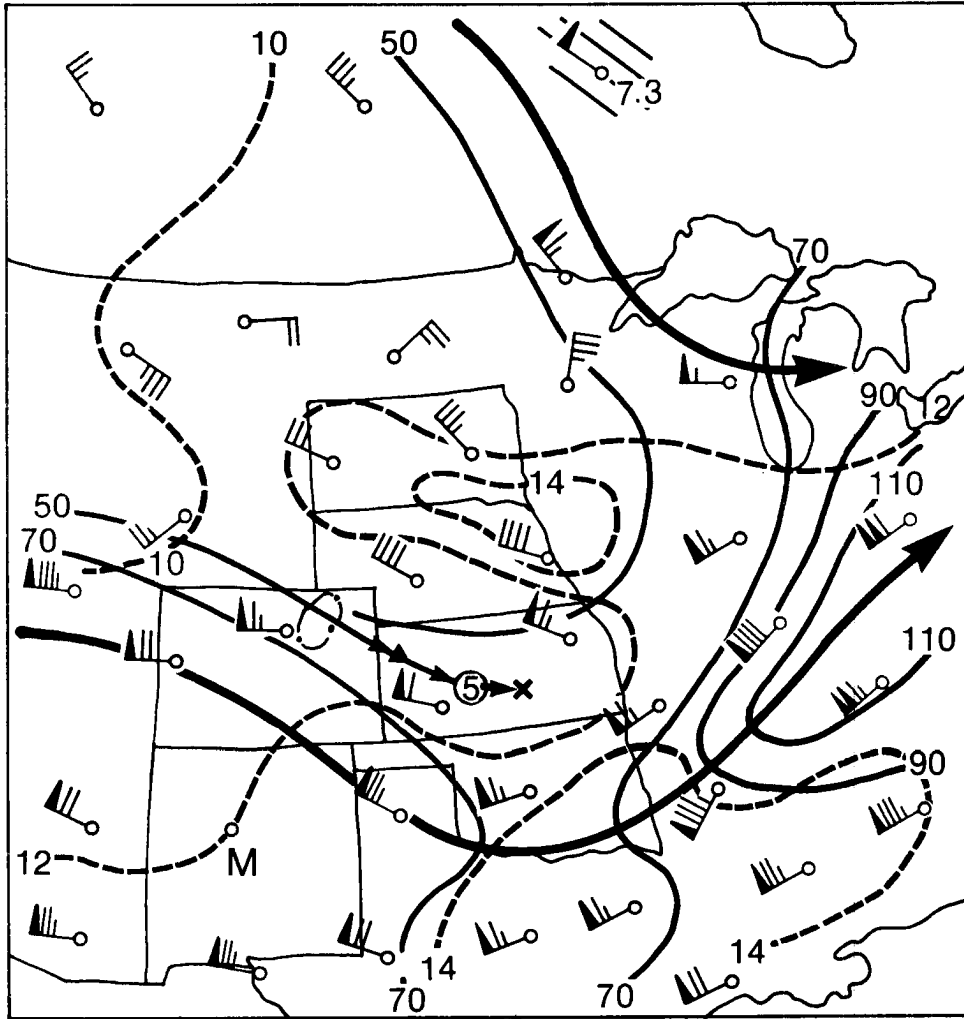


Fig. C36. Maximum observed winds aloft for 0000 GMT 4 June 1978.

Fig. C37. Maximum observed winds aloft for 1200 GMT 4 June 1978.

Fig. C38. Stability chart for 0000 GMT 4 June 1978.

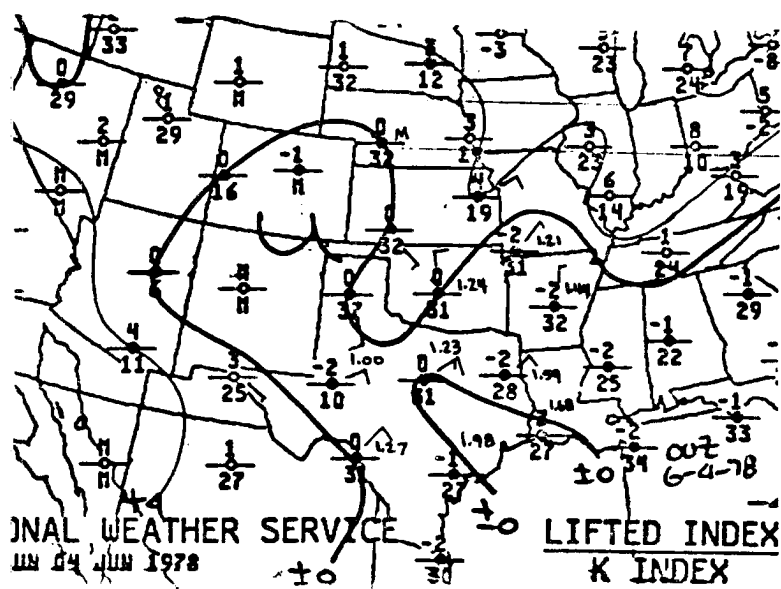
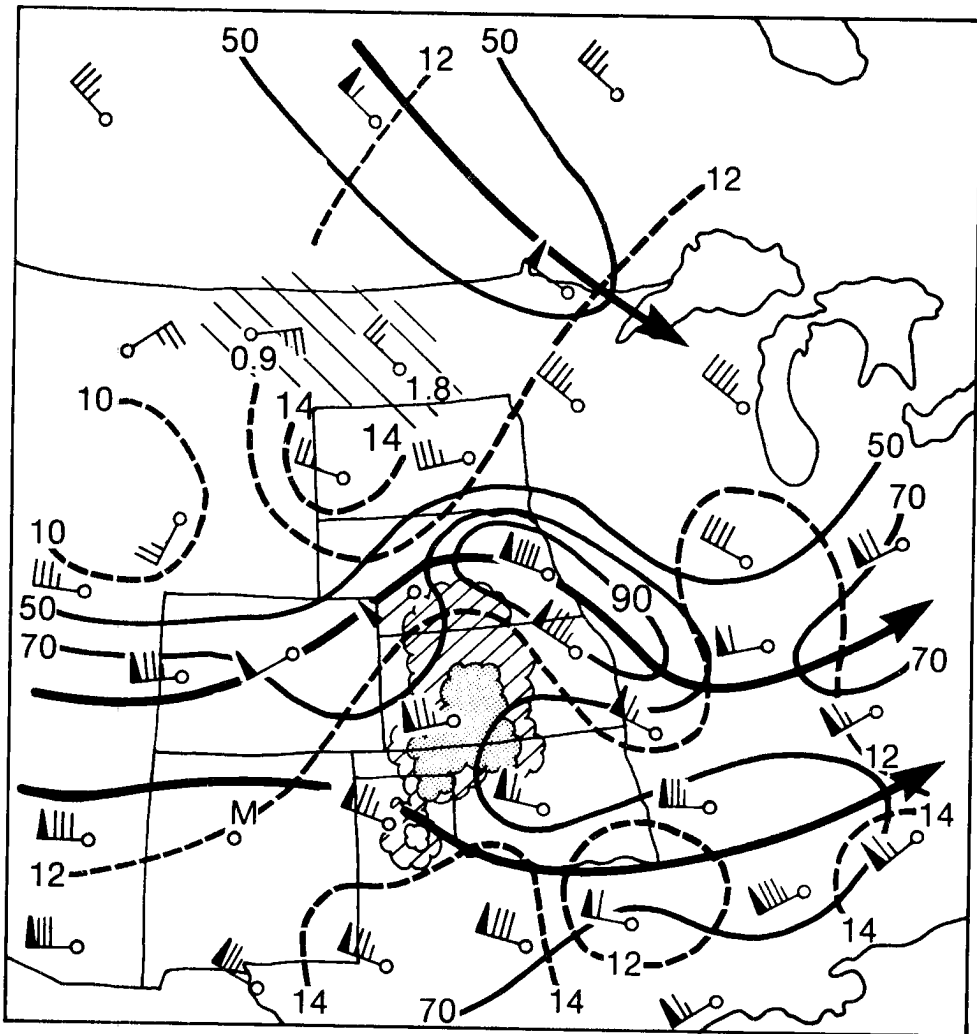
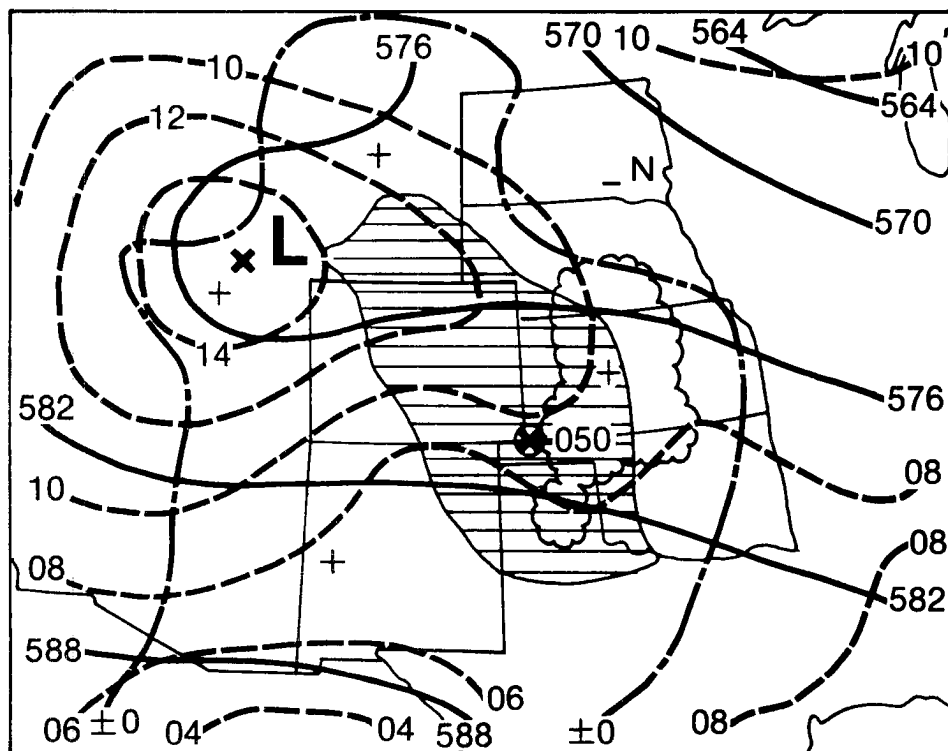
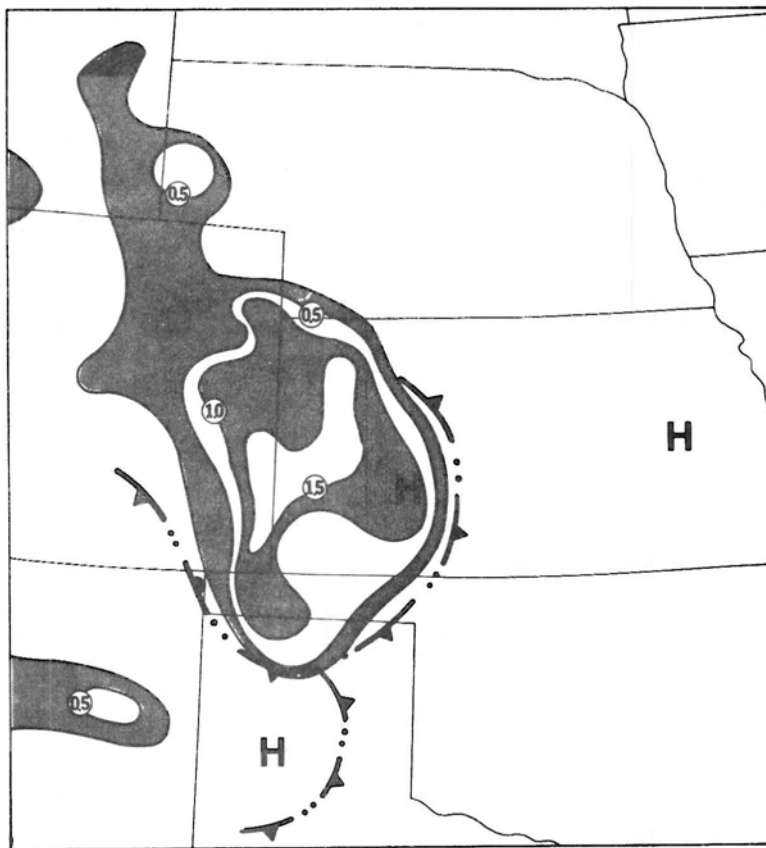


Fig. C39. Accumulated precipitation (in inches) from 0000 to 1200 GMT on 4 June 1978. Surface features at 1200 GMT are also shown.

Fig. C40. Twelve hour LFM numerical forecast valid at 1200 GMT 4 June 1978.



MCC system of those considered. It did, however, produce widespread rains of .5 to 1.5 inches over the plains of eastern Colorado and western Kansas (see Fig. C39). The LFM 12 h forecast (Fig. C40) indicated the precipitation area quite well but with observed amounts again considerably in excess of those predicted. Once again the MCC developed just ahead of a weak short-wave trough that was moving eastward out of a large scale trough to the west (note vertical motion fields on Fig. C40).

C.6 MCC of 19/20 June 1978

This MCC system evolved through a very complicated life-cycle with mergers and interactions among several storm complexes apparent in the satellite imagery. Severe thunderstorms developed over western Kansas about 1930 GMT on 19 June and these rapidly grew and consolidated into a large nearly circular MCC. As this system moved eastward it merged with a large region of storms that had developed over Minnesota and Iowa. Another region of thunderstorms moved eastward out of Colorado and merged into the western part of the system. This MCC is depicted in the satellite image of Fig. C41. The jet stream analyses (Figs. C42 and C43) illustrate a typical evolution of the flow aloft. The initial storms again appear to have developed beneath the right exit zone of a noticeable jet streak. Strong low-level inflow from the south and southwest of the system is indicated by the 1200 GMT analysis (Fig. C43).

The stability, precipitable water and 850 mb wind chart (Fig. C44) illustrates that this system developed within a strongly unstable region (LI -5 to -8) with precipitable water contents of 1.25 to 1.50 inches. A strong low-level jet was present at 0000 GMT. The 12 h rainfall analysis (Fig. C45) shows that this system produced widespread rains and that amounts of 2 to 3 inches were common. The 12 h LFM forecast (see Fig. C46)

Fig. C41. Enhanced IR image for 0630 GMT 20 June 1978.

Fig. C42. Maximum observed winds aloft for 0000 GMT 20 June 1978.

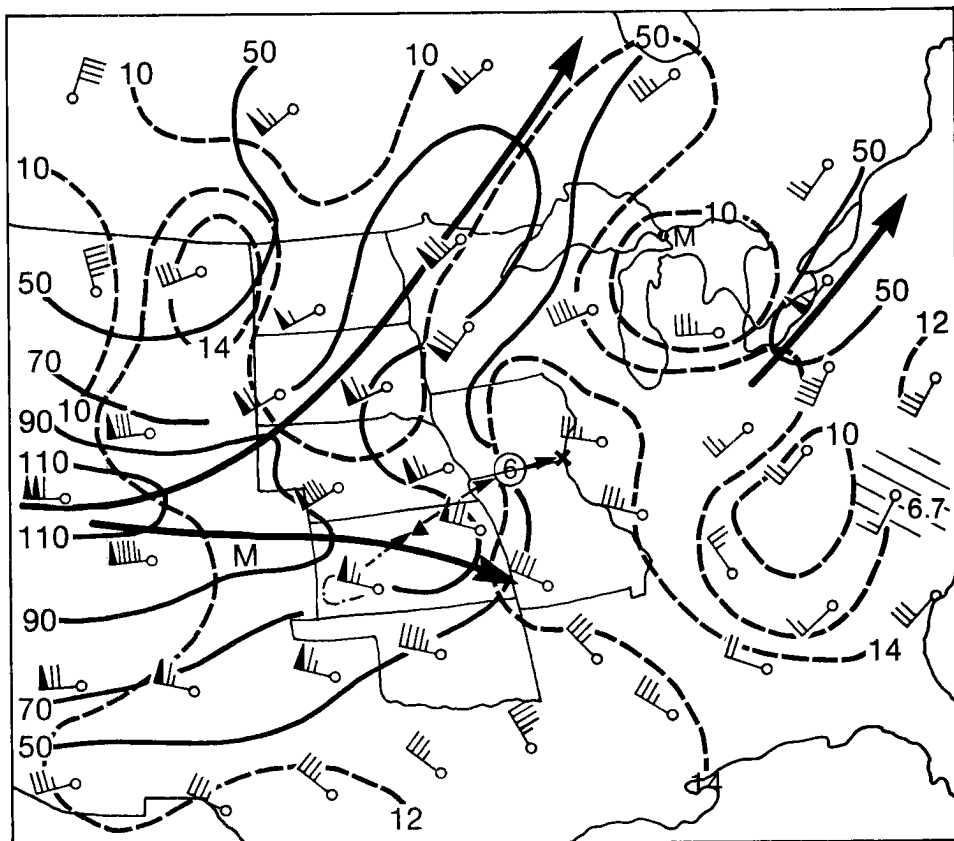
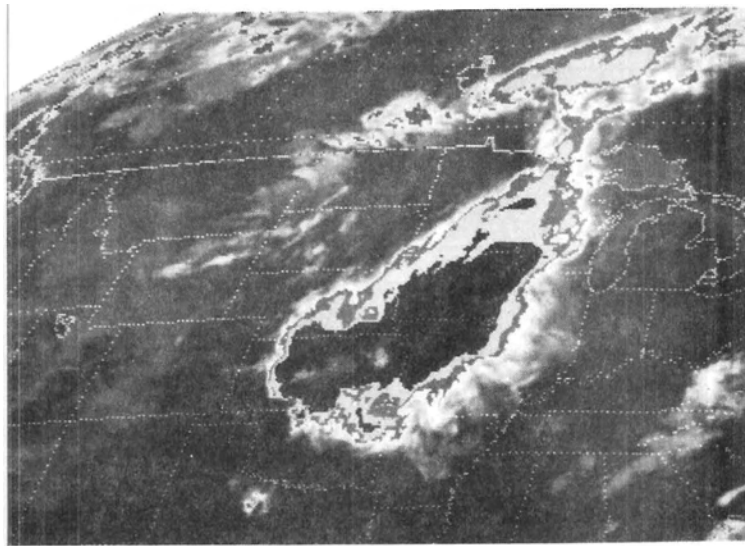


Fig. C43. Maximum observed winds aloft for 1200 GMT 20 June 1978.

Fig. C44. Stability chart for 0000 GMT 20 June 1978.

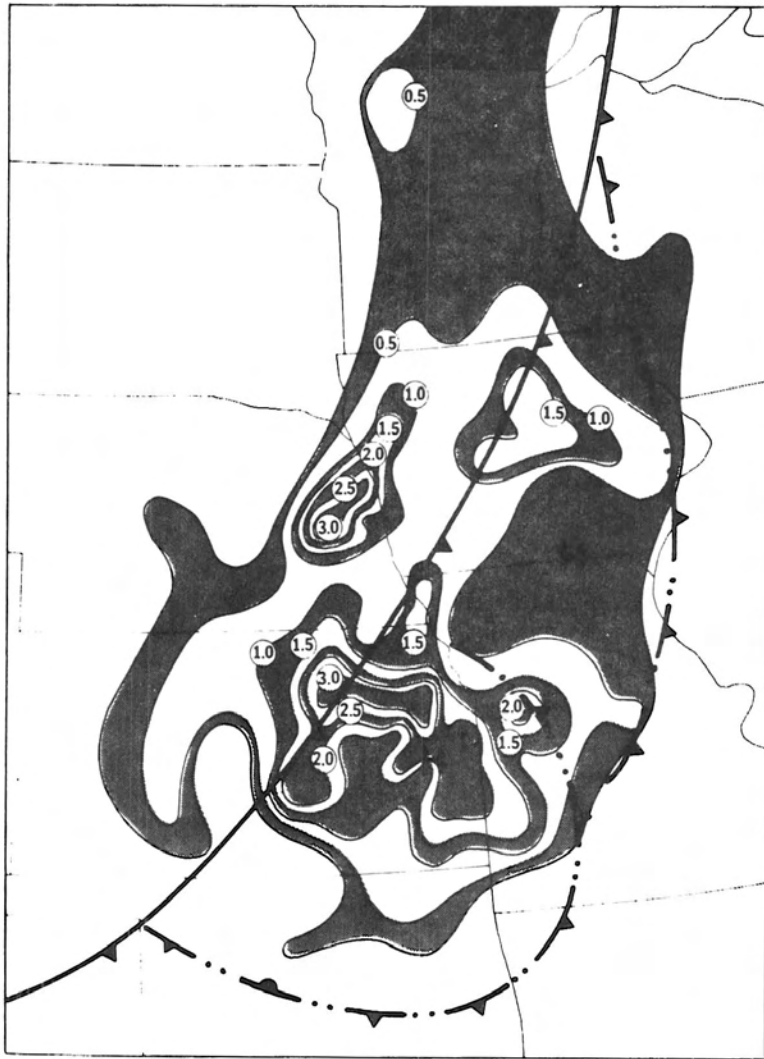


Fig. C45. Accumulated precipitation (in inches) from 0000 to 1200 GMT on 20 June 1978. Surface features at 1200 GMT are also shown.

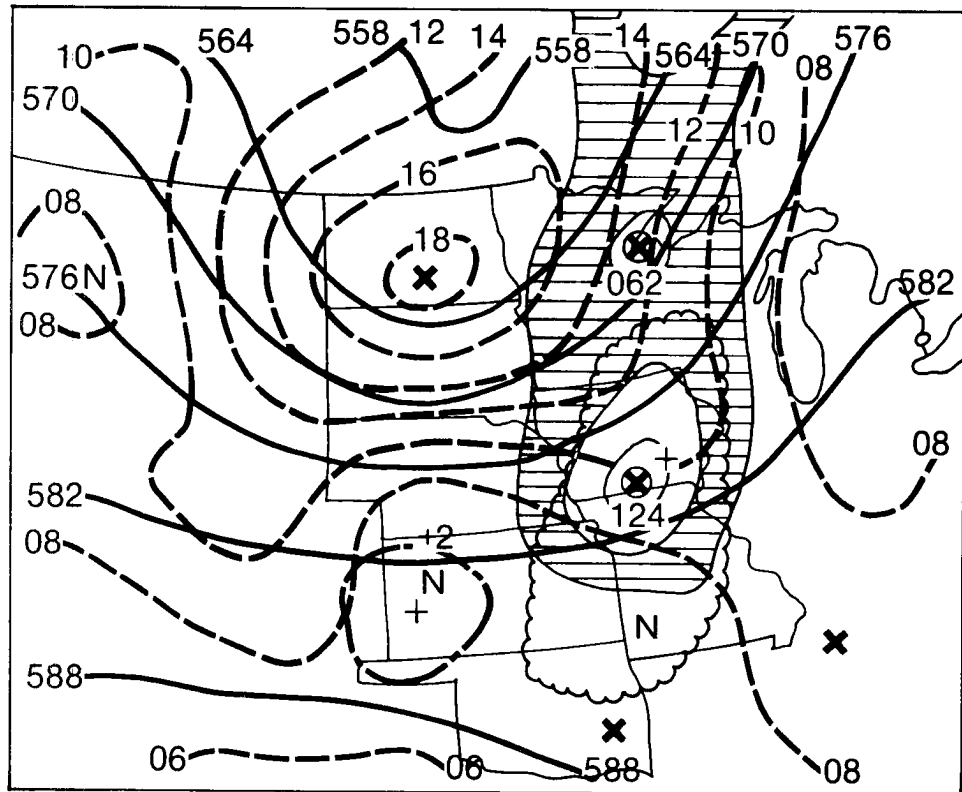


Fig. C46. Twelve hour LFM numerical forecast valid at 1200 GMT 20 June 1978.

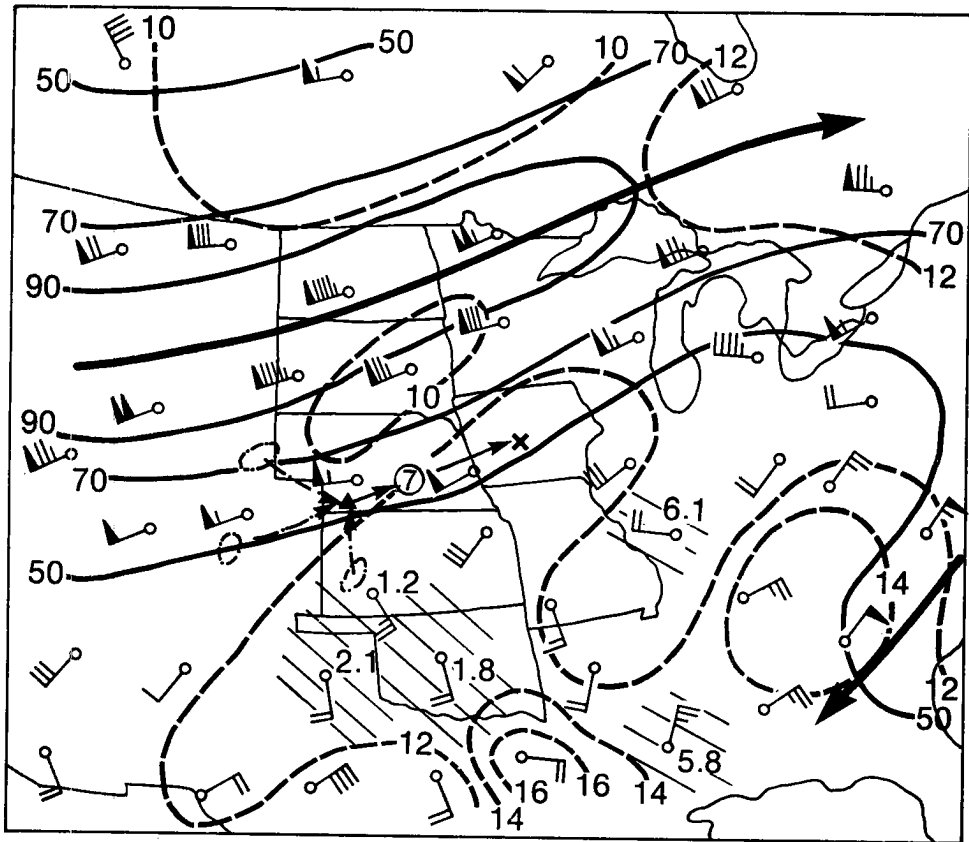
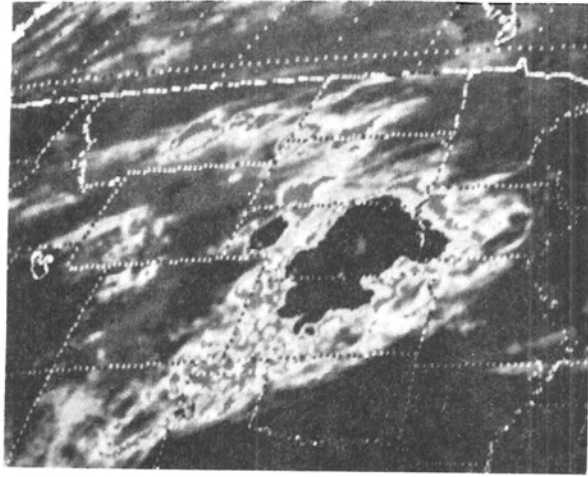
caught the northern half of the precipitation area quite well; however, the significant maximum rain area over Kansas was shifted south and southeast (toward the most unstable air mass) of the model precipitation area. Once again the MCC developed just east of a weak short-wave (see vorticity, height and vertical motion fields) that was embedded within a large scale trough.

C.7 MCC of 19/20 July 1978

Three different clusters of thunderstorms that developed over the High Plains and lee slopes of the Rockies during the late afternoon merged to form the MCC system. Although this system gradually weakened over Iowa during the morning of the 20th it did re-intensify over southern Wisconsin during the afternoon. It once again satisfied the MCC area

Fig. C47. Enhanced IR image for 0800 GMT 20 July 1978.

Fig. C48. Maximum observed winds aloft for 0000 GMT 20 July 1978.



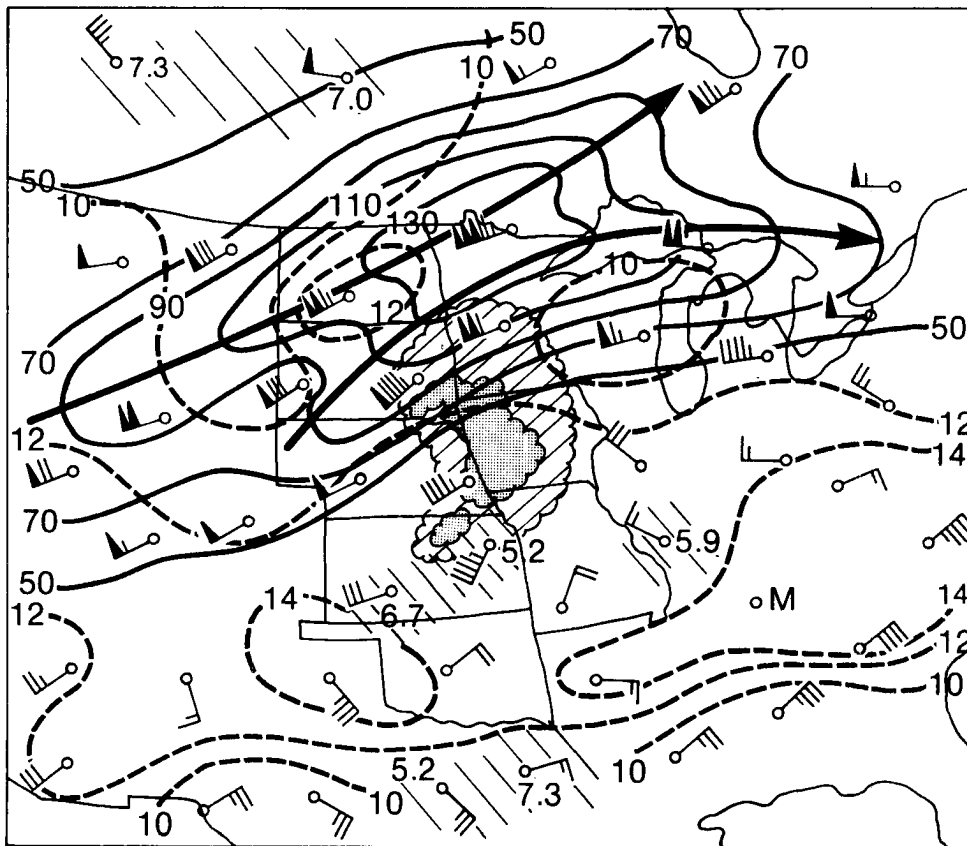


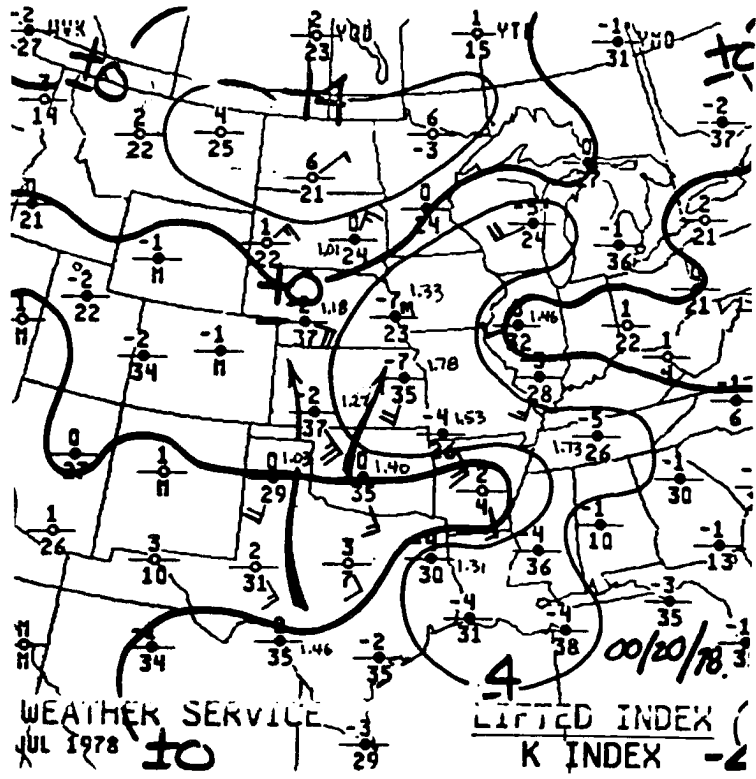
Fig. C49. Maximum observed winds aloft for 1200 GMT 20 July 1978.

requirements; however, this re-invigorated system did not persist for an additional 6 h. The MCC system is portrayed in the satellite image of Fig. C47. The evolution of jet stream level winds (Figs. C48 and C49) was again quite typical. Note the strong low-level flow south and southwest of the system at 1200 GMT.

The precipitable water, stability and 850 mb wind analyses (Fig. C50) show that conditional instability and moisture contents were quite large (LI -4 to -7 and precipitable water 1.25 to 1.75 inches) and that a low-level southerly jet was present. Note again that the MCC developed just south of a col in the 850 mb flow. The rainfall chart (Fig. C51) shows that the MCC system produced widespread precipitation and that 12 h amounts of 1.0 to 2.5 inches were common. The 12 h LFM precipitation

Fig. C50. Stability chart for 0000 GMT 20 July 1978.

Fig. C51. Accumulated precipitation (in inches) from 0000 to 1200 GMT on 20 July 1978. Surface features at 1200 GMT are also shown.



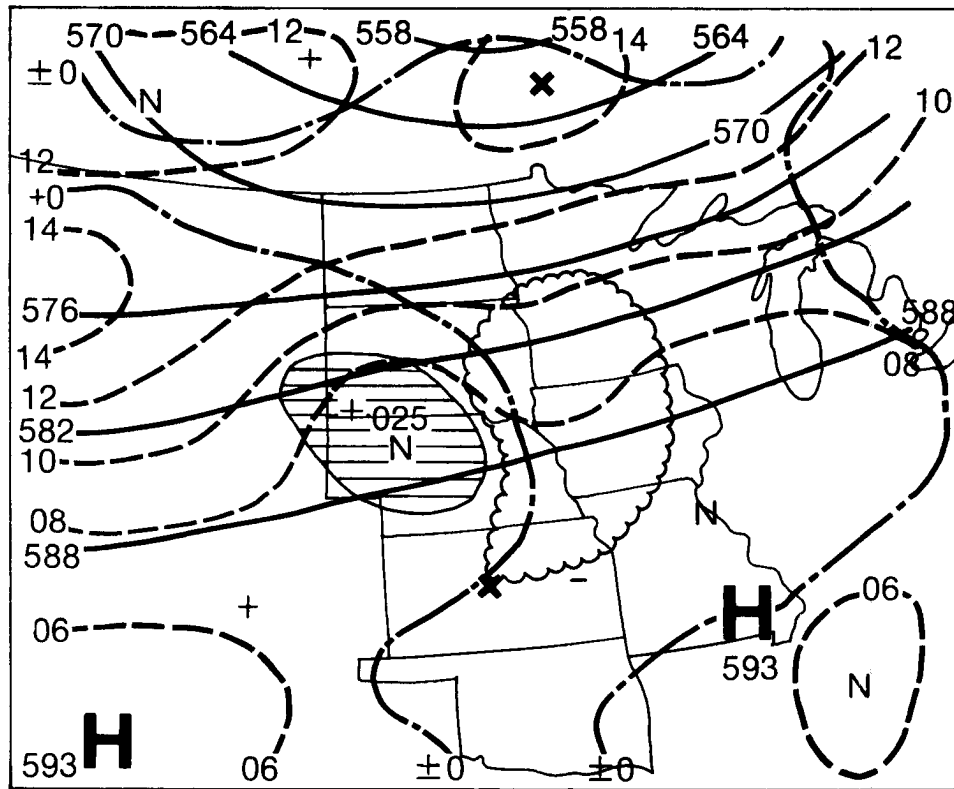


Fig. C52. Twelve hour LFM numerical forecast valid at 1200 GMT 20 July 1978.

prediction (Fig. C52) indicated only a small area of light rainfall to the west of the region over which significant rain actually fell. The forecast did indicate that this system also developed ahead of a very weak short-wave (see vorticity analysis) that was moving eastward through a basically zonal current.

C.8 MCC of 20/21 July 1978

Several groups of thunderstorms developed during the late afternoon and evening over the east slopes of Colorado and then merged over extreme southwestern Nebraska to form the MCC. Another group of storms that developed over northeastern Wyoming eventually merged with the MCC. This system is shown in Fig. C53. Figures C54 and C55 show the jet stream

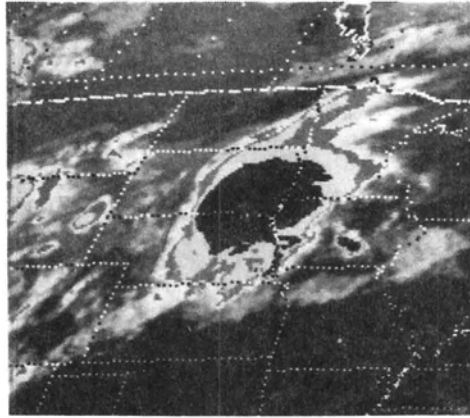


Fig. C53. Enhanced IR image for 0930 GMT 21 July 1978.

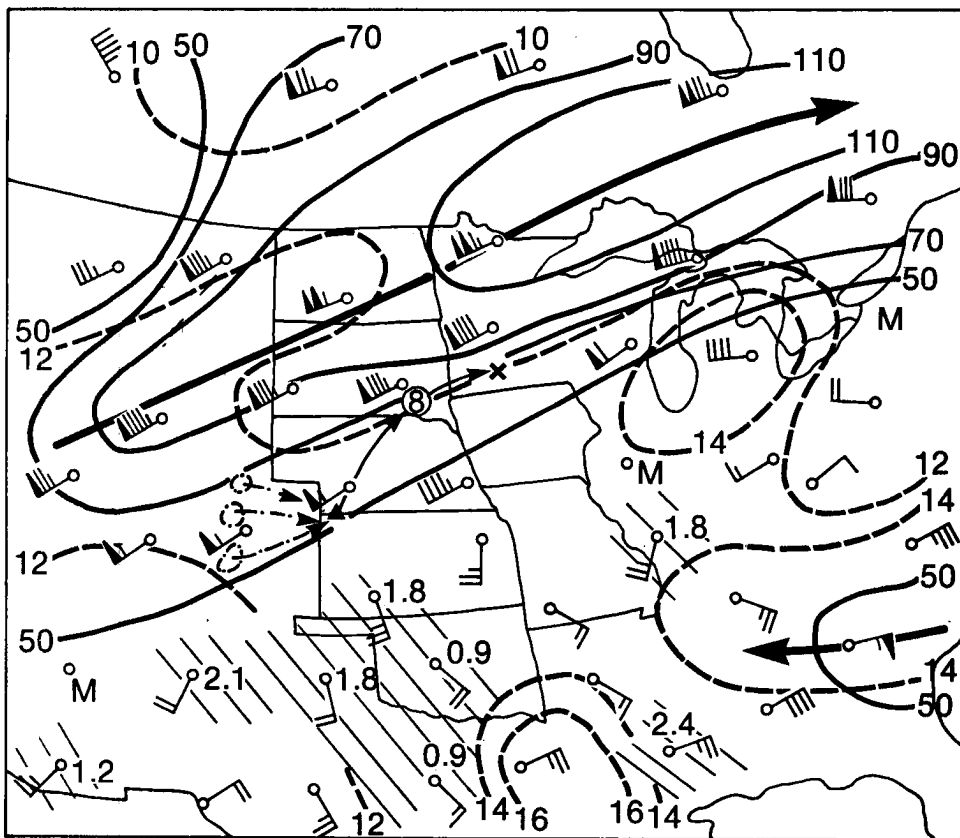
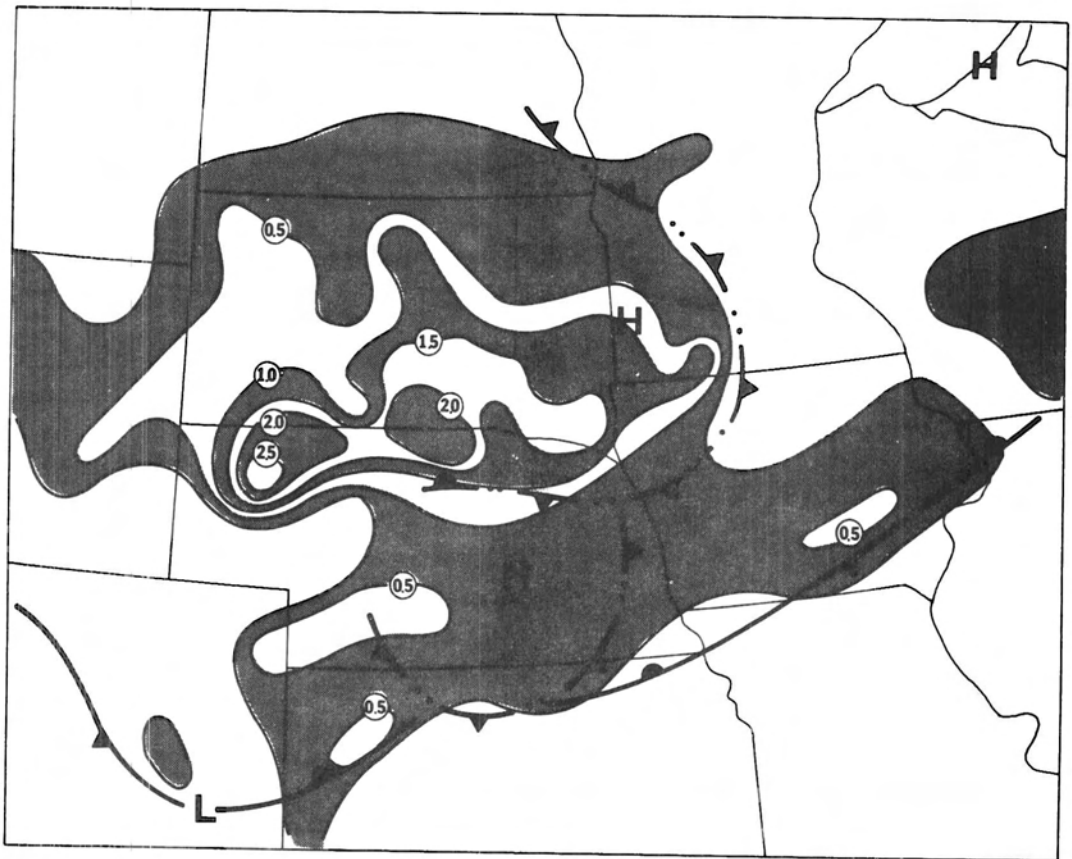
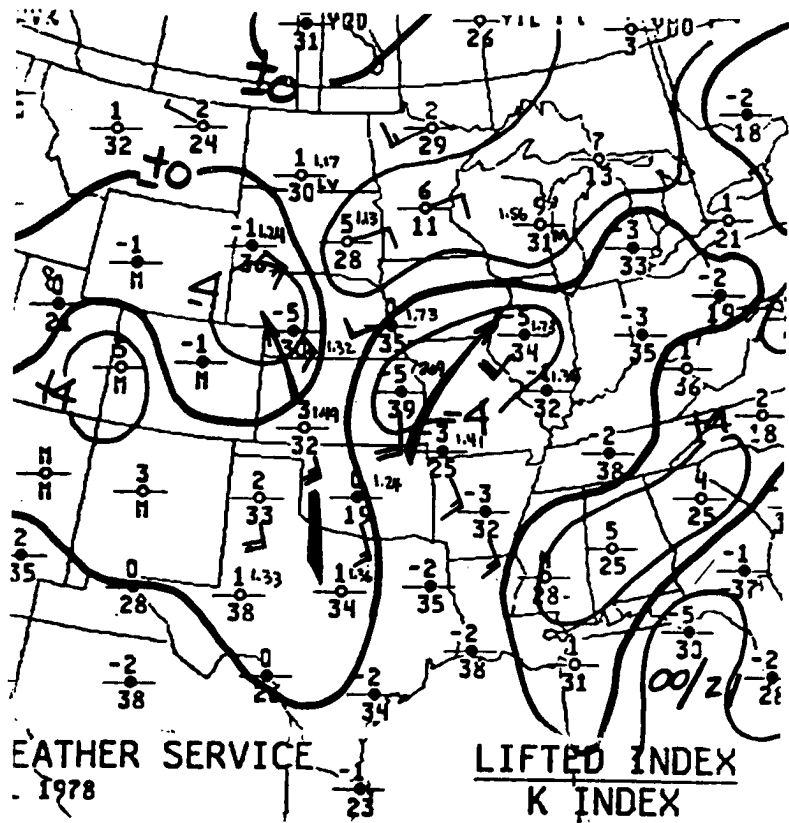


Fig. C54. Maximum observed winds aloft for 0000 GMT 21 July 1978.

Fig. C56. Stability chart for 0000 GMT 21 July 1978.

Fig. C57. Accumulated precipitation (in inches) from 0000 to 1200 GMT on 21 July 1978. Surface features at 1200 GMT are also shown.



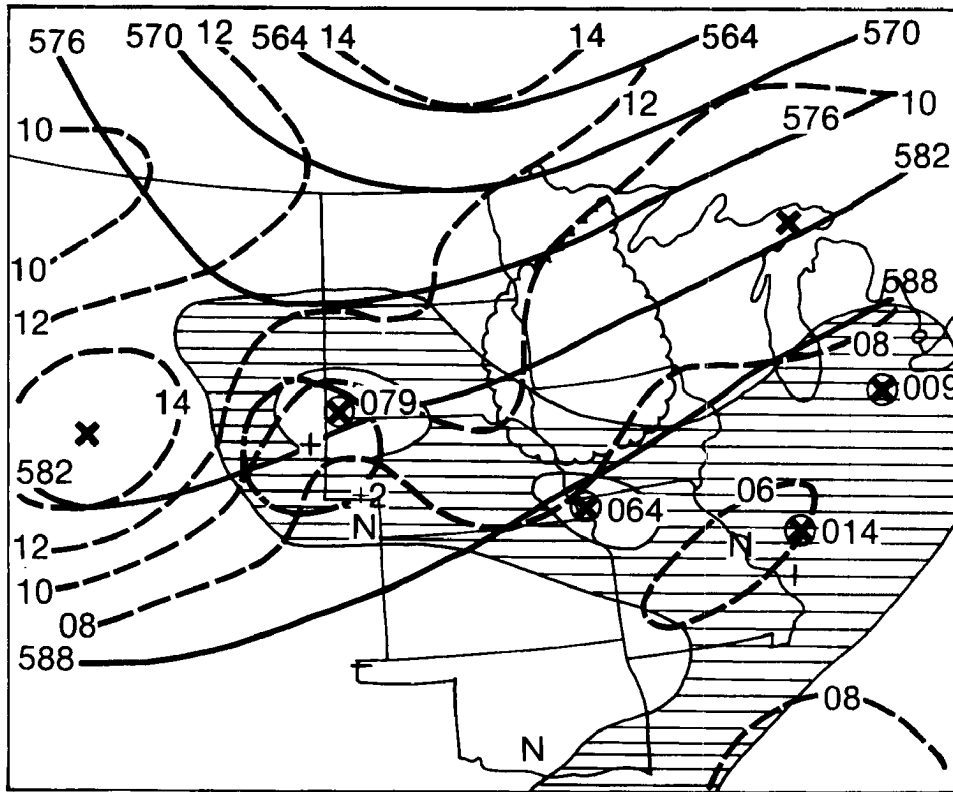


Fig. C58. Twelve hour LFM numerical forecast valid at 1200 GMT 21 July 1978.

the MCC was again occurring (at 12 GMT) just ahead of a weak short-wave (see the vorticity field) within westerly flow.

C.9 MCC of 3/4 August 1977

Large complexes of thunderstorms developed over southeastern Wyoming and northeastern Colorado during late afternoon on the 3rd. These systems grew and merged over western Nebraska and the eventual MCC is captured in the satellite image shown in Fig. C59. The upper-wind analyses shown in Figs. C60 and C61 depict a typical evolution of features. The stability chart (Fig. C62) shows that conditions were very unstable (LI of -6 to -7) and moisture values were high (1.25 to 1.40 inches). A strong south-southwesterly low-level flow was present and the system moved eastward

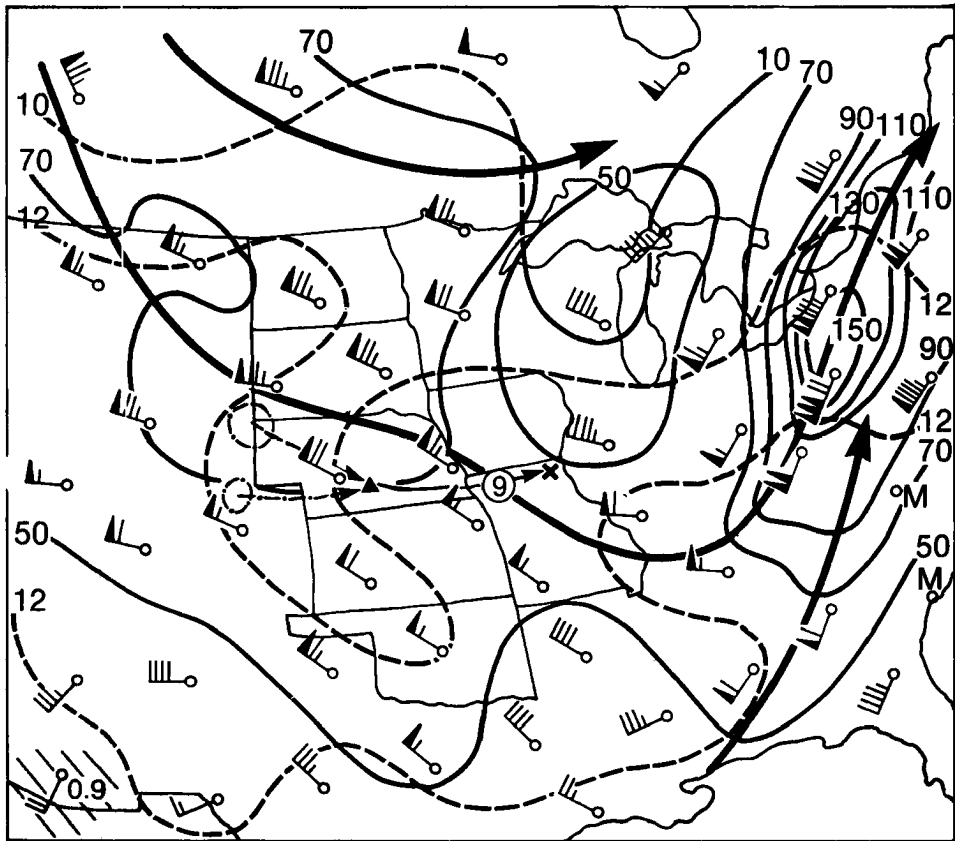
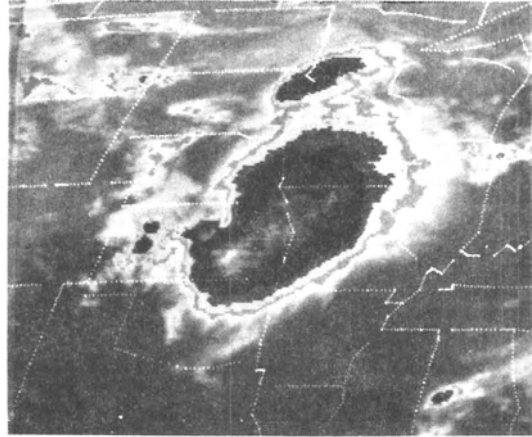


Fig. C60. Maximum observed winds aloft for 0000 GMT 4 August 1977.

Fig. C61. Maximum observed winds aloft for 1200 GMT 4 August 1977.

Fig. C62. Stability chart for 0000 GMT 4 August 1977.

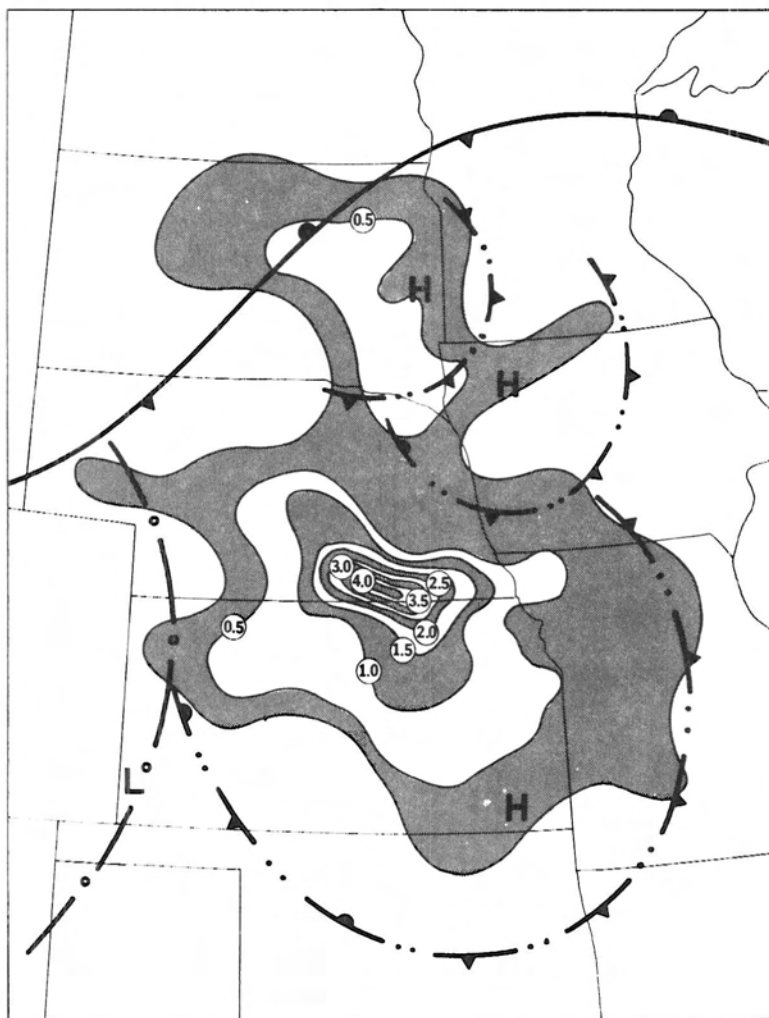


Fig. C63. Accumulated precipitation (in inches) from 0000 to 1200 GMT on 4 August 1977. Surface features at 1200 GMT are also shown.

just south of a pronounced col in the 850 mb flow field. The system produced widespread rains (Fig. C63) with maximum amounts exceeding 4.0 inches over southern Nebraska. Virtually no precipitation was forecasted by the LFM (see Fig. C64) over this region although the vorticity, height and vertical motion fields suggest that the MCC formed just ahead of a very weak short-wave trough.

Time-series plots of surface observations for Lincoln, Nebraska (northern portion of system) and Salina, Kansas (southern portion of system) are shown in Fig. C65. These observations detect considerably more small

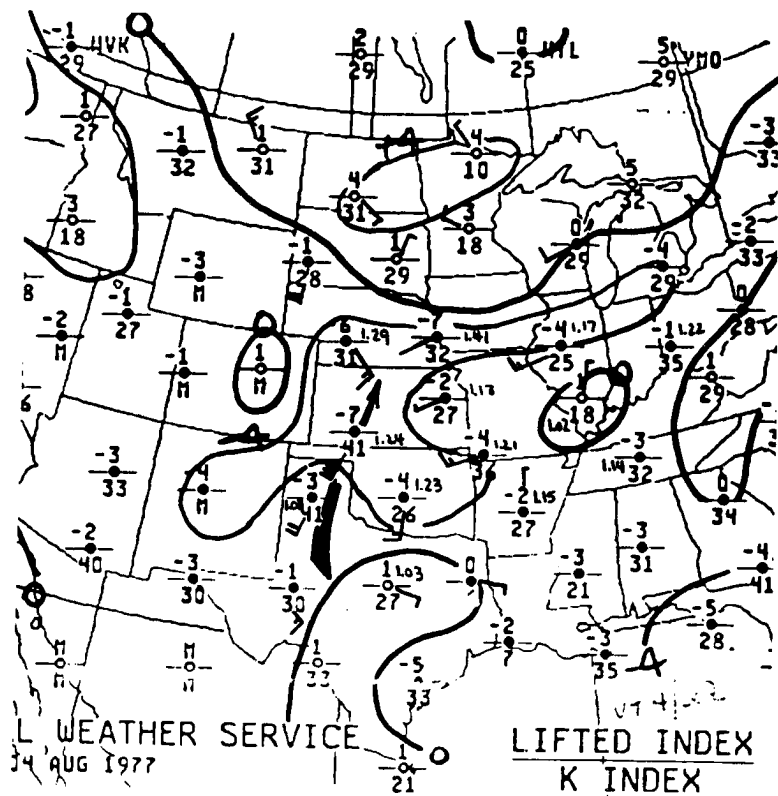
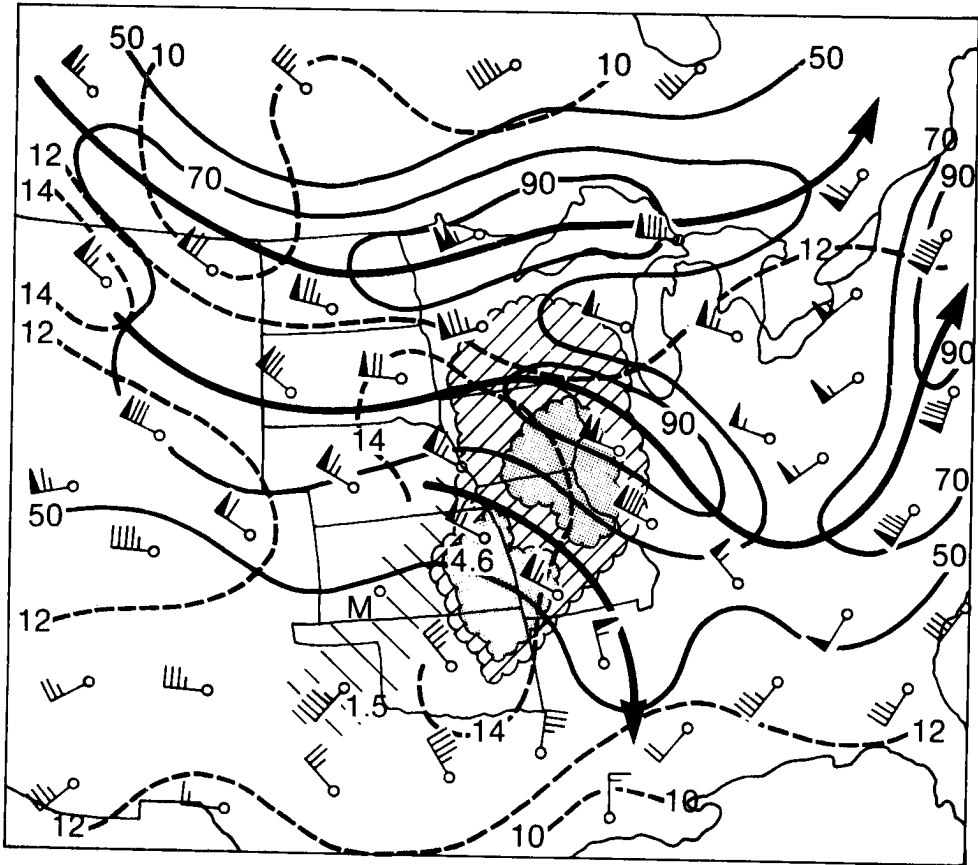
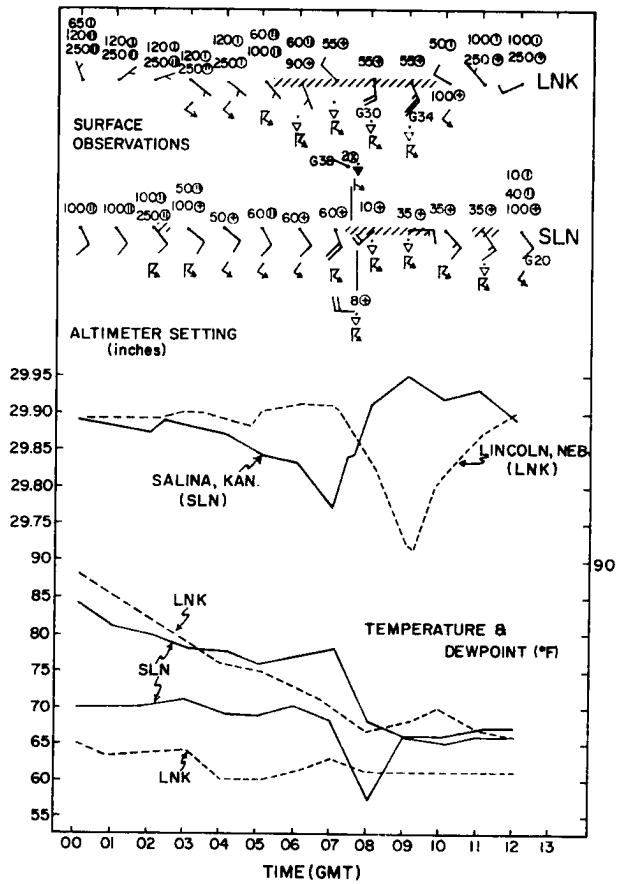
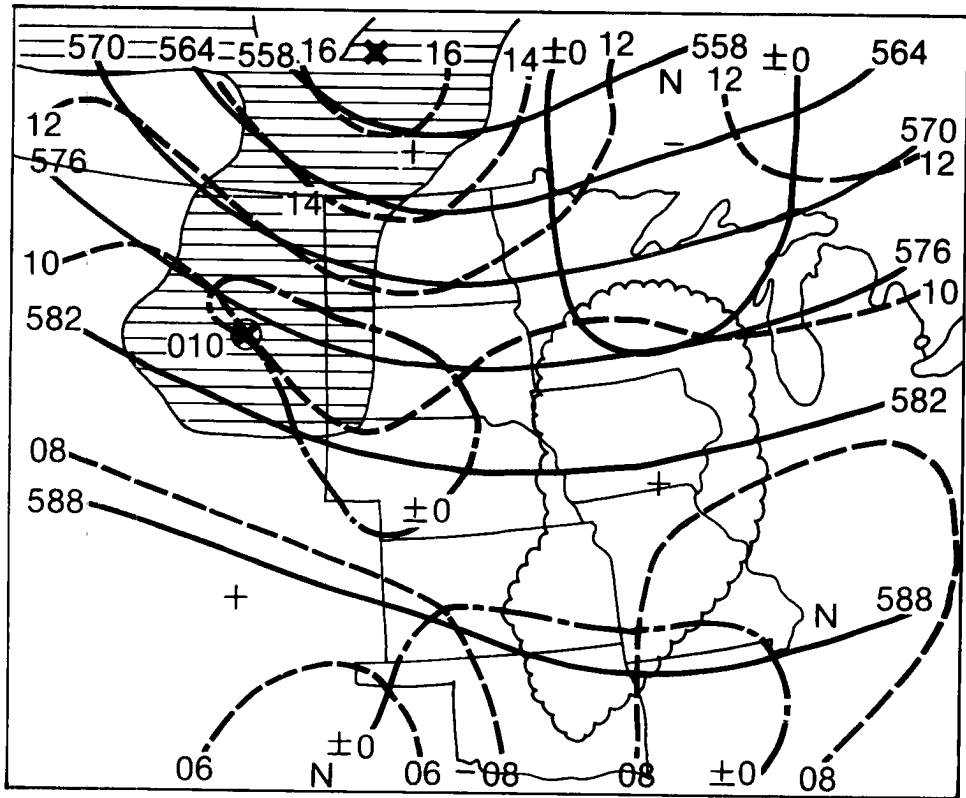


Fig. C64. Twelve hour LFM numerical forecast valid at 1200 GMT 4 August 1977.

Fig. C65. Surface observation time-series for Lincoln, Nebraska and Salina, Kansas. Winds are in knots and are plotted with north to the top of the figure. Cross-hatching indicates periods of reported rainfall.



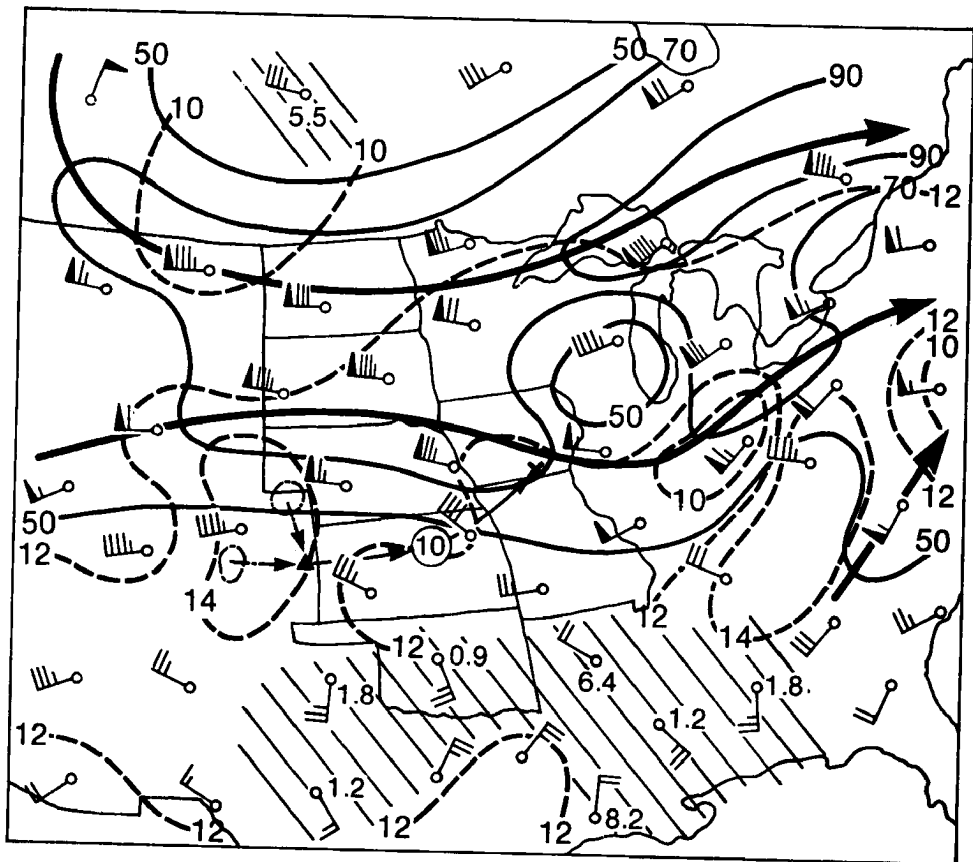
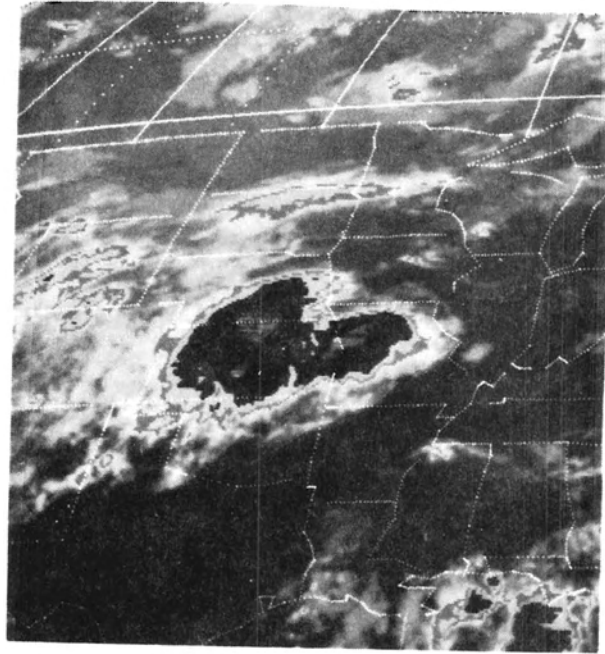
scale structure than did the time series shown in Section II and earlier in this Appendix. Note the large pressure perturbations that attended the system and the difference in the evolution of the pressure field at the two locations. Salina experienced a strong pressure fall ahead of the system (somewhat similar to convective cases studied by Hoxit et al., 1976) followed by an abrupt pressure rise accompanied by marked cooling and moistening. Whereas, Lincoln experienced a brief pressure jump (at about 0430 GMT) that was not accompanied by pronounced temperature or dewpoint changes -- even though precipitation began and continued for more than four hours. Several hours later (about 0700 GMT) a remarkable rapid pressure fall of .25 in. (~ 8 mb) occurred during a 2 h period as an intense wake depression developed along the northwest periphery of the system. Lincoln experienced a gust of 34 knots from the south just ahead of this mesolow. The precipitation at Lincoln fell from a cloud deck based at 5 to 6000 ft. above the ground while the Salina data show a low overcast present for about four hours. Considerable mid-level cloudiness was present at both locations throughout the 12 h period covered in Fig. C65.

C.10 MCC of 4/5 August 1977

This MCC had its roots in thunderstorm activity that developed over the mountains of central Colorado early in the afternoon of the 4th. This activity merged with storms that developed over northeast Colorado and moved eastward eventually merging with another complex of storms that had developed during the early night time hours over eastern Kansas. Another complex of storms developed over south-central Colorado and northern New Mexico during the late afternoon of the 4th; however, this system maintained a separate identity and did not develop into an MCC. The MCC system is shown in Fig. C66 as it began to merge with the storms over

Fig. C66. Enhanced IR image for 0900 GMT 5 August 1977.

Fig. C67. Maximum observed winds aloft for 0000 GMT 5 August 1977.



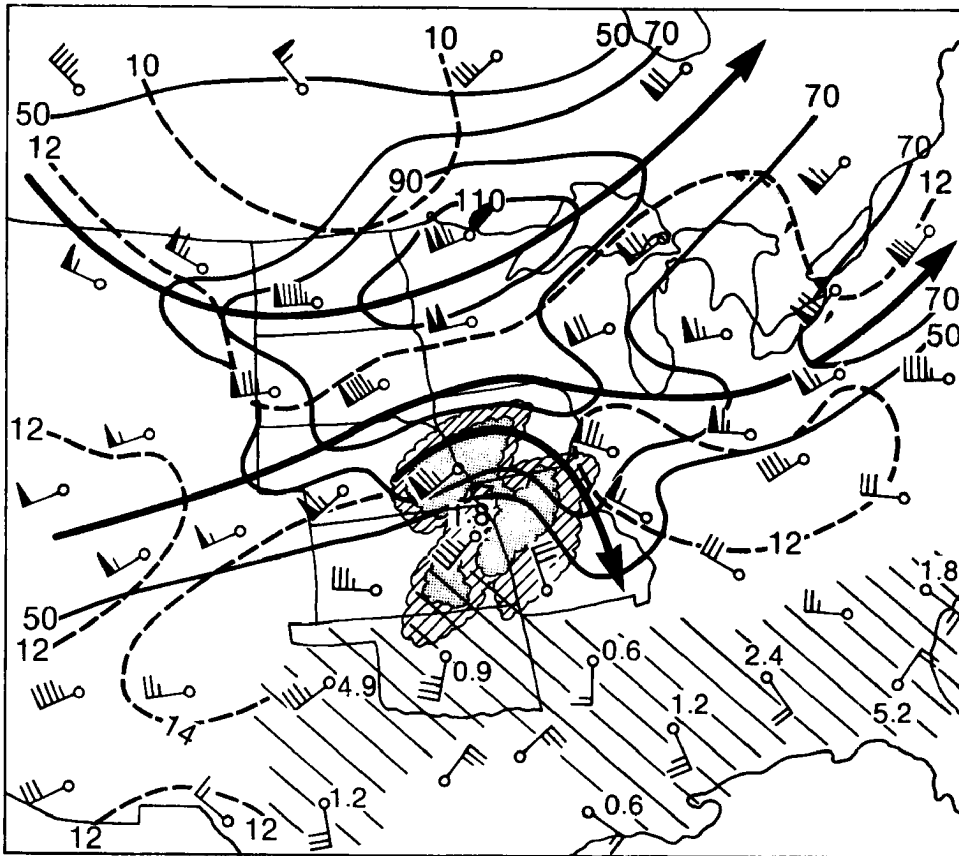


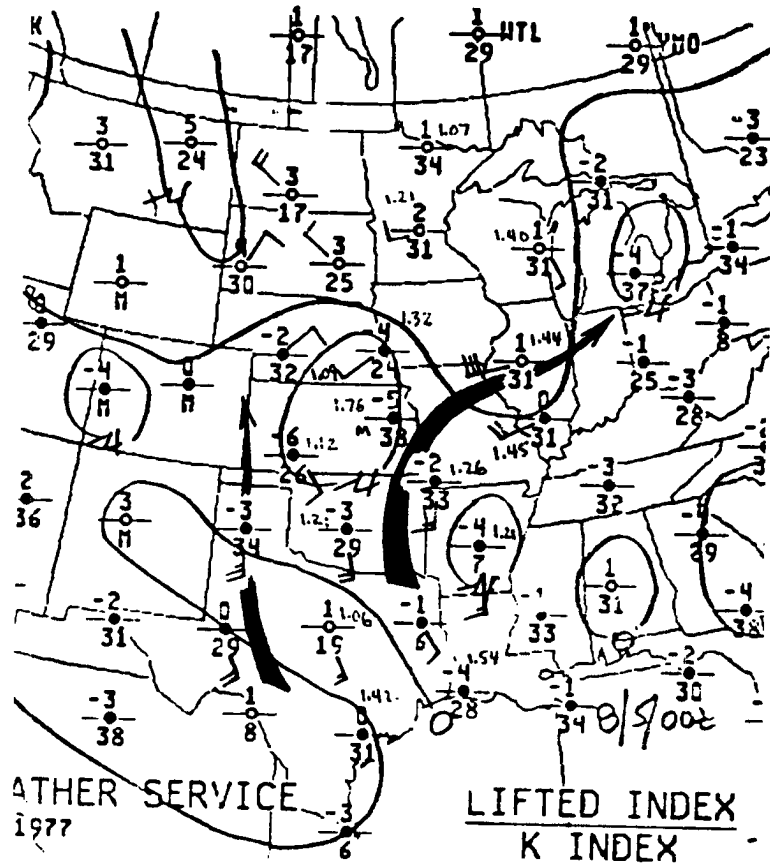
Fig. C68. Maximum observed winds aloft for 1200 GMT 5 August 1977.

eastern Kansas and Missouri. The upper-wind analyses (Figs. C67 and C68) illustrate a typical evolution of jet stream level features. The stability chart (Fig. C69) indicates that conditions were quite similar to those attending the other MCCs. The rainfall chart (Fig. C70) shows that widespread heavy rains fell over parts of Nebraska and Kansas for the second consecutive night. The LFM 12 h forecast (Fig. C71) had indicated light rains over the western part of the region. Once again the LFM vorticity and vertical motion forecasts indicate that this MCC developed and moved eastward and just ahead of a weak short-wave trough.

Figures C72 and C73 illustrate what conditions were typically like 12 h prior to and 12 h after the time that the MCC was well organized (i.e., at the other two data compositing times). At about 0000 GMT on

Fig. C69. Stability chart for 0000 GMT 5 August 1977.

Fig. C70. Accumulated precipitation (in inches) from 0000 to 1200 GMT on 5 August 1977. Surface features at 1200 GMT are also shown.



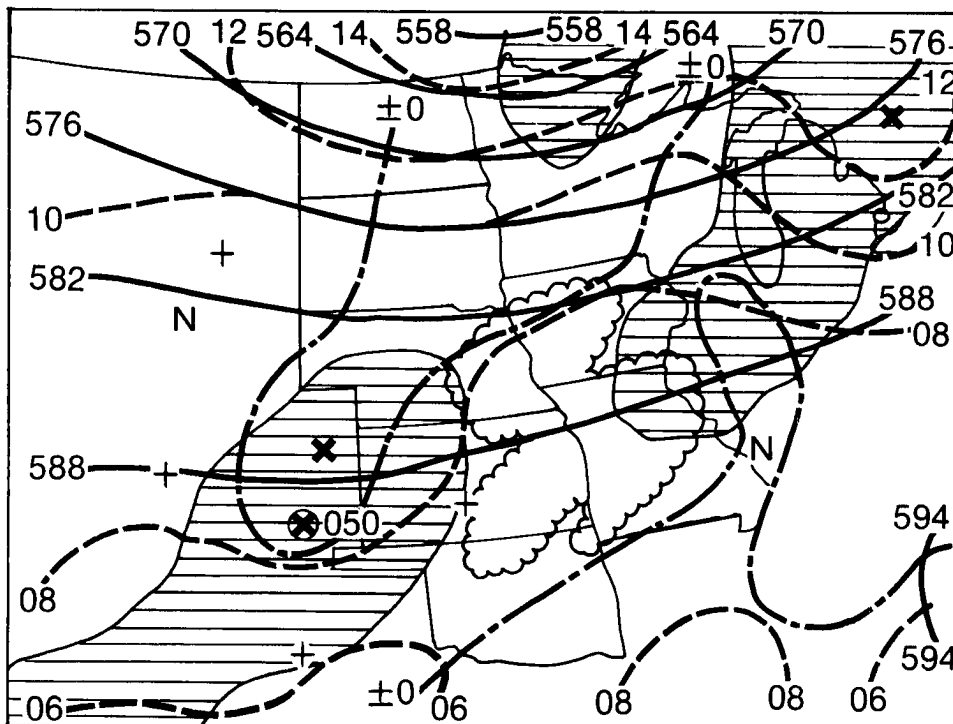


Fig. C71. Twelve hour LFM numerical forecast valid at 1200 GMT 5 August 1977.

the 4th of August the storms that were to develop into the MCC described in C.9 were located over the Nebraska Panhandle. At about 0000 GMT on the 5th of August the storm complex that developed into the MCC discussed in this section was apparent over eastern Colorado, while the debris and remnant cloud masses from the preceding day's MCC were located over the Great Lakes Region. George (1979), Cotton et al. (1981) and Wetzel et al. (1981) have studied the convective systems of 3/4/5 August 1977 and present considerably more detailed discussions of the development and histories of these systems.

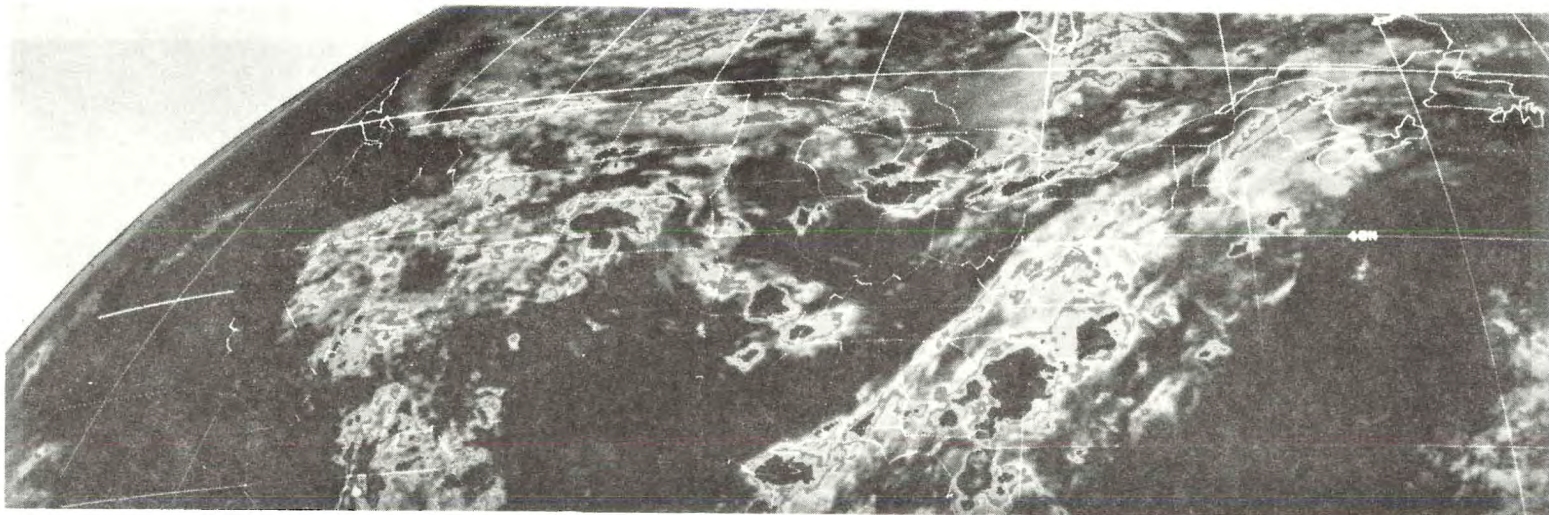


Fig. C72. Enhanced IR image for 0030 GMT on 4 August 1977.



Fig. C73. Enhanced IR image for 0014 GMT on 5 August 1977.